Glaciation Scenario: Safety Assessment for a Deep Geological Repository for Used Fuel

NWMO TR-2010-10 **July 2010**

F. Garisto[1], J. Avis[3], T. Chshyolkova[2], P. Gierszewski[1], M. Gobien[1], C. Kitson[2], T. Melnyk[2], J. Miller[2], R. Walsh[3] and L. Wojciechowski[2]

[1]Nuclear Waste Management Organization
[2]Atomic Energy of Canada Limited
[3]Intera Engineering

nwmo
NUCLEAR WASTE MANAGEMENT ORGANIZATION
SOCIÉTÉ DE GESTION DES DÉCHETS NUCLÉAIRES

Nuclear Waste Management Organization
22 St. Clair Avenue East, 6th Floor
Toronto, Ontario
M4T 2S3
Canada

Tel: 416-934-9814
Web: www.nwmo.ca

Glaciation Scenario: Safety Assessment for a Deep Geological Repository for Used Fuel

NWMO TR-2010-10

July 2010

F. Garisto[1], J. Avis[3], T. Chshyolkova[2], P. Gierszewski[1], M. Gobien[1], C. Kitson[2], T. Melnyk[2], J. Miller[2], R. Walsh[3], and L. Wojciechowski[2]

[1]Nuclear Waste Management Organization
[2]Atomic Energy of Canada Limited
[3]Intera Engineering

ABSTRACT

Title: **Glaciation Scenario: Safety Assessment for a Deep Geological Repository for Used Fuel**
Report No.: **NWMO TR-2010-10**
Author(s): F. Garisto[1], J. Avis[3], T. Chshyolkova[2], P. Gierszewski[1], M. Gobien[1], C. Kitson[2], T. Melnyk[2], J. Miller[2], R. Walsh[3] and L. Wojciechowski[2]
Company: [1]Nuclear Waste Management Organization, [2]Atomic Energy of Canada Limited and [3]Intera Engineering
Date: July 2010

Abstract
A key part of the long-term management of used fuel in Canada is the containment and isolation of the used fuel in a deep geological repository. The reference time frame for the safety assessment of such repositories is one million years, roughly equivalent to the time scale for the radioactivity in the used fuel to decrease to that due to its natural uranium content. Over the past one million years, the most significant natural event across Canada has been repeated glacial cycles. In principle, these will continue since the long-term variation in solar insolation will continue.

In previous Canadian safety assessments of a used fuel repository, the effects of glaciation were considered in geoscience studies and in the engineering design of the repository. However, the potential impacts of glaciation on the safety and performance of the repository were only qualitatively evaluated.

In the current safety assessment study, the effects of an evolving climate with multiple glaciations are quantitatively evaluated. This study is referred to as the Glaciation Scenario to distinguish it from the constant climate scenarios, which presume an unvarying climate, previously investigated. For this study, the repository is assumed to be located at the hypothetical site on the Canadian Shield used in the Third Case Study.

The detailed three-dimensional modelling results confirm the expected significant impact of glaciation on the groundwater flow system, affecting velocity direction and magnitude. The effects are greatest near the surface but extended to the repository level. The open taliks during permafrost periods, in particular, are a dominant factor, focusing system impacts at a discrete location. (A talik is a layer of unfrozen ground that lies in permafrost areas.) Furthermore, the transport calculations indicate that radionuclide mass flows to the surface biosphere are quite different for the transient glaciation model compared to the equivalent constant climate case, with mass flows in the glaciation model both larger and smaller than in the constant climate case. Nevertheless, the overall trends and cumulative mass flows to the biosphere are similar in these two very different climate cases.

For the Glaciation Scenario, the safety assessment calculations indicate that the calculated dose rates are highest during temperate periods. This occurs because only the critical group living during temperate periods uses a well, rather than a lake, as its domestic water source and radionuclide concentrations in well water are typically several orders of magnitude higher than in lake water, leading to higher exposures. In the Reference Case of the Glaciation Scenario, the calculated peak total dose rate is about 3.7×10^{-7} Sv/a, with I-129 contributing the most to the total dose rate. This is similar to the peak dose rate of 1.3×10^{-7} Sv/a for the corresponding case in constant climate scenario. Both these dose rates are well below the dose rate constraint of 3×10^{-4} Sv/a recommended by International Commission on Radiological Protection (ICRP) for disposal of long-lived solid radioactive waste and the average Canadian natural background dose rate of 1.8×10^{-3} Sv/a.

A series of sensitivity cases and probabilistic cases were also investigated. As would be expected, the "what if" sensitivity case in which all containers fail simultaneously gives the highest calculated dose rate. Even for this improbable sensitivity case, the dose rate exceeds the ICRP dose rate constraint of 3×10^{-4} Sv/a for only a brief period of time, at the end of several glacial cycles, but remains well below the average Canadian background dose rate of 1.8×10^{-3} Sv/a.

The results of the Climate State Duration probabilistic case suggests that varying the glacial cycle could lead to higher calculated dose rates compared to the Reference Case of the Glaciation Scenario. Although the 90th percentile calculated dose rate in this probabilistic simulation was 3-fold higher than in the Reference Case, it remained well below the dose rate constraint recommended by ICRP.

In summary, for the hypothetical site and repository of the Third Case Study, calculated peak dose rates for the Glaciation Scenario are approximately of the same order of magnitude as for the corresponding constant (temperate) climate scenario. The calculated peak dose rates for the Glaciation Scenario are well below the ICRP dose constraint and the average natural Canadian background dose rate. Thus, it can be concluded that for the hypothetical Third Case Study site and repository, the impacts of a deep geological repository would be well below regulatory limits when the effects of glaciation are considered.

TABLE OF CONTENTS

LIST OF TABLES

Page

LIST OF FIGURES

Page

1. INTRODUCTION

1.1 BACKGROUND

The selected approach for long-term management of used fuel in Canada is the Adaptive Phased Management Approach (NWMO 2005). A key part of this concept is the containment and isolation of the used fuel in a deep geologic repository in a suitable host rock.

A particular consideration in assessing the performance of a geologic repository in Canada is the potential impacts of future glaciation. Glacial cycles have occurred approximately every 120,000 years over the past million years. The main factor that initiated these events in the past – notably solar insolation variation due to Earth orbital dynamics – is still present. In the absence of human-induced changes such as greenhouse gases, glacial cycles would certainly continue over the next million years. Although current levels of greenhouse gases in the atmosphere may delay the onset of the next glaciation, the glacial cycles are likely to reassert themselves in the long run (Berger and Loutre 2002).

During past glacial cycles, much of Canada was covered by kilometre-thick ice sheets. Because these glacial cycles represent such a large potential perturbation to a site on time scales of interest to long-term safety assessment, the Canadian used fuel disposal program has been examining the implications of glaciation. Much of this effort has focussed on understanding the effects of glaciation underground, notably through examining the palaeohydrogeological record for the effects of glaciation on the rocks and porewaters of the Canadian Shield (e.g., McMurry and Ejeckam 2002, Gascoyne et al. 2004).

The general conclusion is that there should be sites within the Canadian Shield where a deep repository can be safely sited, even when considering the potential effects of glaciation. Similar observations have been made for other northern countries, notably Sweden and Finland (SKB 2006a, 2006b; Smith et al. 2007).

Three major safety assessment case studies have been considered within the Canadian used fuel disposal program: the Environmental Impact Assessment (EIS) study (AECL 1994, Goodwin et al. 1994); the Second Case Study (SCS) (Goodwin et al. 1996); and the Third Case Study (TCS) (Gierszewski et al. 2004a, Garisto et al. 2005a). Each study considered a different combination of engineering design and site characteristics, and assumed that the climate was constant throughout the simulation. Although these studies qualitatively discussed the potential effects of glaciation, they did not present any quantitative analyses.

The purpose of the current case study is to quantitatively assess the long-term safety implication of glacial cycles on a deep geological repository for used nuclear fuel located on the Canadian Shield. Specifically, we carry out a postclosure safety assessment of a deep repository for an illustrative Glaciation Scenario. In this Glaciation Scenario, the climate changes, with several glacial cycles occurring during the simulation time.

1.2 REPORT OUTLINE

This report is organized as follows:

- **Section 2** summarizes the context of the safety assessment for the Glaciation Scenario, and the analysis approach.
- **Section 3** describes the reference glacial cycle used in the assessment calculations.
- **Section 4** describes the evolution of the repository and site during a glacial cycle in general terms.
- **Section 5** describes the conceptual models used in the assessment of the Glaciation Scenario
- **Section 6** describes the detailed groundwater modelling results.
- **Section 7** describes the results of the detailed I-129 transport calculations.
- **Section 8** describes the system level safety assessment modelling calculations carried for the Glaciation Scenario.
- **Section 9** compares the safety assessment results for the Glaciation Scenario with the corresponding results for a constant climate scenario in which the climate remains constant throughout the simulation time.
- **Section 10** gives a summary of the results and the conclusions.

2. ASSESSMENT CONTEXT

Analysis of the features, events and processes (FEPs) for a deep geological repository for used fuel on the Canadian Shield (e.g., Gierszewski et al. 2004c) identified an important external FEP – climate change, in particular glaciation. Although the implications of glaciation were qualitatively assessed in previous safety assessments, detailed quantitative analyses were not done (McMurry et al. 2003).

2.1 OBJECTIVES

The purpose of the present study is to assess the implications of glaciation on the safety performance of a deep geological repository for used fuel in the Canadian Shield. That is, we carry out a postclosure safety assessment of a used fuel repository for a Glaciation Scenario. The study is conducted for a hypothetical site, but the overall results are expected to be more generally applicable.

The study focuses on groundwater flow, contaminant transport and potential dose impacts under glaciation. Some containers are assumed to have failed. Other aspects of glaciation, such as the potential intrusion of oxygenated meltwater into the geosphere or the mechanical response of the containers, are not addressed here but are discussed elsewhere (e.g., Spiessl et al. 2009, McMurry 2000, McMurry et al. 2003).

2.2 REPOSITORY SITE AND SYSTEM DESIGN

In order to provide a quantitative assessment of the performance of a deep repository under glacial cycles, it is necessary to consider a specific site and repository design.

Since there is presently no specific candidate site, recent Canadian work has considered a hypothetical site within the Canadian Shield, referred to as the Third Case Study site (Gierszewski et al. 2004a,b). This hypothetical site is assumed to be composed of crystalline (granitic) rock, intersected by a complex set of interconnecting fractures (see Section 6). Within this setting, a number of regional and local scale modelling studies have been carried out:

1. hydrogeological modelling (Sykes et al. 2003a,b; 2004);
2. safety assessments (Gierszewski et al, 2004a, Garisto et al. 2004a, 2005a,b);
3. glacial effects on hydrogeology (Chan and Stanchell 2004, 2008; Chan et al. 2003, 2005, Normani 2009);
4. alternative design concepts - in-room emplacement (Gierszewski et al. 2004a; Garisto et al. 2004a), and horizontal borehole layout (Garisto et al 2005a).

For the present study, it is convenient to build on the analyses undertaken for these studies. Therefore, the present case study considers a repository located at the Third Case Study site and an underground repository at approximately 670 m depth. The design of a repository is adjusted to suit the characteristics of the host rock, and several concepts are under consideration in the Canadian program. The repository design considered here is the horizontal borehole emplacement concept (HBC), as was used in the HBC safety assessment study (Garisto et al. 2005a).

In the HBC, similar to the KBS-3H design in Sweden and Finland (Smith et al. 2007, Seidler and Faucher 2004), used fuel containers are placed in long horizontal boreholes drilled into the host rock from access tunnels (see Figure 2.1). The containers are surrounded by a close-fitting dense bentonite layer, held in place during handling by a perforated steel jacket (Seidler and Faucher 2004). The emplacement gap between the steel jacket and host rock is filled with pellets of dense bentonite after each container package has been inserted.

Scoping calculations indicated that a borehole spacing of about 50 m would be acceptable based on thermal and mechanical considerations (Garisto et al. 2005a). For this spacing, the area of the repository is about 4.1 km^2. The (single-level) repository layout is illustrated in Figure 2.2 (Garisto et al. 2005a).

After a borehole is filled, the borehole is closed with a buffer/concrete plug (see Figure 2.1). On closure of the facility the tunnels and shafts would also be sealed with a clay based materials (see Figure 2.1). The shaft sealing methodology has not yet been defined. However, in this study, we assume that, throughout the time frame of interest, the shaft does not provide a preferential groundwater pathway to the surface.

After closure, the repository would slowly saturate with groundwater from the surrounding rock. The rock around the repository will also initially increase in temperature due to the decay heat from the used fuel.

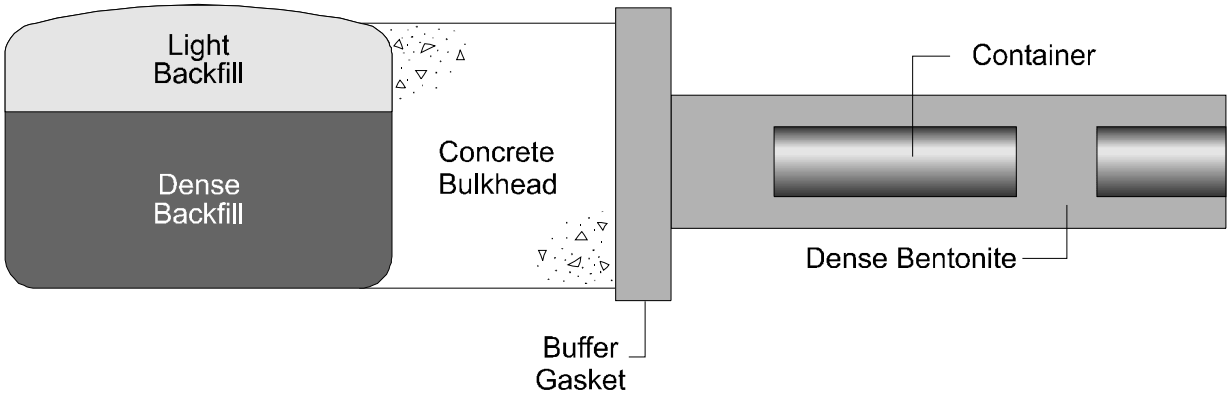

Figure 2.1: Schematic representation of the horizontal borehole emplacement concept.

2.3 ASSESSMENT CRITERIA

Previous studies have indicated that the most significant postclosure impacts from a repository for used fuel are those associated with radiological doses to potential human groups living or working near the repository site (Goodwin et al. 1994). Communities living further away are generally less impacted due to dilution. In keeping with the concept of a critical group, we conservatively assume that people live on or near the repository site in the future, and have

lifestyles that maximize their potential exposure doses while behaving in an otherwise reasonable manner.

The impact considered is the radiological dose rate to humans.

As in the previous TCS and HBC safety assessments, we compare calculated human dose rates to the dose constraint of 0.3 mSv/a recommended by the International Committee on Radiation Protection for scenarios involving natural processes (ICRP 2000). This is less than the Canadian regulatory limit of 1 mSv/a for members of the public. As well, dose rates are compared to the average Canadian natural background dose rate of about 1.8 mSv/a (Grasty and LaMarre 2004).

2.4 TIME SCALES AND SPATIAL SCALES

Guidance from the Canadian Nuclear Safety Commission (CNSC) given in P-290 (CNSC 2004) and in G-320 (CNSC 2006) indicates that the assessment time frame should include the period over which the maximum impacts are expected.

The deep geological repository is expected to be capable of isolating the used fuel such that the maximum impact would occur well beyond 10,000 years. Since 98% of the used fuel is natural uranium, as radionuclides decay, the radioactivity in the repository will eventually become similar to that of uranium ore bodies found in other locations on the Canadian Shield. This occurs on time scales of about five hundred thousand to one million years (Gierszewski et al. 2004a). Based on previous Canadian safety assessments, peak dose rates are also attained during this period. Therefore, in this study, the impacts of a deep geological repository are assessed over a time period of one million years.

Since a typical glacial cycle lasts about 120,000 years (see Section 3), over this time frame of one million years there could be several glacial cycles, each involving one or more periods of ice sheet coverage at the site.

The subsurface spatial domain needs to consider the effect of key topographic boundaries and major interconnected fractures that control the groundwater flows on long time scales. The surface spatial domain needs to consider the primary discharge areas for any radioactivity released from the repository, and the related surface watershed at which any released radioactivity would be collected. In this area, concentrations of nuclides released from the repository and, therefore, calculated dose rates, would be the highest. Further downstream from this location, radionuclide concentrations are expected to be significantly diluted, resulting in substantially lower dose rates to the people residing there.

The general area considered therefore is a subregional watershed area of approximately 100 km^2 around the repository site (see Figure 2.2). Previous studies have indicated that this is a suitable domain for modelling contaminant transport from a repository under current climate conditions (Garisto et al. 2004a, 2005a), in part because of the generally low topographic relief across the Canadian Shield. However, during the period of ice sheet advance and retreat, it is possible that there will be longer range influences from the ice sheet edge (or terminus). Therefore a somewhat larger area than considered in the HBC study has been used for detailed groundwater and transport modelling (see Section 6).

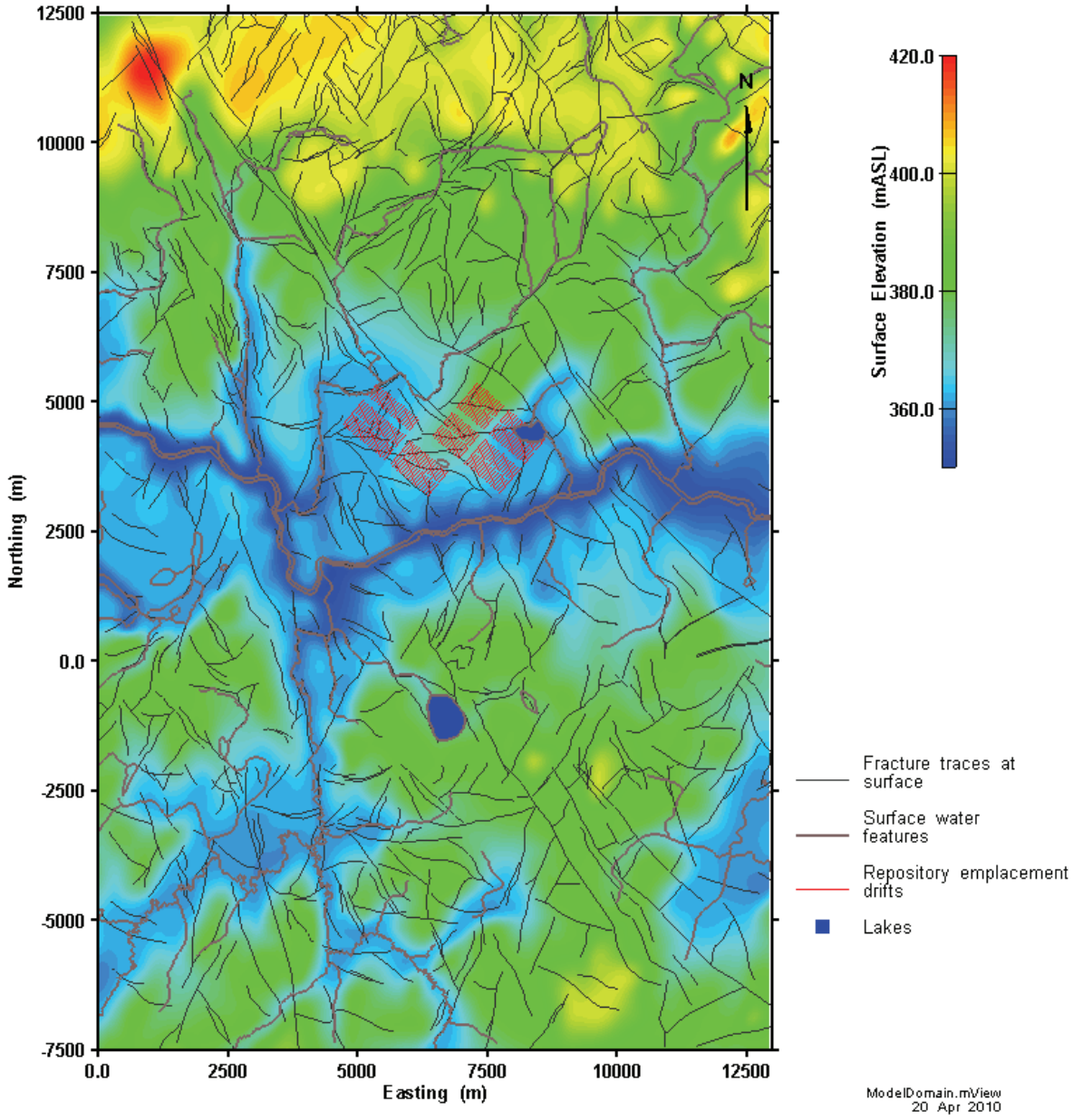

Figure 2.2: Surface features at the hypothetical site, including the surface fracture network. The location of the repository is also shown.

2.5 REPOSITORY ASSUMPTIONS

The repository, including the containers, is assumed to be built and sealed as designed. The repository uses the horizontal borehole emplacement method and is designed to hold 3.6 million fuel bundles (in about 11,000 fuel containers), as in the HBC study (Garisto et al. 2005a). In

comparison, the present projected lifetime output from existing Canadian CANDU reactors falls in the range 2.8 to 5.5 million fuel bundles (Garamszeghy 2008).

The repository is assumed to be constructed, operated and closed according to the following time lines:

- used fuel bundles are at least 30 years old at emplacement,
- repository operation (i.e., container emplacement) lasts 30 years,
- the post-operation monitoring period with open access tunnels lasts 70 years, and
- the repository is quickly closed and sealed.

The site is then monitored for some period afterwards, but it is assumed that after 300 years there are no controls remaining on the repository site.

2.6 FUTURE HUMAN BEHAVIOUR ASSUMPTIONS

We assume that future humans will, in general, largely resemble present day humans in terms of societal behaviour, capabilities and actions. Briefly, this means the following:

- There is no credit taken for advances in science and technology that might reduce the risk from the repository.
- There is no catastrophe that has significantly contaminated the biosphere around the repository site and made it unsuitable for human habitation.
- Human activities affect the local environment only in a minor way.
- People live in circumstances consistent with North American practice. Their lifestyles are plausible, but selected so as to increase their potential exposure to any contaminants from the repository (e.g., they live on or near the repository site, and grow or hunt food near the repository site).

The people living near the repository are assumed to adapt their lifestyle, as needed, to the changing climate. Consequently, the characteristics of the critical group living near the repository site change. Three critical groups with different lifestyles have been selected to represent the people living near the repository: a self-sufficient farmer critical group, present during periods of temperate climate; a self-sufficient hunter critical group, present during periods of permafrost; and a self-sufficient hunter-fisher critical group, present during periods when a large proglacial lake[1] is present at the site. Finally, it is assumed that no people live near the repository when the site is ice covered.

2.7 MODELLING AND DATA APPROACH

The intent is to use best-estimate (realistic) values in general for the safety assessment calculations. The uncertainty in the value of a parameter can be expressed via a probability density or parameter distribution function, and included in probabilistic analyses or in specific sensitivity studies. For this study, the probabilistic analyses will be mainly limited to assessing

[1] A proglacial lake is a lake formed during the retreat of a melting glacier. These lakes are known as proglacial lakes because ice forms a part of their shoreline.

the effects of changes to (1) the glacial cycle itself and (2) the number, location and time of container failures, and not to changes in other system parameters. The probabilistic analyses carried out in the previous Third Case Study assessments (Garisto et al. 2004a, 2005a) have already explored the impact of the uncertainties in the other system parameters.

The models used are intended to be either realistic or conservatively simple for the processes they represent.

One important conceptual model uncertainty is related to the geosphere model. Since the site is hypothetical there are no data available. For the Third Case Study, a geostatistically-generated fracture network model was constructed (Gierszewski et al. 2004a,b). This network was extended to cover the larger model domain used in the Glaciation Scenario study (see Figure 6.1). Sensitivity analyses are used to assess the effects of the hydrogeological boundary conditions and the rock storage coefficient on the groundwater flow and radionuclide transport results.

Another important uncertainty is the glaciation model. The selected model is plausible and consistent with current understanding and is based on the continental model developed by Peltier (2006). However several aspects of the model such as the ice sheet profile, the effect of surface topography, and internal hydraulic head were assumed and are uncertain. Uncertainties arising from future climate evolution (and therefore the details of glacial cycles) have been addressed, in part, by carrying out a probabilistic simulation in which the glacial cycle is allowed to vary.

The Glaciation Scenario is different from all other scenarios considered in previous Canadian safety assessment studies because the climate varies with time. This has important consequences. For example, in the HBC study, the groundwater flow system was time invariant, i.e., the groundwater flow system attained steady state. This is not the case for the Glaciation Scenario because of the changes to the groundwater flow system caused by, e.g., the formation of permafrost and the advance or retreat of ice sheets. For this reason, a transient groundwater flow model is needed here. This was addressed through use of the FRAC3DVS-OPG groundwater flow modelling code (Therrien et al. 2007), with a combination of transient boundary conditions and stepwise-changes in properties to represent the presence and depth of permafrost boundary conditions (see Section 6); and through the use of a state-based SYVAC3-CC4 system model for the safety assessment calculations, with a different fixed groundwater flow field for each of the main climate states within a glacial cycle (see Section 8).

3. THE GLACIAL CYCLE

In order to explore the possible impacts of glaciation events, a representative glacial cycle for the future needs to be defined in terms of the climate and surface boundary conditions. In this section, an illustrative glacial cycle is described. The implications of this glacial cycle on the repository, geosphere and biosphere are discussed in the next chapter.

3.1 GLACIATION MODEL

In order to develop a representative glacial cycle for the future, we use information obtained from past glacial cycles. In particular, we focus on the last glacial cycle which started about 120,000 years ago.

The development of models of continental scale glaciation and deglaciation has been a focal point of modern geophysical research for at least the past decade. Aside from the Glacial Systems Model (GSM) developed at the University of Toronto (Peltier 2003) that is employed for this study, other models currently exist at a number of other laboratories. These include the model of Huybrechts (1986; Belgium/Germany), the model of Payne and Dongelmans (1997; the United Kingdom), the model of Ritz et al. (1996; France) and the model of Marshall and Clarke (1997a,b; Canada). These models, together with the GSM, have been compared in the context of the European Ice Sheet Modelling Initiative (EISMINT; Payne et al. 2000). The majority of models agreed closely with one another.

The uniqueness of the GSM derives from three of its design characteristics. Firstly, it is fully coupled to the global theory of the glacial isostatic adjustment process. This process significantly contributes to the magnitude of the climate forcing as a continental scale ice sheet evolves, and is required to accurately predict relative sea levels and modern geodetic data. The second key characteristic of the GSM concerns the level of detail with which basal processes are described. Of these, the incorporation of a space dependent sediment thickness together with a space dependent variation of heat flow from the Earth's interior into the base of the ice sheet is especially important. The third attribute of the GSM is that it has been successfully linked to a detailed model of meltwater runoff into the oceans.

The key input to the GSM is climate data, such as from Greenland ice core logs for the last glaciation. The model is then calibrated by performing a Monte Carlo scan of solutions by randomly sampling the parameters of the model within a-priori specified ranges of plausibility (Peltier 2003). The output of this ensemble of runs is analysed to find the set of model parameters that enable the model to best fit the constraint data. This methodology essentially constitutes a means whereby the inverse problem is solved – "given the available observations, what must have been the evolutionary history of the Laurentide Ice Sheet?". The data that are employed to constrain the model consist of the following (Peltier 2003):

1. Radiocarbon dated relative sea level records from sites on the Canadian coastline,
2. Radiocarbon dated locations of the position of the margins of the Laurentide Ice Sheet,
3. Measurements of the present day time rate of change of the surface gravitational acceleration at sites that were once ice covered, and
4. Measurements of the present day rate of vertical motion of the Earth's crust.

Based on this calibrated continental-scale model, a series of possible scenarios were produced for the history of the Laurentide Ice Sheet (see Figure 3.1) over the northern part of the North American continent over the past 120,000 years (Peltier 2006). The results of the model include surface boundary conditions (normal stress, surface temperature, permafrost depth and meltwater production) across North America on a grid scale of 50-km on a side.

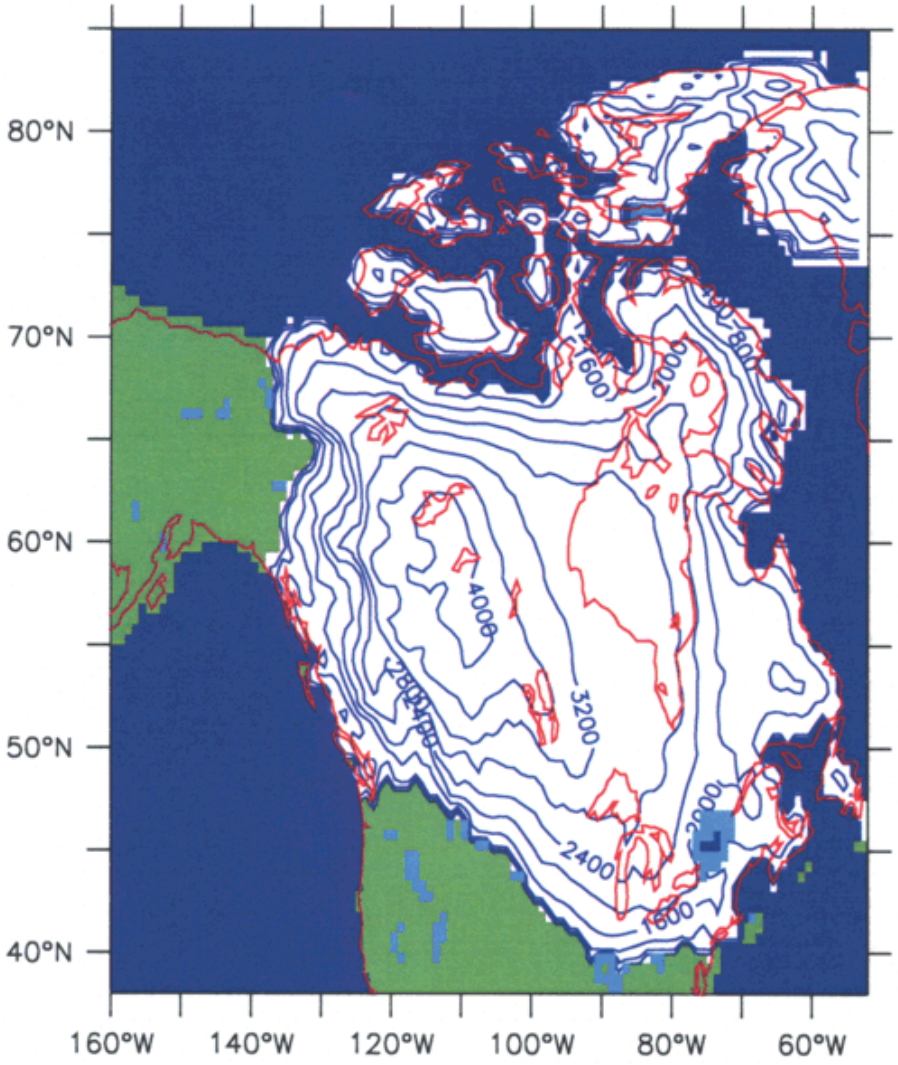

Figure 3.1: Illustration of Laurentide Ice Sheet coverage over North America during the last glaciation maximum at 24000 years before the present (Peltier 2006, Simulation nn2778). The ice covered region is shown in white and proglacial lakes are shown in light blue. Contours of ice sheet height relative to sea level (in m) are also shown.

3.2 A WARM-BASED GLACIAL CYCLE

As noted above, Peltier (2006) derived several plausible histories of the past Laurentide Ice Sheet. However, one particular history, Simulation nn2778, was selected for further consideration in the current study. For this particular simulation, the ice sheet at the repository site includes both “warm-based” and “cold-based” periods, but is generally “warm-based”. That is, at the repository site, the temperature at the bottom of the ice sheet site is equal to the ice’s pressure melting point for a large fraction of the time during which the site is covered by ice. In contrast, the temperature at the bottom of a "cold-based" ice sheet is below the pressure melting point for ice. The difference clearly affects the extent and duration of permafrost under the ice sheet. A warm-based glacier is of interest because it is anticipated that without the isolating permafrost layer there is greater opportunity for the deep groundwater flow to be affected by passage of the ice sheet.

In this section we describe the data extracted from Simulation nn2778 for a location representative of the Third Case Study site. Figures 3.2 and 3.3 present some of the results for Simulation nn2778. The glacial cycle for Simulation nn2778 lasts about 121,000 years. Note the multiple advances and retreats of the ice sheet across the site over this period. The last 12,000 years represent current temperate conditions.

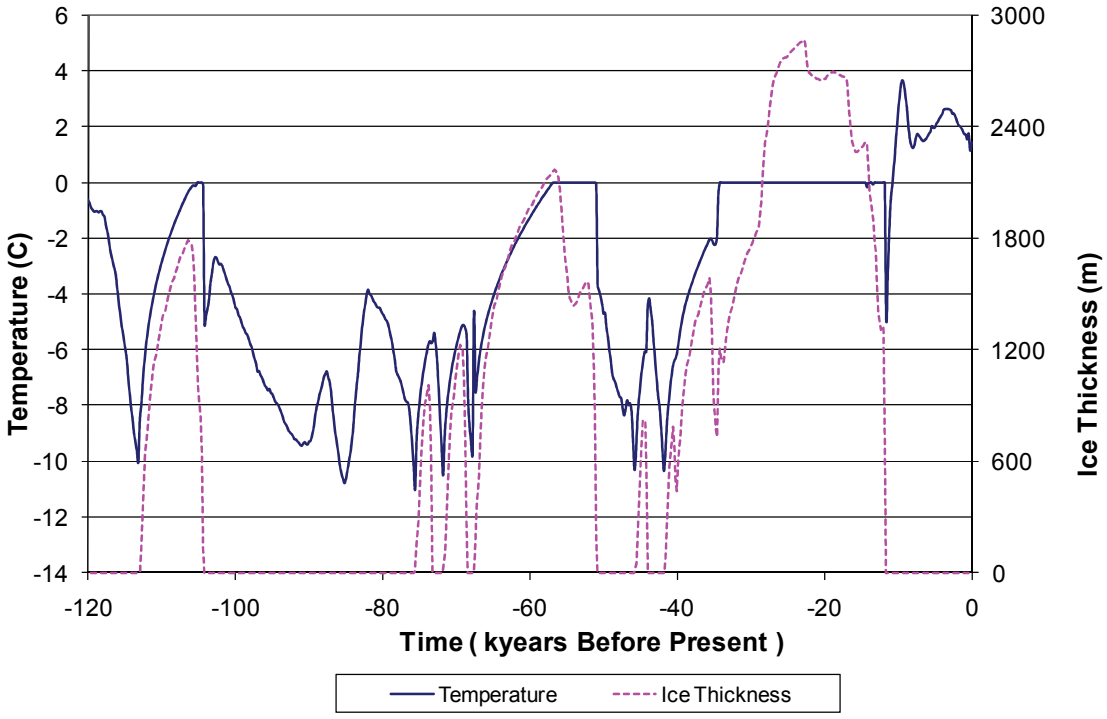

Figure 3.2: Calculated land (surface) temperature (relative to pressure melting point) and ice thickness at site (Simulation nn2778). The pressure melting point is defined as the temperature at which ice under a given pressure begins to melt.

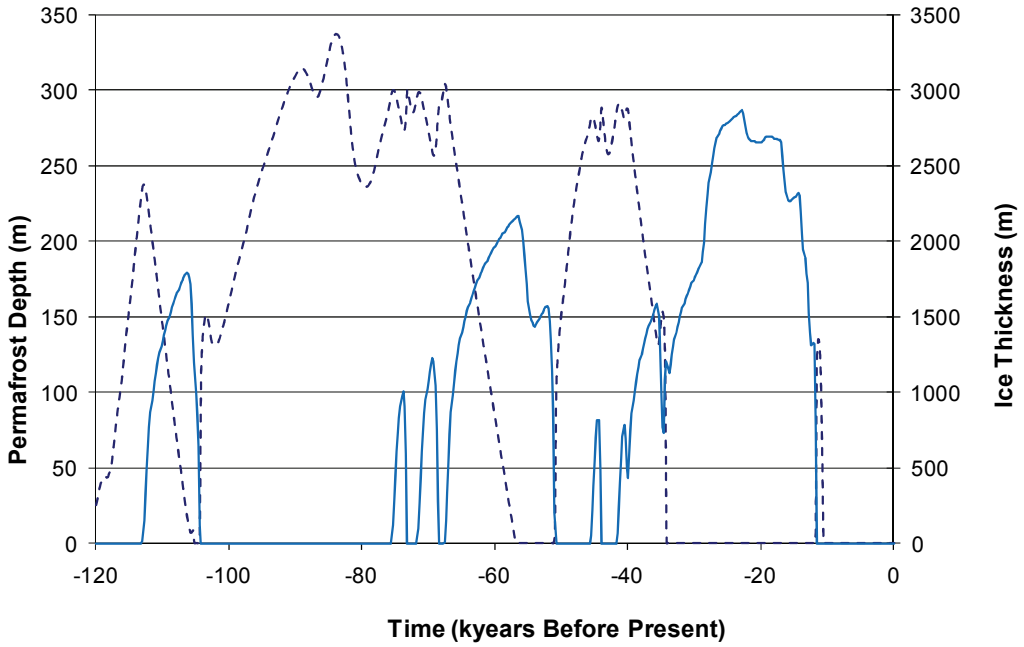

Figure 3.3: Calculated permafrost depth at the repository site for Simulation nn2778 (dashed line). The ice thickness is also shown (sold line). Note that the permafrost gradually thaws under the ice-sheets.

For the purposes of developing a safety assessment model, this glacial cycle was divided into four states or periods: Temperate State, Permafrost State, Ice Sheet State and the Proglacial Lake State (see Section 4). The durations of the various states of the glacial cycle were calculated based on the data in Figures 3.2 and 3.3, and are shown in Table 3.1.

The Permafrost State, which represents periods during the glacial cycle when there is permafrost but no ice sheet (and no proglacial lake), existed for about 46,500 years during the last glacial cycle. The Ice Sheet State existed for 62,800 years. However, the Permafrost and Ice Sheet States are discontinuous, with periods of the Permafrost State interspersed with periods of the Ice Sheet State (see Figure 3.3). Finally, the Temperate and Proglacial Lake States existed for only 10,500 and 1200 years, respectively, during the last glacial cycle.

3.3 FUTURE CLIMATE EVOLUTION

The glacial cycle described in the previous sections provide a plausible description of the conditions over the past 120,000 years. However, for evaluating the potential impacts of glaciation on a repository, we need a reference future glaciation scenario.

The first question is whether there will be a future glacial cycle. The second is whether and how we could usefully estimate what such a future glaciation would look like.

Table 3.1: Duration of Glaciation States (Simulation nn2778)

Glaciation Period or State	Overall Duration during a Single Glacial Cycle (years)
Temperate or Interglacial Period (Land temperatures > 0°C, no proglacial lake)	10,700
Permafrost Period (Land temperatures < 0°C, no ice sheet and no proglacial lake)	46,300
Ice Sheet Period	62,800
Ice sheet with permafrost beneath ice	34,400
Ice sheet with no permafrost beneath ice	28,400
Proglacial Lake	1,200
Total duration of glacial cycle	121,000

With respect to the first question, glacial cycles are believed to be driven by the variation in the solar insolation (particularly at high latitudes) and the location and size of the continents. Over the next one million years, the continents will not change and the variation in solar insolation is predictable based on known earth orbital dynamics. Specifically, over the next 100,000 years or so, the amplitude of insolation variations will be smaller than during the last glacial cycle (Berger and Loutre 2002, Loutre and Berger 2000). Thus, the current interglacial period (which has already lasted more than 10,000 years) may last much longer than previous interglacial periods, which lasted about 10,000 years (Marsh 2008, Berger and Loutre 2002).

Furthermore, it is also clear that the composition of greenhouse gases is presently significantly larger than usual. As the Intergovernmental Panel on Climate Change reports (IPCC 2007), these concentrations are likely to lead to climate changes, with a general trend towards increased global temperatures, especially at higher latitudes. Such conditions could suppress the initiation of a glacial cycle for at least 50,000 years, especially given the comparatively small reduction in solar insolation over this period (Berger and Loutre 2002).

Nevertheless, looking ahead over a one million year period, it is likely that glacial cycles will reassert themselves (Archer and Ganopolski 2005, Berger and Loutre 2002). For example, there is a finite amount of fossil fuels, and after they have been burned, various natural processes could gradually reduce the high levels of greenhouse gases and therefore their ability to suppress glaciation in the long-term. Moreover, the variation in solar insolation will continue over this period, with a comparatively larger reduction in solar insolation anticipated in future periods relative to the next 50,000 years, and thus a stronger trigger to initiate a new glacial cycle.

It is therefore prudent for repository assessments over a one million year period to consider the possibility of future glaciations. In this context, we specifically assume that the current interglacial period lasts a further 50,000 years, due in large part to the impact of current global warming (SKB 2006b; Cedercreutz 2004; Berger and Loutre 2002; Loutre and Berger 2000). During this period, we assume that climate conditions on the Canadian Shield remain similar to current conditions. We recognize that a small amount of climate change could significantly

affect specific ecosystems, but current projections of likely climate changes in this area suggest that the area will remain temperate.

Earlier initiation of a glacial cycle appears to be unlikely, and while longer delays (up to 500,000 years) have been proposed (Archer and Ganopolski 2005), it is expected that early resumption of glaciation would potentially have a larger impact on repository performance and therefore is appropriate to consider within this case study.

We therefore assume that the future climate will evolve to initiate and support glacial cycles. The past glacial cycle as described in the Section 3.2 is taken to be representative or illustrative of the conditions expected at the repository site under glaciation in future years. Since we are interested in a one-million year period, we will represent the future climate as a repeating set of this 121,000-year glaciation sequence. Although the assumed period of the glacial cycles is in accord with Earth's temperature history over the last million years (Raymo and Nisancioglu 2003), it is acknowledged that the climate during future glaciations could be different than during the past glacial cycle due to differences in, for example, solar insolation. Nevertheless, for illustrating the potential effects of glaciation on the safety of a used fuel repository, use of the past glacial cycle is considered appropriate.

3.4 REFERENCE GLACIAL CYCLE

The future climate at the repository site must be known to carry out the safety assessment calculations for the Glaciation Scenario. The assumed future climate at the site is described in this section.

First, based on the discussion in the previous section, it is assumed that the current interglacial or temperate period lasts another 50,000 years. Second, following this long temperate period, the climate at the repository site is assumed to be described by repeating cycles of a simplified version of Simulation nn2778 (Peltier 2006), which was described in Section 3.2. A total of 8 glacial cycles occur over the time frame of interest, i.e., the next one million years.

With these climate assumptions, the ice thickness at the repository site is shown in Figure 3.4 for the first 180,000 years of the Glaciation Scenario. Ice first covers the site at about 60,000 years in the future and the ice thickness at the site reaches a maximum of about 2800 metres at about 150,000 years into the future.

As illustrated in Figure 3.4, the history of a glacial cycle can be fairly complicated, with several advances and retreats of the ice sheet over the repository site. For the purposes of the current safety assessment, particularly the hydrogeological modelling, this glacial cycle was simplified. Specifically, the two short periods of ice cover at the site that occur between 95,000 and 101,000 years, just before the longer period of ice cover, were neglected as was the short period of ice cover at about 126,000 years.

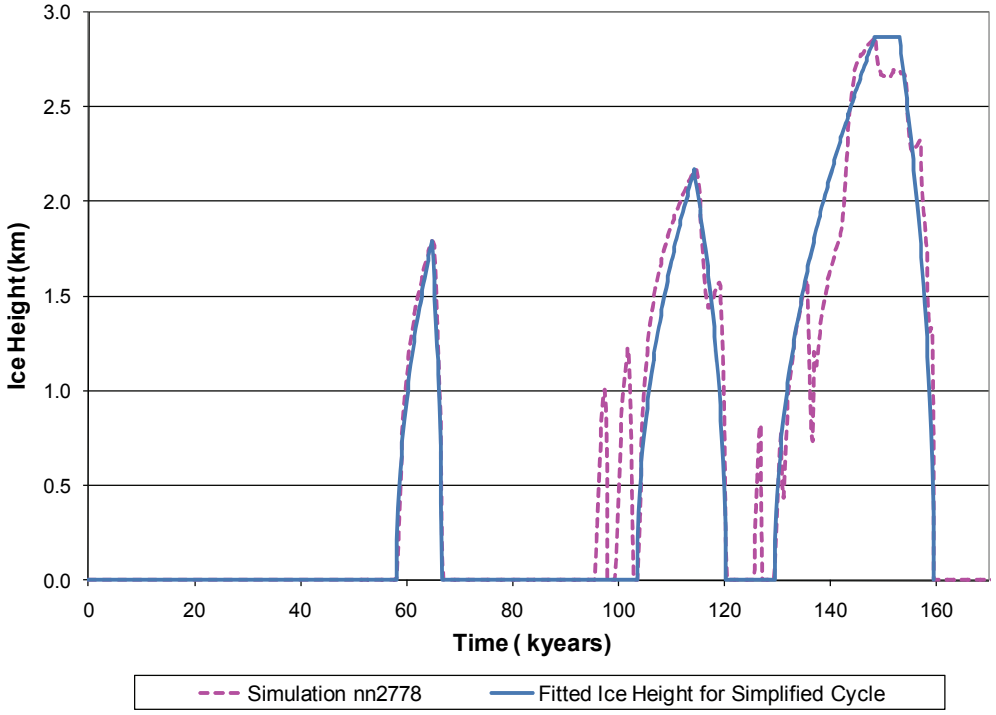

Figure 3.4: Comparison of ice sheet height at the site for the reference glacial cycle with the full history from Simulation nn2778. The short periods of ice sheet cover at the site just before the 2nd and 3rd major ice sheet advances are neglected in the simplified glacial cycle.

The transient behaviour of the groundwater flow in the geosphere that occurs as a result of ice-sheet movement across the site is of key interest. However, the time needed for ice sheets to advance or retreat through the model domain could not be directly calculated from the data extracted from Simulation nn2778. Hence, a simple approach was used to estimate the time needed for the ice sheet to cross the model domain and for the ice sheet to reach its maximum thickness over the repository site. First, the ice-sheet profile, h(x), during early advance and late retreat was specified by an analytic equation given by Oerlemans (2005):

$$h(x) = \sqrt{\frac{2\tau_0}{\rho g(1+\delta)}\,x} \qquad (3.1)$$

where h(x) is the height of the ice sheet at the distance x from the ice edge or terminus, τ_0 is the yield stress (Pa), ρ is the ice density (900 kg m^{-3}) and δ is the isostatic depression parameter. Oerlemans (2005) suggests values of 50 kPa to 300 kPa for yield stress and 0.33 for δ. We have assumed that τ_0 = 50 kPa. Application of these values to Equation 3.1 results in the profile shown in Figure 3.5. The ice sheet thickness is converted to an equivalent freshwater hydraulic head by multiplying ice-sheet thickness by ice-sheet density. The fraction of the ice load carried by the pore water, i.e., the loading efficiency, depends on the properties of the rock mass (Walsh and Avis 2010).

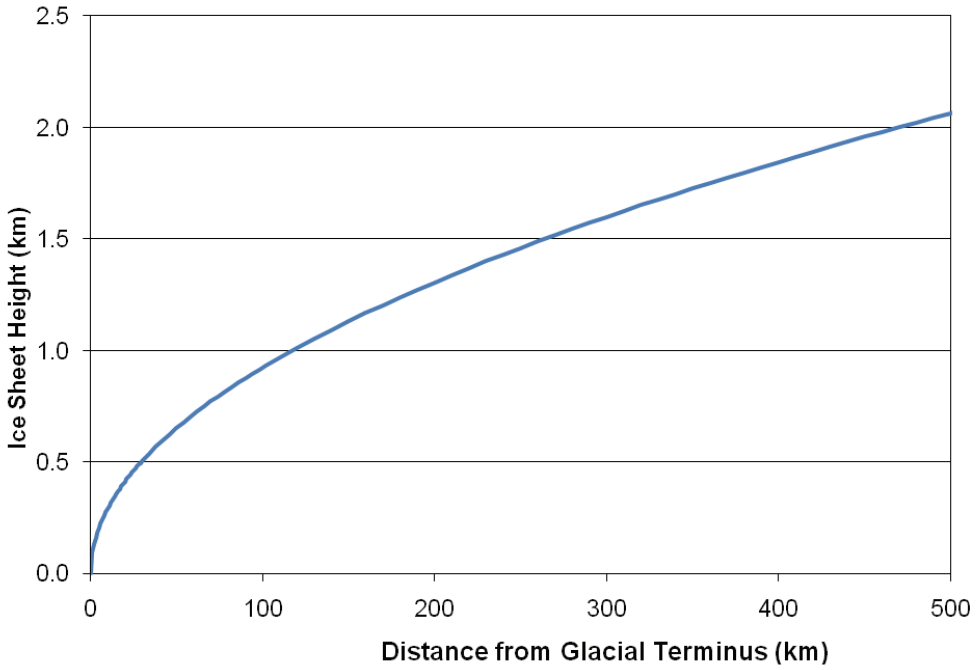

Figure 3.5: Ice sheet edge profile.

Second, the ice height curves from Simulation nn2778 were fitted using the ice profile curve, assuming that the ice sheet travels at a constant velocity over the site in a north-south direction during advance and a south-north direction during retreat. The fitting of the ice height curves was achieved by varying the ice velocity until a good match was obtained. The fitted ice height over the site is compared to Simulation nn2778 in Figure 3.4.

The ice velocities needed to fit the ice height curves depend on the ice profile curve (Figure 3.5), which in turn depends on the selected value of τ_0. The value of τ_0 was selected so that the velocities needed to fit the ice height curves match the ice sheet velocities inferred from field data. Literature data generally indicate that ice advance rates are in the range 25 to 120 m/a and ice retreat rates are in the range 50 to 230 m/a, with ice retreat rates generally more than twice as fast as ice advance rates (see Appendix A).

The velocity of the ice sheet needed to fit the ice height curves are as follows:

1. Advance starting at 58,200 years: 56 m/a
2. Retreat starting at 65,000 years: 198 m/a
3. Advance starting at 103,600 years: 51 m/a
4. Retreat starting at 114,400 years: 92 m/a
5. Advance starting at 129,400 years: 51 m/a
6. Retreat starting at 153,200 years: 150 m/a

Note that these velocities describe the rate at which the ice sheet terminus (or edge) advances or retreats and does not necessarily represent the rate of movement of the ice sheet itself. Retreat of the ice sheet is, for example, mainly due to melting of the ice sheet.

In addition to the simplifications made to the ice sheet height shown in Figure 3.4, the curve describing the thickness of the permafrost layer was simplified, making it feasible to implement the hydrogeological simulations for the Glaciation Scenario. The permafrost depth curves for Simulation nn2778 and the (simplified) reference glacial cycle are compared in Figure 3.6.

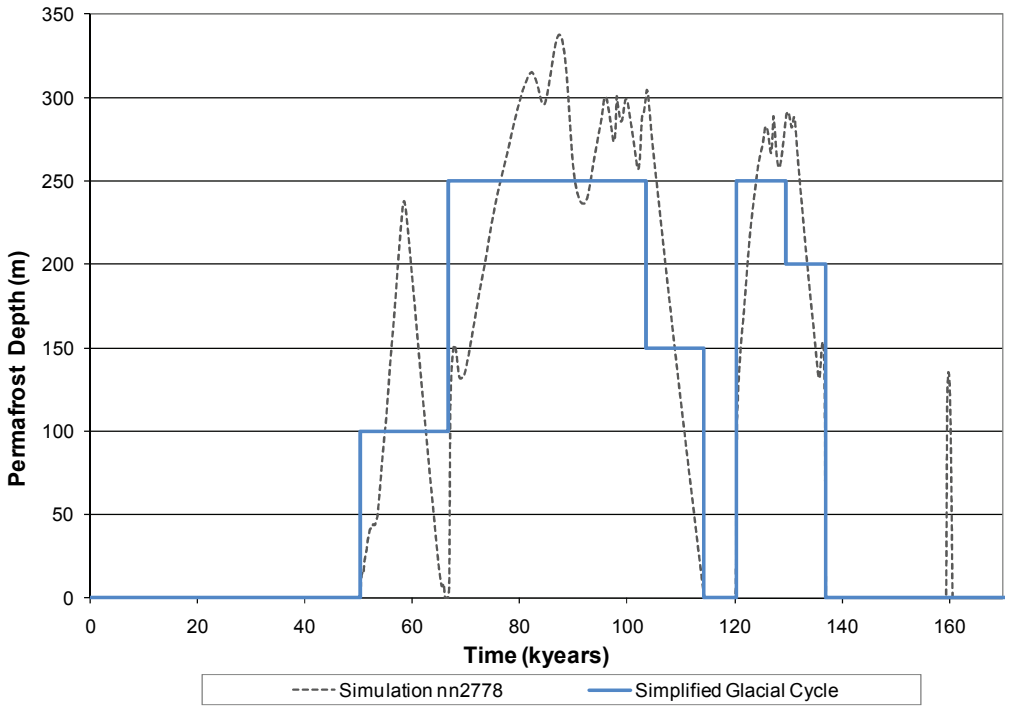

Figure 3.6: Comparison of permafrost depths for reference glacial cycle at the site with the permafrost depths from Simulation nn2778.

In summary, after the long current temperate period, which is assumed to last another 50,000 years, the climate at the repository site is defined in terms of repeated cycles of the reference glacial cycle. The reference glacial cycle is defined by the sequence of glaciation states shown in Table 3.2. It begins at the start of the first Permafrost State (stage 2 in Table 3.2) and ends at the close of the Temperate State (stage 13 in Table 3.2). The total durations of the different glaciation states in the reference glacial cycle are given in Table 3.3. The ice height and permafrost depth during the reference glacial cycle are illustrated in Figures 3.4 and 3.6 respectively.

The reference climate at the repository site during the Glaciation Scenario is shown up to 300,000 years in the future in Figures 3.7 and 3.8.

Table 3.2: Time History for Reference Glacial Cycle

Stage[#]	Relative Time Period (years)[1]	Actual Times During First Cycle (years)	Duration of State (years)	Description of Glaciation State
1	----------	0 – 50,300		Temperate (current Interglacial)
2	0 – 7,800	50,300 – 58,100	7,800	Permafrost
3	7,800 – 14,500	58,100 – 64,800	6,700	Ice Sheet Advance, permafrost underneath
4	14,500 – 16,400	64,800 – 66,700	1,900	Ice Sheet Retreat, permafrost underneath
5	16,400 – 53,200	66,700 – 103,500	36,800	Permafrost
6	53,200 – 64,000	103,500 – 114,300	10,800	Ice Sheet Advance, permafrost underneath
7	64,000 – 70,000	114,300 – 120,300	6000	Ice Sheet Retreat, no permafrost underneath
8	70,000 – 79,200	120,300 – 129,500	9,200	Permafrost
9	79,200 – 86,600	129,500 – 136,900	7,400	Ice Sheet Advance, permafrost underneath
10	86,600 – 102,700	136,900 – 153,000	16,100	Ice Sheet Advance, no permafrost underneath
11	102,700 – 109,200	153,000 - 159,500	6,500	Ice Sheet Retreat, no permafrost underneath
12	109,200 – 110,400	159,500 – 160,700	1,200	Proglacial Lake
13	110,400 – 121,200	160,700 – 171,500	10,800	Temperate

[1]In the Glaciation Scenario the current interglacial period is assumed to extend 50,000 years into the future and immediately precedes the start of the first glacial cycle at 50,300 years. The glacial cycle repeats itself starting at: 171,500; 292,700; 413,900; etc. years.
[#]Stage number used to identify particular state in following sections.

Table 3.3: Duration of Glaciation States for Reference Glacial Cycle

Glaciation Period or State	Overall Duration during a Glacial Cycle (years)
Temperate or Interglacial Period	10,800
Permafrost Period	53,800
Ice Sheet Period	55,400
Proglacial Lake Period	1,200
Total duration of glacial cycle	121,200

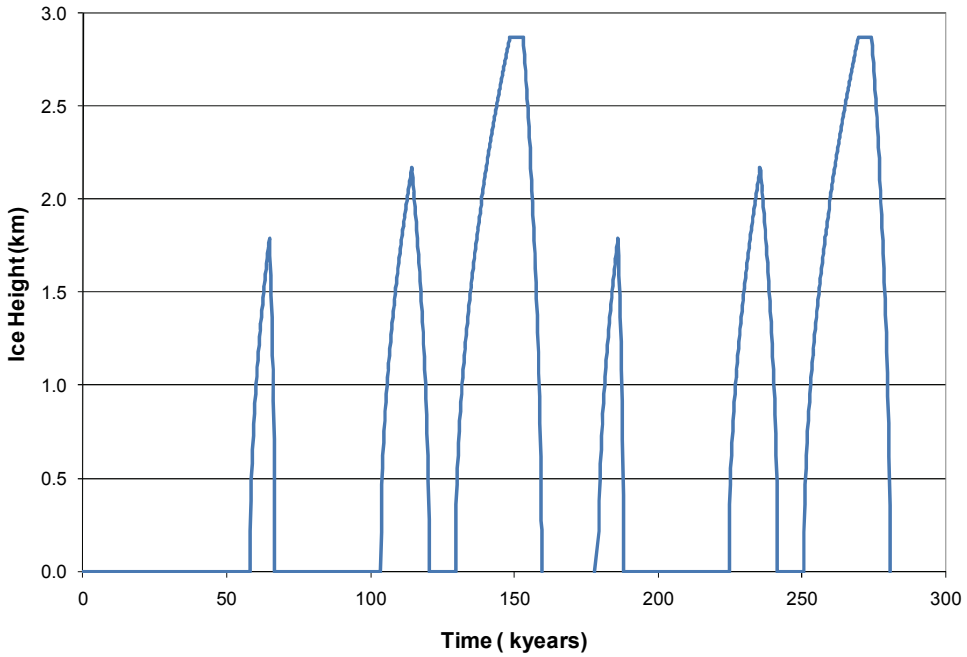

Figure 3.7: Ice thickness at site for the Glaciation Scenario up to 300,000 years into the future. The reference glacial cycle repeats after 292,700 years.

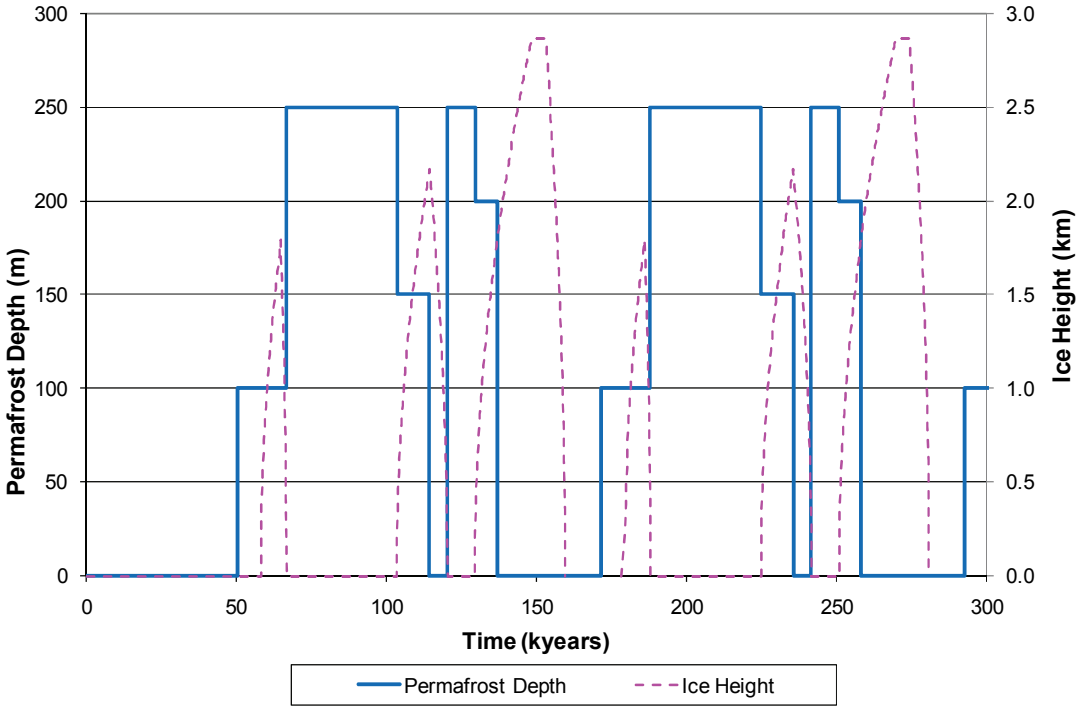

Figure 3.8: Permafrost depth and ice height at the site for the Glaciation Scenario up to 300,000 years in the future. The reference glacial cycle repeats after 292,700 years.

4. REPOSITORY SYSTEM EVOLUTION

4.1 INTRODUCTION

The repository is assumed to be located on the Canadian Shield interior. Consequently, the repository will be affected by glaciation, as described in the previous section. However, sea level changes will not directly affect the repository site.

During the course of the next one million years, there will be variation in time of the repository or near-field environment, the geosphere, and the biosphere. Consistent with the emphasis in the current study on the implications of glaciation, we discuss the system evolution in this chapter with emphasis on the glacial cycle stages or states.

In particular, we can consider the glacial cycle as involving 4 main states: the Temperate State, the Permafrost state, the Ice Sheet State and the Proglacial Lake State. A glacial cycle involves a progression between these states, with each occurring at least once during a glacial cycle. At the end, the climate returns to the Temperate State.

In this section we describe

1. the properties and characteristics of these 4 states, and

2. the important processes occurring during these 4 states.

The descriptions include the effect, if any, of the four different glaciation states on the features and processes of the near-field, geosphere and biosphere. The main emphasis will be on the features and processes of importance for the Defective Container Glaciation Scenario, which is described below.

In the Defective Container Glaciation Scenario it is assumed that the repository is built to design specifications, except that some containers are emplaced with small undetected defects that penetrate the copper shell of the containers (McMurry et al. 2004). Such defects could lead to early development of a pathway for radionuclide releases from the defective containers into the groundwater around the repository and, thereafter, to the surface environment. Thus, the focus of the analyses for this scenario is on radionuclide releases from used fuel, transport of radionuclides through the container, vault and geosphere to the surface, and on radionuclide movement within the local biosphere, leading to radiological doses to humans living in the vicinity of the repository.

Except for the climate, the Defective Container Glaciation Scenario is similar to the Defective Container Scenario of the HBC study. In the HBC study, the climate was constant throughout the 1 million year simulation time and was representative of the current day climate on the Canadian Shield. In the following, this latter case is referred to as the Defective Container Constant Climate Scenario.

In this safety assessment we only investigate the impacts of emplacing undetected defective containers in the repository. Therefore, the Defective Container Glaciation Scenario and Defective Container Constant Climate Scenario are simply referred to as the Glaciation Scenario and Constant Climate Scenario, respectively.

4.2 TEMPERATE STATE

4.2.1 Description

During the Temperate State, climate conditions are assumed to be approximately represented by current climate conditions, as they have been for the past 10,000 years or so, since the end of the last glaciation.

In the reference Glaciation Scenario, the next ice age does not initiate until approximately 50,000 years from today (see Section 3.4). Furthermore, the climate becomes temperate at the end of each glacial cycle. The Temperate State is sufficiently long that steady state conditions are attained in the biosphere and geosphere during this time.

4.2.2 Biosphere

The biosphere during the Temperate State is assumed to resemble closely the biosphere used in the TCS and HBC studies (Garisto et al. 2004b). This biosphere is based on central Canadian Shield conditions, and the surface ecosystem is temperate boreal. A general description of the Canadian Shield biosphere is provided in Davis et al. (1993). Farming is, for example, practiced in some favourable parts of the Canadian Shield.

The surface topography on the Canadian Shield is generally relatively flat with many lakes and rivers. The granitic rock of the Canadian Shield extends close to the surface throughout most of the site. The water table is fairly close to the surface and there are no aquifers.

Global warming (or natural variations) could certainly lead to changes in the climate over this period that would be important to humans and to specific ecosystems. However, at the level of model detail within this safety assessment, the specific changes are not likely to be important. For example, the site is assumed to be far from the sea, and remains so during this period (i.e., the site does not become inundated by rising sea levels). Current estimates for Canada suggest that in many areas there may be an increase or decrease in rainfall, which will affect the flow rates of water through watersheds and the water table elevation, but it is not expected to turn current Canadian Shield boreal areas into desert (Government of Canada 2004). The climate changes will undoubtedly affect specific ecosystems (e.g., boreal forest may change to deciduous and/or vice versa over such a period), but the basic conditions are likely to remain suitable for agriculture.

4.2.3 Geosphere

The physical and chemical characteristics of the geosphere for the Temperate State are generally the same as those of the hypothetical Canadian Shield site used in the Third Case Study and are described in Gierszewski et al. (2004b) and Garisto et al. (2004b) (see also Section 6).

The site is assumed to be composed of granitic rock, intersected by a complex set of interconnecting major fractures and discontinuities (see Section 6). The derivation of the fracture network is based on Canadian Shield fracture statistics, and was generated as described in Srivastava (2002a,b). Only one conceptual fracture model for the site is used.

The local groundwater flow in the geosphere (i.e., within the boundaries of the watershed area in which the repository is located) is expected to be driven by surface topography because the water table is close to the surface (Sykes et al. 2003a, 2003b, 2004).

A characteristic feature of the geosphere within Canadian Shield settings is the increase in the salinity of the groundwater with depth, with concentrations ranging between approximately 10 and 100 g/L dependent on site-specific conditions. From a hydrogeochemical perspective, such saline waters may be indicative of stagnant or sluggish groundwater flow domains associated with extremely long residence times (Gascoyne 2004, McMurry 2004). These variable salinity distributions may also introduce density gradients that could render the flow domain insensitive to external perturbations (e.g., long-term climate change) and contribute another line-of-reasoning for flow system stability in the repository safety case.

The composition of the water in the geosphere is site specific, but would likely be consistent with the groundwater composition at depth in other locations on the Canadian Shield. For the hypothetical TCS site, the groundwater composition from the Whiteshell Research Area has been adopted because it is well characterized (McMurry 2004).

The heat generated by the radioactive decay of the used fuel would result in the slow heating of the rock around the repository, followed by a gradual return to ambient conditions over a period of about 100,000 years (McMurry et al. 2003). Details of the evolution of the temperature would depend on the specific characteristics of the site and the repository, but the general effects can be summarized as follows (McMurry et al. 2003):

1. After 1000 years, the geosphere within a few hundred metres of the repository would be warmed (to about 60°C);
2. After about 10,000 years, the thermal plume in the geosphere would reach its broadest extent, and the geosphere around the repository begins to cool ; and
3. After about 100,000 years the repository-induced heat effects are insignificant compared to ambient temperatures.

4.2.4 Near Field

The repository design consists of a series of long horizontal boreholes drilled into the rock at the vault level from the access tunnels, as described in Section 2.5. Containers are emplaced within these boreholes, surrounded by a layer of buffer (dense bentonite).

The near field also includes the excavation damaged zone (EDZ) in the rock wall adjacent to the horizontal borehole and access tunnel. Within this zone, cracks or fractures are created during excavation which provide locally increased porosity and flow permeability.

The containers are based on a corrosion-resistant copper shell, surrounding a structural steel vessel. As the containers are robustly designed and carefully inspected before emplacement, no container failures are expected for hundreds of thousands of years. During this period, the radioactivity in the used fuel continues to decay (McMurry et al. 2003). The gamma radiation field outside the copper containers is low (Hanna and Arguner 2001), and is unlikely to cause

any physical changes in the surrounding materials. Consequently, the impact of the containers is primarily through the heat source from radioactive decay.

Each reference container holds 324 used fuel bundles. Based on an average burnup of 220 MWh/kgU and a conservative average age at emplacement of 30 years, each container generates about 1140 W at emplacement and the heat generated by the containers in the repository at emplacement is about 3.11 W/m^2, where the footprint of the repository is assumed to be 4.1 km^2 (see Table 4.1).

The heat generated by the fuel in the repository is expected to increase the temperature of the surrounding materials and rock. Thermal analyses indicate that the temperature in the near-field would rise rapidly, reaching a maximum of about 90°C within about 100 years. The temperature would remain high for up to 10,000 years and then slowly decrease, reaching ambient conditions after about 100,000 years (McMurry et al. 2003).

Table 4.1: Thermal Power from Fuel, Container and Repository

Age of Used Fuel (years)	Thermal Power from Fuel (W/kgU)	Thermal Power per Container (W)	Thermal Power from Repository (W/m^2)
3.00E+01	1.83E-01	1.14E+03	3.11E+00
5.00E+01	1.32E-01	8.19E+02	2.24E+00
7.50E+01	9.30E-02	5.79E+02	1.58E+00
1.00E+02	7.07E-02	4.40E+02	1.20E+00
1.50E+02	4.98E-02	3.10E+02	8.49E-01
2.00E+02	4.18E-02	2.60E+02	7.13E-01
3.00E+02	3.55E-02	2.21E+02	6.04E-01
5.00E+02	2.90E-02	1.81E+02	4.95E-01
1.00E+03	2.01E-02	1.25E+02	3.42E-01
1.00E+04	7.13E-03	4.44E+01	1.22E-01
1.00E+05	4.10E-04	2.55E+00	6.98E-03
1.00E+06	1.48E-04	9.22E-01	2.53E-03

The near field is assumed to re-saturate about 100 years after repository closure. The evolution of the near field properties (e.g., transition from oxidizing to reducing conditions due to consumption of the oxygen remaining in the repository at closure) during this short period are neglected in the safety assessment since radionuclides are assumed to be released from the defective containers only after saturation of the repository.

Defective Containers

It is possible that some of the 11,000 containers in the repository might fail sooner than expected. For example, weld defects in the container fabrication could lead to early failure of the copper shell. For an early failure probability of 1 in 5,000 (Garisto et al. 2004b), 1 to 2 containers might fail early. For these failed containers, groundwater would eventually enter the

container (McMurry et al. 2004). This would likely be accompanied by the formation of rust on the carbon steel vessel and hydrogen gas within the container.

The flooding of the defective container, which is assumed to occur soon after repository saturation, provides a possible path for fuel failure, release of radionuclides into the container, and eventually release of radionuclides into the surrounding buffer material. The transport of these radionuclides is specifically considered in the safety assessment (see Sections 7 and 8). Since the released radionuclides are present only in dilute concentrations, the failed containers likely have only a small effect on the overall repository system evolution. As such, container failure and radionuclide releases are not considered further in this chapter on repository system evolution, but is discussed in Sections 7 and 8.

The composition of the water reaching the used fuel within the defective containers would be that of the surrounding host rock groundwater but conditioned by passage through the buffer and container (Garisto et al. 2004b). For example, changes could arise due to exchange of calcium ions in the groundwater with sodium ions in the bentonite buffer or due to dissolution of the minor mineral components of the buffer (Arcos et al. 2000, Lemire and Garisto 1989). The pH and Eh of the contact groundwater are of particular importance because they strongly affect the solubility and dissolution rate of the used fuel and, hence, the radionuclide source term. These would be buffered to near-neutral and reducing conditions by the bentonite and reactions with the carbon-steel container.

4.3 PERMAFROST STATE

4.3.1 Description

The glacial cycle includes long cooling stages (see Figure 3.2) during which permafrost may develop. Permafrost is defined as ground that remains at or below 0°C for a period of at least two continuous years. Permafrost formation depends mainly on the air temperature.

The Permafrost State considers conditions during which continuous permafrost exists at the repository site and there is no ice sheet at the site. Permafrost can also exist below ice sheets (see Figure 3.8 and Table 8.2)

In Canada, the permafrost line coincides with the -1°C isotherm for annual mean air temperature. Along this isotherm the permafrost is not continuous, i.e., there are areas with no permafrost. The boundary between the discontinuous and continuous permafrost zones appears to lie in the vicinity of the -8.5°C mean annual air isotherm, corresponding approximately to the location of the -5°C mean annual ground temperature isotherm. The thickness of the permafrost near the southern limit of continuous permafrost zone is about 60 m (Brown 1974).

Even in a permafrost region, however, the ground beneath large lakes and rivers can be free of permafrost. The permafrost free zone below a water body is called a talik. It is has been observed that a deep (> 4 m or so) circular lake with a radius greater than 0.6 times the thickness of the surrounding undisturbed permafrost is big enough to maintain an open talik, i.e., there is no permafrost zone beneath the lake (SKB 2006b, p. 102). For lakes with a smaller radius, the talik is closed, i.e., permafrost exists at some depth below the lake.

4.3.2 Biosphere

In permafrost regions, the climate is generally cold and relative dry (about 50% of current day precipitation on the Canadian Shield).

The biosphere and periglacial climate description below is based on the Southern Arctic Ecozone as defined by Environment Canada (2009). In this zone, the mean annual precipitation varies from 200 mm to 500 mm; the mean summer temperatures range from 4°C to 6°C; the mean winter temperatures range from -28°C to -17.5°C; and the mean annual temperatures range from -11°C to -7°C. For the reference glacial cycle, the mean annual land temperatures are shown in Figure 3.2.

Soils during the Permafrost State are underlain by continuous permafrost. At the surface, an active (thaw) layer exists that is usually moist or wet throughout the summer. The landscape is studded with lakes, ponds and wetlands. The impermeable permafrost layer prevents deep groundwater from discharging directly to surface soils, ponds and wetlands. In fact, during this state, surface discharges of deep groundwaters can only occur at lakes that support open taliks. Hence, during the Permafrost State, open taliks would likely be the only surface discharge points.

Vegetation in a periglacial climate is characterized by dwarf shrubs, such as dwarf birch and willow. These are commonly mixed with various herbs and lichens. Wetlands are common and mainly support sedge-moss vegetation.

The Southern Arctic Ecozone is a major summer range for large caribou herds. Caribou are migratory animals and may reside, for example, near a repository site for only a fraction of the year. This is necessitated in part by the limited productivity of an arctic ecosystem, which requires large grazing areas. Other characteristic mammals include bears, wolves, moose, arctic ground squirrels, and brown lemmings. The zone is also a major breeding and nesting ground for a variety of migratory birds, including loons, snow geese, and ptarmigans.

Because the biosphere is so different during the Permafrost State compared to the Temperate State, the representative human groups will be different for these two states. Farming, for example, would not likely be practiced during Permafrost States. Hence, the lifestyle of the people living during the Permafrost State would be quite different from those living during the Temperate State. A potential critical group for the Permafrost State would be a tundra hunter who leads a self-sufficient hunter lifestyle (i.e., plants make up only a small fraction of the critical group diet).

4.3.3 Geosphere

During the Permafrost State, the existence of continuous permafrost affects the evolution of the geosphere. The permafrost depth during the (simplified) reference glacial cycle is shown in Figure 3.6.

The depth of the permafrost layer in the reference glacial cycle is not the same for all Permafrost States. The permafrost depth can be 100 m or 250 m, depending on time during the glacial cycle that the Permafrost State appears (see Figure 3.8 and Tables 8.2 and 8.4).

Hydraulic

The presence of the permafrost layer strongly affects the groundwater flow regime at the repository site because it has a very low hydraulic conductivity and is essentially impermeable, limiting both groundwater flow and radionuclide transport. Permafrost also restricts infiltration and groundwater recharge and, consequently, despite low precipitation rates in permafrost regions, large areas are waterlogged during the summer.

Because the permafrost layer is essentially impermeable, the open taliks near the repository site are the only surface discharge points for groundwater. Furthermore, at sites with several open taliks, vertical flow systems may develop in a network of open, water conducting taliks that are hydraulically connected below the permafrost. More importantly, open taliks, depending on the hydrogeologic regime, could also serve as a conduit for radionuclides, released from the repository, to reach the surface biosphere. Section 7 describes the detailed radionuclide transport modelling results, including the effects of open taliks on radionuclide transport during the Permafrost State.

Chemical / Biological

Because of the lower temperatures in the permafrost zone, reactions (chemical and microbial) would be slower than during the Temperate State. The lower temperatures would also affect mineral solubilities, e.g., carbonate minerals become more soluble as the temperature approaches 0°C.

Dissolved salts are expelled from groundwater as it freezes. Salt exclusion could produce a plume of more salty water beneath the permafrost zone (Vidstrand et al. 2006). (Although the magnitude of the increase in the salt concentration is uncertain, it would be limited if the surface groundwaters are not saline.) In permeable rock, this plume would gradually move downward because of the resulting density gradient, possibly affecting the hydrogeochemical characteristics of the groundwater. However, for closed systems such as isolated fractures and pore fluids, the system would likely return to its original state after the permafrost thaws, so salt exclusion would produce little change in hydrogeology or geochemistry (Gascoyne et al. 2004).

4.3.4 Near-Field

The formation of permafrost has no direct effect on the repository because the repository is much deeper (670 m) than the maximum depth of the permafrost layer (about 300 m).

The heat generated by the fuel in the repository has decreased more than 100-fold (see Table 4.1) by the end of the (long) current interglacial period and, therefore, the permafrost thickness should not be affected by the heat flux from the repository. After about 100,000 years, the thermal effect of the used fuel becomes insignificant and temperatures around the repository return to ambient conditions (McMurry et al. 2003). At this time, it is possible that the cold climate during the Permafrost State could cause the temperature around the repository to decrease by up to 5°C, but it remains above freezing.

4.4 ICE SHEET STATE

4.4.1 Description

During the Ice Sheet State, the regional area around the repository site becomes fully covered with an ice sheet, i.e., the ice terminus is far from the site. The ice surface elevation at the site would generally reflect the continental-wide ice sheet profile (see Figure 3.5) and, therefore, would be relatively uniform across the area of the repository if the ice terminus is far from the site (see Figure 6.7) (Gogineni et al. 2001). In consequence, the thickness of the ice sheet at the site varies with the topography of the underlying land surface.

The land under the ice sheet will be depressed because of the weight of the ice sheet, with the greatest depression occurring under the ice sheet center, and less at the edges. The topographic gradients induced by the ice sheet occur across continental distances; with estimates in the central area of the order of 1 m per km (Ahlbom et al. 1991). This depression is not likely to be a significant factor at the repository level because the entire crust moves up and down.

The onset and termination of the Ice Sheet State are important aspects of this state since the movement of the ice sheet over the site can cause significant transient changes to the groundwater flow regime. The advance and retreat of the ice sheet are modelled as described in Section 3.4.

4.4.2 Biosphere

During ice sheet advance over the site, soil and overburden are eroded away. The average glacial erosion during a full glacial period is between 0.2 m and 4 m in a previously glaciated site that has been scraped down to the granite bedrock (Passe 2004). Excluding the extremes, the average glacial erosion is about 1 m per glacial cycle. In contrast, during ice sheet retreat, deposition of gravel, sand and till occurs.

During the Ice Sheet State, there is no vegetation and the only fauna might be visiting birds. Current Arctic ice cap wildlife and vegetation (e.g., algae) are associated with the marine environment and ice edges adjacent to the sea. More importantly, there are no humans living near the site during the Ice Sheet State so there is no potential dose exposure to people during this time.

4.4.3 Geosphere

Thermal

The ice sheet covering the repository site can be either cold based or warm based, as shown in Figures 3.3. (Cold-based ice sheets move more slowly because they adhere more strongly to the ground surface.) The ice sheet is generally cold based directly after the ice sheet moves over the site. During these periods permafrost exists beneath the ice sheet and there is no basal melting. The permafrost under the ice sheet would affect the groundwater flow regime in the geosphere.

After the glacier moves over the repository site, the ground beneath is insulated from the cold air and the permafrost beneath the glacier begins to melt due to the geothermal flux from the earth. After the permafrost has melted, the ice sheet is considered to be warm-based. A warm-based ice sheet has liquid water at the base of the ice sheet. This water has a temperature equal to the pressure melting point of the ice (see Figure 3.2). The pressure melting temperature is approximately -1.6°C for a 2 km thick ice sheet.

The open taliks that exist beneath large lakes during the Permafrost State likely freeze, i.e., permafrost forms beneath the lakes, after a cold based ice sheet moves over the lakes. This assumption seems reasonable given that (1) the ice sheet pushes the water out of the lake and (2) there is no influx of heat into the lakes during the summer months after the ice sheet moves over the lakes. It is the heat absorbed by lake water during the summer months that keeps the water at the bottom of the lake from freezing during winter months, thereby preventing permafrost formation beneath the lake.

Hydraulic

For a cold-based ice sheet, the ground and base of the ice sheet are frozen (i.e., there is no basal meltwater flow) and so water infiltration rates into the geosphere are low. For a warm-based ice sheet, subglacial groundwater flows would be directed downward and subglacial groundwater discharges may occur close to the ice terminus (which is far from the repository site during the Ice Sheet State). Near the edge of the ice sheet, groundwater may flow upward due to differential hydrostatic pressure, potentially moving deep groundwaters upwards, as illustrated in Figure 4.1. Because of the potentially large hydraulic heads and gradients near the ice terminus, glacial melt water could, in theory, penetrate deep down into the bedrock and groundwater flows could be substantially larger than under present day conditions (Chan et al. 2005).

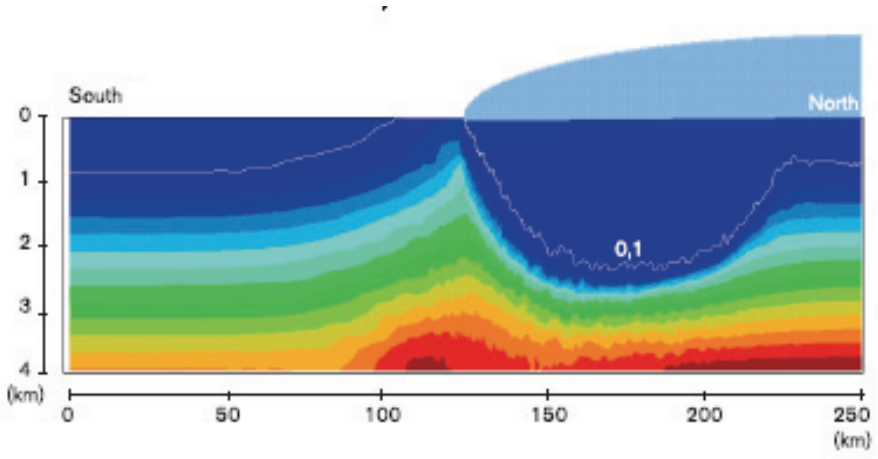

Figure 4.1: Illustration of upconing of saline water (after SKB 1999). The total dissolved salt density increases with depth.

Groundwater flow beneath the ice sheets (or permafrost, if it exists) is affected by consolidation effects due to the ice load, which can increase the subsurface hydraulic pressures at depth by 30% to 80% of the total imposed load (Wang 2000). For a warm based ice sheet, the hydraulic pressures would be further increased, if, for example, the water table is near the top of the ice sheet.

After the ice sheet retreats, the high water pressures at depth caused by the ice sheet would cause groundwater to flow upwards towards the surface until the high pressures are dissipated (Chan and Stanchell 2008). This can take a long time, possibly thousands of years, depending on the permeability of the system (Chan and Stanchell 2008).

However the actual effect of the ice sheet on groundwater conditions at repository depth will be muted. First, the occurrence of permafrost under the advancing ice sheet will restrict the depth of penetration of glacial meltwater into the geosphere. Second, the denser saline groundwaters at depth will also resist changes. Thirdly, the low and decreasing permeability of the rock with depth will also naturally isolate the deep repository. Evidence in the chemistry of porewater samples from various deep rock sites on the Canadian Shield indicates that these waters are very old, possibly millions of years (Gascoyne 2004). This means that they have not been much affected by the multiple glaciations over the past million years. A good candidate site for a repository would be expected to show similar behaviour.

Mechanical

As the ice sheet moves over the repository site, the vertical stresses under the ice sheet increase, the lithosphere bends and the mantle flows laterally due to the load of the ice sheet. This will result in a depression beneath the ice sheet and an up-warping bulge outside the ice sheet terminus. This depression and bulging occurs over hundreds of kilometres. While it is important to the overall evolution of the ice sheet, it is only gradual on the scale of the regional site model considered in this study.

The weight of the ice sheet is impressed onto the rock and porewater underneath the ice. The balance of the imposed load between the rock and the water depends on the porosity and the compressibility of each material. In one limit, the weight is entirely carried by the rock. In the other limit, the weight is entirely carried by the pore water. In practice, estimates of the balance of the load between the rock and water for granitic rock suggest that the pore pressure increase at depth would range from 30% to 80% of the total imposed load.

The higher water pressures (due to the weight of ice) decrease the effective normal stresses on faults and thereby reduce their shear strength, lowering fault stability. This could in theory cause hydraulic jacking or fracturing of the rock at shallow depths (< 60 m) (Hökmark et al. 2006).

The vertical stresses due to the ice load tend to stabilize the mantle, reducing the probability of seismic activity. However, after the ice sheet retreats, the vertical load on the rock decreases rapidly. The changing loads also mean that the stresses can change direction relatively quickly. The changing stress regime can cause horizontal and gently dipping fractures to widen. More importantly, seismic activity increases immediately (0 to 2000 years) after deglaciation (SKB 2006b, Stewart et al. 2000, Adams 1989). However, fault movement would preferentially take place as reactivation of existing fracture zones, not creation of new faults, because these are

pre-existing weak areas. Reactivation of existing fractures could potentially affect the groundwater flow field.

Chemical / Biological

During the Ice Sheet State, the rates of chemical and microbial processes are lower than during the Temperate State because of the lower temperatures, particularly in the shallower geosphere zones.

Because of the high hydraulic heads at the bottom of the ice sheet, it is possible that glacial meltwaters will penetrate deep into the geosphere if the glacier is warm-based. Of more importance, however, is the depth of penetration of the oxygen in glacial meltwater, which contains about 45 mg/L of oxygen, since arrival of oxygenated groundwater into the repository could significantly increase radionuclide source terms.

However, evidence from paleohydrogeological studies at the Whiteshell Research Area (Lac du Bonnet, Manitoba) on the Canadian Shield indicates that oxygenated groundwaters have not penetrated more than about 50 m into the bedrock during the last million years, which includes about 8 complete glacial cycles (Gascoyne et al. 2004, McMurry and Ejeckam 2002). The oxygen does not travel far into the geosphere because it reacts with Fe(II) minerals in the granite bedrock (Spiessl et al. 2009, Gascoyne 1999). Moreover, the periods over which large vertical hydraulic gradients occur are limited since the ice edge (or terminus) passes relatively rapidly across the repository site. The important findings from the field studies include the following:

1. Oxygenated recharge water typically only percolated through the shallowest part of the flow system (< 50m).
2. The upper 200m of bedrock in the Canadian Shield was affected by previous glaciations. Groundwater in that layer has a warm climate isotopic signature, and a residence time of tens to thousands of years (Gascoyne 2000).
3. Groundwaters from depths of 200 m to 400 m have a cool-climate isotopic signature that corresponds to the last glacial cycle, indicating either incursion by glacial meltwater or a dilution by freeze out from a deep permafrost formation (Zhang and Frape 2002). Fracture lining minerals have not preserved evidence of reaction with oxidizing water but do suggest that downward percolation of young glacial meltwater is limited (Blyth et al. 2000).
4. At depths greater than 400m, groundwater also typically has a warm-climate isotopic signature, but one that correlates with residence times greater than a million years, i.e., it is unaffected by glacial meltwater.

Although these results are from a specific site, it is expected that sites on the Canadian Shield can be found where oxygenated waters have not penetrated deep into the bedrock and where glacial meltwaters have not penetrated below typical repository depths.

It has been suggested that as the highpressure water under the ice sheet moves down into the bedrock it could cause deeper more saline water to move upwards, as illustrated in Figure 4.1 (SKB 2006c, Jaquet and Siegel 2006, SKB 1999). In simplistic terms, the high pressure of the melt water causes the upward displacement of the denser deep groundwater. This upconing could, in theory, cause the deeper, more saline groundwater to reach the repository. However,

any effect of upconing on repository performance may be limited because the ice sheet edge is in the vicinity of the repository for a relatively short time.

4.4.4 Near-Field

The hydrological and chemical conditions in the near field are largely unaffected by the processes occurring at the surface during the Ice Sheet State, for reasons discussed above. In particular, it is expected that oxygenated and/or freshwaters will not reach the repository depth. Thus, reducing, saline, and stagnant conditions will remain at the repository level. However, as mentioned above, upconing saline groundwaters could reach the repository during ice sheet advance. The higher salinity could affect repository performance (e.g., buffer swelling pressures, radionuclide solubilities, etc.).

The mechanical stresses in the near field change as the ice sheet advances (or retreats) above the repository. For example, the presence of an ice sheet above the repository causes the external load on intact containers to increase significantly because of the increased hydraulic pressure at depth induced by the high hydraulic heads at the base of the ice sheet. For this reason, containers are designed to withstand the additional load during the Ice Sheet State (Poon et al. 2001).

4.5 PROGLACIAL LAKE STATE

4.5.1 Description

A proglacial lake is a lake formed either by the damming action of a moraine or ice dam during the retreat of a melting glacier, or one formed by melt water trapped against an ice sheet due to isostatic depression of the crust around the ice. These lakes are known as proglacial lakes because ice forms a part of their shoreline.

Deglaciation, at the end of the glacial cycle, occurs relatively rapidly. About 10,000 years after glacial maximum, intense periglacial conditions have returned and by about 2000 years later the periglacial environment has been eliminated and the mean surface temperatures are restored to temperate climate values. As the ice sheet melts, large amounts of water are generated and proglacial lakes likely form. For example, the GSM results predict that vast proglacial lakes formed adjacent to the southern margin of the Laurentide Ice Sheet during the retreat phase of the last glacial cycle (see Figure 4.2).

The Proglacial Lake State is relatively short lived (about 1200 years in the reference glacial cycle). During this period, proglacial lakes can fill up and catastrophically empty many times, typically as the ice melts and uncovers a path for the water to flow out. The depth of the proglacial lake in the reference glacial cycle is assumed to be about 165 m, based on the GSM results for Simulation nn2778 (Peltier 2006).

4.5.2 Biosphere

Proglacial environments are found at or just beyond glacial ice margins. Landforms are considered proglacial if they are proximal to ice margins.

The Hudson Plains Ecozone as defined by Environment Canada (Environment Canada 2009) is used to describe the climate state for the Proglacial Lake State. This ecoregion is marked by cool, short summers and cold winters. The mean summer temperature is 11.5°C and the mean winter temperature is -16°C. The mean annual precipitation ranges from 700 to 800 mm.

The Hudson Plains ecoregion consists largely of flat, poorly drained plains with subdued fluvial and marine features. Throughout the area, there are gravelly, well-drained belts of raised beaches, resulting from postglacial, isostatic rebound. Wetlands cover 50 to 75 % of the area.

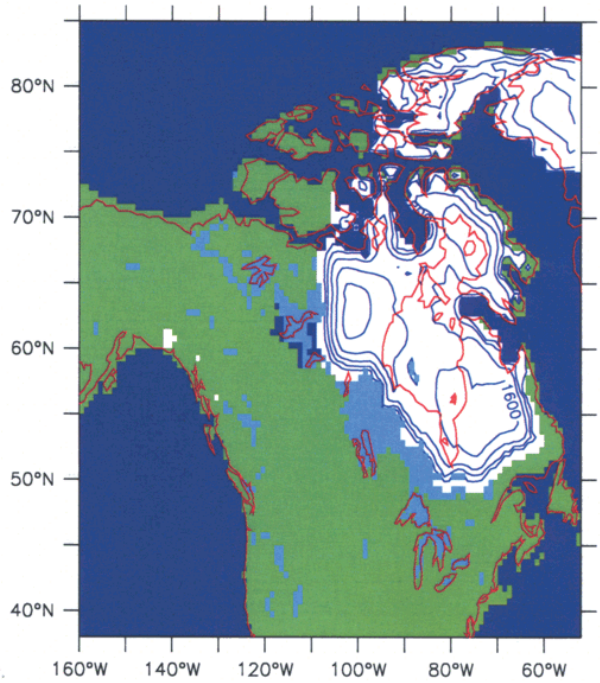

Figure 4.2: Example of a large proglacial lake (light blue colour) formed during retreat of the Laurentide Ice Sheet 10,000 years before the present (Peltier 2006)

Following the withdrawal of the ice-sheet, the land surface would everywhere be devoid of vegetation and desert-like, with wind action leading to formation of sand dunes. However, recolonization by plant life proceeds rapidly, such that within a few centuries an initial tundra biome would be replaced first by open woodlands and later by closed forest.

Characteristic wildlife of the Hudson Plains ecoregion includes barren-ground caribou, black bear, wolf, moose, lynx, and snowshoe hare. Bird species include the Canada goose, ruffed grouse, and American black duck.

When people arrived at the Hudson Plains ecoregion after the last glaciation, they would have encountered spruce-pine forests, many small lakes and probably one large proglacial lake. (Paleoindian sites in the Canadian Prairies are often found in association with the margins of large proglacial lakes.) Subsisting primarily by hunting, the early people moving into the area after the last glaciation followed a seasonal cycle. In spring and summer, they camped on the shore of the lakes, which would have provided rich opportunities for hunting as well as for

fishing and the gathering of edible plants. In fall and winter, they moved inland to sheltered hunting areas, establishing smaller and more temporary campsites than those on the shore, which were occupied over and over again.

4.5.3 Geosphere

Thermal

Because of the short duration of the Proglacial Lake State and the low thermal conductivity of the rock, it is assumed that the thermal regime during this state is similar to that during the end of the Ice Sheet State except near the surface which is heated by solar radiation during the summer months. These seasonal thermal effects are not expected to propagate far down into the geosphere during this short state.

Hydraulic

The proglacial lake is assumed to cover the entire modelling domain during the Proglacial Lake State; therefore, the elevation of the lake surface controls the hydraulic heads at the top of the model domain. Consequently, there are no horizontal gradients driving horizontal flows across the model domain. However, the large hydrostatic pore pressures in low permeability rock produced during the Ice Sheet State are expected to decrease only gradually, maintaining an upward hydraulic gradient for thousands of years after the ice sheet has retreated (Chan et al. 2003, 2005). The upward flowing groundwater discharges into the proglacial lake.

Mechanical

The weight of the water in the proglacial lake increases the mechanical stresses in the geosphere relative to those during the Temperate State. However, the mechanical stresses due to the lake will be much lower than those caused by the ice sheet during the Ice Sheet State.

Chemical / Biological

Because of the lower temperatures during glaciation, the rates of chemical and microbial processes are lower during the Proglacial Lake State than during the Temperate State, particularly in the shallower geosphere zones.

The upward groundwater flow, resulting from the high hydrostatic pressures produced during the Ice Sheet State, could in theory cause more saline waters from beneath the repository to enter the repository. However, this effect is not expected to be significant because of the low permeability of the rock at repository depth and the effect of gravity.

4.5.4 Near-Field

It is believed that the conditions in the near field, e.g., hydraulic pressures, will slowly return to those existing during the Temperate State after the end of the glacial cycle. However, this may not be achieved by the end of the Proglacial Lake State. The presence of the large proglacial lake above the repository is not expected to affect the evolution of conditions in the near field because of the large depth of the repository, although the stresses will be higher in the

repository during the Proglacial Lake State than during the Temperate State because of the weight of the water above the site.

4.6 INFUENCE OF GLACIAL CYCLING

The reference glacial cycle for the Glaciation Scenario is described in Section 3. For convenience, the glacial cycle was divided into the four main climate states described above: the Temperate, Permafrost, Ice Sheet and Proglacial Lake states. The duration and sequence of these states during the reference glacial cycle is also described in Section 3. The features, processes and events occurring during these four states are described in Sections 4.2 to 4.5.

Because we are interested in a time frame of one million years, the future climate in the Glaciation Scenario is represented by a repeating set of the 121,000 year reference glacial cycle.

As noted above, there are processes and events that could affect the properties of these four states (e.g., stress changes during deglaciation could cause the opening of existing fractures; erosion and deposition could cause the topography of the repository site to change; lakes could disappear or be formed; etc.). However, we do not take these processes or events into account in the current safety assessment. Rather, each particular state is assumed to have the same "basic" near-field, geosphere and biosphere properties regardless of time of occurrence of that state. In other words, for example, all the Temperate States that occur over the one million years time frame have identical physical and chemical properties. The same is true for the Ice Sheet, Permafrost and Proglacial Lake States. This stylized approach is appropriate for the long time scale of interest in the safety assessment of a used fuel repository (CNSC 2006).

Some processes that are modelled exhibit some differences between similar states. For example, not all Ice Sheet States are warm-based or have the same thickness of ice, and not all Permafrost States have the same thickness of permafrost. Similarly, the explicit time-dependence of radionuclide transport means that radionuclide concentrations in the biosphere will, for example, not be the same for each Permafrost State.

Finally, it is interesting to note that the groundwater flow regime reaches a steady state during the Temperate State (see Section 6). Consequently, the evolution of the groundwater flow regime subsequent to the Temperate States will be identical for all glacial cycles that occur during the one million year time frame, assuming that the geosphere and biosphere properties do not change as a result of glaciation (e.g., no new fractures are created, the topography at the repository site remains the same, etc.). For this reason, it will only be necessary to describe the groundwater flow regime during the first glacial cycle.

5. SCENARIO AND CONCEPTUAL MODELS

5.1 SCENARIO DESCRIPTION

While the reference copper containers are designed to survive glaciation when emplaced in a suitable site (McMurry et al. 2003, Maak and Simmons 2001), it is of interest to consider the safety implications of container failures, as in the Defective Container Glaciation Scenario. In this scenario, the repository is built to design specifications except that some containers are assumed to be emplaced with small, undetected defects that penetrate the copper shell, due to, for example, fabrication flaws.

Based on experience with other high-quality nuclear-grade components, the number of containers that would have full penetration defects in the copper shell and escape detection is expected to be small. Based on the estimated probability of undetected defects (Maak et al. 2001), we assume that two of the approximately 11,000 containers in the repository could have full penetration defects at the time of emplacement in the Defective Container Glaciation Scenario.

The other defining aspect of this scenario is that the container defects are present at the time of emplacement. Therefore, there is the possibility for early release of radionuclides from the defective containers into the groundwater around the repository and, thereafter, to the surface environment. Since radionuclide inventories generally decrease with time (as radionuclides decay), the potential radiological consequences of early radionuclide releases would be larger than if the containers failed at a later time.

It should be noted that a small penetration in the copper shell (i.e., small enough that it escapes detection) would not necessarily lead to immediate radionuclide releases; rather, substantive releases from the container are likely only after at least ten thousand years (McMurry et al. 2004). However, it will be conservatively assumed that this release pathway develops immediately after groundwater has saturated the vault around the defected container. In this early failure model, we assume that the defective container is intact except for a small hole through the copper shell, and we do not take credit for the containment offered by the steel inner vessel or the Zircaloy cladding.

After the used fuel is contacted by groundwater, a pathway exists for radionuclides to be released from the container and to move through and with the groundwater toward the surface biosphere. The focus of the analysis for the Defective Container Glaciation Scenario is, therefore, on radionuclide release from the used fuel, transport of radionuclides through the container defect, vault, geosphere, and to the surface, and on radionuclide transport within the local biosphere, leading to radiological doses to humans living in the vicinity of the repository.

Sensitivity analyses will also be carried out to understand the influence of the location of the failed containers and the number of failed containers on calculated impacts.

5.2 CONCEPTUAL MODEL

The Defective Container Glaciation Scenario considers a case in which some containers fail early because of the presence of undetected manufacturing or installation flaws, and the system model calculates the subsequent release of radionuclides from the used fuel and container, their transport through groundwater to the surface, and the consequences to people living in the vicinity of the repository.

Figure 5.1 illustrates the general conceptual model for the Defective Container Glaciation Scenario, outlining some of the key factors. It is similar to that used in the Defective Container Scenario for the TCS and HBC studies (Garisto et al. 2004a, 2005a). The major difference between these two scenarios is the varying climate during the Defective Container Glaciation Scenario caused by the onset of glaciation.

The varying climate affects the biosphere, including the critical group characteristics, and the geosphere, especially the groundwater flow system.

5.2.1 Biosphere

The surface biosphere near the repository site has the characteristics of the Canadian Shield region of central Canada. The properties of the biosphere vary with time as the glacial cycle moves through its various states: Temperate State, Permafrost State, Ice Sheet State and Proglacial Lake State. For each distinct state, there is a distinct biosphere, as described in Section 4. The main features of these states are summarized here:

1. The Temperate State biosphere resembles the current climate biosphere of a typical Canadian Shield location (Gierszewski et al. 2004b). Of particular note, the biosphere at the repository site includes the North Lake, located above the east corner of the repository, and the South Lake, located south of the repository (see Figure 2.2).

2. The main features of the Permafrost State biosphere are: the continuous permafrost layer; the periglacial climate, flora and fauna; and the two open taliks, referred to as the North and South taliks, beneath the two large lakes in the model domain (see Figure 6.2). The existence of open taliks under these lakes is a reasonable assumption given their assumed depths (4.6 m) and sizes (widths of North and South lakes are greater than 300 m and 600 m, respectively).

3. During the Ice Sheet State, an ice sheet moves over the repository site, covering the repository site and surroundings with a thick layer of ice, and then retreats. It is assumed that no humans live near the site during this state.

4. Finally, in this study, the Proglacial Lake State biosphere is assumed to resemble the Permafrost State biosphere except for the presence of a large proglacial lake above the repository site.

The biosphere parameter values describing the properties of these states are presented in Appendix A.

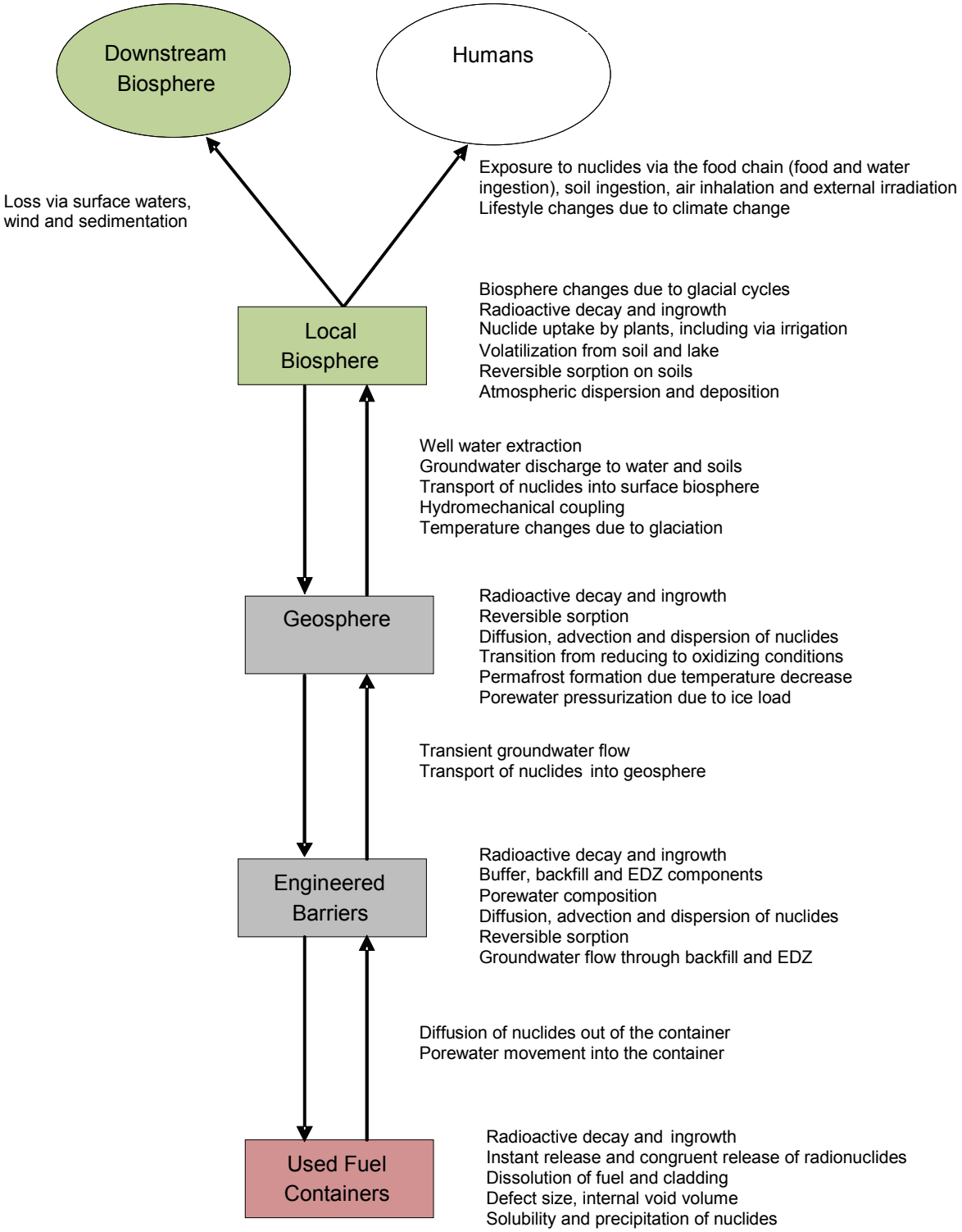

Figure 5.1: General conceptual model for the Defective Container Glaciation Scenario. The arrows indicate interactions or nuclide transfers between the model components. The important processes modelled for each model component are also indentified.

An important feature of the biosphere is the people who would be affected by the repository. Following international practice, we assume that the site is occupied by a group of people (the "critical group") that behaves in a plausible manner but one that maximizes their exposure to any radionuclides released from the repository into the biosphere. The characteristics of the critical group change with the climate. We identify 3 critical groups: the self-sufficient farmer, living during the Temperate State; the self-sufficient tundra hunter, living during the Permafrost States; and the self-sufficient tundra hunter-fisher living during the Proglacial Lake State. For conservatism, we assume that these people spend all their lives in the vicinity of the repository and obtain all their food and water from this area. The detailed characteristics of these critical groups are described in Appendix A.

The self-sufficient farmer critical group has the same characteristics as previously described for the TCS and HBC studies, i.e., he or she uses a well that intercepts the contaminant plume from the repository; grows its own crops and raises animals. The food ingested by this group includes plants grown in a garden, domesticated animals and fish. This lifestyle is more self-sufficient than current habits and will lead to higher estimates of impacts.

The tundra hunter critical group that lives during Permafrost States is also self-sufficient but survives mainly by hunting. Its diet consists mostly of caribou, augmented with some fish (from the lake), fowl (Canada geese) and plants (berries). These foods are processed, as required, for winter usage. This group is assumed to use the lake at the repository site (i.e., the North Lake) for all water needs (drinking, bathing, etc.). In winter, the lake is also used for water by boring through the ice, although melted snow may also be used.

The tundra hunter-fisher critical group lives during Proglacial Lake States. Its lifestyle and characteristics are assumed to be similar to those of the tundra hunter critical group found during the Permafrost State, except that its diet consists of much more fish (and less caribou). The fish are taken from the large proglacial lake.

Plants growing near the repository can become contaminated directly by atmospheric deposition of radionuclides that reach the North Lake (or North talik) and become volatilized (e.g., I-129) or suspended due to aerosol formation (all nuclides). They can also become contaminated due to root absorption of radionuclides that have been deposited to the soil from the atmosphere. Lichens, an important foodstuff for caribou, are only contaminated by atmospheric deposition.

Caribou are migratory animals and reside near the repository site for only a fraction of the year. While near the repository site, the caribou are assumed to drink water from the local lake and eat lichen growing near the repository site.

During ice sheet advance over the site, soil and overburden are eroded away. However, in the current model, the effects of erosion on the biosphere or geosphere are neglected. Consequently, for example, each Temperate State is assumed to have the same topography regardless of the time of its occurrence, and residual contaminants in the soil are not swept away by erosion and are present during subsequent states of the glacial cycle.

The biosphere model includes only the local biosphere near the repository, since doses to the critical group living near the repository should be higher than for any individual living further away from the repository because radionuclide concentrations would be higher in the local biosphere. Radionuclides are lost from the local biosphere by radioactive decay, by discharge from the local lake to downstream watershed locations, and by loss to the deep sediments at

the bottom of the lake and river (see Figure 5.1). For a few volatile nuclides, losses to the downstream airshed due to winds and atmospheric dispersion are also important.

The conceptual biosphere model is generally similar to that used in the Third Case Study (Garisto et al. 2004a,b), except for the additional critical groups. The conceptual model is implemented in the SYVAC-CC4 code. Additional model details can be found in Gierszewski et al. (2004d).

Radionuclides released from the repository reach the surface biosphere in several ways: via the well that intercepts the radionuclide plume; via groundwater discharge to lakes and other surface water bodies; and via groundwater discharges to terrestrial areas. Given these radionuclide discharge rates from the geosphere, the SYVAC3-CC4 biosphere model then:

- describes the movement of nuclides through soil, plants and animals, the water and sediment of a lake, and the atmosphere near the groundwater discharge locations;
- calculates the concentrations of nuclides in water and air in the local habitat of the critical group; and
- calculates radiological dose rates to an individual in the critical group caused by ingestion and inhalation of nuclides and by external exposure to radiation from nuclides in the environment (air immersion, water immersion, and groundshine). The internal and external exposure pathways are similar to those used to calculate derived release limits for normal operation of a nuclear facility (CSA 2008).

In the biosphere model, all radionuclide mass flows out of the geosphere also enter the (North) lake. Although this overestimates the nuclide mass in the biosphere, it simplifies the modelling because many processes that recycle radionuclides within the local biosphere are accounted for implicitly, such as surface runoff into the lake.

5.2.2 Geosphere

This section describes the main features of the geosphere and geosphere model that are important to the postclosure safety assessment of the Defective Container Glaciation Scenario. The geologic features at the hypothetical repository site and the geosphere property data are described in Gierszewski et al. (2004b) and briefly in Section 6.

The principal components of the geosphere and the corresponding principal processes included in the geosphere conceptual model are shown Figure 5.2.

The assumed geosphere has a defined fracture network, and bulk rock and fracture permeabilities varying with depth. The permeability versus depth profiles are shown in Figure 6.4 and Table 6.1. For the bulk rock, the permeability profile used in the Glaciation Scenario is the same as used in the HBC and corresponds to a rock with medium permeability (Garisto et al. 2005a). Following Normani et al. (2007), the permeability of the fractures is taken to be depth dependent in the current study, whereas in the HBC study the permeability of the fractures was independent of depth (Garisto et al. 2005a).

The detailed 3-dimensional groundwater flow and contaminant transport calculations are carried out with the FRAV3DVS-OPG code, Version 1.1 (64 bit) (Therrien et al. 2007). Henceforth, this code is simply referred to as FRAC3DVS, although the complete name may be used for emphasis.

Simplifications

As part of the HBC study (Garisto et al. 2005a), FRAC3DVS simulations were undertaken to explore the influence of spatially variable salinity distributions on groundwater flow. For the flow system considered in the HBC, comparative steady-state groundwater simulations revealed only small differences between fresh and saline water realizations. This outcome appeared, in part, related to the site-specific flow domain permeability distributions and assumed boundary conditions.

Normani (2009) carried out studies of the paleoevolution of pore fluids in glaciated geological settings, including the TCS watershed area. He used the glacial cycle based on Simulation nn2778 (see Section 3, Peltier 2006) and carried out simulations for both brine and freshwater systems. Comparison of his results for Scenario 1 (brine with TDS = 300 g/L at 1500 m depth and about 20 g/L at repository depth) and Scenario 3 (same as Scenario 1 but with freshwater) shows that the calculated velocity magnitudes are similar but that the brine affects the flow direction at depth, preventing deep flow paths from developing compared to the freshwater case (Normani 2009, p.103). Thus, mean travel times for particles to reach the surface from the repository are somewhat greater for the saline system.

The results discussed above suggest that the influence of salinity at the TCS site is not particularly large (at least at repository depths) and that the neglect of salinity would be conservative (Normani 2009, Sykes et al. 2003a,b). For these reasons, salinity is not incorporated in the FRAC3DVS groundwater and mass transport simulations for the Glaciation Scenario.

Since salinity is not modelled, several aspects of the transient groundwater movement during ice sheet advance/retreat over the site cannot be studied, including the potential for upconing of saline groundwater during ice sheet advance over the site (see Section 4.4.3 and Figure 4.1).

In the HBC study (Garisto et al. 2005a), as an approximation for the effect of repository heating, a zone at a steady temperature of 40°C was defined around the repository. However, the thermal plume would have essentially dissipated at the end of the initial long Temperate State. After this period, the evolution of the groundwater flow system would be much more influenced by the changing climate conditions (i.e., permafrost formation, ice sheet advance, etc.) than by the remaining small thermal gradients arising from the repository. Consequently, the thermal effects due to the heat generated by the fuel in the repository are neglected. This approximation is expected to have very little influence on the radionuclide transport calculations for the Glaciation Scenario.

As the ice sheet moves over the repository site, the weight of the ice produces a depression in the lithosphere beneath the ice sheet and an up-warping bulge outside the ice sheet terminus. This depression and bulging occurs over hundreds of kilometres. While this process is important to the overall evolution of the ice sheet, it is only gradual on the scale of the regional site model considered in this study and is, therefore, neglected. Similarly, any potential changes to the geosphere properties due to seismic activity resulting from ice sheet advance/retreat is not taken into account in the current study, as discussed previously.

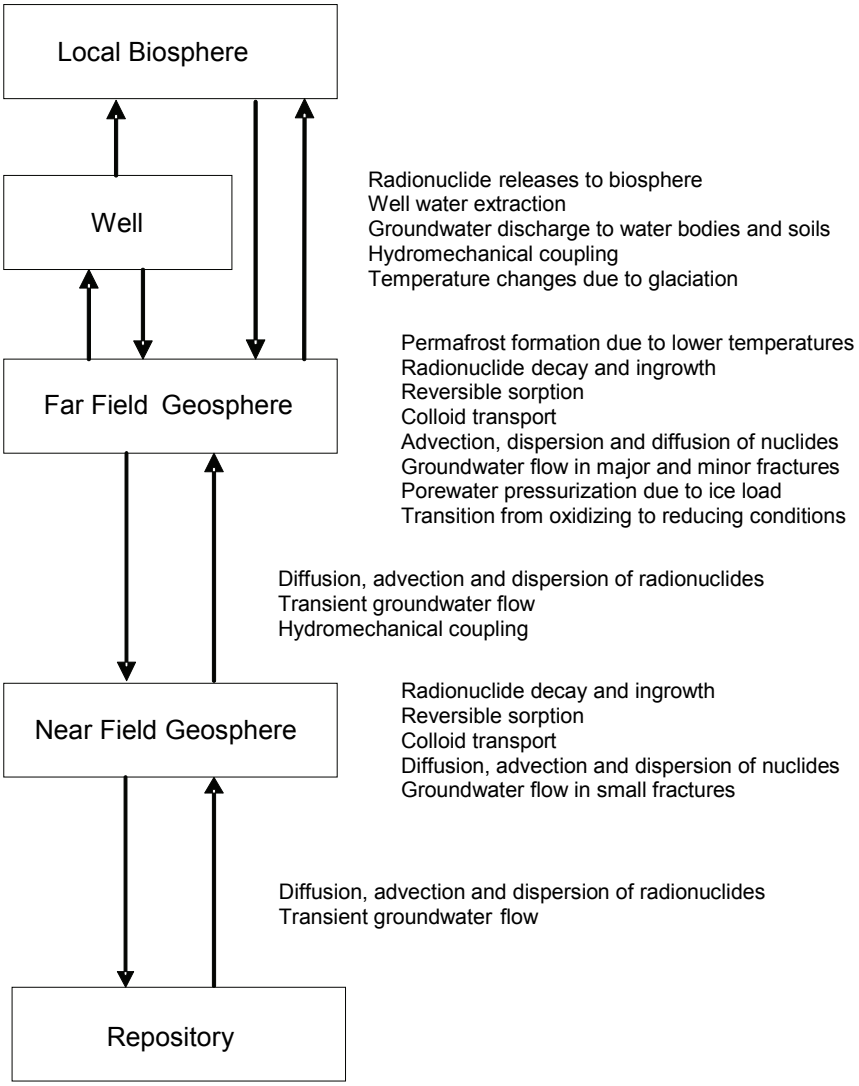

Figure 5.2: Conceptual model for the geosphere. The arrows indicate interactions or nuclide transfers between the model components. The important processes modelled for each model component are also indentified.

The depth of the permafrost layer in the geosphere for the reference glacial cycle is derived from the results of Simulation nn2778 (Peltier 2006), as discussed in Section 3, and thus is model input. The permafrost depth has been simplified in the reference glacial cycle to make the transient groundwater modelling feasible; hence there are abrupt changes in permafrost depth between the various glaciation states (see Figure 3.8). These sudden property changes are imposed on a hydraulic head distribution that is a function of the preceding property specification, and this will cause short-lived disruptions in the modelled flow field as the system moves towards a new equilibrium. These disruptions are essentially an accelerated version of what might happen in a real system in which these properties change more gradually. Transitory spikes in flow rate and perhaps radionuclide transport are a potential consequence, although the effect on the overall model predictions will be small due to the very short duration of these flow disruptions.

Groundwater and Transport Modelling

For the Glaciation Scenario, a transient groundwater flow regime exists in the geosphere. The transient groundwater flow is driven by the changes in the climate caused by the glacial cycle, particularly the advance and retreat of ice sheets over the repository site.

Eight glacial cycles occur during the one million year time frame of interest. As noted in Section 4.6, it is assumed that the geosphere and biosphere properties do not change as a result of glaciation (i.e., no new fractures are created, the topography at the repository site remains the same, etc.). Consequently, since the groundwater flow system attains the same steady state during the Temperate State, which occurs at the end of each glacial cycle, the groundwater flow system repeats itself during subsequent glaciations following the first complete glacial cycle (see Section 6). The steady state groundwater flow field attained during the Temperate State is illustrated in Figure 6.9.

The boundary conditions used in the calculation of the groundwater flow field depend on the glaciation state and are described in Section 6 and in more detail in Walsh and Avis (2010). During the Ice Sheet State, for example, the presence of an ice sheet over the model domain causes the hydraulic heads at the surface of the model to increase substantially. (The hydraulic heads are proportional to the ice height.)

During the Temperate State the hydrogeological model includes a 100 m well, at a specified location, which draws water from a fracture zone at a specified rate. The influence of the well on the overall groundwater flow field is small. The well is used as a water source by the self-sufficient farmer critical group.

An important consideration in the Glaciation Scenario, arising from the advance of an ice sheet over the repository site, is the effect of the changing ice load on the groundwater flow system. This has been approximately taken into account in the modelling for the Glaciation Scenario by using the one-dimensional hydromechanical coupling module in FRAC3DVS-OPG, as described in Section 6 and Walsh and Avis (2010). This model assumes that the glacial load results in purely vertical strain of the underlying rock. Deep within an ice field, where the ice load is relatively uniform, this assumption is very good. In the vicinity of the ice sheet terminus, where the vertical load varies significantly across the model domain, this hydromechanical coupling model provides a rough approximation of the true stress state and resulting induced hydraulic pressures and gradients.

The weight of the ice sheet is impressed onto the rock and porewater underneath the ice. The balance of the imposed load between the rock and the water depends on the porosity and the compressibility of each material. For granitic rock, estimates of the balance of the load between the rock and water range widely (Wang 2000). In the present study, we assume an increase in the porewater pressure equivalent to about 1/3 of the basal normal stress applied by the glacier (Chan et al. 2005).

In the FRAC3DVS-OPG geosphere model, an equivalent porous medium model is used to model transport of (dissolved) radionuclides in the fractures and in the bulk rock between the defined fractures (Garisto et al. 2004a, Therrien and Sudicky 1996). The results of the equivalent porous medium model have been shown to be similar to those obtained derived using a discrete fracture network approach (Garisto et al. 2005a).

In the Glaciation Scenario, the high hydraulic heads at the bottom of warm-based ice sheets have the potential to drive water (e.g., glacial meltwater rich in oxygen) downward into the geosphere. However, field evidence (isotopic measurements) at the Whiteshell Research Area indicates that there are sites on the Canadian Shield where there are no glacial (cold) water signatures below depths of about 350 m, i.e., glacial meltwaters do not infiltrate below 350m at this site (Gascoyne et al. 2004). More importantly, the paleohydrogeological evidence at this site suggests that oxygen in the meltwaters is consumed in the upper 50 m or so of bedrock and does not penetrate to depths greater than 50 m (Gascoyne et al. 2004).

The evolution of the groundwater flow system during the Glaciation Scenario is described in Section 6.

Chemical

The mineral composition of the fracture in-filling material is assumed to be the same as that used in the EIS study (Davison et al. 1994), which was derived from studies at the Whiteshell Research Area. The mineral composition of the fracture material depends on depth, with two fracture compositions defined – one for fractures below the redox divide in which reducing conditions are assumed to prevail and one for fractures above the redox divide in which oxidizing conditions prevail. Only radionuclide sorption coefficients are affected by the composition of the fracture in-fill material and, for redox-sensitive elements, by the location of the redox divide.

5.2.3 Near Field

Since the intact containers are designed to withstand the additional load during the Ice Sheet State (Poon et al. 2001, Maak and Simmons 2001), the current safety assessment assumes that no intact containers fail as a result of the higher loads experienced during the Ice Sheet State. However, the effect of multiple container failures is examined in Section 8 with both deterministic and probabilistic sensitivity case studies.

The effects of changes to the mechanical stresses in the near field on, for example, groundwater flow within the vault are neglected in the current study of the Glaciation Scenario. However, the potential importance of such effects needs to be assessed in the future.

Radionuclide transport in the near-field (out of the defective container, through the buffer, through the excavation damaged zone (EDZ) and into the surrounding geosphere) is modelled in the SYVAC3-CC4 system model (Chapter 8).

The FRAC3DVS model for the Glaciation Scenario uses a minimum grid size of 50m. Hence, the model does not include a detailed representation of the repository. (In the previous HBC study, a detailed vault model was nested within the larger site model, but this was not practical for the present study.) Consequently, radionuclide transport through the near-field is not directly modelled in the current FRAC3DVS simulations. Instead, the radionuclide fluxes out of the repository calculated in the HBC study (Garisto et al. 2005a) were used as source terms for the detailed FRAC3DVS radionuclide transport calculation in the Glaciation Scenario (Chapter 7). This is expected to be a good approximation because previous results indicate that the radionuclide fluxes out of the HBC repository are not overly sensitive to the groundwater flows near the repository (Garisto et al. 2005a)

In the near-field geosphere around the vault, the rock is sparsely fractured and chemically reducing conditions are assumed to prevail. Also, the temperature in this near field zone will be initially warmer than in the surrounding geosphere due to radioactive decay heating. However, because the thermal gradients will have decayed away by the time of the onset of the first glacial cycle (following the long current interglacial period), this hot zone has been neglected in the hydrogeological modelling for the Glaciation Scenario.

5.2.4 Wasteform and Container

The reference wasteform in this study is a standard CANDU 37-element fuel bundle with a burnup of 220 MWh/kgU and a fuel power of 455 kW/bundle. The radionuclide inventories in this fuel bundle are given in Garisto et al. (2004b).

The wasteform has two distinct components: the UO_2 fuel itself and the Zircaloy cladding. Radionuclides within the UO_2 fuel are released by two mechanisms, which operate on very different time scales (Garisto et al. 2004b). First, radionuclides in the fuel/sheath gap, in fuel cracks and in grain boundaries are released rapidly after water contacts the fuel. Second, radionuclides trapped in the UO_2 fuel grains are released congruently as the fuel matrix dissolves. This relatively slow process controls the release of the major portion of the radionuclides in the fuel. Under the expected repository conditions, the fuel dissolution rate depends on the rate of production of oxidants by the radiolysis of water induced by radiation from the fuel (Appendix E, Garisto et al. 2004b). The fuel dissolution rate decreases with time as the strength of the radiation fields from the fuel decrease.

Radionuclides trapped in the Zircaloy cladding are assumed to be released congruently as the cladding dissolves. The cladding dissolution rate is calculated using a solubility-limited dissolution model, and dissolution continues until the cladding completely dissolves.

The reference container has a copper outer shell with a steel inner vessel for structural support. The lid of the steel inner vessel is bolted into place. The inner steel components of the container are not specifically included in the conceptual model, except for maintaining the void volume inside the container that connects to the defect in the copper shell. In practice, the steel components would corrode, producing H_2 gas and iron oxides. Although H_2 could substantially reduce the dissolution rate of the UO_2 fuel (Shoesmith 2008), this effect is not included in the present conceptual model. Similarly, formation of iron oxides would reduce the void volume of the container and provide a high surface area for adsorption of some of the radionuclides released from the fuel. In the present model, the possible effects of iron oxide formation are neglected. Omission of the effects of H_2 gas and iron oxides will generally lead to overestimation of radionuclide releases from the container.

6. HYDROLOGICAL MODELLING

6.1 INTRODUCTION

In this section we describe results from FRAC3DVS-OPG (Version 1.1, 64 bit), a three-dimensional (3-D) groundwater flow and transport model. This code is used to investigate the evolution of the groundwater flow domain over a single reference glacial cycle, the impact of a talik feature on groundwater flow, and the effect of multiple glacial cycles on the transport of radionuclides from a hypothetical defective container. FRAC3DVS-OPG is a quality assured version of the FRAC3DVS code used in the previous TCS and HBC studies.

Additionally, preliminary numeric studies were undertaken to assess the depth of glacial meltwater penetration, using the conservative assumption of constant density fluid. This preliminary work predicted that limited quantities of glacial meltwater could penetrate to the depth of the repository, but his deep infiltration is highly dependent on the presence of permeable fractures. The detailed results can be found in Walsh and Avis (2010).

The methodology focuses on detailed 3-D groundwater flow modelling and 3-D transport modelling for a single radionuclide (I-129). The study is limited to one hypothetical repository site, but looks at transport from hypothetical failed canisters at two separate locations within the repository footprint. The potential effects of the mechanical ice load on transient groundwater flows were included in the calculations through use of the 1-D hydromechanical coupling module in FRAC3DVS (Therrien et al. 2007). The study is referred to as the Glaciation SCenario (GSC) study model.

The radionuclide transport calculations are described in Section 7.

The total glacial response over the 1 Ma simulation period is produced by eight sequential applications of the single reference glacial cycle (see Section 3). The reference glacial cycle is described in Section 3 and is compared with the original glacial cycle derived by Peltier (2006) in Figures 3.4 and 3.6.

A major interest in this modelling project is the transient behaviour of the flow system occurring as a result of ice-sheet movement across the model domain (see Section 6.2.2) during ice-sheet advance and retreat periods. Ice sheet thickness data can be extracted from the stress data obtained from Simulation nn2778 (see Section 3), but the GSM results had insufficient spatial resolution to determine variation over the model domain. Therefore, a simplified model was selected where the transient ice-sheet profile was specified by an analytical model, as discussed in Section 3. The equation for the glacial surface profile is given in Equation 3.1 and the profile is shown in Figure 3.5.

6.2 MODEL CHARACTERISTICS

6.2.1 General Approach

The objective of the current modelling exercise is the assessment of sub-regional scale glacial cycle impacts. This requires the use of a transient flow model over the entire model domain to capture the changes induced by glacial cycling. In steady-state systems, fixed heads at vertical boundary nodes of the embedded transport model can be easily specified. However, for transient flow models the variable boundary conditions must be specified at each vertical boundary node of the model over the duration of the simulation.

The model developed for use in the Glaciation Scenario uses a horizontal grid resolution of 50 m in the vicinity of the repository, which increases to 100 m at the model boundary. This relatively coarse resolution precluded direct incorporation of repository features and required use of relatively large dispersivity values (longitudinal and transverse dispersivity values of 80 m and 8 m, respectively). These are acceptable compromises as the primary purpose of the current model is to examine the general features of flow and transport within the system. The greater dispersivity is a conservative assumption that enhances the rate of solute transport from the repository to the biosphere.

The GSC model domain is 13 km East to West and 20 km North to South. This domain is larger than that used in the earlier studies (Garisto et al. 2004a, 2005a), as shown in Figure 6.1. This change was made to increase the distance of the north and south boundaries from the repository, potentially reducing the impacts of model boundary conditions on modelling results near the repository. The north and south boundaries are the most important because the ice sheet is assumed to advance and retreat over the model domain in the north/south direction and a zero vertical gradient is imposed at this boundary in the Reference Case model. The model was further refined by making fracture zone permeability depth dependent.

In addition to the changes outlined above, a major difference between this and previous studies is the incorporation of simplified 1-D hydromechanical coupling in the model (Therrien et al. 2007). The FRAC3DVS hydromechanical (HM) coupling module, which is based on the work of Neuzil (2003), assumes purely vertical strain. This allows a great simplification of the hydromechanical analysis, allowing transient flow due to hydromechanical coupling to be fully represented by the fluid flow equation alone (Walsh and Avis 2010). Using this simplified expression implies that the horizontal gradients in fluid pressure and stress are small compared to the vertical gradients. These assumptions are reasonable for a relatively homogeneous and extensive vertical load, such as would occur underneath a glacier (Neuzil 2003). This assumption is not valid where vertical loads vary significantly within the model domain, as would occur during the early stages of a glacial advance when the ice terminus is within the model domain. However, the interval during which the ice terminus crosses the model domain is short (350 to 400 years during glacial advances, shorter during retreats). This means that for most of the time the one-dimensional HM model is reasonably accurate and provides an acceptable estimate of how transient glacial loading might impact the flow field and resulting transport solution.

Changes in geosphere permeability caused by the increased load and large-scale depression of the crust are similarly unaccounted for in the model.

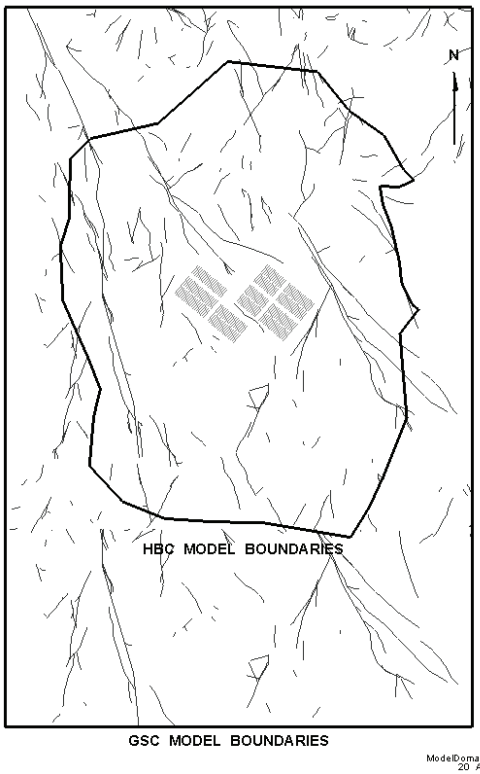

Figure 6.1: Model domain of GSC and earlier HBC models.

6.2.2 Model Domain

Figure 6.2 illustrates the model extent, surface topography, surface water features, fracture zones at the repository depth of -300 mASL (metres above sea level) or approximately 670 mBGS (metres below ground surface), and the location of the hypothetical repository emplacement drifts. As stated earlier, the model used a horizontal grid resolution of 50 m in the vicinity of the repository, which was increased to 100 m at the model boundary. For the vertical discretization the element thickness was generally 50 m, but thinner layers were used near the surface.

The lake above the eastern edge of the repository (called the North Lake) was identified in previous studies as a discharge zone and was the terminus of the shortest flow pathline from the repository. For the current study, the lake has been designated an open talik, under which permafrost conditions will not occur during permafrost periods. The larger lake roughly five kilometres south of the repository (called the South Lake), which was not present in earlier studies (Garisto et al. 2005a) has also been designated a talik, to examine whether multiple zones of discontinuous permafrost with different hydraulic potentials could cause significant flows during permafrost periods. For the majority of modelling scenarios the taliks are assumed to exist only during permafrost periods, and to freeze over when covered by ice. One calculation case examines the effect of areas of unfrozen ground in the sub-glacial permafrost.

6.2.3 Fracture Network

As in earlier modelling work (Garisto et al. 2004a, 2005a), the discrete fracture set from Srivastava (2002a,b) was used. However, below a Northing of roughly -2000 m, the fracture distribution was duplicated in order to extend the fracture system all the way to the model boundary. This provided a representative fracture system for this portion of the model domain that is consistent with the rest of the fracture system. The complex three dimensional fracture network used as a basis for the GSC model is illustrated in Figure 6.3.

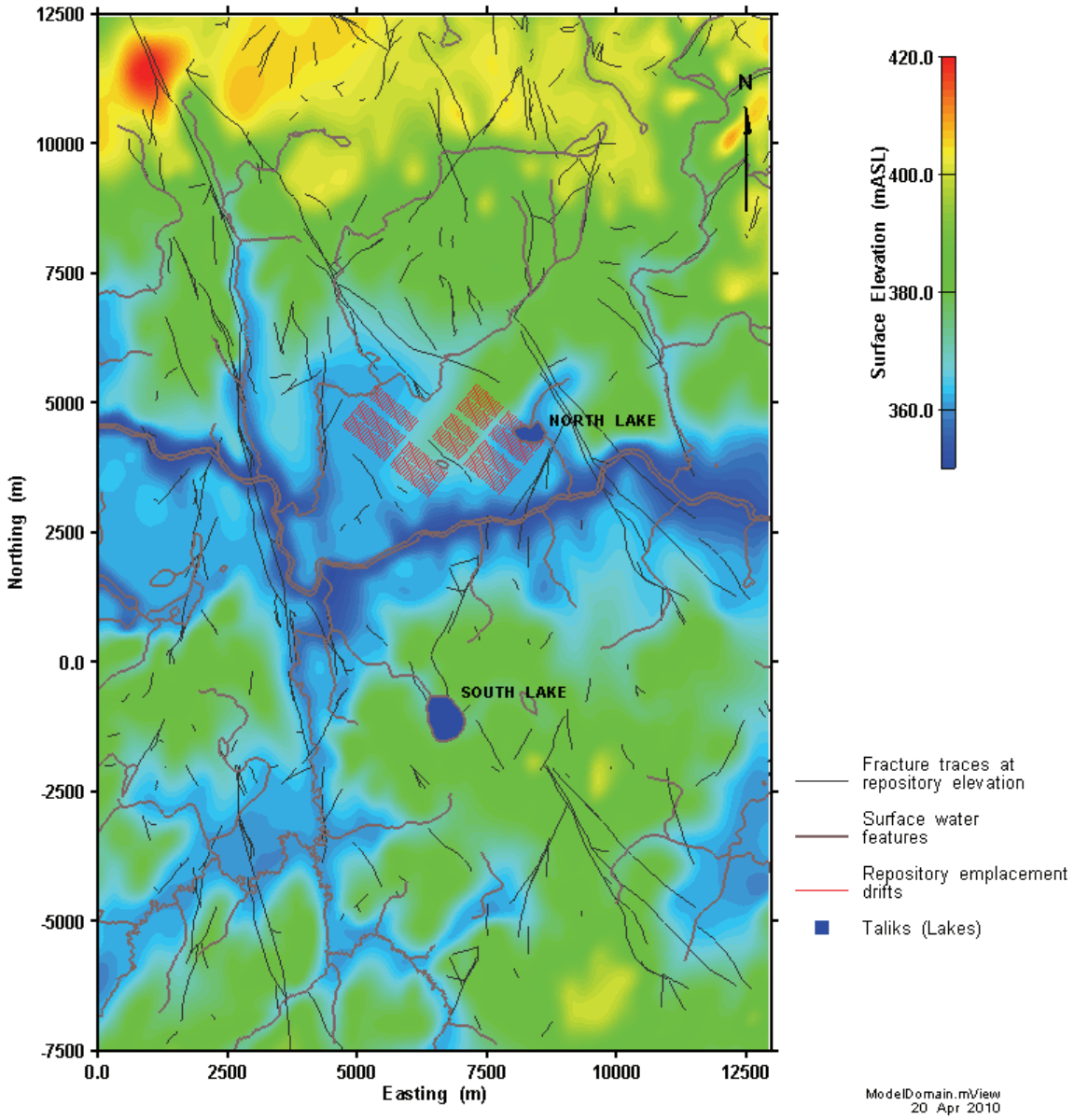

Figure 6.2: Glaciation flow and transport model domain. Note the two taliks, referred to as the North Lake (Northing ≈ 4500 m) and South Lake (Northing ≈ -1200 m)

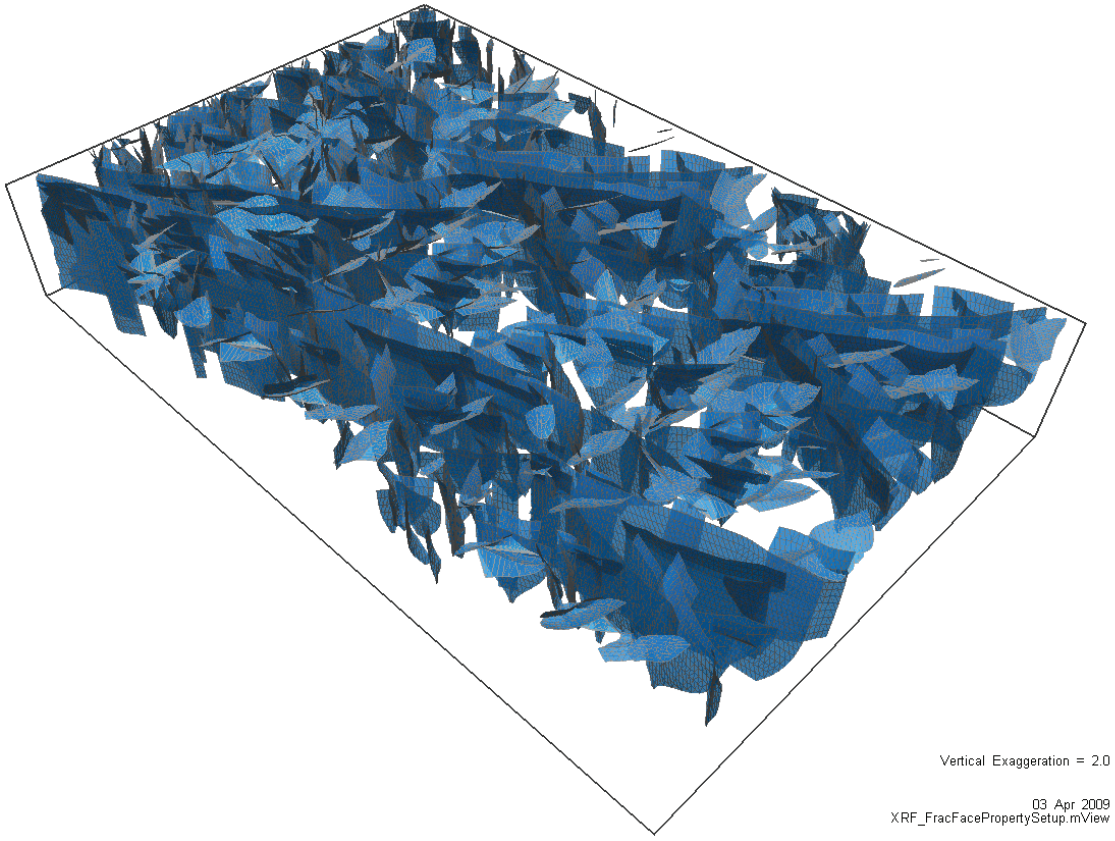

Figure 6.3: Fracture network realization for the GSC model.

6.2.4 Material Properties

At the Third Case Study site, the material properties of the rock are assumed to vary only vertically. The variation in material properties is represented as a series of horizontal layers with homogeneous and isotropic material properties within the layer. These layers span the entire model domain. The hydraulic conductivity values are based on the Case 2 permeability values described in Gierszewski et al. (2004a). Porosity of intact rock was set to 0.003 throughout the model domain, to be consistent with Garisto et al. (2005a). For the transient flow model, the storage coefficient defines the speed of the time dependent response of the flow system. The one-dimensional storage coefficient (which assumes uni-axial strain, Neuzil (2003)) was calculated as described in Walsh and Avis (2010). Hydraulic conductivities and storage coefficients for the model layers are shown in Table 6.1. These are the only parameters that vary between layers.

The final material property to be defined is the one-dimensional loading efficiency. This term is analogous to Skempton's coefficient, but is valid for the assumption of uni-axial strain (Neuzil 2003). In order to maintain consistency with the work of Chan and Stanchell (2008), a loading efficiency of approximately one third was selected (Walsh and Avis 2010).

Table 6.1: Material properties that vary between flow model layers.

Depth Range*	Hydraulic Conductivity (m/s)	Storage Coefficient (m^{-1})
Ground Surface to 10 mBGS	7.00E-07	3.63E-07
10 to 70 mBGS	7.00E-08	3.63E-07
70 to 150 mBGS	8.00E-10	3.63E-07
150 mBGS to 75 mASL	7.00E-11	1.97E-07
75 to -125 mASL	3.00E-11	3.18E-08
-125 to -325 mASL	7.00E-12	3.18E-08
-325 to -1225 mASL	1.00E-12	3.18E-08

*Near surface layers follow topography. Ground surface is at about 350 mASL.

6.2.5 Fracture Properties

The layer permeabilities are modified to account for the existence of fracture zones in the model domain. Earlier work used a constant value for fracture permeability, but the current model uses a depth dependent fracture zone permeability. The fracture zone permeability function was defined according to the work done by Normani et al. (2007). Permeability values were based on the 50^{th} percentile fracture permeability (Normani et al. 2007). The impact of this change on radionuclide mass flows to the biosphere is relatively minor, as discussed in Walsh and Avis (2010).

Fracture information was incorporated into the model through the equivalent porous medium (EPM) approach (Walsh and Avis 2010). The equivalent porous medium hydraulic conductivity of elements containing fractures is variable and anisotropic. Figure 6.4 shows the depth dependent hydraulic conductivity profiles of the intact rock, the discrete fractures (from Normani et al. 2007), and the average EPM vertical hydraulic conductivity of elements intersected by fracture zones. Figure 6.5 shows the spatial distribution of hydraulic conductivity within the model domain. Note the blended hydraulic conductivities used for modelling fracture zones as EPM elements.

6.2.6 Permafrost Implementation

Permafrost is modelled by modifying the hydraulic conductivity of all materials above a given depth to 10^{-13} m/s. The depth of the continuous permafrost varies between 100 and 250 m, depending on the permafrost period (see Figure 3.8). During permafrost periods, model cells underlying the talik are not modified, that is, they retain their original permeability. Figure 6.6 shows the assigned hydraulic conductivities during a permafrost period with 250 m deep permafrost, and two open taliks.

The implementation approach, described in preceding sections, couples flow regimes by nodal head at each sequence transition. As a consequence, the transition between permafrost and non-permafrost states is instantaneous. This is clearly not realistic, as permafrost will develop from surface down over a period of time. However, the instant application of permafrost is a simplifying assumption that will not substantially alter the resulting flow domain over longer time periods.

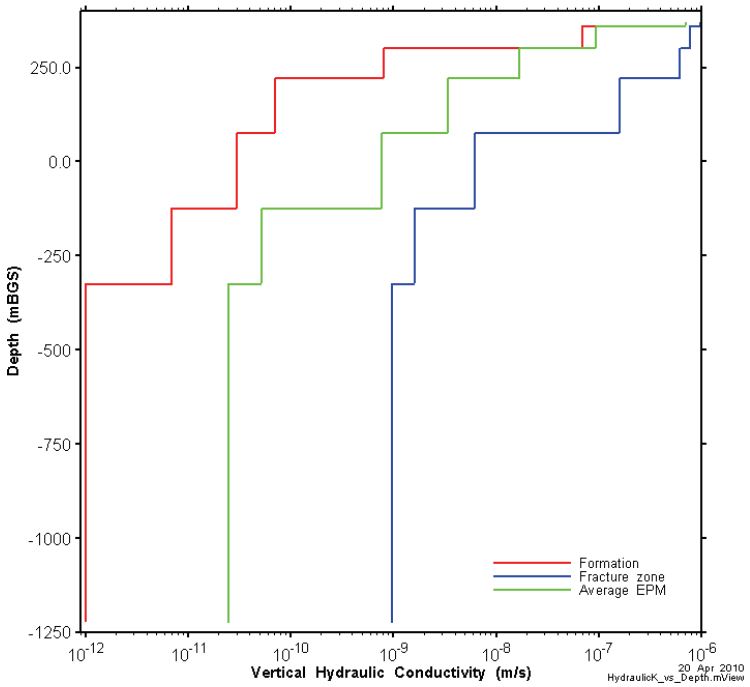

Figure 6.4: Vertical hydraulic conductivity profiles for rock formation, fracture zone and EPM elements.

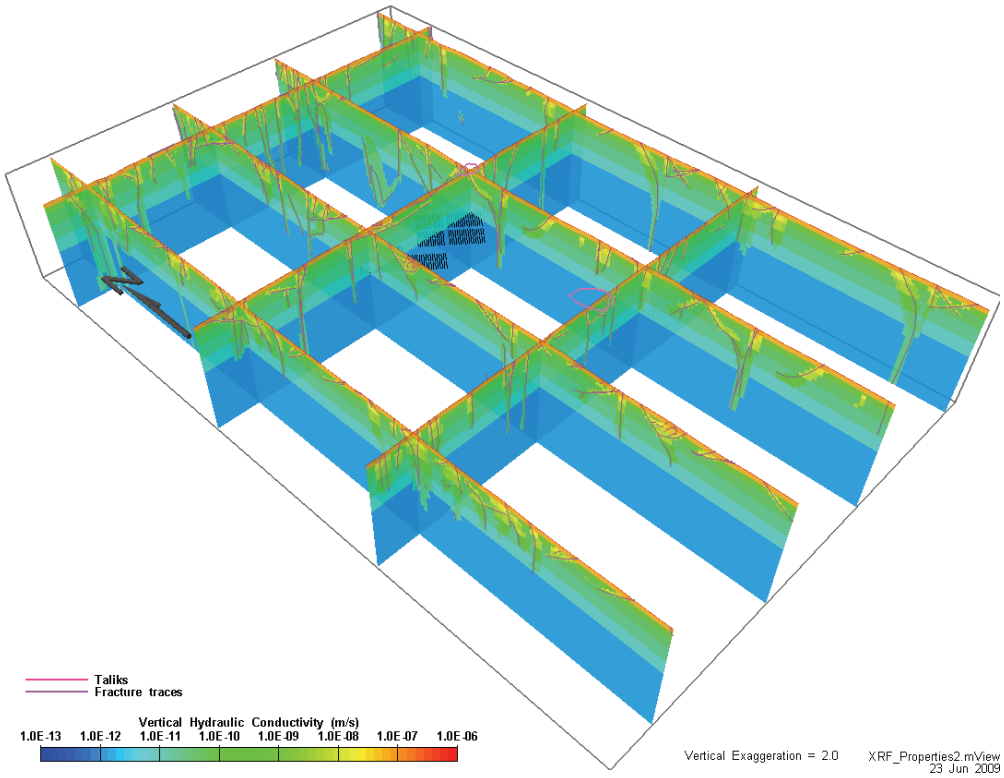

Figure 6.5: Geosphere hydraulic conductivity distribution during temperate periods.

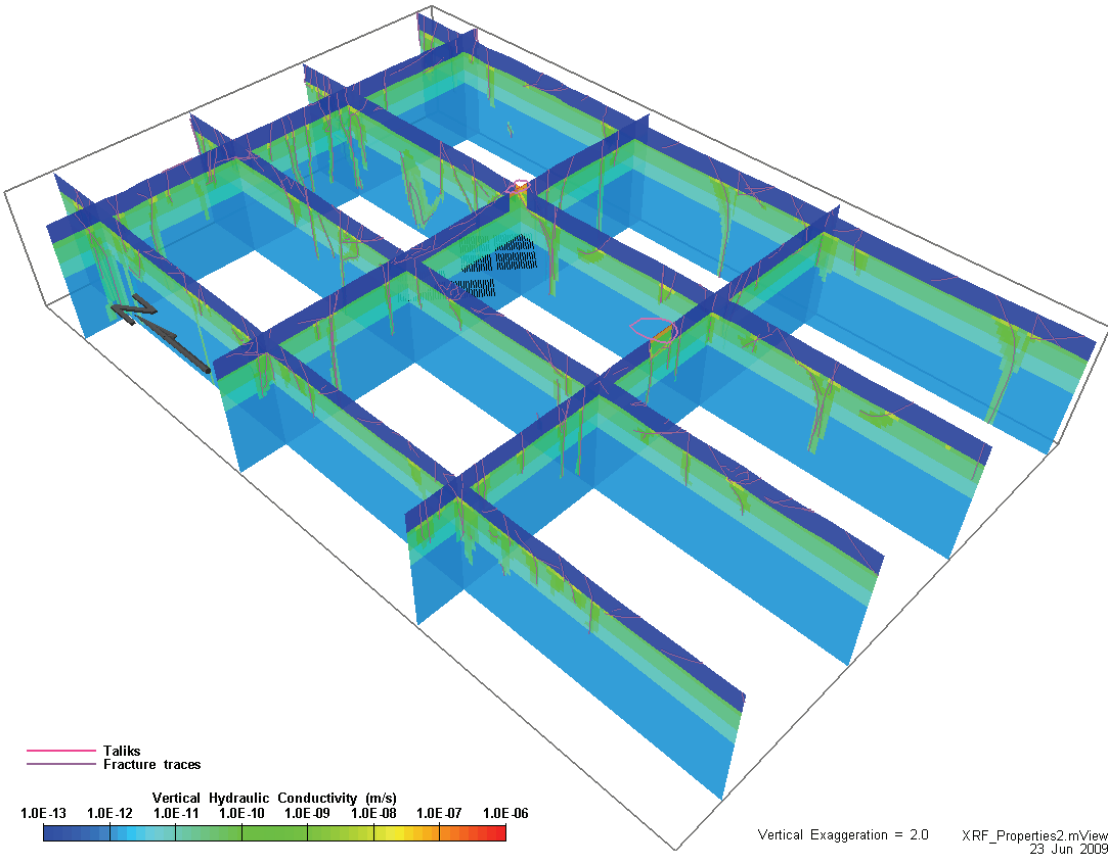

Figure 6.6: Geosphere hydraulic conductivity distribution during permafrost periods, with 250 m deep permafrost and two open taliks.

6.2.7 Boundary Conditions

The bottom boundary is zero flow.

The continental glacier was assumed to traverse the model domain from North to South, with relatively little variation in thickness (and therefore hydraulic pressure) in the East-West direction. Therefore, the East and West boundaries were set as zero flow.

For the Reference Case, the North and South boundaries were modelled as constant head boundaries, with the head set equal to the head at the surface. This allows horizontal flow into and out of the model domain, and implicitly assumes that the vertical hydraulic gradient is zero at these boundaries. The advantage of having such a boundary condition is that it allows the pressure gradients caused by the glacier to push water ahead of it as it advances. This process could enhance radionuclide transport, and is therefore of interest. To ensure that these boundary conditions do not have an undue effect on the model results, a calculation case with no-flow Neumann boundary conditions on all boundaries (except the surface) was undertaken. The fixed head and no-flow boundary conditions are bounding bases, with the true behaviour of such a system likely falling between these two extremes.

Boundary conditions at ground surface are fixed hydraulic head at ground surface elevation for all temperate and permafrost periods. During the proglacial lake periods, hydraulic head at the surface is uniform across the model domain and is set equal to the elevation of the lake surface. During periods of ice cover, the surface boundary heads are transient with variable pressure head calculated to reflect the ice load over the site as glaciers advance and retreat (Walsh and Avis 2010). Below the ice sheet it is assumed that free water exists over the ground surface and recharges to or discharges from the hydrogeologic system. The pressure head at ground surface was determined from the ice-load, calculated as the ice thickness multiplied by ice density (assumed 900 kg m^{-3}). During cold-based glaciation stages, the hydraulic connection between the glacier and underlying geosphere is severely impeded by the presence of continuous permafrost.

Rather than using a perfectly smooth glacial profile as depicted in Figure 3.5, a smoothed surface which reflects a 50% moderation of the topographic variation was created. In nature, the surface elevation and subsurface hydraulic head may not closely track the subsurface topography (Gogineni et al. 2001). However, with a perfectly smooth ice surface, the resulting hydraulic pressure distribution would have caused relatively stagnant flow underneath the ice sheet, with very few local flow systems. The presence of drainage channels beneath glaciers requires some variation in subsurface hydraulic heads and the presence of local flow fields. Although using a moderation of the surface topography is not strictly correct, it is a simple way to allow local circulation systems to exist under the glacial ice. This will tend to enhance spreading and transport beneath the glacier, particularly during the later stages of ice advance, or early stages of ice retreat, when the glacial slope is low.

Figure 6.7 shows the boundary condition heads at various times during a glacial advance along a North-South transect through the site. Times shown on the figure represent time since the start of the ice-sheet advance sequence. Profiles for later ice sheet advances have the same overall shape, although the advance rates are slightly different and the maximum ice depths are greater (see Figure 3.7). For ice-sheet retreats, the profile is the same but reversed in time.

6.2.8 Water Supply Well

The GSC model includes a water supply well that is only active during the Temperate State of each glacial cycle. The well is approximately 100 m deep and uses a constant pumping rate of 738 m^3 a^{-1}. It is conservatively located, next to the North Lake, so as to intercept the radionuclide plume from defective containers at location DC1 (see Figure 7.3). Groundwater travel times from the repository to the surface are shortest for the DC1 repository location in the Constant Climate Scenario described below.

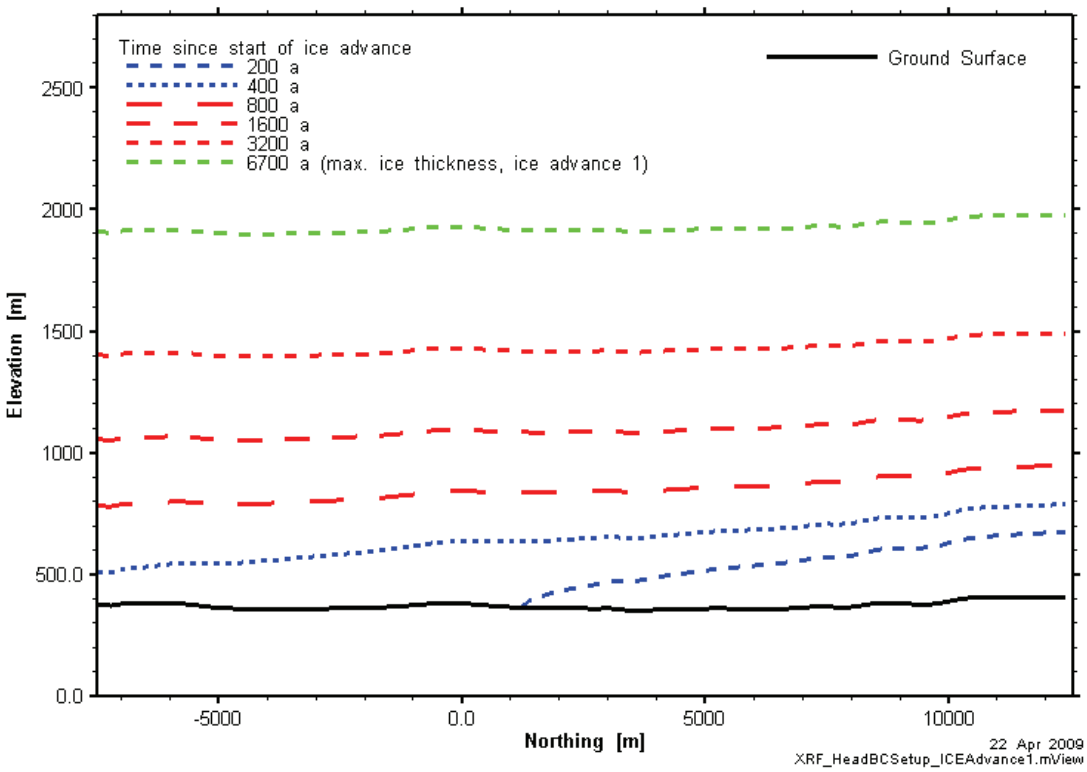

Figure 6.7: Ice surface boundary condition heads during the first glacial advance.

6.3 MODELLING CASES

Detailed groundwater modelling was performed for a reference case (RC) model and for a number of parameter and conceptual model sensitivity cases. The RC model may be summarised as follows:

- Transient model, with sequential variations in climate and boundary conditions simulating periods of temperate, permafrost, ice sheet (with and without permafrost), and proglacial lake conditions;
- During permafrost periods, two taliks are left open (since permafrost is represented by areas where the permeability is reduced to simulate frozen ground, the taliks are represented by areas where the permeability is not reduced);
- During periods where glacial ice is advancing over permafrost, taliks are frozen over; and
- Constant density water flow.

Modelling sensitivity cases have been defined to assess the sensitivity of model predictions to alternate boundary conditions, geosphere properties, or long term climate conditions. Table 6.2 describes all the defined sensitivity cases.

For the GSC-CC case, there were two versions - with and without a well. The presence or absence of a well significantly affects the surface discharge locations of radionuclides released from the repository.

For the GSC-HS case the storage coefficient was increased by an order of magnitude throughout the model domain while all other parameters were held constant.

Table 6.2: Modelling sensitivity cases.

Model Name	Abbreviated Name	Description
Reference Case	GSC-RC	As described in Section 6.3
Constant Climate Scenario	GSC-CC	Temperate state conditions persist for the entire assessment period. This is a steady-state flow model. Useful for understanding the influence of glaciation on radionuclide mass flows to the biosphere.
High Storage Coefficient	GSC-HS	Geosphere storage coefficients increased by one order of magnitude throughout model domain. Used to study the importance of system response time on the results.
No-Flow N-S Boundaries	GSC-NF	Boundary conditions at the North and South vertical boundaries changed from specified head boundaries to no-flow boundaries. All other boundary conditions remain unchanged. Studies the influence of boundary conditions on the results.
“Talik” under Glacier	GSC-TK	Existing taliks remain open when ice is advancing over permafrost (see Table 3.2). Used to explore the impact of a regions of unfrozen ground in the sub-glacial permafrost on flow and transport.

6.4 GLACIAL SEQUENCE MODELLING RESULTS

6.4.1 Head and Velocity Distribution

Chronologically ordered visualizations of flow model results in this section show the transient nature of the flow system response over a single glacial cycle. The figures portray results on a vertical cross-section on a North-South transect (the direction of glacial advance) cutting through the North talik that is above the repository. The location of this cross-section is shown in Figure 6.8. The figures on the following pages present head contours at several different scales over different head magnitudes, as well as velocity vectors and advective velocity magnitude as a colour field. The large variation in hydraulic head at different times means that the hydraulic head range varies between figures. The advective velocity scale is maintained constant between all figures.

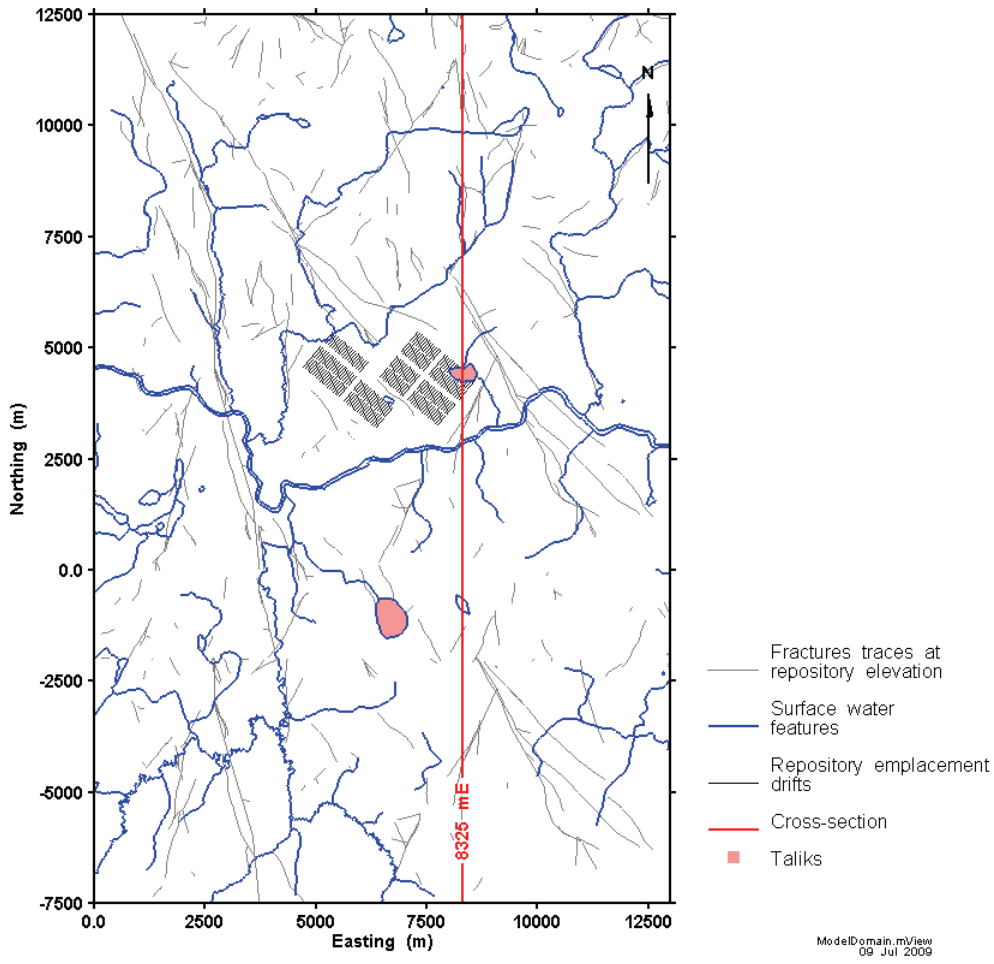

Figure 6.8: Location of cross-section line

6.4.1.1 Reference Case

Figure 6.9 illustrates the steady-state flow domain that exists during the initial temperate period. During this stage, the head boundary condition is equal to the surface elevation, so flow is topographically driven. This results in small-scale flow circulation systems, with the vast majority of flow occurring in the more permeable shallow system. There is some minor flow at greater depths, particularly within the fracture system. (As noted earlier, these results do not include any salinity effects.)

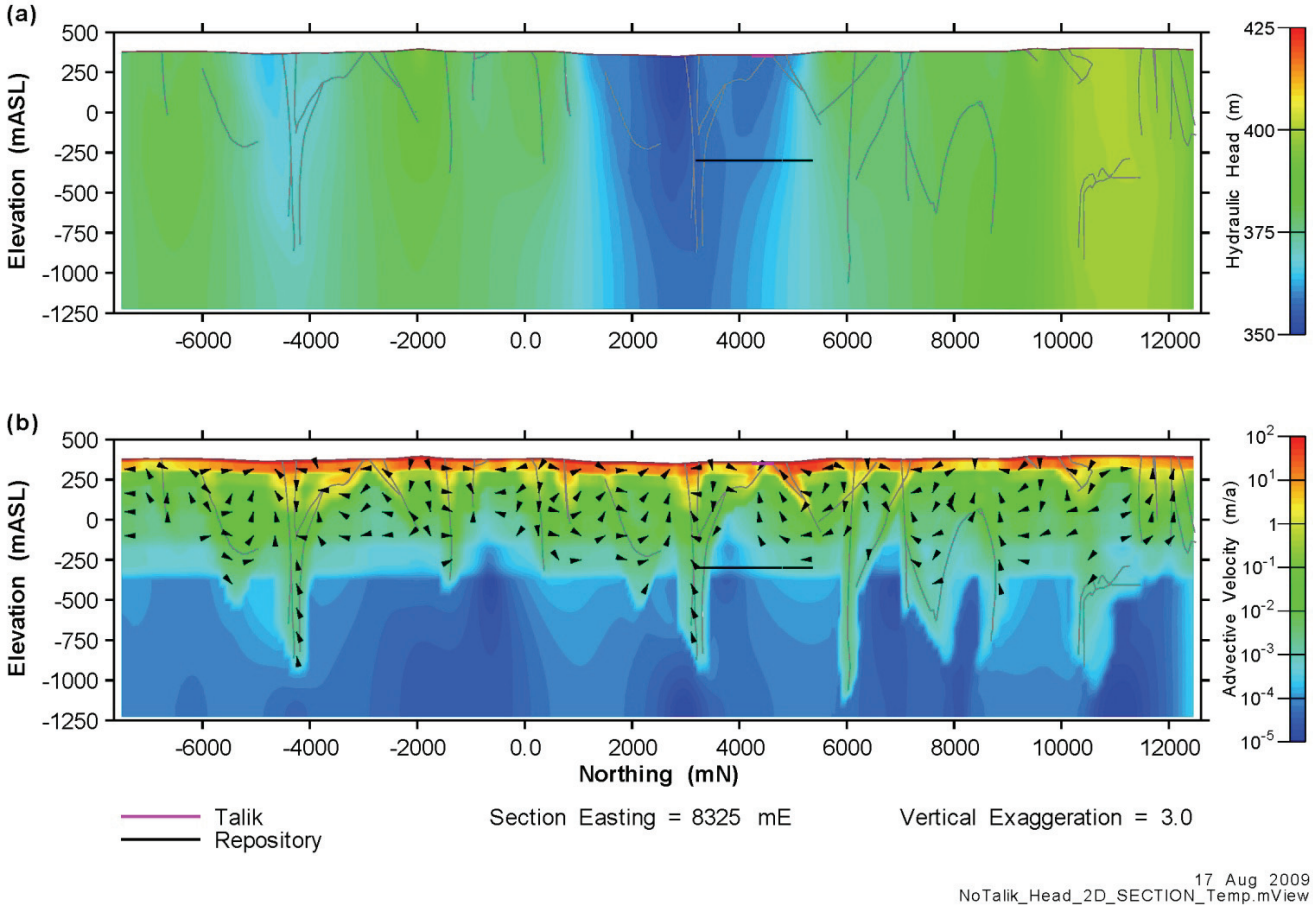

Figure 6.9: GSC-RC flow model results during initial temperate phase (stage 1 – temperate). The hydraulic head distribution is shown in (a), while the advective velocity distribution is shown in (b). Velocity vectors are plotted where the velocity exceeds 1 mm/a.

Figure 6.10 shows the flow field 300 years into the first glacial advance. At this time, ice largely covers the model domain, except for the southernmost 2000 m. The subsurface below the glacier is significantly pressurized. This pressurization comes from two sources, namely the hydromechanically induced pressures in the subsurface and the fixed head hydraulic boundary condition on the northern boundary. The boundary condition causes an instant pressurization on the right hand boundary. Throughout the remainder of the model domain, the transmission of heads from surface to depth is dampened by storage effects. The overall impact of the advancing glacial front is to cause predominantly southward flows below the permafrost and above approximately -125 mASL.

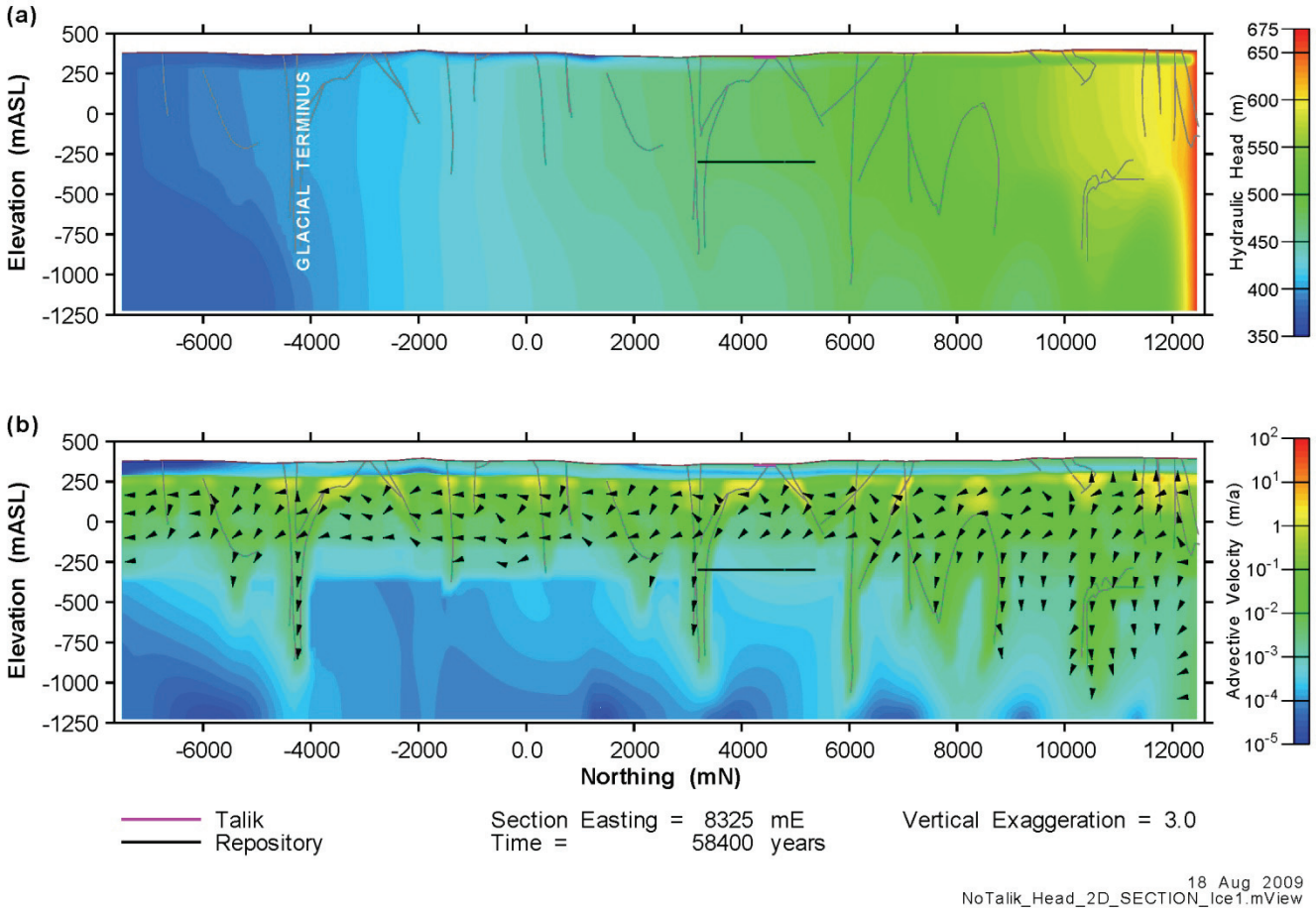

Figure 6.10: GSC-RC flow model results at 58,400 years (beginning of stage 3 – ice advance, cold based glacier). The hydraulic head distribution is shown in (a), while the advective velocity distribution is shown in (b). Velocity vectors are plotted where the velocity exceeds 1 mm/a.

Figure 6.11 shows the head and velocity contours during the first glacial retreat. In this cold-based retreat, the only hydraulic outlets for stored, glacially-induced heads are the northern and southern boundaries. This leads to a rather unusual flow regime, with divergent flow from the center of the model towards the northern and southern boundaries. In the vicinity of the repository, the flow direction is vertically upward toward the more permeable layers. For this particular period, no-flow boundaries around the entire model domain might provide more realistic results. However, the major flow-system discrepancies are limited to the near-boundary area. Flow within the centre zone of the model where transport occurs is likely representative.

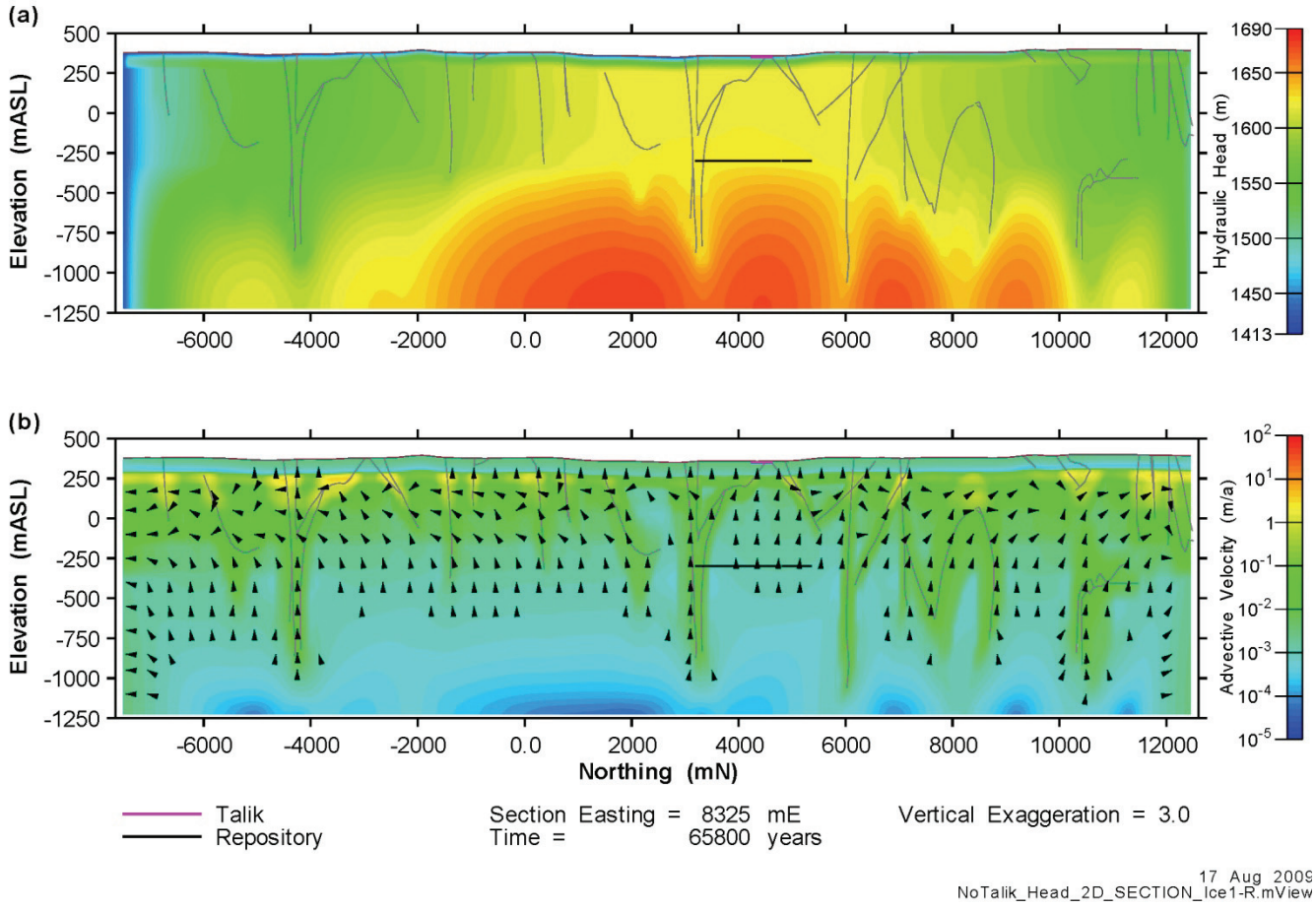

Figure 6.11: GSC-RC flow model results at 65,800 years (midpoint of stage 4 – ice retreat, cold based glacier). The hydraulic head distribution is shown in (a), while the advective velocity distribution is shown in (b). Velocity vectors are plotted where the velocity exceeds 1 mm/a.

Figure 6.12 shows an intermediate transition period approximately 2000 years after the start of the second permafrost sequence. After 2000 years, elevated heads caused by the relatively rapid glacial retreat remain at greater depths, especially where there are no fracture zones to provide drainage. Impermeable permafrost covers most of the surface, locking in the pressure and directing flow towards the only hydraulic outlets of the system, the North-South boundaries and the two taliks. The North talik, above the repository, is at a lower elevation than the southern talik, and consequently a larger proportion of the flow is focused here. (Note that the southern talik is not intersected by the cross-section in Figure 6.12.)

In the transport results, this flow into the North talik leads to a significant increase in the I-129 mass flow into this talik (see Section 7). In fact, for source location DC1 (see Figure 7.3), the I-129 mass flows into the North talik are highest at the beginning of the second permafrost period in each glacial cycle (see Section 7). This occurs because the preceding glacial retreat is cold based (i.e., a continuous permafrost layer is still present under the glacier) and the high pressures induced by the ice load are unable to dissipate out the top of the model.

The high pressure zone seen at the top right of Figure 6.12 (a) is an artefact caused by the instantaneous application of permafrost down to a depth of 250 m. This traps some relatively high hydraulic heads in the low-permeability permafrost zone. These heads take some time to dissipate, but have a minor effect on the flow field in the underlying more permeable zones.

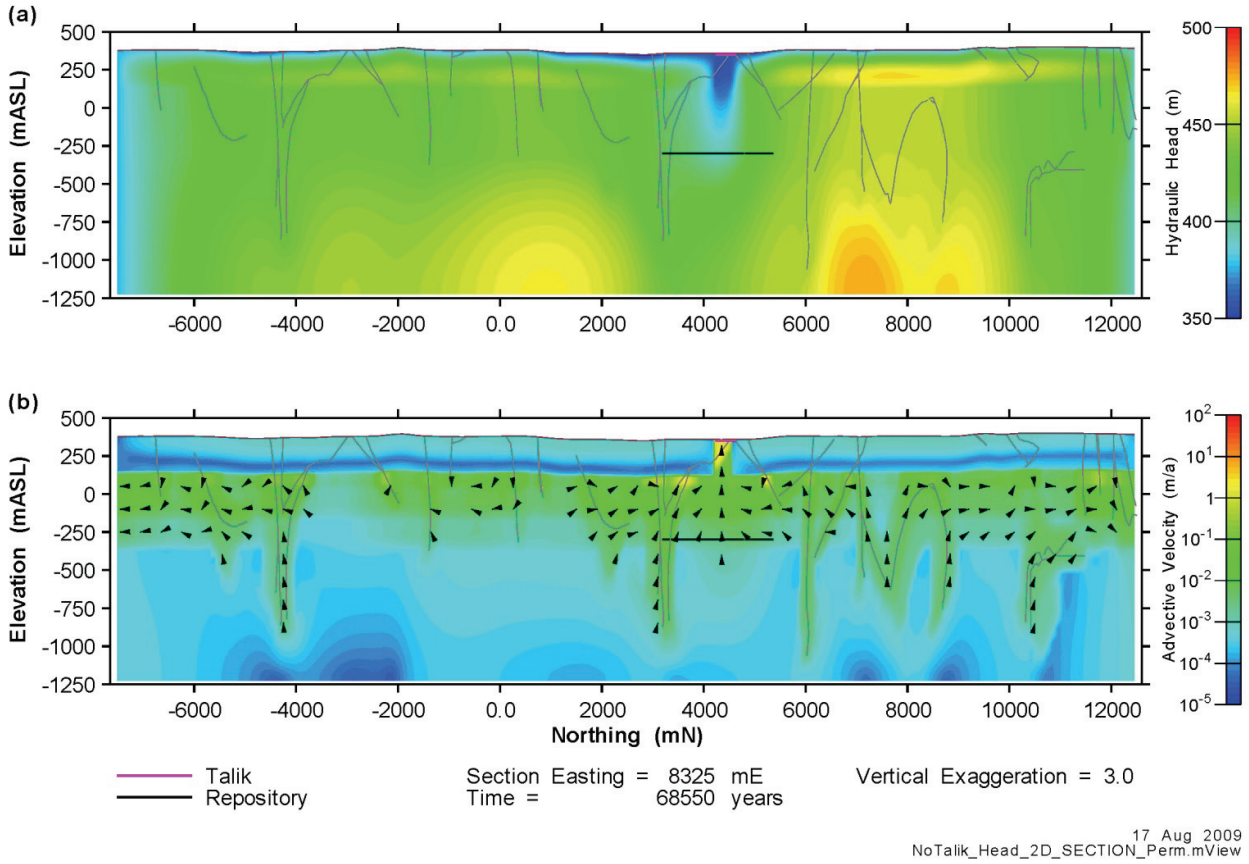

Figure 6.12: GSC-RC flow model results at 68,550 years (start of stage 5 – permafrost). The hydraulic head distribution is shown in (a), while the advective velocity distribution is shown in (b). Velocity vectors are plotted where the velocity exceeds 1 mm/a.

Figure 6.13 shows the flow field at a time near the end of the second permafrost period. The system has long since reached a steady state. Head gradients at depth have been reduced as water has been released from the system. Flow in the less permeable parts of the model (below -300 mASL and within the permafrost) is effectively stagnant. In the more permeable zones between the permafrost and deeper low-permeability rock some flow persists. This flow is driven by the specified hydraulic heads at the North-South boundaries and the two taliks. As the North talik has the lowest fixed hydraulic head within the model, it serves as the primary hydraulic outlet, meaning that the flow converges on this talik. Consequently, the overall groundwater flow and radionuclide mass transport rates through the talik remain high relative to other stages in the glacial cycle.

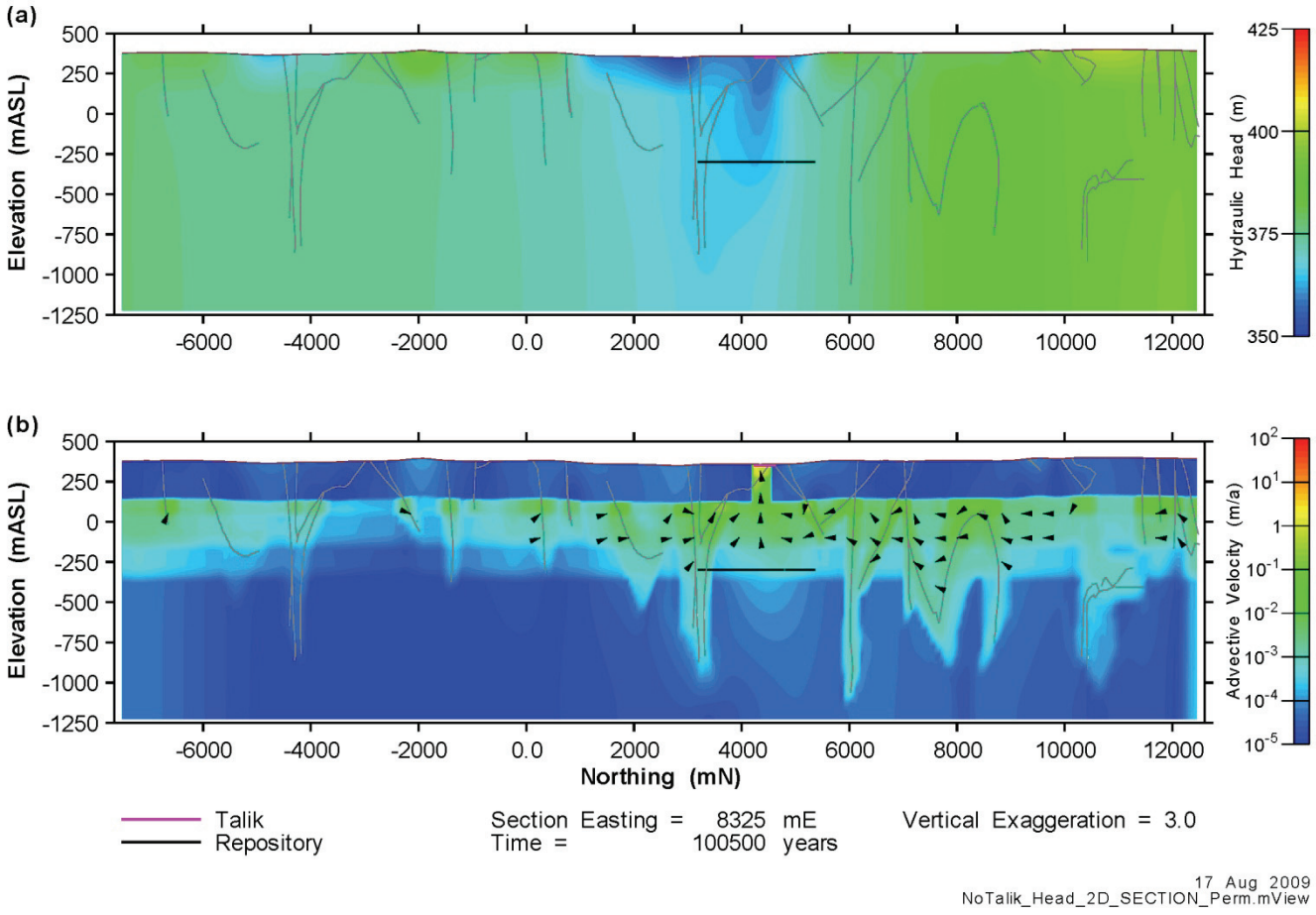

Figure 6.13: GSC-RC flow model results at 100,500 years (end of stage 5 – permafrost). The hydraulic head distribution is shown in (a), while the advective velocity distribution is shown in (b). Velocity vectors are plotted where the velocity exceeds 1 mm/a.

Figure 6.14 shows the flow field at the midpoint of glacial stage 10, a warm-based glacial advance. Ice covers the entire model domain, with a depth of approximately 2.2 km. This flow field contrasts with that shown in previous figures largely because the glacier is now warm-based, with no permafrost barrier impeding the transmission of the very high hydraulic heads at the base of the glacier, and the ice sheet is significantly thicker. In the shallow system, flow is driven by the topography of the ice-sheet elevation boundary condition. At the elevation of the repository and deeper, the low rates of flow are directed downward toward under-pressurized zones at greater depth.

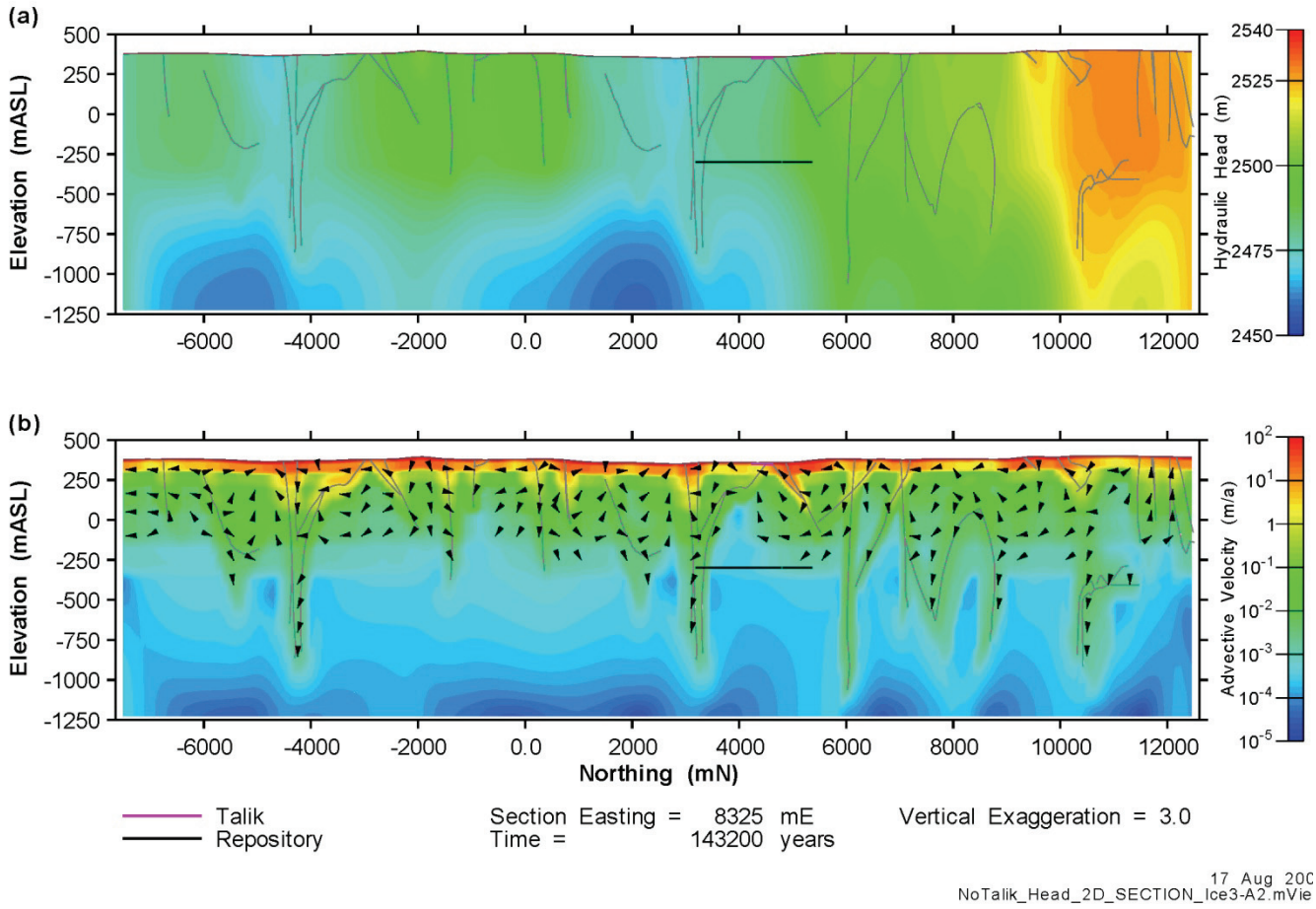

Figure 6.14: GSC-RC flow model results at 143,200 years (midpoint of stage 10 – ice advance, warm based glacier). The hydraulic head distribution is shown in (a), while the advective velocity distribution is shown in (b). Velocity vectors are plotted where the velocity exceeds 1 mm/a.

Figure 6.15 shows the flow field near the end of stage 11, during a warm-based glacial retreat stage. Ice still covers the entire model domain, but the ice thickness and therefore the specified heads at the surface have dropped relatively rapidly from their peak values. This leads to a reversal of the prevailing downward flow direction during the preceding ice advance stage. High hydraulic heads remain stored in the deeper, less permeable system while the heads at the surface have dropped rapidly. Consequently, below roughly 200 mASL the predominant flow direction is vertically upward.

Above 200 mASL, the flow direction shifts to predominantly horizontal and southward. This is caused by the slope of the retreating ice sheet on the surface. So, although the flow from the repository is vertically upward with a velocity of millimetres to centimetres per year, very little radionuclide actually reaches the North talik at this stage, as the plume above the repository is swept to the south and diluted (see Section 7).

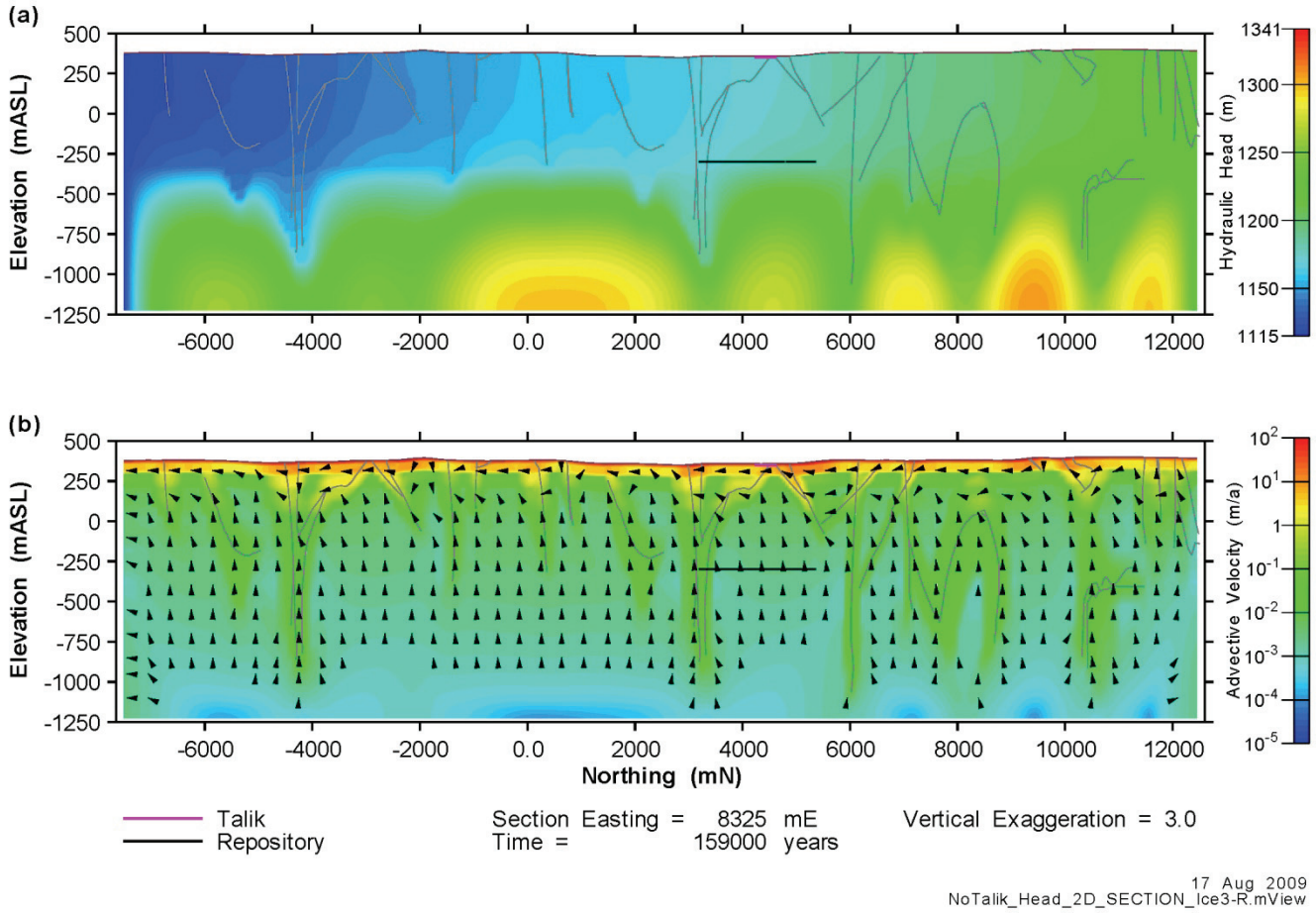

Figure 6.15: GSC-RC flow model results at 159,000 years (end of stage 11 – ice retreat, warm based glacier). The hydraulic head distribution is shown in (a), while the advective velocity distribution is shown in (b). Velocity vectors are plotted where the velocity exceeds 1 mm/a.

Figure 6.16 shows the flow field midway through stage 12, at which time a constant head boundary of 540 m is applied at the surface to simulate a proglacial lake. Water is still being released from storage in the deeper formations, driving flow vertically upward throughout the model domain. The stored overpressures persist into the following temperate period, finally returning to the initial steady state flow field 3500 years after the end of stage 12 (at approximately 164,200 years).

Because the groundwater flow system attains a steady state during temperate periods, the flow fields of the subsequent glacial cycles required to reach the end of the performance period are identical to those described above.

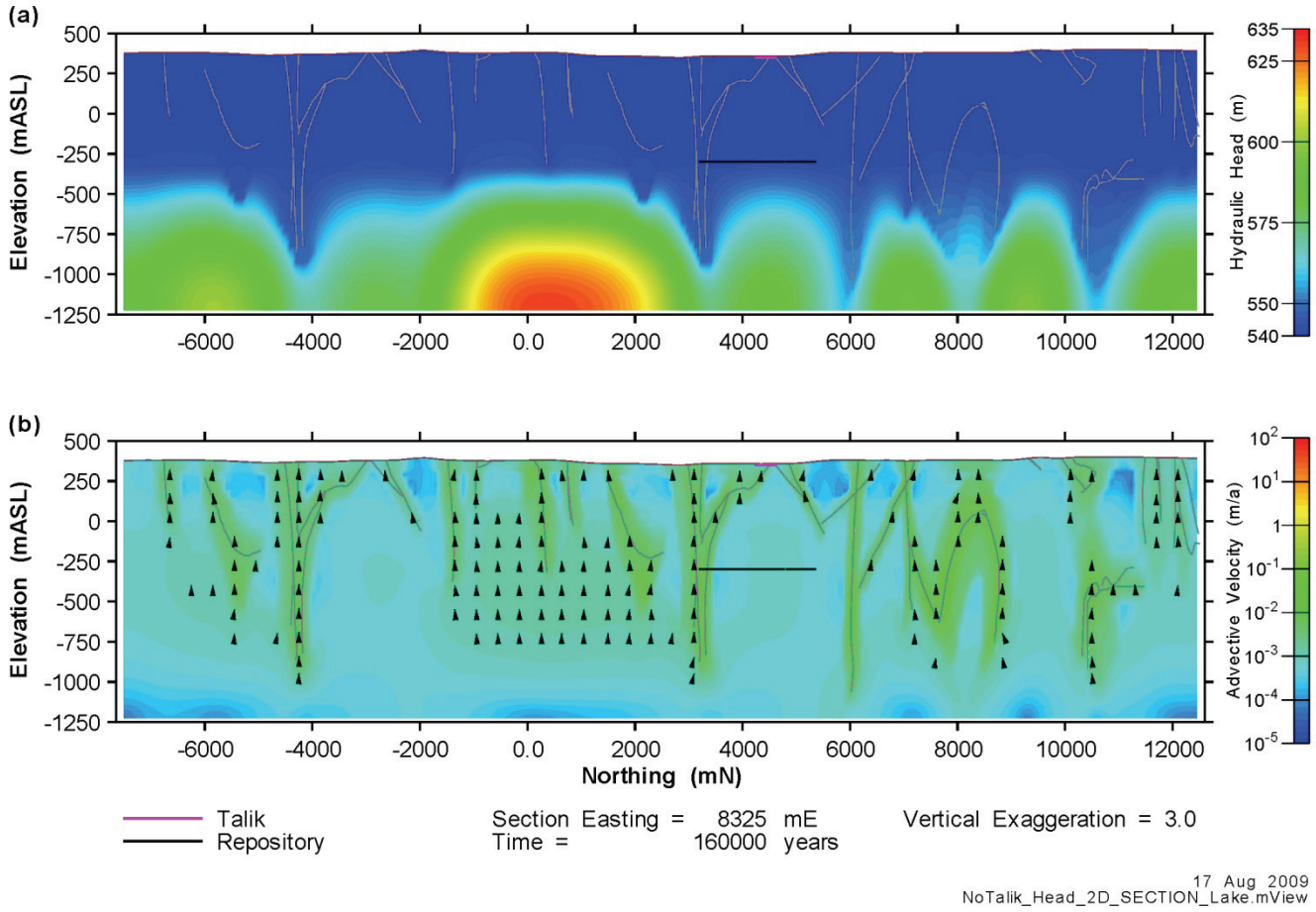

Figure 6.16: GSC-RC flow model results at 160,000 years (midpoint of stage 12 – pro-glacial lake). The hydraulic head distribution is shown in (a), while the advective velocity distribution is shown in (b). Velocity vectors are plotted where the velocity exceeds 1 mm/a.

6.4.1.2 High Storage Coefficient Case

The High Storage Coefficient Case (GSC-HS) is identical to the reference case, with the exception that storage coefficients throughout the model were increased by one order of magnitude. The higher storage coefficient causes a delay in the reaction of the system to changes in boundary conditions. Hydraulic head in the system increases more slowly during glacial advances than in the GSC-RC. Conversely, when the ice retreats the glacially induced overpressures in the subsurface persist for a longer time. During permafrost periods the onset of steady state conditions is delayed. As an example, Figure 6.17 shows the head distribution below the advancing ice sheet 300 years into the first glacial advance. In comparison to Figure 6.10, the high hydraulic heads produced by the glacier and the northern hydraulic boundary have not penetrated as far into the model domain. Overall advective velocities are somewhat lower throughout the model domain and within the repository footprint.

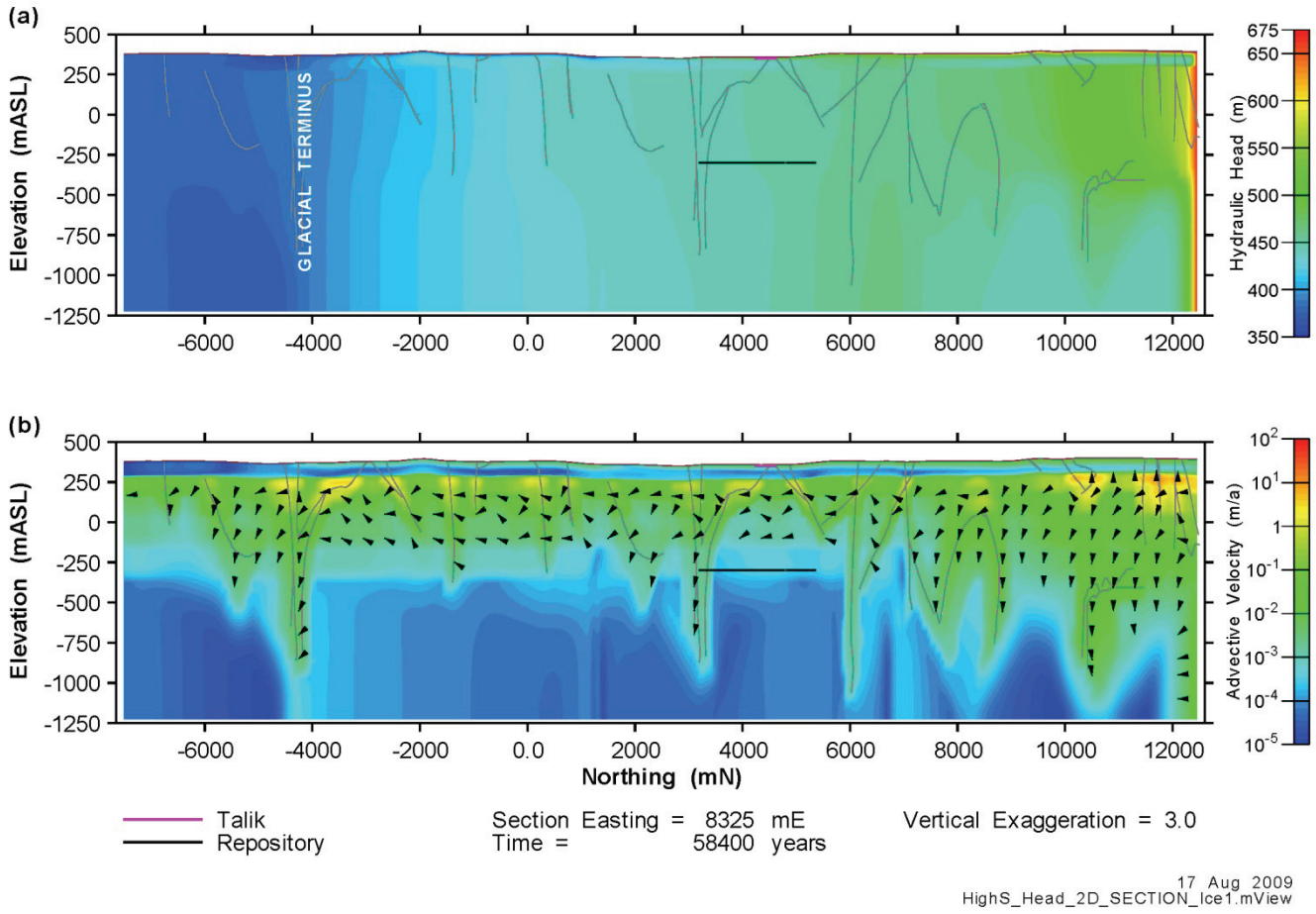

Figure 6.17: GSC-HS flow model results at 58,400 years (beginning of stage 3 – ice advance, cold based glacier). The hydraulic head distribution is shown in (a), while the advective velocity distribution is shown in (b). Velocity vectors are plotted where the velocity exceeds 1 mm/a.

Comparing results at 68,550 years, the start of the second permafrost stage (GSC-HS in Figure 6.18, GSC-RC in Figure 6.12), the effect of the higher storage coefficients is reversed. In the GSC-HS model significantly higher hydraulic heads remain stored in the deep geosphere, driving much higher flow rates and flow velocities throughout the model and within the repository footprint itself. The thin layer of high hydraulic potential at the top of the model in Figure 6.18 is an artefact in the model caused by the instantaneous application of low permeability permafrost down to a depth of 250 m. This traps pressurized water in this upper zone. This is not realistic, but has a minimal effect on the flow field in the more permeable units below, as shown by the hydraulic head and velocity distributions. Flow from this permafrost zone is very low in comparison to the volumes of flow in the unfrozen formations below the permafrost.

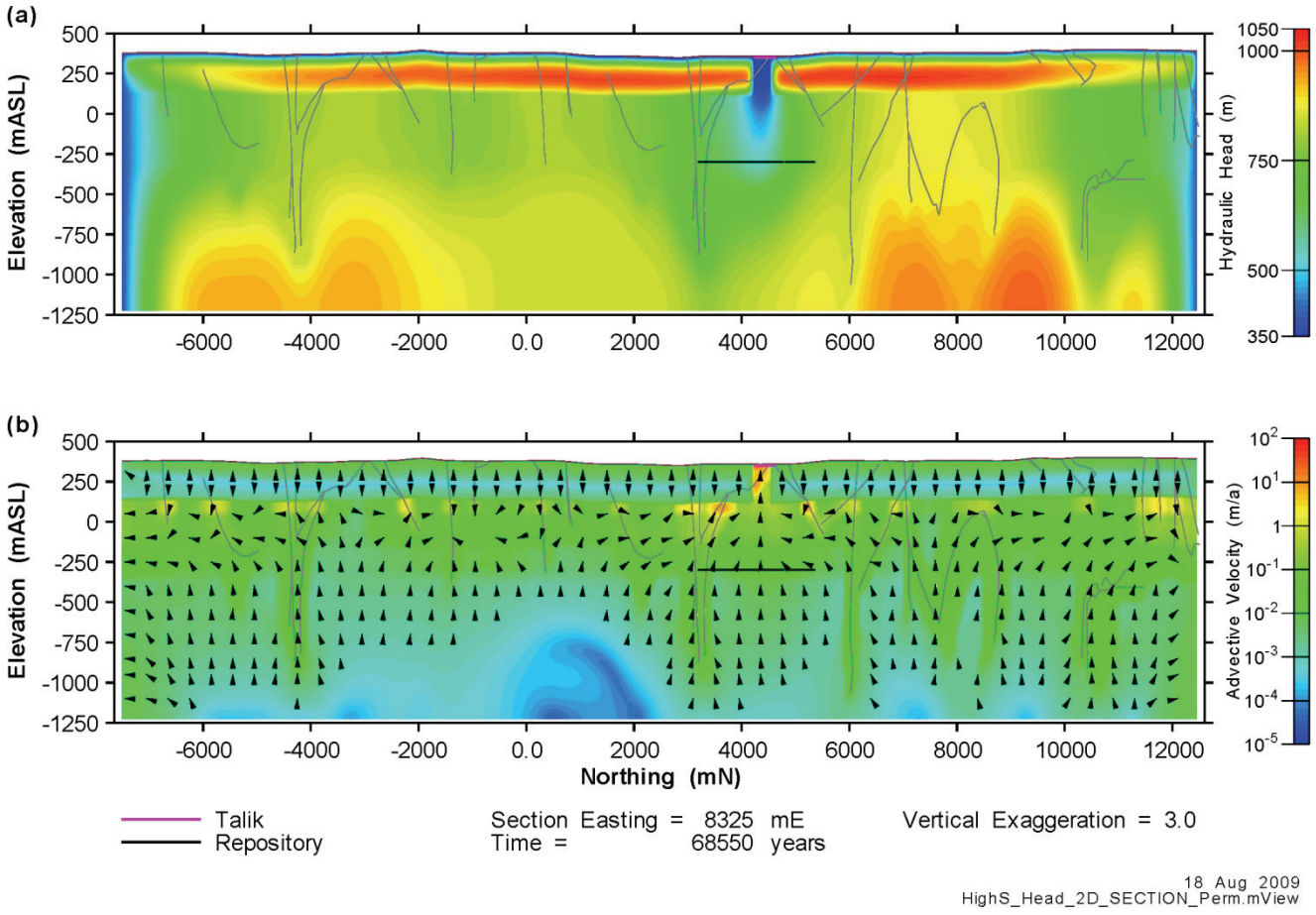

Figure 6.18: GSC-HS flow model results at 68,550 years (start of stage 5 – permafrost). The hydraulic head distribution is shown in (a), while the advective velocity distribution is shown in (b). Velocity vectors are plotted where the velocity exceeds 1 mm/a.

6.4.1.3 No-Flow North-South Boundaries Case

The No-Flow North-South Boundaries Case (GSC-NF) differs from the reference case (GSC-RC) in that the North and South boundaries are no-flow boundaries. In GSC-RC, the North and South boundaries are set as constant head, equal to the applied head at the surface (i.e., no vertical head gradient). Neither boundary condition perfectly describes the actual likely boundary conditions that would be present in the real physical system. Rather, they represent two endpoints bounding the likely behaviour of the hydrogeological system. The choice of boundary condition has a sizeable impact on the flow behaviour of the model system. However, as discussed in Section 7, their impact on radionuclide mass transport to the biosphere is far less significant.

Figure 6.19 shows the GSC-NF flow field 300 years into the first glacial advance, and is directly comparable to Figure 6.10. The pressurization of the subsurface due the hydraulic boundary condition on the northern boundary observed in Figure 6.10 is absent in Figure 6.19. There is a moderate pressurization of the subsurface due to hydromechanical coupling. This causes some higher horizontal flow velocities in the more permeable units, particularly in the general vicinity of the ice sheet terminus where the hydraulic gradient is the highest. Overall, the velocities are much lower than those observed for GSC-RC.

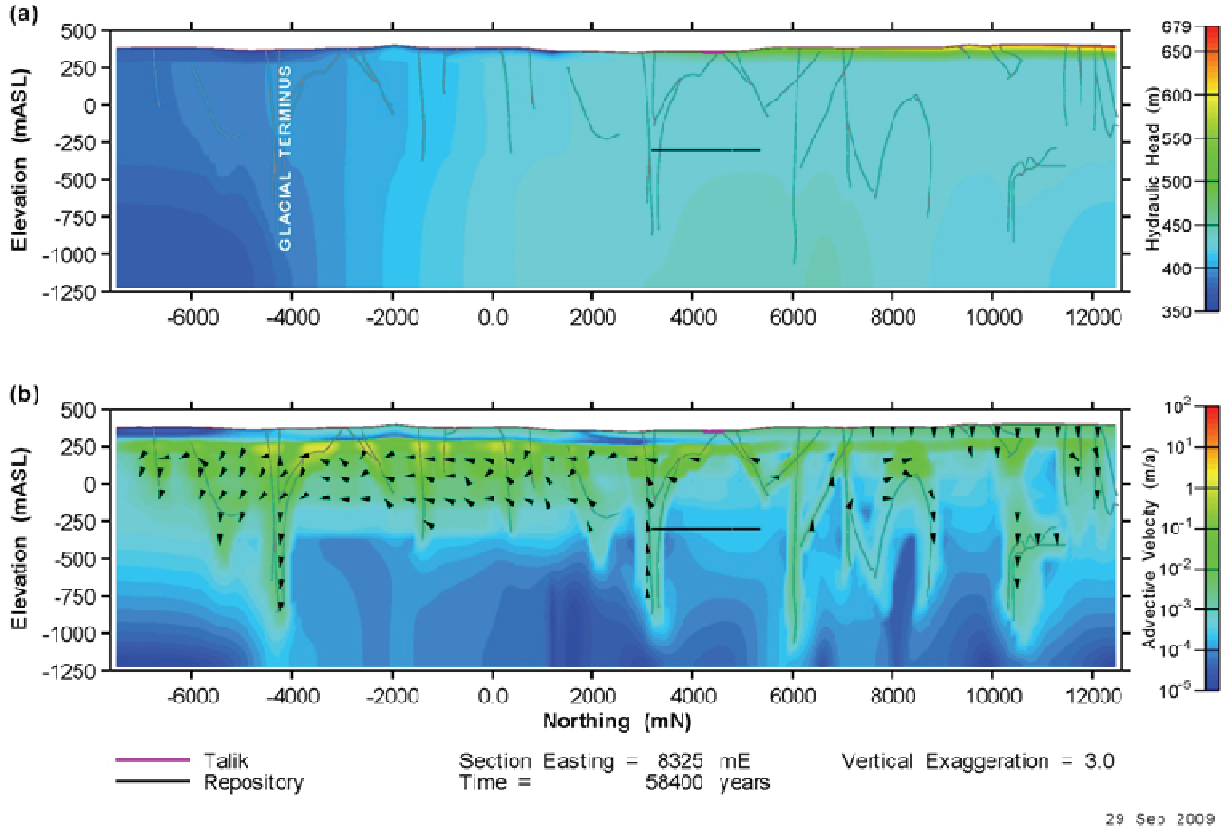

Figure 6.19: GSC-NF flow model results at 58,400 years (beginning of stage 3 – ice advance, cold based glacier). The hydraulic head distribution is shown in (a), while the advective velocity distribution is shown in (b). Velocity vectors are plotted where the velocity exceeds 1 mm/a.

Figure 6.20 shows the GSC-NF model results during cold-based glacial retreat, and may be compared directly with Figure 6.11. The average head in the GSC-NF model is of a similar magnitude to the GSC-RC model, but the variation in the hydraulic head below the permafrost is much lower, and the flow field is virtually stagnant. This is unsurprising, as no flow boundaries on the sides and bottom, and the frozen upper surface mean that the hydraulic system is essentially a closed box. It is likely that in the interior of a continental glacier, underlain by permafrost, such a stagnant system could exist. However, the real flow system under a retreating glacier is likely to be somewhere between the GSC-RC and GSC-NF models, with some horizontal flow gradients in the upper system, greater than in model GSC-NF, but less than in GSC-RC.

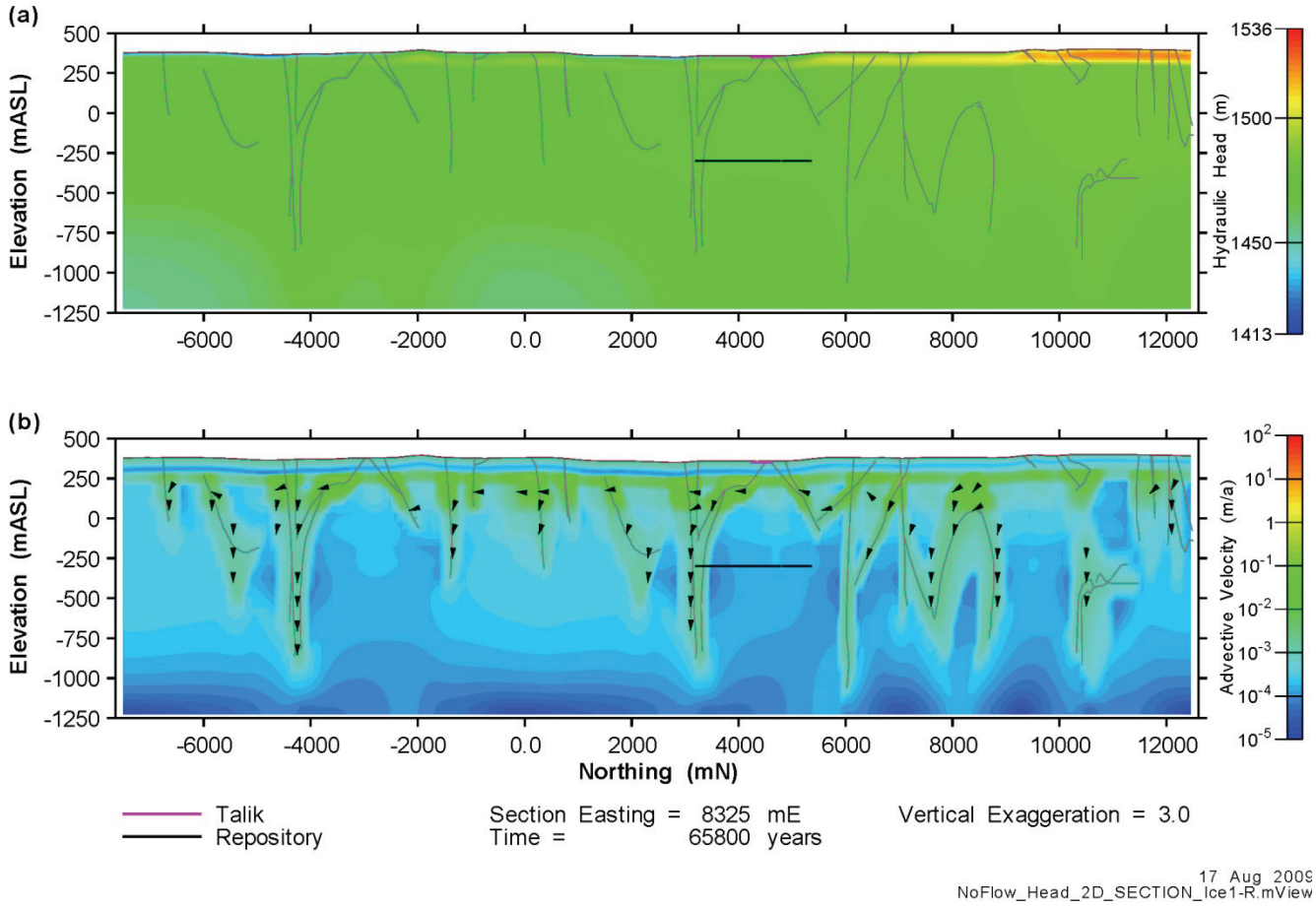

Figure 6.20: GSC-NF flow model results at 65,800 years (midpoint of stage 4 – ice retreat, cold based glacier). The hydraulic head distribution is shown in (a), while the advective velocity distribution is shown in (b). Velocity vectors are plotted where the velocity exceeds 1 mm/a.

During the ice advance over permafrost, the no-flow northern and southern boundaries had the effect of reducing the flow velocities in the repository, and thereby reducing the rate of advective transport from the repository. The exact opposite occurs during the second permafrost stage.

Figure 6.21 shows a cross-section of the flow field approximately 2000 years after the start of the second permafrost sequence. In the GSC-RC model (Figure 6.12), there are 4 hydraulic outlets for the glacially induced heads, the two taliks and the North and South boundaries. In the GSC-NF model (Figure 6.21) the stored pressures cannot escape at the North and South boundaries, causing higher heads and hydraulic gradients to persist for a longer time. During this permafrost stage the two taliks also form a hydraulic dipole system, with the southern talik (not present in the cross-section shown in Figure 6.21), which is at a higher elevation, forming the source, while the smaller North talik acts as the only sink in the model.

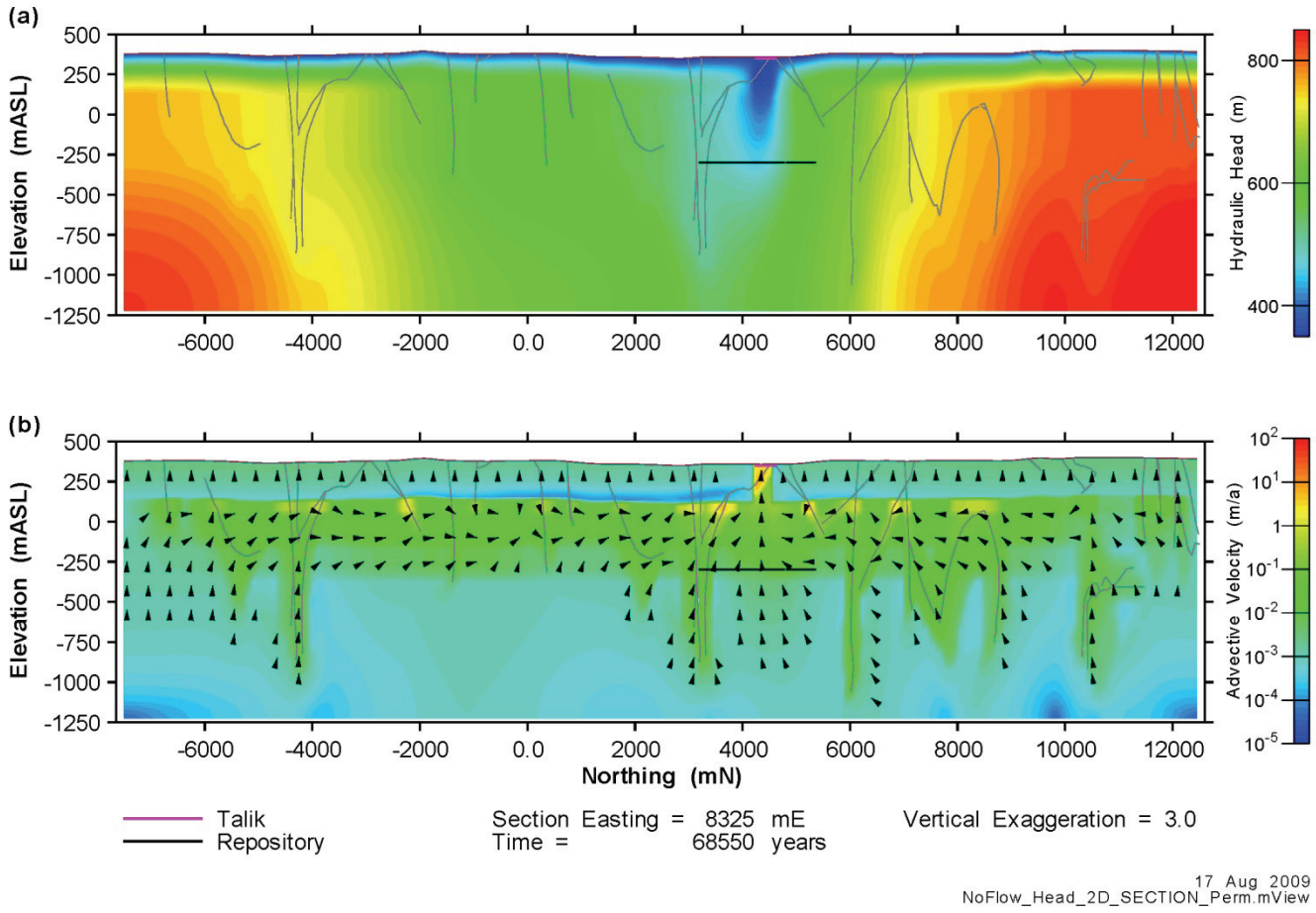

Figure 6.21: GSC-NF flow model results at 68,550 years (start of stage 5 – permafrost). The hydraulic head distribution is shown in (a), while the advective velocity distribution is shown in (b). Velocity vectors are plotted where the velocity exceeds 1 mm/a.

6.4.1.4 Talik under Glacier Case

The Talik under Glacier Case (GSC-TK) is identical to the reference case GSC-RC, except that taliks in the permafrost layer remain open during the cold based glacier stages (stages 3, 4, 6, and 9 in Table 3.3). Figure 6.22 shows a cross section of the flow field at the 58,400 years, the beginning of the first glacial advance. Comparing it to Figure 6.10, it is evident that presence of areas of unfrozen ground in the sub-glacial permafrost has had a minimal impact on both the hydraulic head and velocity distributions, except very near the talik. However, as the repository is located directly below the talik, it did impact the flow field in the repository, causing increased vertical flow rates. In Figure 6.22 the flow direction is downward, and velocity is roughly an order of magnitude higher than seen in the GSC-RC model (Figure 6.10). The same occurs during the cold-based glacial retreat (stage 4), except that the flow direction at the repository during the retreat is vertically upward.

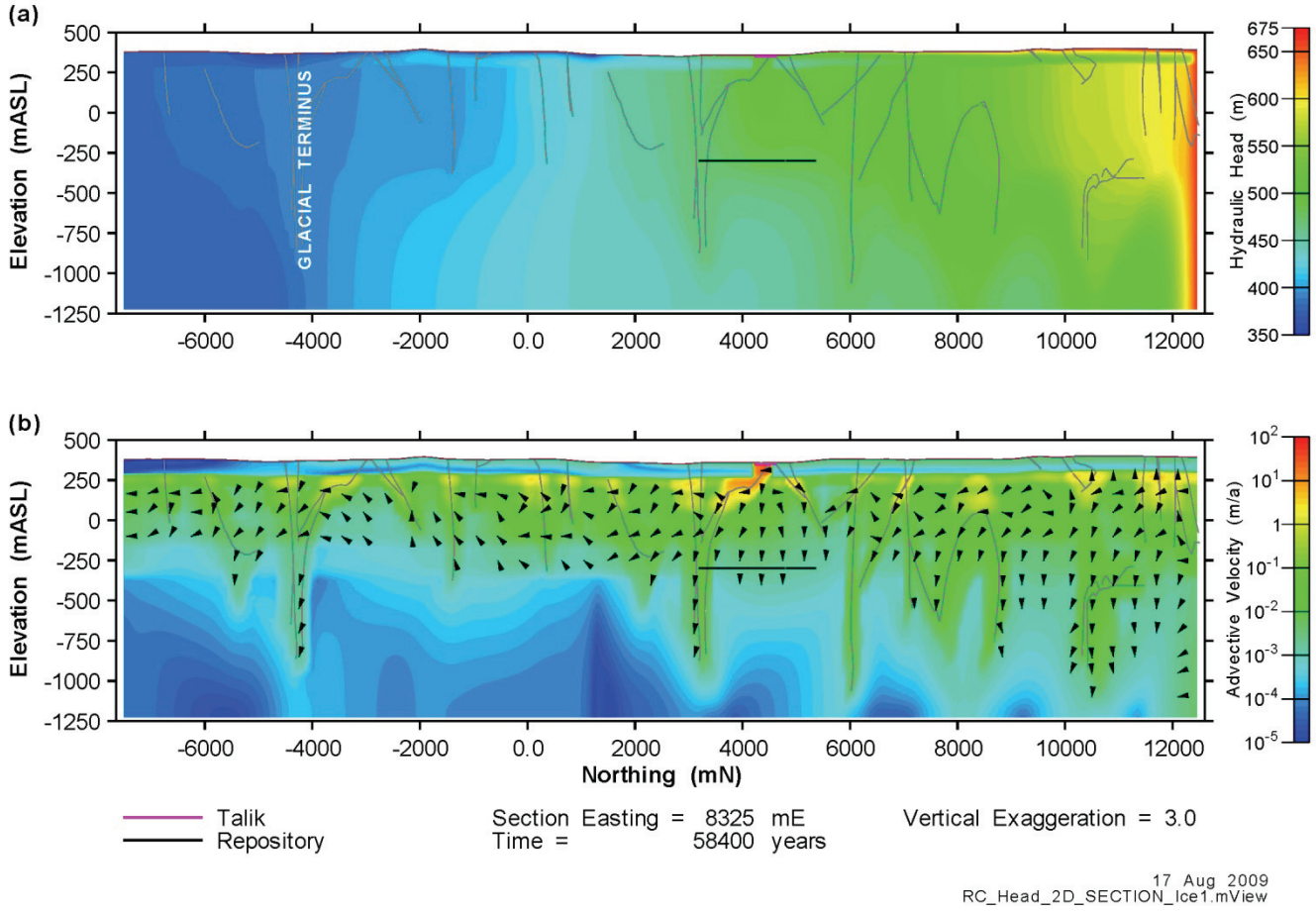

Figure 6.22: GSC-TK flow model results at 58,400 years (beginning of stage 3 – ice advance, cold based glacier). The hydraulic head distribution is shown in (a), while the advective velocity distribution is shown in (b). Velocity vectors are plotted where the velocity exceeds 1 mm/a.

6.4.2 Effect of Hydromechanical Coupling

The inclusion of hydromechanical coupling in modelling sub-glacial hydrogeology is an important feature of the model. To understand how hydromechanical coupling affects the flow system, the first (cold-based) glacial stage of the GSC-NF model was run with the hydromechanical coupling module deactivated. This case should show the most extreme contrast between the models with and without hydromechanical coupling, as the model is closed on all sides. The base and sides of the model have no-flow boundary conditions, while the top of the model is covered with a continuous 100 m thick permafrost layer.

Figure 6.23 shows the head and velocity contours at the beginning of the glacial advance, when the model domain is not yet entirely covered by ice. It is evident in the figure that a small amount of water passes through the permafrost layer, due to the extremely high hydraulic gradient. However, the head and velocity increase in the deeper geosphere is very small. Comparing these results to Figure 6.19 (GSC-NF results with hydromechanical coupling) shows that hydromechanical coupling significantly increases hydraulic heads and velocities in the subsurface. During a warm based glacial advance, the effect of hydromechanical coupling on head and velocity is reduced.

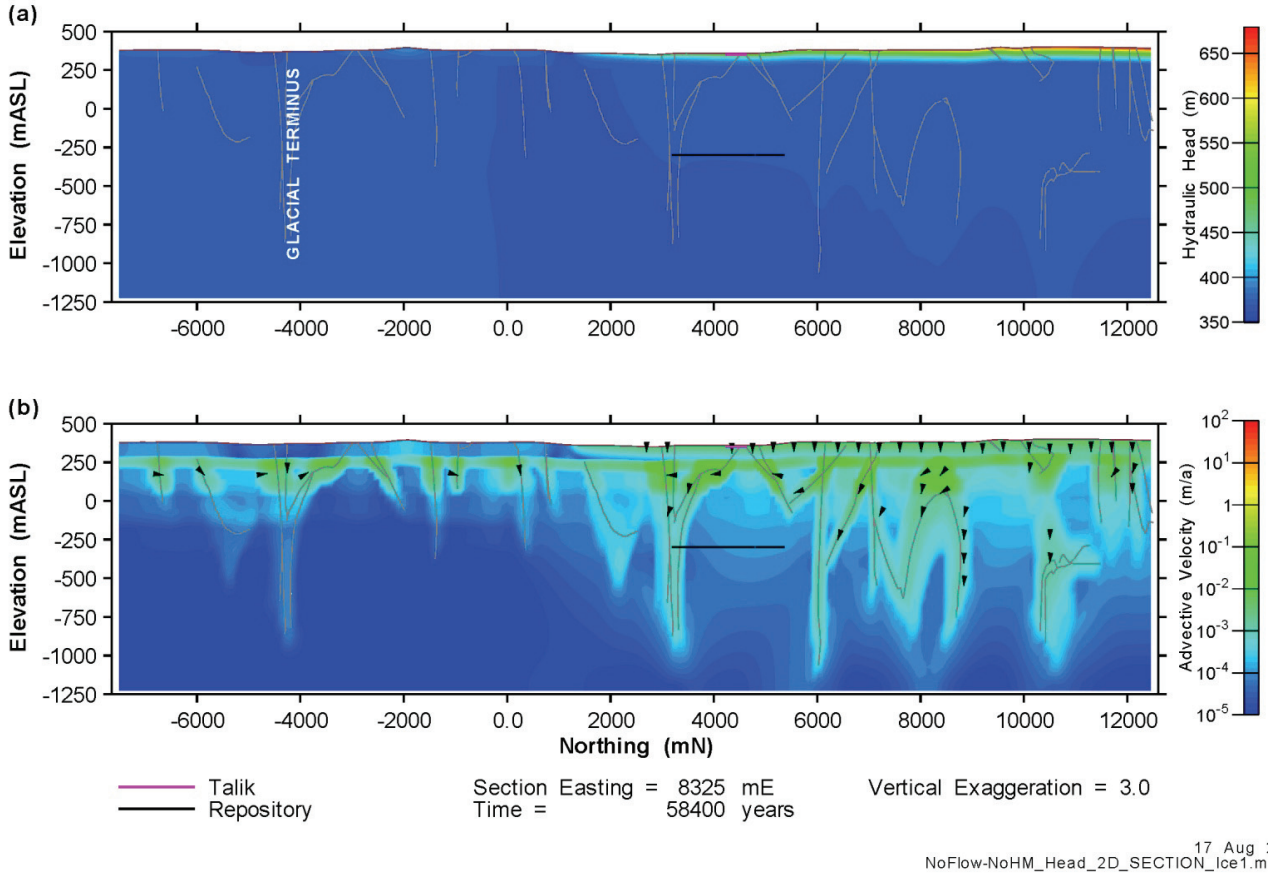

Figure 6.23: GSC-NF with no hydromechanical coupling. Results at 58,400 years (beginning of stage 3 – ice advance, cold based glacier). The hydraulic head distribution is shown in (a), while the advective velocity distribution is shown in (b). Velocity vectors are plotted where the velocity exceeds 1 mm/a.

Figure 6.24 shows the advective flow velocity magnitude for model GSC-NF divided by the velocity magnitude for case GSC-NF without hydromechanical coupling at three times. Early in the glacial advance the difference is striking, particularly in the vicinity of the glacial terminus where velocities are 100 to 1000 times higher in the model with hydromechanical coupling (Figure 6.24 (a)). However, this is a very transient effect. As the glacial advance proceeds the difference between the models is greatly reduced, as shown in Figure 6.24 (b) and (c).

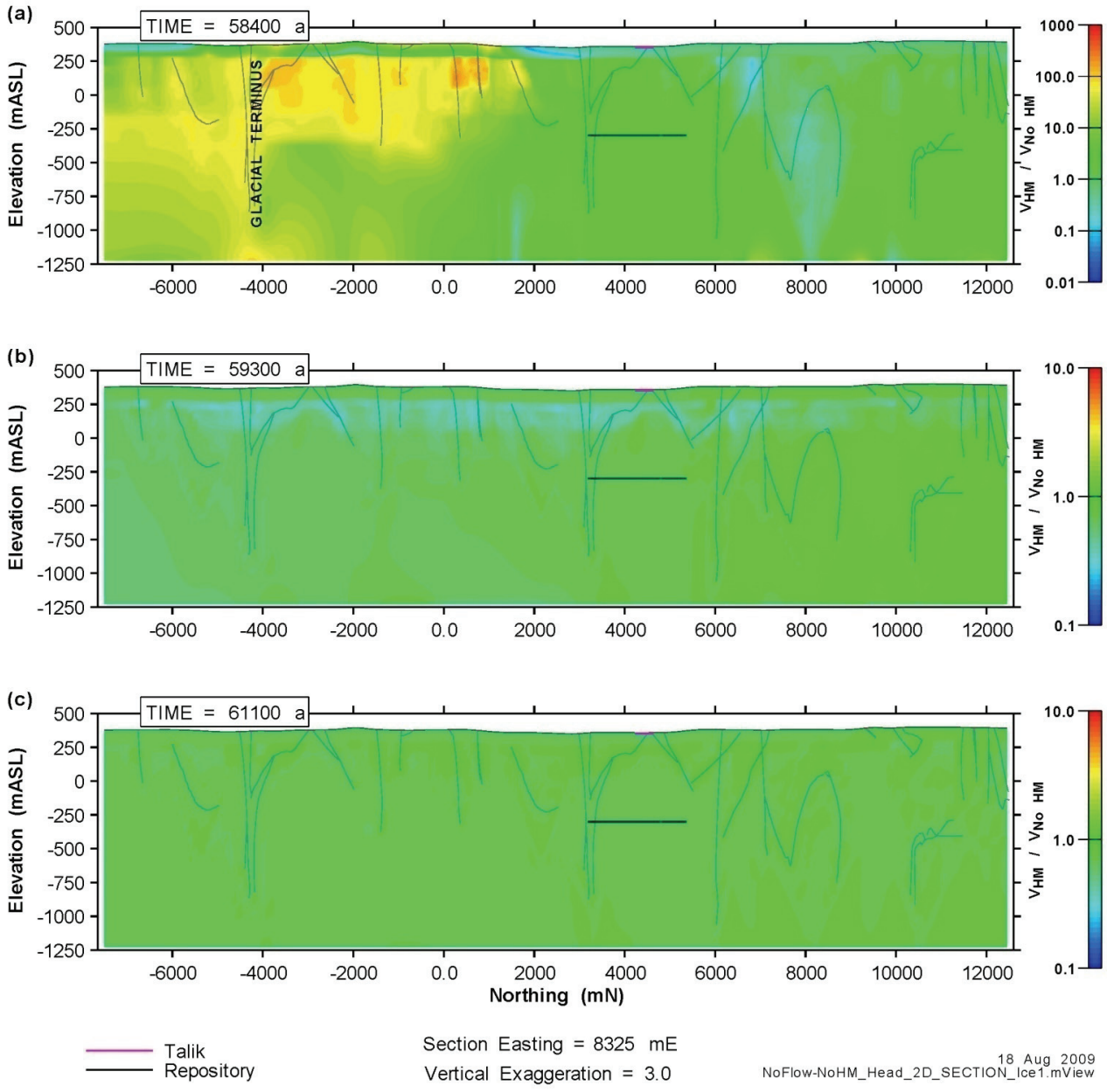

Figure 6.24: Ratio of the advective flow velocity magnitude for GSC-NF with and without hydromechanical coupling. Results are shown at (a) 58,400 years (300 years into cold based glacial advance), (b) 59,300 years (1200 into glacial advance), and (c) 61,100 years (3000 years into glacial advance)

6.4.3 Repository Velocity Calculations

The figures in the preceding section provide a snapshot of the flow field in the model domain, at one time and across one vertical slice through the repository. These plots are helpful, but do not to provide a continuous description of the flow field. Figure 6.25 shows how the average vertical component of the advective velocity within the repository footprint changes with time and varying boundary conditions. The plot makes clear how the different hydraulic boundary conditions impact on the flow field in the repository. Advancing glaciers, both cold- and warm-based, lead to larger negative or downward vertical velocities. Retreating glaciers have the reverse effect, and this effect persists into the following permafrost stages, as the rapid retreat does not allow all the pressure stored during the glacial advance to dissipate.

Integrating the velocities shown in Figure 6.25 gives the average vertical travel distance within the repository footprint during one glacial cycle, see Figure 6.26. The total positive (upward) movement only slightly exceeds the sum of the negative (downward) movement. As a result, the cumulative vertical distance travelled is only about one meter after a 121,000 year long glacial sequence. This means that although the glacial cycling leads to increases in velocity and changes in flow direction, within the repository, the hydraulic impacts of glacial advances and retreats almost cancel each other out. This is also evident in the I-129 mass flow curves presented in Section 7, where the cumulative I-129 mass flows to the biosphere in the Reference Case (GSC-RC) only moderately exceeds the cumulative flow for the corresponding Constant Climate case (GSC-CC). Given the much larger flow velocities in the transient Reference Case, larger I-129 mass flows in the Reference Case model (compared to case GSC-CC) might have been expected, but were not actually observed in the model results.

A caveat needs to be added to the preceding analysis. Although Figure 6.26 seems to imply that the cumulative advective travel distance at the end of one glacial cycle will be on the order of one meter, particle track simulations (see Section 6.4.4) and transport simulations (see Section 7) show that material does escape and travel much further from the repository. Although average velocities are very low within the repository itself, there is significant variation between the lowest and highest velocities within the repository, so that, at certain locations, particles (i.e., contaminants) need travel only a short distance from the repository before they enter a fracture zone, where velocities are higher. The particle tracking and transport simulations also indicate that, during the course of a glacial cycle, radionuclide transport near the repository varies between advection (and, hence, dispersion) dominated transport and diffusion dominated transport (Walsh and Avis 2010). The relatively high dispersivity value used in the model overestimates the contribution of advective transport.

Figure 6.25 also shows some evidence of numerical instability in the flow solution, particularly during the second (warm-based) ice retreat between 235,500 and 241,500 years. This numerical instability is brought about by a very sudden alteration of the flow field and boundary conditions, caused by the instantaneous removal of the permafrost layer and the shift from an advancing to a retreating glacier. This numerical instability reduces the accuracy of the model to a limited degree during this stage of the glacial cycle. However, the oscillations remain relatively small and decay as the glacial retreat proceeds, so the results are still sufficiently accurate for the purposes of this report.

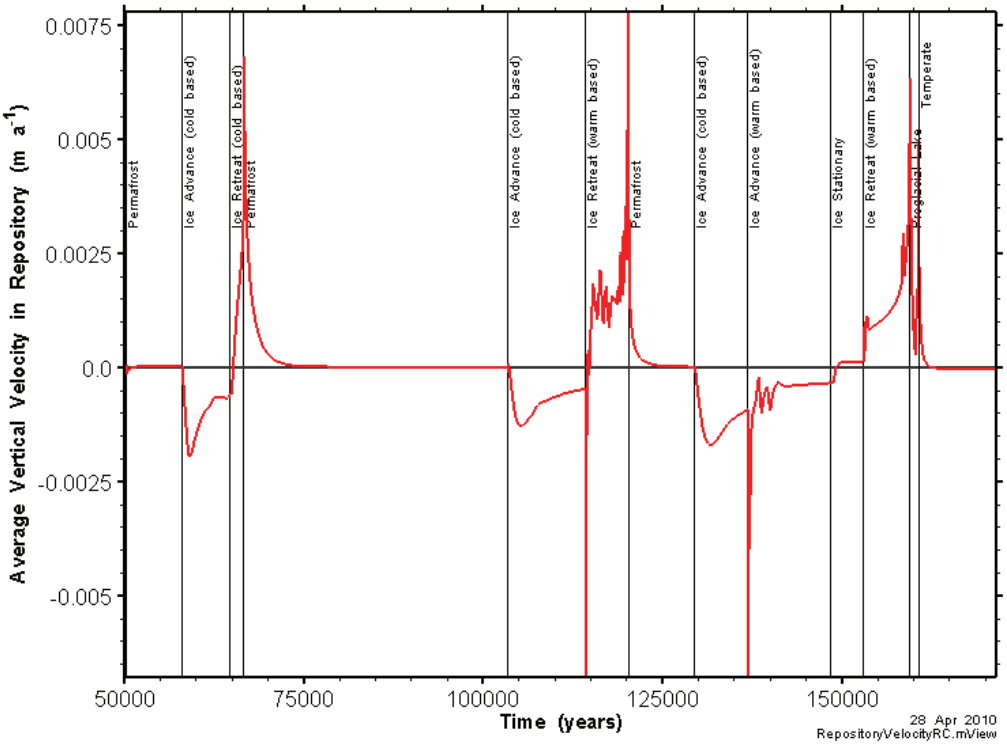

Figure 6.25: GSC-RC flow model, average vertical component of advective velocity within the repository footprint. Positive velocities are up, negative velocities are down.

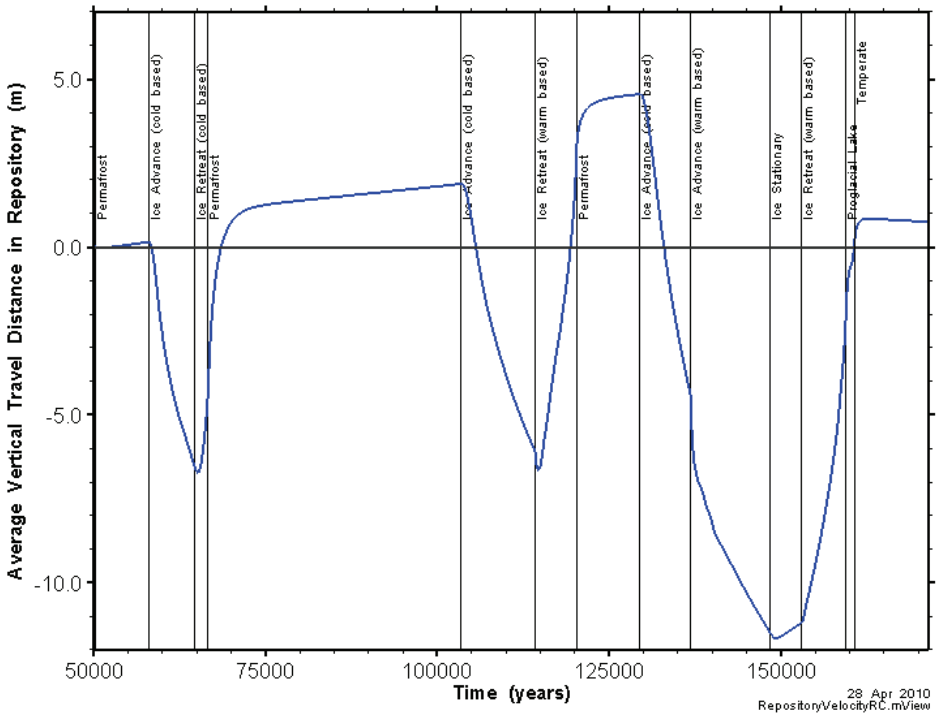

Figure 6.26: GSC-RC flow model, cumulative average vertical advective flow distance within repository footprint. Calculated by integrating the curve in Figure 6.25 over time.

The calculation case with a flow field that differs most from the Reference Case (GSC-RC) is the high storage coefficient case (GSC-HS). The higher storage coefficients cause glacially induced heads to persist for much longer, leading to increased flow and velocity for a longer time. The effect on the repository vertical advective velocity is shown in Figure 6.27. Note that the Y-axis range is much larger than in Figure 6.25.

If the curve in Figure 6.27 is integrated over time, we obtain the curve shown in Figure 6.28. Although the advective flow distance can be significant during a given stage of the glaciation scenario, the positive and negative vertical flows tend to cancel one another. For the GSC-HS case this leads to a net travel distance of about -14 m at the end of the glacial cycle.

As before, this analysis must be qualified by the observation that the transport simulations for case GSC-HS (see Section 7) show that radionuclides released from the repository do escape and travel further from the repository, upward as well as downward. Again, although average velocities are very low within the repository itself, there is significant variation between the lowest and highest velocities within the repository, so that, at certain locations, particles (i.e. contaminants) must travel only a short distance from the repository before they enter a fracture zone, where velocities are higher.

However, the analysis of the vertical velocity and total travel distance within the repository footprint does clearly show how the changing boundary conditions during glacial advances and retreats affect the repository flow field. The analysis suggests that because the head added during a glacial advance and subsequently removed during a glacial retreat are equal and opposite, the periods of positive and negative vertical velocity tend to cancel one another, making the net effect of glacial advances and retreats rather small, especially when one considers the sizable imposed hydraulic heads during glacial advances. This is confirmed by comparison of the transport and mass flow results of the GSC-RC and GSC-CC models in Section 7.

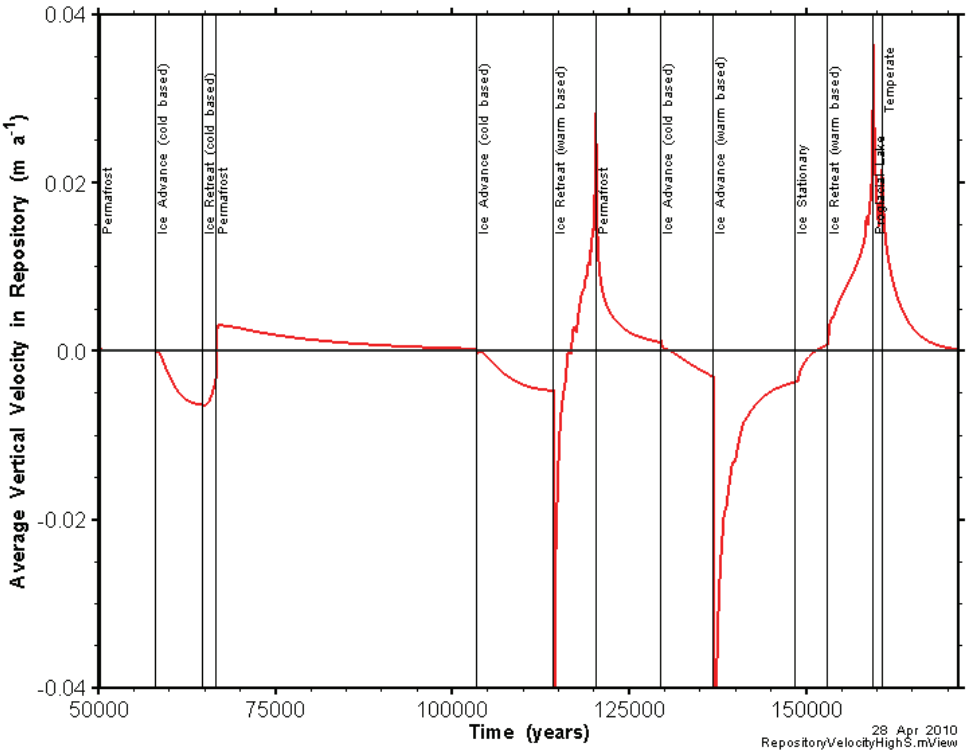

Figure 6.27: GSC-HS flow model, average vertical component of advective velocity within the repository footprint. Positive velocities are up, negative velocities are down.

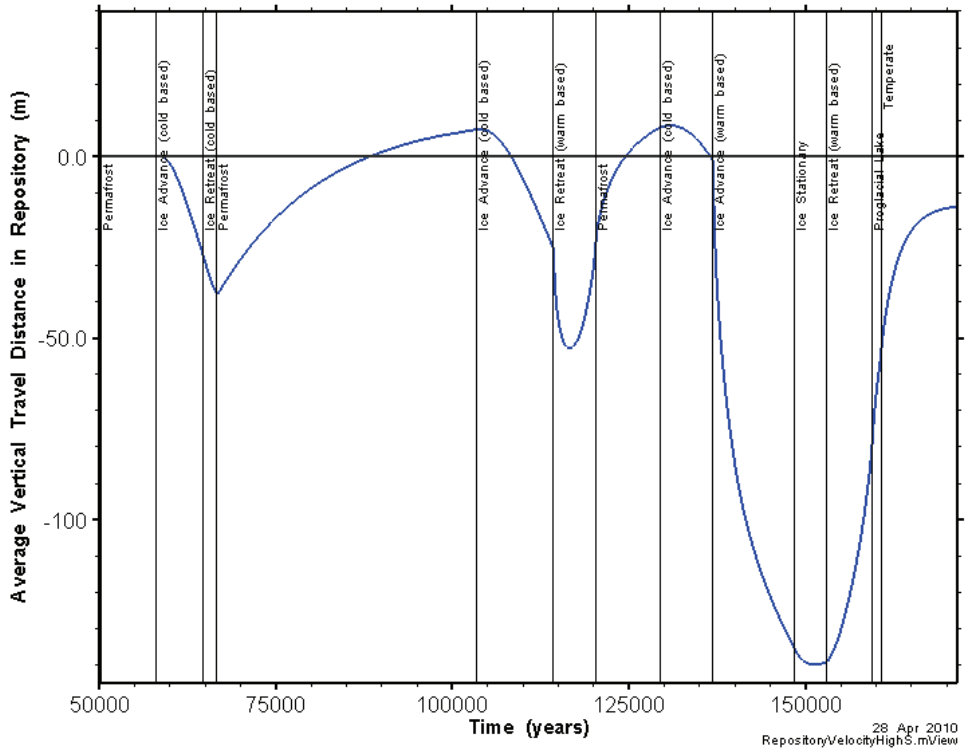

Figure 6.28: GSC-HS flow model, cumulative average vertical advective flow distance within the repository footprint. Calculated by integrating Figure 6.27 over time.

6.4.4 Particle Tracking Results

In addition to the repository velocity, another metric was developed to qualitatively assess effects on transport, at the repository horizon, of the various flow systems present throughout a glacial cycle. Velocities at selected times were used to generate particle tracks for particles originating at repository nodes. In calculating these particle tracks, it was assumed that the selected velocity field is constant with time. The tracks were then processed to calculate the distance traveled by each particle in a 100 year period after release. Calculated distances were further processed as cumulative distribution functions (CDF) to present the range of particle distances over the entire repository. This metric allows for a simple comparison of the advective velocity fields, and is a useful complement to the average repository velocity presented in the preceding section. It is important to note that although the curves do provide the travel distance, they do not show the travel direction. Results of the simulations at selected times are presented n Figure 6.29.

Differences in the flow systems are readily apparent with median travel distances varying over roughly 1.5 orders of magnitude. There can be a very large variation in behaviour within one stage. For instance, the two dotted red lines in Figure 6.29 show the 100 year travel distance near the start and towards the end of the second permafrost cycle. At the start of the cycle, stored heads from the preceding glaciation drive relatively high velocities in the repository footprint, but eventually the high heads dissipate and the system reaches a steady state at much lower velocities.

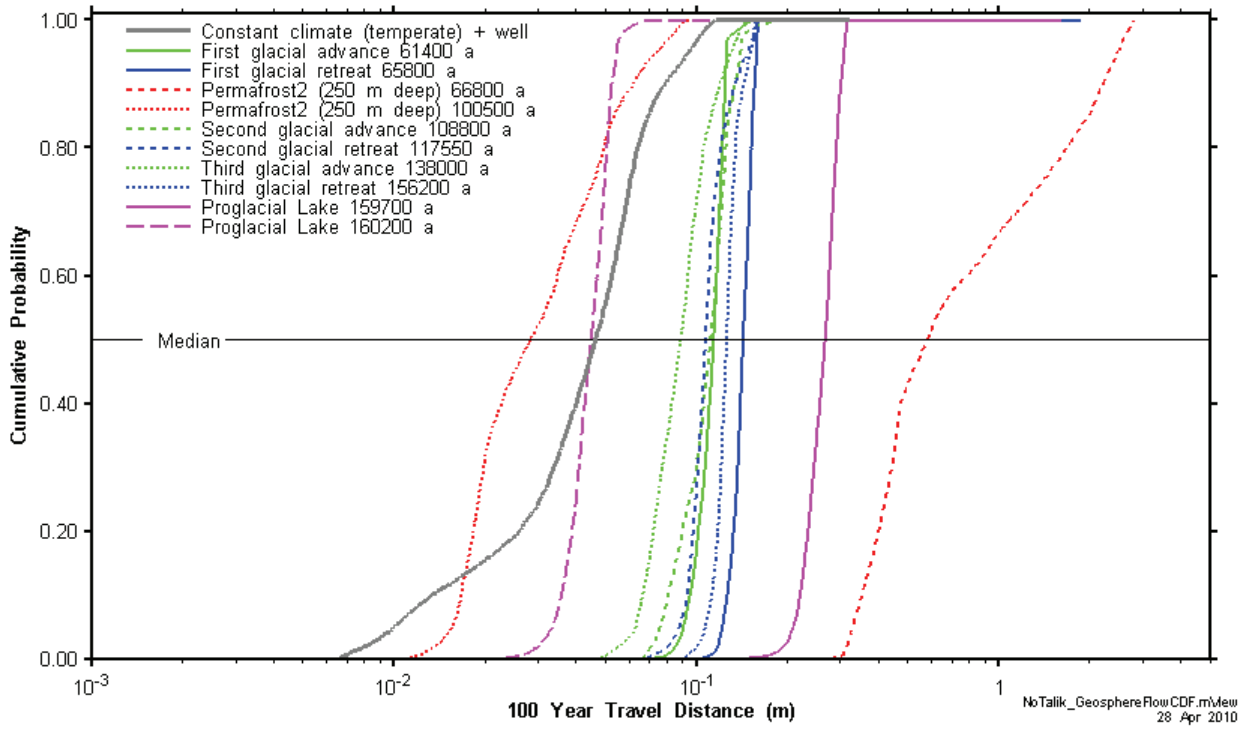

Figure 6.29: 100 year particle travel CDFs for selected flow times, GSC-RC model.

The particle track results are also useful in examining variations in groundwater discharge locations. The location of the defective containers (in the Reference Case) was selected from the start location of the particle with the fastest travel time to the surface, based on the Constant Climate case flow field (GSC-CC). Figure 6.30 is a map of travel time from the particle release location to discharge for the GSC-CC model. The fastest particle, located almost directly beneath the discharge talik, takes approximately 610,000 years to travel from the repository to discharge in the well adjacent to the North Lake. This differs from the peak concentration time shown in Figure 7.4 (385 ka). If transport from DC1 source location to the surface was advective, the travel time of the fastest particle and the peak of the I-129 mass flux across the North Lake should be approximately coincident. This suggests that diffusion or dispersion (which are not included in the particle track calculations) are important transport mechanisms.

Particle track results for several flow fields are needed to generate the geosphere transport networks used by the SYVAC3-CC4 system model (see Appendix B). This latter model is used for the deterministic and probabilistic safety assessment calculations described in Section 8.

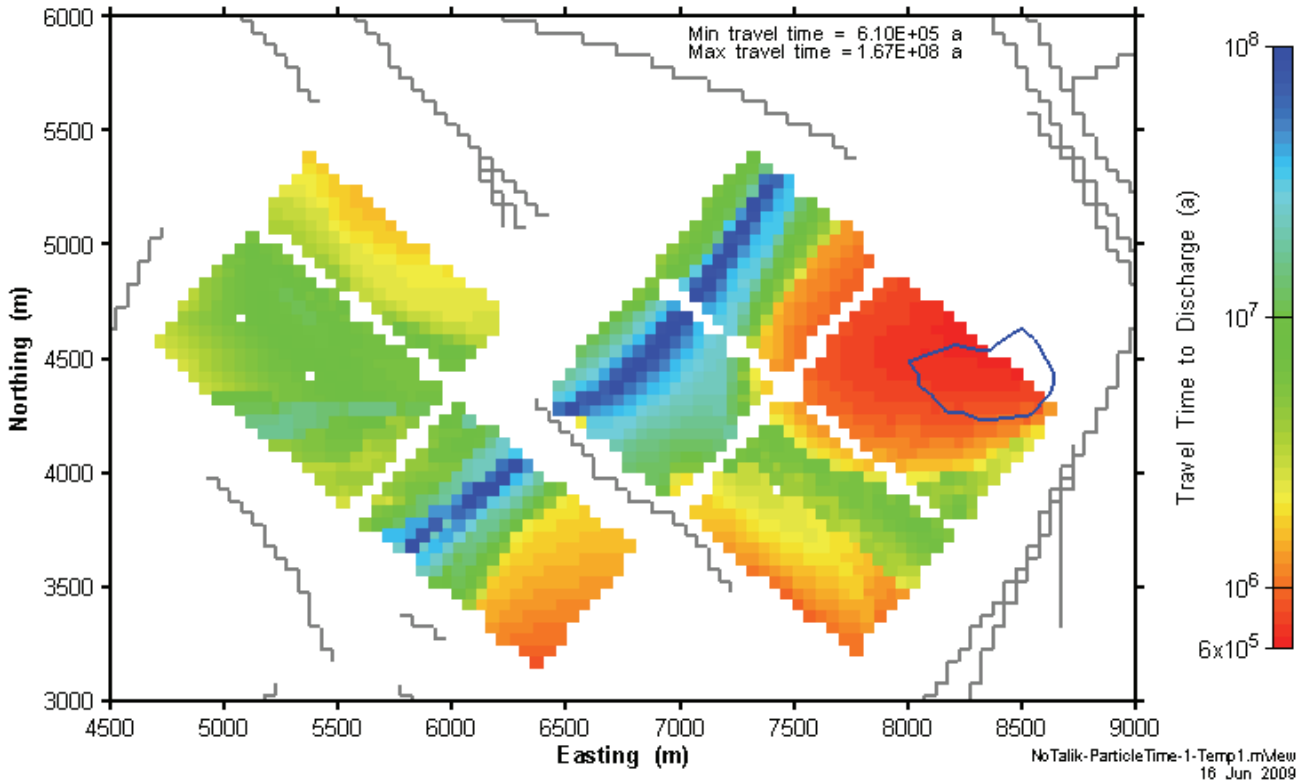

Figure 6.30: Particle travel time to discharge for steady-state temperate flow system.

Figure 6.31 shows how the elevation of the fastest particle changes with time, and whether the particle is travelling in intact rock or a fracture zone. For roughly 600,000 years the particle travels very slowly in the intact rock, after which the particle reaches a fracture zone and traverses the remaining distance to the well relatively rapidly. In contrast to the particle tracking analysis, contaminants from the source zone reach the fracture zone much more rapidly in the transport calculations due to diffusion/dispersion processes. Thus, for the Constant Climate case model (GSC-CC), transport from the repository is diffusion/dispersion dominated. However, during some short stages of the GSC-RC model, advective transport may become important even in the vicinity of the repository as shown in Figure 6.25Figure 6.25:.

Particle tracking simulations can also provide a reasonable three-dimensional snapshot of the local flow system during any particular stage of the glacial cycle. The pictures on the following pages show particle tracks generated by extracting the velocity field at a particular time, and running steady-state particle tracking on that flow field. Thus, the particle tracks and travel times are not in fact true representations of how the particles would move in the transient flow field, but are only used to illuminate flow paths. Typically, the travel time to discharge of even the fastest particles far exceeds the duration of a given configuration of the flow system, meaning no particle leaving the repository would actually follow one of the depicted flow paths. However, the particle tracks do offer an alternative method of visualizing the three-dimensional flow field, and the figures on the following pages provide an excellent illustration of the variability of the flow system during a glacial cycle. Additional results are shown in Walsh and Avis (2010).

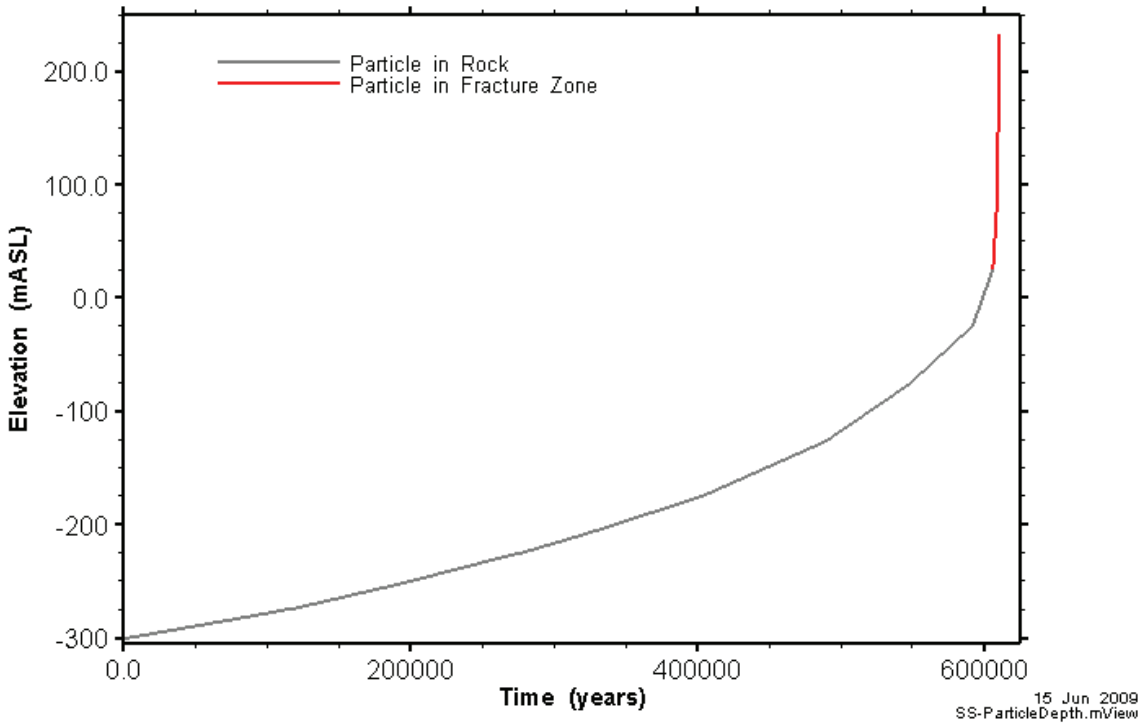

Figure 6.31: Particle elevation with time of fastest travelling particle.

As an example, Figure 6.32 shows particle tracks for the flow system extant at the beginning of the second permafrost period. High heads stored in the system from the preceding glaciation, combined with the fact that the North talik is the primary hydraulic outlet of the system, draw particles vertically upwards through the low permeability intact rock above the repository. When particles reach the more permeable, shallower fracture system, all the paths converge towards North talik. The high head gradients in this system mean that a few of the fastest particles reach the talik in as little as 6000 years. However, this is due to the rather extreme gradients and velocities at the start of the permafrost period, which do not persist for long. Velocities are reduced to half of the initial velocity within roughly 300 years, to a quarter of the initial velocity within 900 years, and have reached much lower steady-state velocities within approximately 5000 years. In addition, it is unknown whether the sudden application of a few small openings (taliks) in the permafrost layer post-glaciation provides a good representation of reality. There are no readily available data in the scientific literature describing the evolution of taliks in a permafrost environment.

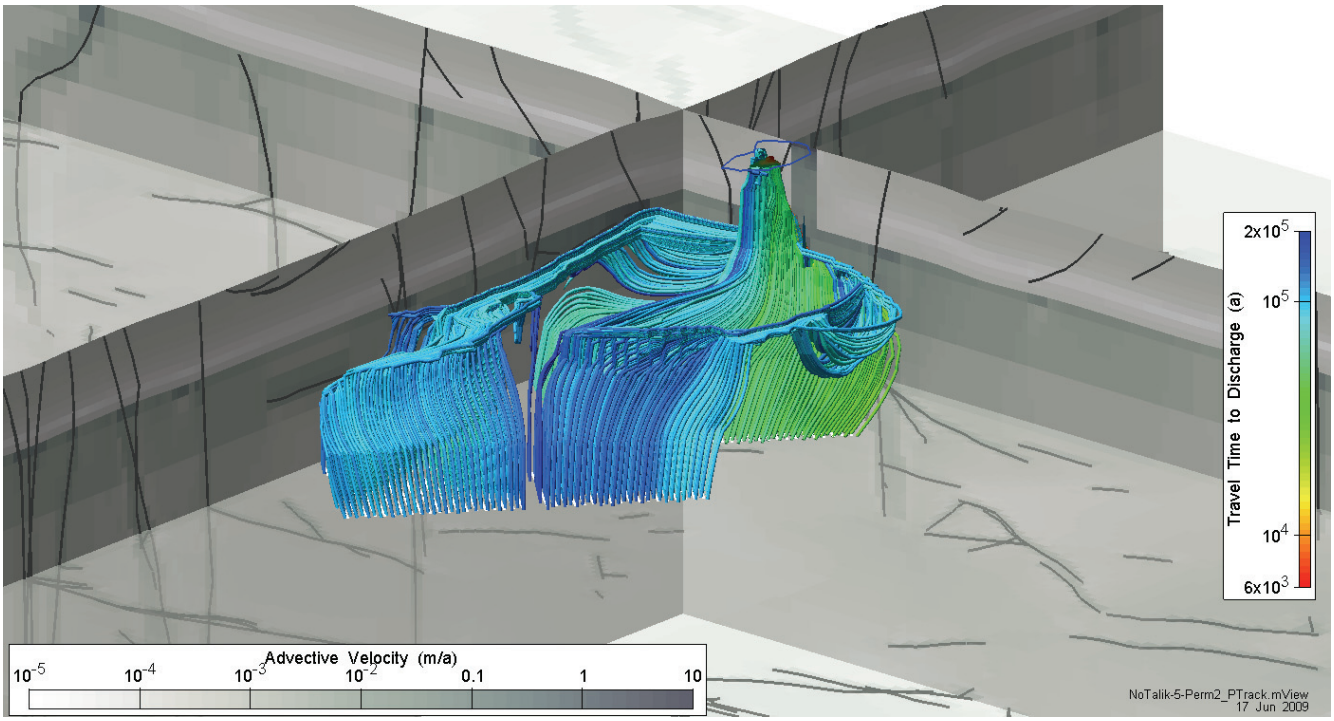

Figure 6.32: 3-D visualisation of particle tracks at 66,800 years, flow system at the start of the second permafrost period.

Figure 6.33 shows the particle tracks near the end of the second permafrost period. The flow system has attained a steady-state, with complete dissipation of all glacially induced heads. While the North talik remains the primary outlet for the particles, the paths travelled by the particles are significantly altered, and the fastest particle now requires just over 250,000 years to reach the surface.

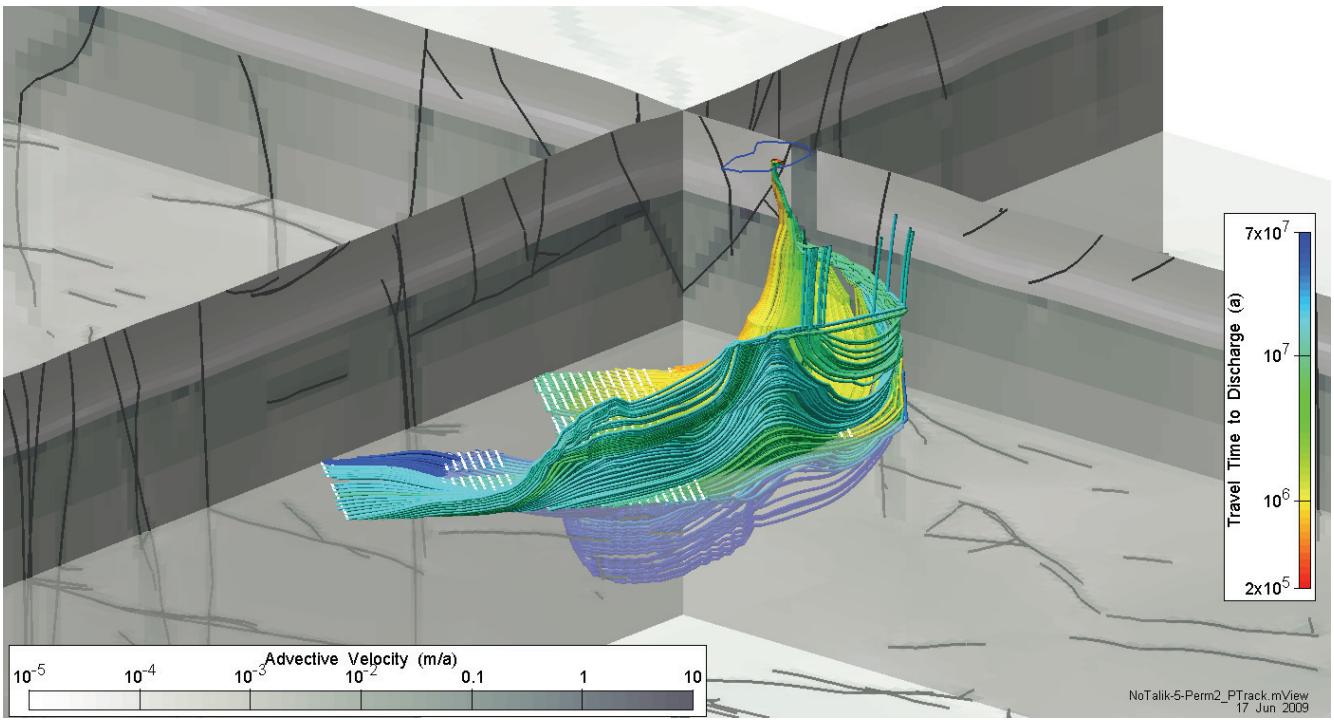

Figure 6.33: 3-D visualisation of particle tracks at 100,500 years, flow system near the end of the second permafrost period.

Figure 6.34 shows particle tracks during the Proglacial Lake State, when the entire model domain is covered by a proglacial lake. The tracks move vertically and exit the model at the surface. Travel times to the surface are rather long, with the fastest particle requiring 600,000 years to reach the surface. However, these velocities are only representative of this snapshot of the flow system. Travel times at the start and the end of the Proglacial Lake State are shorter.

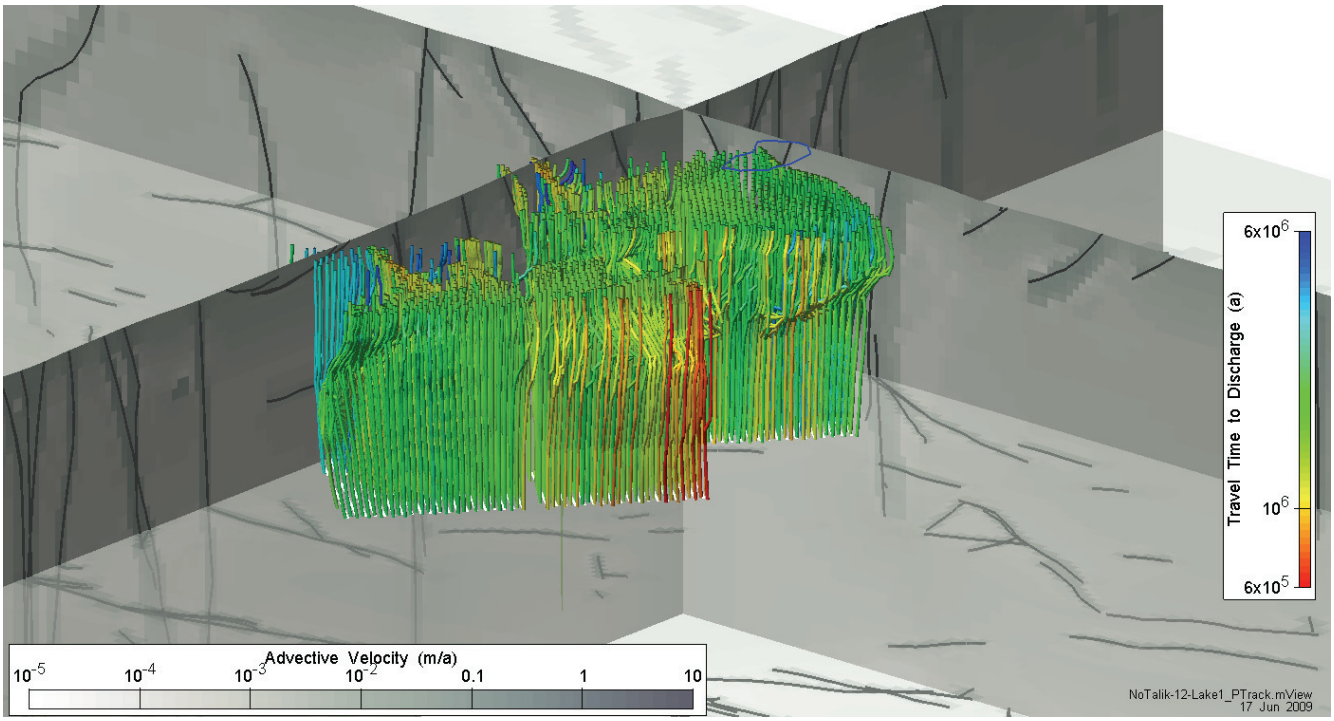

Figure 6.34: 3-D visualisation of particle tracks at 160,200 years, flow system midway through the Proglacial Lake State.

For the Reference Case, the defective containers were located at the repository location with the shortest groundwater travel time to the surface, as identified with the steady state (temperate) (GSC-CC) groundwater flow field. However, the groundwater flow system is transient during a glacial cycle and conditions can change quickly as illustrated in the figures above. It is possible that particles released from alternate source locations could travel to discharge faster than indicated by the steady-state flow model.

6.5 SUMMARY OF GROUNDWATER MODELLING RESULTS

A general approach was developed which captures the impact of glacial cycles on a complex, fractured flow system. Results of the simulations are informative, showing the wide range of advective velocities that occur at the repository horizon, and also the profound variation in flow path structure between the different climate periods. The modelling results indicate that impacts of glaciation induced surface boundary conditions and geosphere changes are significant and have an extensive effect on flow system, affecting direction and magnitude of flow.

In the transient flow model, the taliks are a dominant factor, focusing flow from a large portion of the model domain at a discrete location. These isolated gaps in the permafrost act as pathways for the dissipation of hydraulic pressure from preceding glacial events. After the stored glacial pressure has been drained and the system reaches equilibrium, the inclusion of two taliks also leads to a dipole flow system from the talik at higher elevation to that at a lower elevation. The presence of additional taliks could significantly reduce the duration of glacially induced overpressures and perhaps also the volume of water flowing through individual taliks, decreasing the influence of an individual talik.

Altering the storage coefficient (GSC-HS) had a dramatic effect on the modelling results. When the storage coefficient was increased by a factor of 10, more persistent glacial overpressures during the post-glacial permafrost period resulted in persistent upward flows of water.

Changing the northern and southern boundaries from constant head to no-flow boundaries (GSC-NF) also had a significant effect on the flow solution. During cold-based glacial advances and retreats the flow velocity was greatly reduced as compared to the Reference Case. Since no water was able to escape across the northern and southern boundaries, the glacially induced heads persisted for a much longer time, and all flow in the model was towards the two taliks.

The results presented in this section represent a small set of parameter choices, many of which are uncertain (e.g., glacier profile, geosphere storativity, fracture permeability, loading efficiency, permafrost properties, material property spatial distributions, and talik locations), and conceptual models (e.g., simplified hydromechanical coupling and constant-density flow). The instantaneous changes in permeability in the upper layers, used to simulate the application of permafrost, may also be a source of error, and may potentially magnify spikes in radionuclide mass flows to the surface (see, for example, Section 7). Furthermore, the model does not consider how high surface loading and hydraulic pressure might lead to permanent or transient alterations of the hydraulic conductivity of the rock mass.

The groundwater and transport modelling results will clearly vary with other parameters or model choices, but the parameters considered here are plausible (and in some cases bounding – e.g., taliks always present over the repository). Of course, analysis of more cases will improve our confidence in the conclusions.

7. TRANSPORT MODELLING

In the Glaciation Scenario considered in this report, it is assumed that some containers fail early, leading to releases of radionuclides. Detailed transport modelling, using FRAC3DVS-OPG, was performed to determine the I-129 mass flows to the surface biosphere for the Reference Case (GSC-RC) and for the sensitivity cases described in Section 6. The simulations were carried out to about 0.8M years, well beyond the time of the peak I-129 mass flows to the biosphere. Six complete glacial cycles occur during this time period.

The results of these calculations are presented in this section.

7.1 NUCLIDE RELEASE FROM CONTAINER

For the Defective Container Glaciation Scenario, it is assumed that 2 containers are emplaced in the repository with undetected defects in the copper shell. The container defect is small and its size is assumed to be time invariant. The two defective containers are assumed to flood soon after the vault is closed (i.e., 100 years after container emplacement), creating a continuous pathway for release of radionuclide from inside the container to the buffer. Models and parameters are used to characterize the defective container (e.g., defect size, void volume), radionuclides in used fuel (e.g., inventory, solubility), radionuclide release rates from the UO_2 fuel (e.g., release mechanisms, radiation field strengths) and radionuclide transport out of the container, yielding estimates of radionuclide release rates from the container.

The model used to calculate the rate of fuel dissolution assumes that the conditions in the repository are reducing and that oxidative dissolution of the fuel occurs because of the production of oxidants by radiolysis of the water near the fuel surface (Garisto et al. 2004b). As discussed in Section 4, it is expected that reducing conditions in the vault will prevail throughout the glacial cycle(s). Thus, the radionuclide release rates from the defective container in the Glaciation Scenario should be identical to those in corresponding HBC study, since the assumed defect size and other relevant parameters are identical in the two cases.

FRAC3DVS transport simulations are done only for I-129, the most important dose rate contributor. I-129 is not adsorbed by the rock in the geosphere. The I-129 mass transport rate out of two defective containers in the Reference Case is shown in Figure 7.1.

7.2 RADIONUCLIDE SOURCE TERM

In the HBC study (Garisto et al. 2005a), radionuclide transport was modelled using nested models. Two model grids were developed for modelling transport on the scale of the Engineered Barrier System (EBS) (i.e., for transport in the near field) and scale of the geosphere. The radionuclide mass flow out of the defective containers (see Figure 7.1) was used as input to the EBS transport model. The EBS scale model, which included a detailed representation of the emplacement borehole and associated engineered barrier system, provided the radionuclide source term to the geosphere transport model.

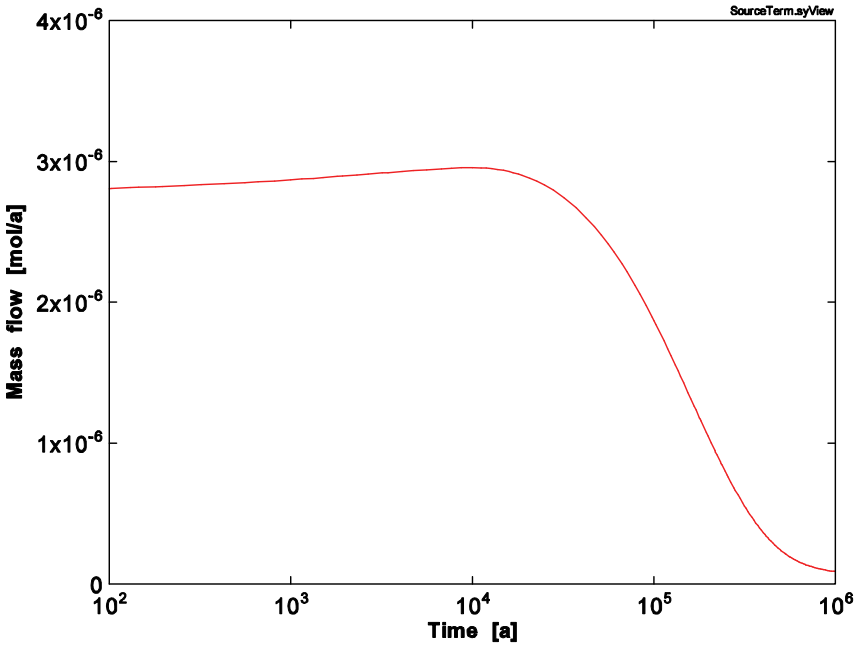

Figure 7.1: I-129 mass transport rate out of two defective containers in the Reference Case as calculated by SYVAC-CC4 (Garisto et al. 2005a).

To minimize model runtimes as much as possible, this approach was not used in the present study of the Glaciation Scenario. Instead, the total I-129 mass flow into the intact rock, as calculated by the EBS scale transport model in the HBC study (Garisto et al. 2005a) was used as a source term in the GSC model (see Figure 7.2). This total mass flow was divided by four and applied, in the GSC model, to the four upper corners of the hexahedral element which enclosed the selected source location in the repository (i.e., elevation -300 mASL).

To examine the effect of alternative source locations, the source term was applied at two locations within the repository footprint, as shown in Figure 7.3. These locations were selected based on having relatively short travel times to the ground surface during different stages of the glacial cycle. The location designated Defective Container 1 (DC1), was the location with the shortest travel time in the Temperate State. The second location, Defective Container 3 (DC3), also has a relatively short travel time to the surface, notably during the Proglacial Lake State.

Two approximations are involved in applying this source term to the Glaciation Scenario models. First, the HBC vault model used the HBC steady-state flow model to provide flow boundary conditions, with a flow system based on the temperate state. This is not consistent with the current model, where the flow field varies throughout the simulation. This approximation is greater for source location DC3, as the flow field in this location is less similar to that in the HBC model. Nevertheless, this is an acceptable approximation since previous results indicate that the radionuclide fluxes out of the HBC repository are not overly sensitive to the local groundwater flows near the repository (Garisto et al. 2005a)

Second, the source term is applied at nodes which are a greater distance (maximum 50 m) from the source location than in the HBC model (maximum 27.5 m). This approximation is somewhat

conservative since, in effect, about 10 m of intact rock is bypassed causing more rapid transport of contaminants away from the source.

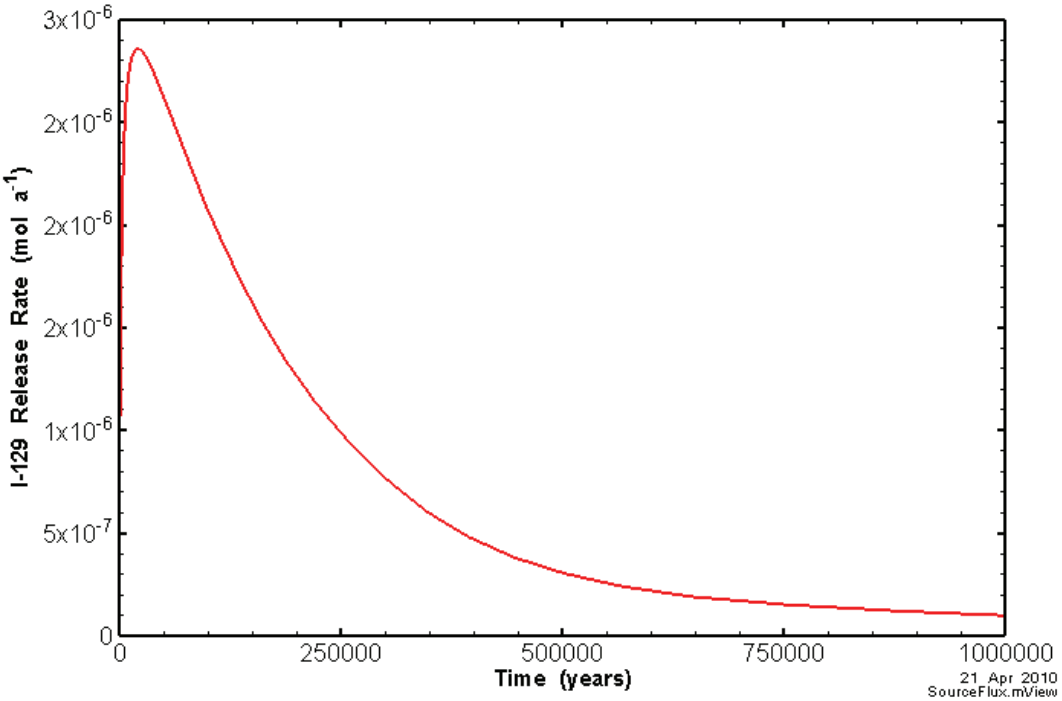

Figure 7.2: Release rate of I-129 into the geosphere

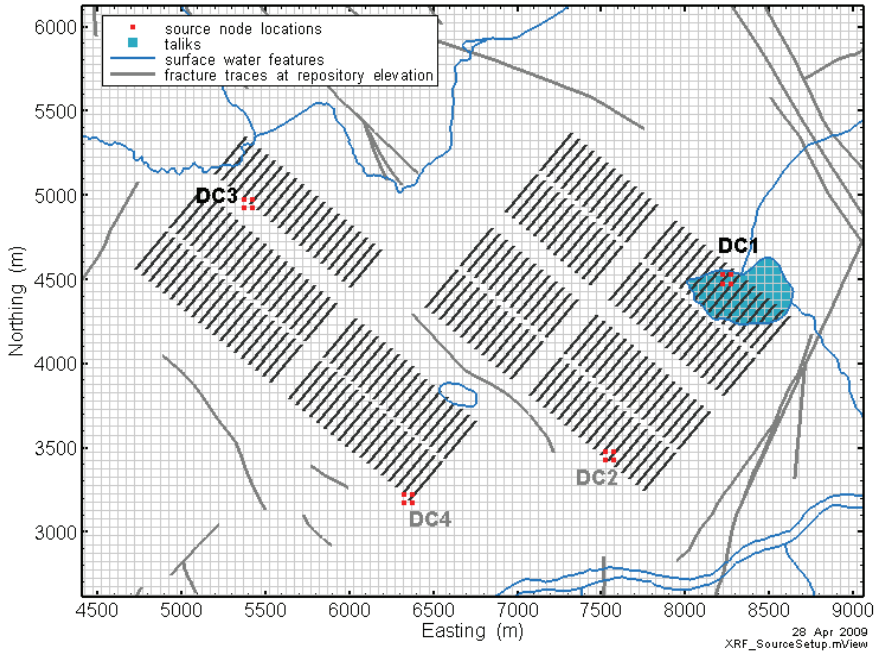

Figure 7.3: Defective container source locations. Only DC1 and DC3 were assessed for the complete performance period.

7.3 BOUNDARY CONDITIONS AND PERMAFROST IMPLEMENTATION

For transport, model boundaries are set as Neumann type boundaries with a concentration gradient of zero on all sides of the model (Frind 1988). This allows solute to leave the model domain with the advective flow, but assumes that the dispersive and diffusive fluxes are equal to zero at the model boundaries.

The permafrost layer is assumed to have the same transport properties as intact rock. Thus, permafrost has a porosity of 0.003; and the radionuclide free solution diffusion coefficient in permafrost is set at a very high value of $1x10^{-9}$ m^2 s^{-1}, with a tortuosity of 1.0. These are very conservative assumptions for the permafrost layer and so radionuclide transport through the permafrost will be unrealistically high. However, as will be seen, during permafrost periods most of the radionuclide mass enters the biosphere via the open taliks. Thus, these conservative values should have minimal impact on the overall transport results.

7.4 COMPARISON TO HBC REFERENCE CASE

The GSC model approach differs numerically from that used for the HBC study, e.g., grid discretization is coarser, and dispersivity is larger (80 m longitudinal in the GSC model versus 50 m in the HBC study). As previously noted, the larger dispersivity is required to reduce numeric effects from the larger discretization and is not based on field measurements. Consequently, dispersive transport is probably overestimated in the model.

A single verification case (GSC-CC) was performed to ensure that the GSC model results are broadly comparable with previous studies. The verification case assumed no water-supply well, steady-state boundary conditions and no permafrost in the geosphere. The basis for the comparison is the I-129 mass flux to the North Lake and results are presented in Figure 7.4.

The GSC-CC model results in a peak mass flow rate into the North Lake similar to the HBC model; but, the peak mass flow rate occurs much earlier (385 ka for GSC-CC, 485 ka for HBC). This earlier arrival of the peak in the GSC-CC model is mainly due to the higher dispersivity value used in this model compared to the HBC model. However, the altered flow field also influences the arrival time, as discussed further below.

To assess the impact of the depth dependent fracture permeability in the GSC model, a further simulation with constant hydraulic conductivity fractures (with $K_{fracture} = 10^{-6}$ m/s) was performed. The results are also shown in Figure 7.4. The higher fracture conductivities result in a slightly lower and earlier peak mass flow to the North Lake; but, the total mass flows to the biosphere are similar in the two cases (with more mass flow going to the River discharge for the constant $K_{fracture}$ case). The limited impact of the fracture conductivity reduction is likely due to the very low hydraulic conductivity of the intact rock formation and the relatively large distance between the radionuclide source and the nearest fracture zone.

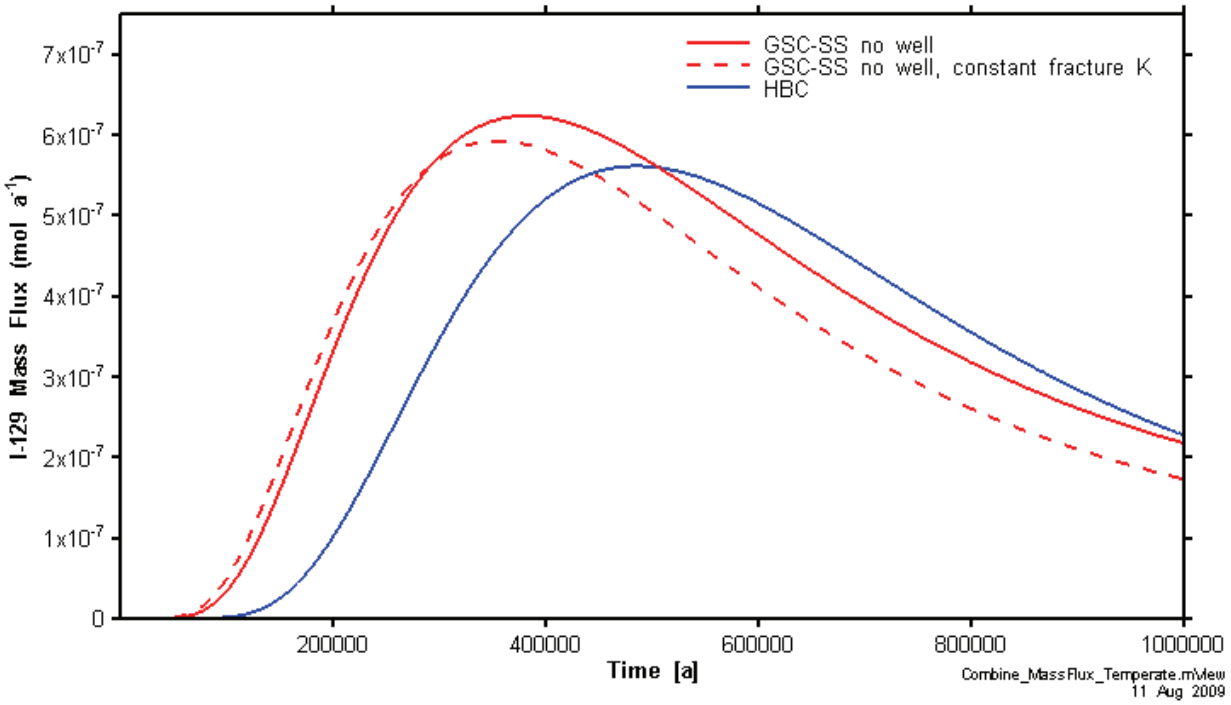

Figure 7.4: Comparison of mass flux to the North Lake for the no-well case for the HBC and GSC-CC models.

7.5 MULTIPLE GLACIAL CYCLE TRANSPORT RESULTS

Transport model results show how the transient nature of the flow system response over many glacial cycles affects the fate of radionuclides released from the repository. The figures in this section present plan sections and vertical cross-sections through the radionuclide plume in the vicinity of the repository for the DC1 source location. Additional transport modelling results, including those for the DC3 source location, can be found in Walsh and Avis (2010).

Plan sections are shown at elevation 0.0 mASL (about 350 mBGS) and cross-sections are shown on a North-South transect at easting 8325 mE, which passes directly through the DC1 source location (see Figure 6.8). The figures present concentration contours on a logarithmic scale that is consistent for all figures. To better display the plume shape, very low I-129 concentrations are shown, i.e., as low as 10^{-9} mol/m^3 (or equivalently 0.84 Bq/m^3). A person drinking 1 m^3/a of water with this low concentration of I-129 would receive a dose rate of less than 0.1 μSv/a.

During the course of a given glacial cycle the shape and location of the plume changes constantly. The six "snapshots" of the plume provide a representative picture of plume evolution during the course of the entire assessment period.

Figure 7.5 to Figure 7.7 show detailed cross-sections of the GSC-RC radionuclide plume (for the DC1 source location) for times bracketing the second glacial advance and retreat (see Table 3.2). This series of figures is intended to illustrate the general impact of a glacial advance and

retreat on flow and transport. The figures start at 103,500 years as the plume has developed sufficiently by this time for the transport implications to be observable without complicating the analysis by including the superimposed effects of previous multiple advances and retreats.

Figure 7.5 shows the radionuclide plume and velocity field at the end of the second permafrost period. By this point, there has been 50,300 years of temperate conditions, followed by 7800 years of permafrost, 6700 years of cold-based glacial advance, 1900 years of cold-based glacial retreat, and 36,800 years of permafrost. The plume has spread in all directions, being drawn upward towards the North talik in particular during the permafrost period. As explained in Section 6, this is due to the North talik being the primary hydraulic outlet for the entire system during the permafrost period.

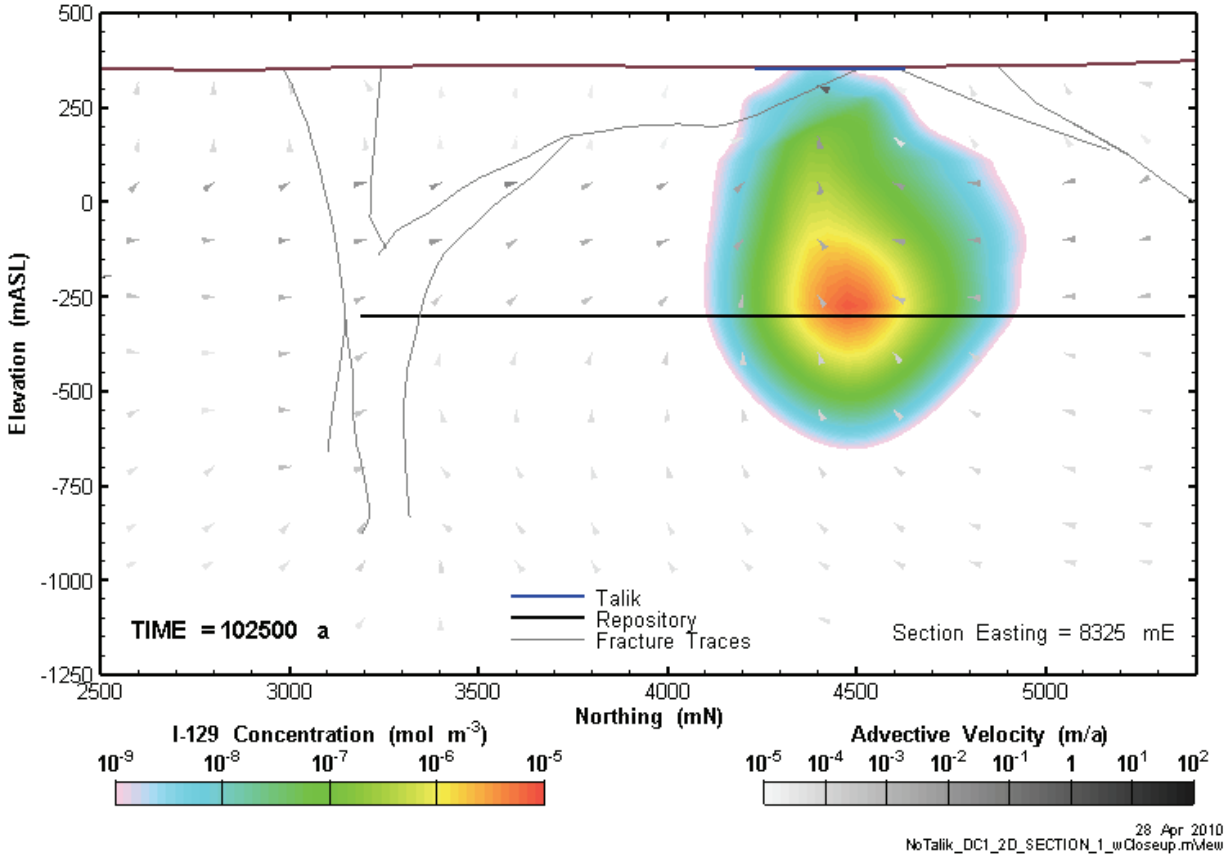

Figure 7.5: GSC-RC DC1, Y-Z cross section showing I-129 plume after 103,500 years, the end of the second permafrost period. Arrows illustrate direction and magnitude of the advective velocity.

Figure 7.6 shows the radionuclide plume at the end of the second glacial advance. This advance is cold-based, and the high hydraulic heads on the ground surface do not penetrate to great depth through the permafrost. Nevertheless, the hydromechanically induced heads and the specified heads at the north and south boundaries do lead to a general North-South gradient, and promote flow towards the south in the upper, more permeable units. At the elevation of the repository the flow direction is downward, as more pressurised water in the

shallower units moves to equilibrate the heads. The downward flow is caused largely by the very high specified heads at the northern and southern boundaries, which pressurize the more permeable shallower units. As expected, the flow field in the more permeable units drives the upper part of the I-129 plume to the south. As a consequence, the glacial advance spreads the plume laterally at the top, and pushes it deeper at the bottom.

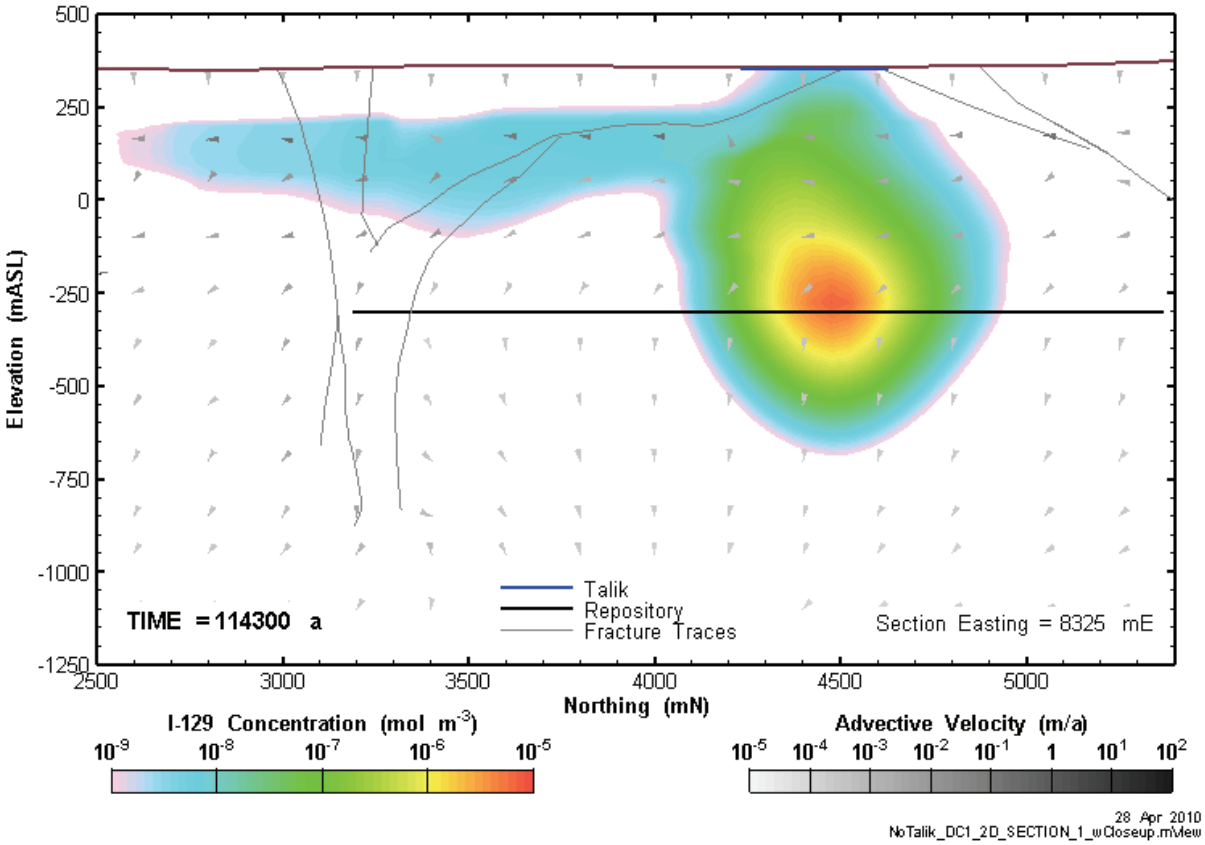

Figure 7.6: GSC-RC DC1, Y-Z cross section showing I-129 plume after 114,300 years, the end of the second glacial advance (cold-based). Arrows illustrate direction and magnitude of the advective velocity.

Figure 7.7 shows the plume at the end of the second glacial retreat, which is warm based. Where sufficient ice covers still exists (i.e., north of ≈ 3000 mN), there is a southward flow at the top of the model, caused by the slope of the retreating glacier. At the elevation of the repository the advective flow direction is upwards. This upward flow is due to the pressurized fluid stored during the preceding glacial advance. Although the prevailing flow direction in the upper units is still southward, the southernmost reaches of the plume seem to contract during this stage. This can be attributed largely to dilution, as the I-129 is drawn upwards into the permeable shallow aquifer and swept away to the south more rapidly than it can be replaced from below. This effect is much weaker if the retreat is cold-based.

The effects of a typical glacial advance-retreat cycle on the contaminant plume are largely confined to the upper part of the plume in the more permeable, shallower units. Comparing Figure 7.5 to 7.7 it is evident that the core of the plume, above concentrations of 10^{-7} mol/m^3,

remains relatively unaffected by the massive hydraulic perturbations induced by the advancing and retreating ice field. This is largely due to the low permeability of the deeper geosphere, and the roughly equal and opposite effects of the glacial advance and retreat stages. Within the repository footprint, the flow direction is generally downward during ice advances, and upward during retreats. At all times, the velocities within the repository footprint remain very low, i.e., on the order of millimetres per year or less.

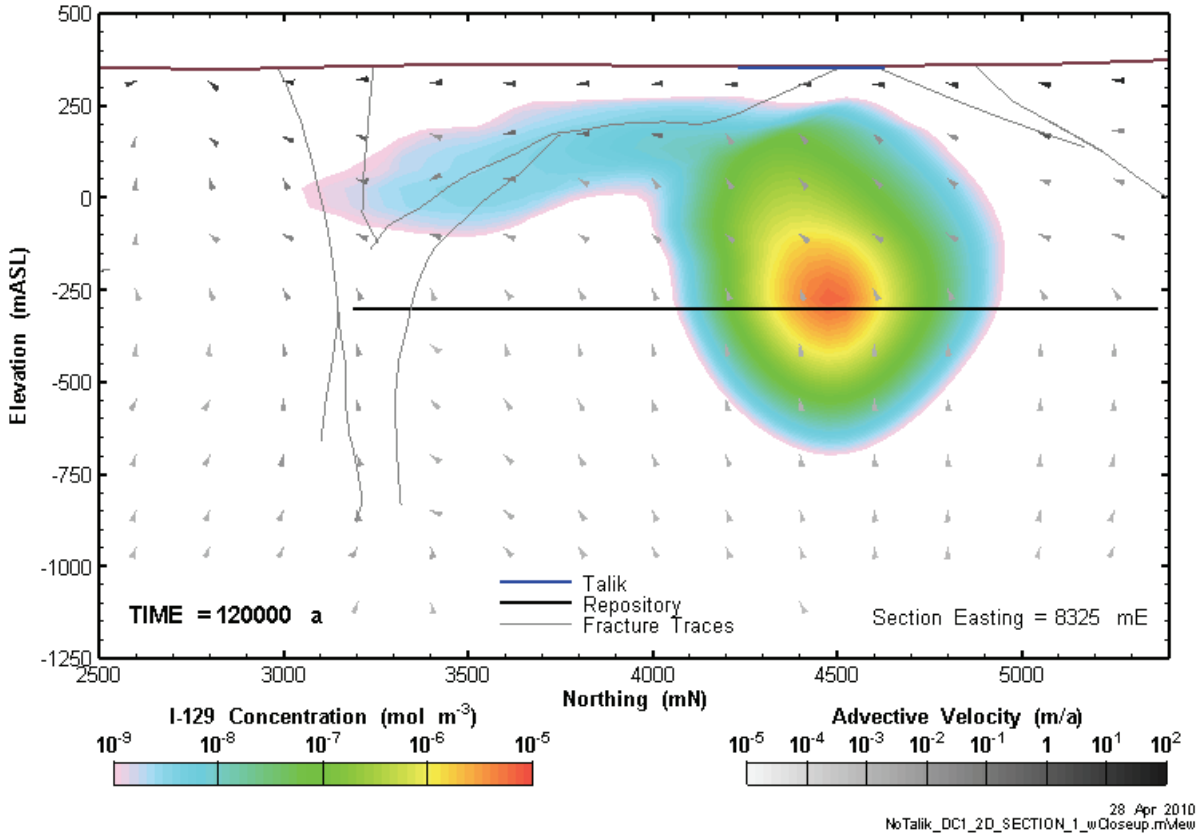

Figure 7.7: GSC-RC DC1, Y-Z cross section showing the I-129 plume after 120,000 years, the end of the second glacial retreat (warm-based). Arrows illustrate direction and magnitude of the advective velocity.

Figure 7.8 shows plan sections of the DC1 plume for case GSC-RC at 6 different times during the entire 0.8 Ma simulation period. These plan sections are at elevation 0.0 mASL, or 300 m above the repository horizon. As shown in the preceding figures, the outer reaches of the plume advance and retreat during different parts of the glacial cycle, but the core remains largely stable.

Figure 7.9 shows a North-South cross section through the centre of the plume at the same six times as Figure 7.8.

It is difficult to determine when the I-129 plume reaches its maximum extent, but the plume in Figure 7.8 (d) at 402,600 years is close to the maximum. Before this point the outer reaches of the plume generally grow larger, while after this point the plume generally shrinks.

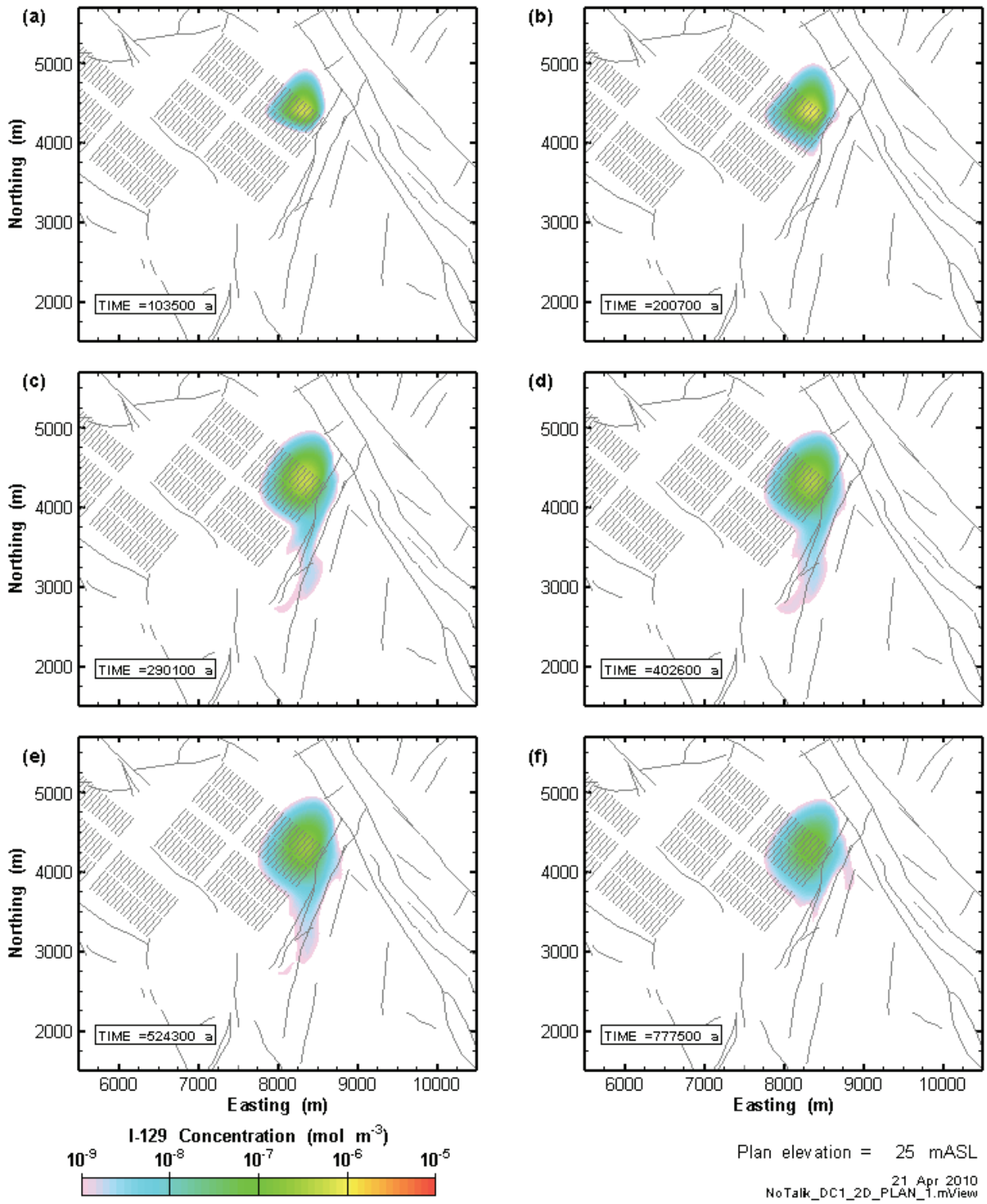

Figure 7.8: GSC-RC (Reference Case) DC1 X-Y planar section of transport model results at 6 times during the simulation period. Section elevation of 0.0 mASL (approximately 370 mBGS).

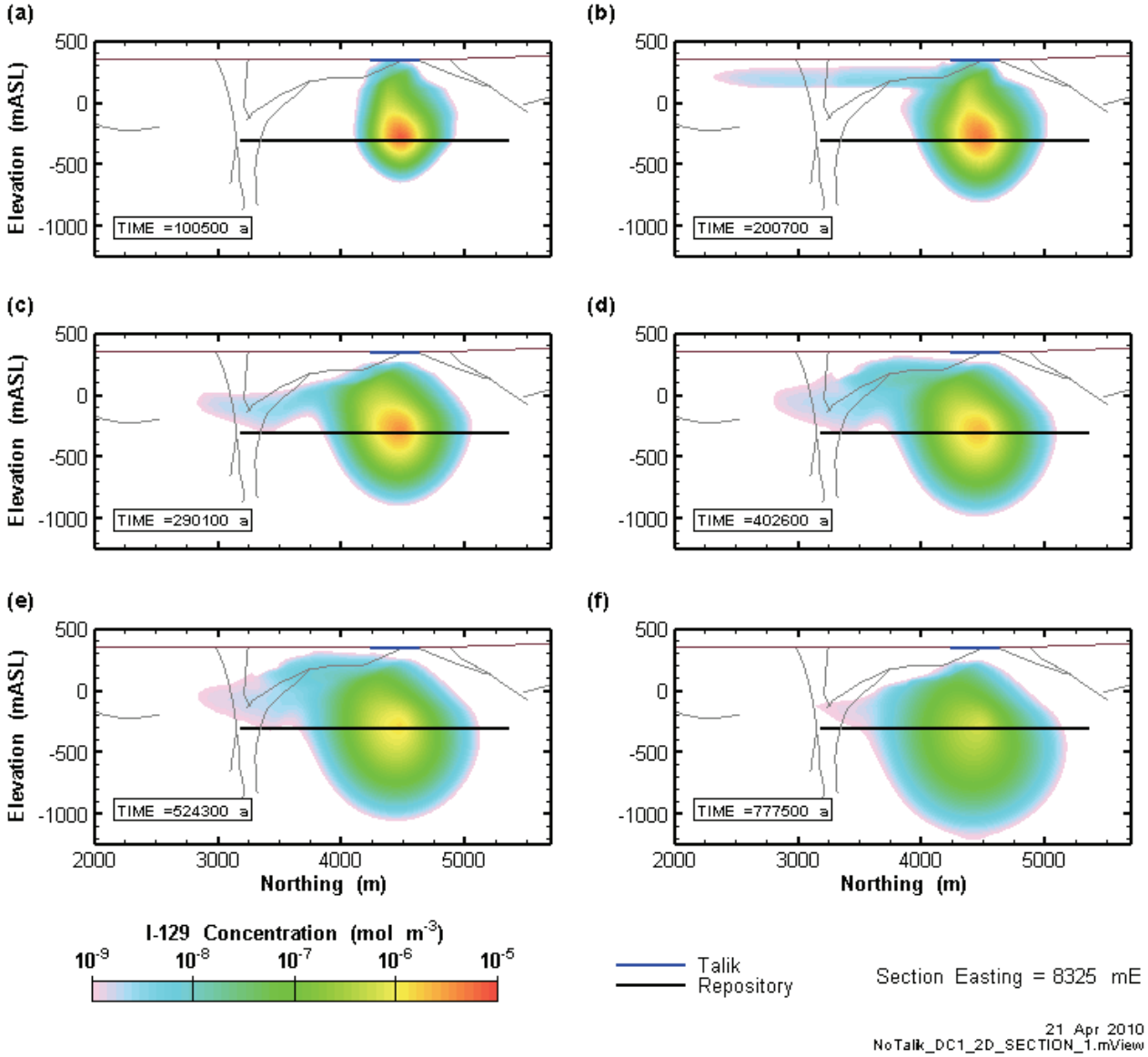

Figure 7.9: GSC-RC DC1 (Reference Case) Y-Z cross section of transport model results at 6 times during the simulation period. Section easting of 8325 mE.

Figure 7.10 shows plan sections for modelling case GSC-CC (Constant Climate case) for the plume from the DC1 source location at 6 different times during the simulation period.

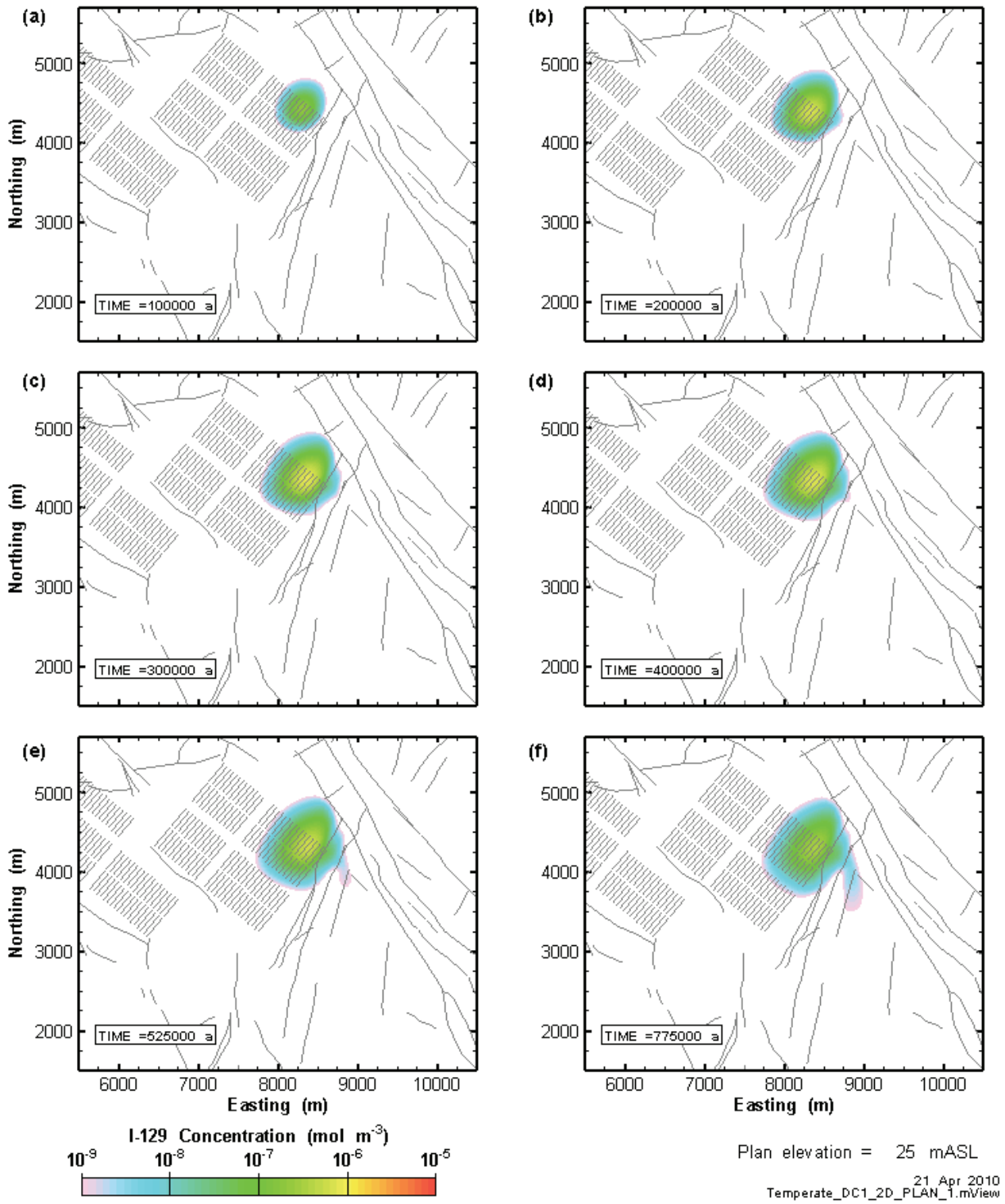

Figure 7.10: GSC-CC (Constant Climate) DC1 X-Y planar section of transport model results at 6 times during the simulation period. Section elevation of 0.0 mASL (approximately 370 mBGS).

Comparing Figure 7.10 to Figure 7.8, there are clear differences between the two plumes. Because there are no glacial advances and retreats in the GSC-CC model, the outer part of the plume does not spread as far as in GSC-RC case. However, above roughly 10^{-8} mol/m^3, the steady state GSC-CC and the GSC-RC plumes do not differ greatly. The concentrations at the centre of the GSC-CC plume remain somewhat higher than for the Reference Case plume because of the lower average flow velocity at the source. The higher velocities in the GSC-RC spread the plume over a larger area, with lower concentrations resulting. The differences between plumes in the GSC-CC and GSC-RC cases are much less than might be expected, given the extreme perturbations of the hydraulic system induced by glacial loading and unloading. Figure 7.11 shows six North-South cross sections through the centre of the GSC-CC plume, at the same times as shown in Figure 7.10. Once again, the similarity to the GSC-RC plume is evident although the GSC-CC plume is slightly more compact.

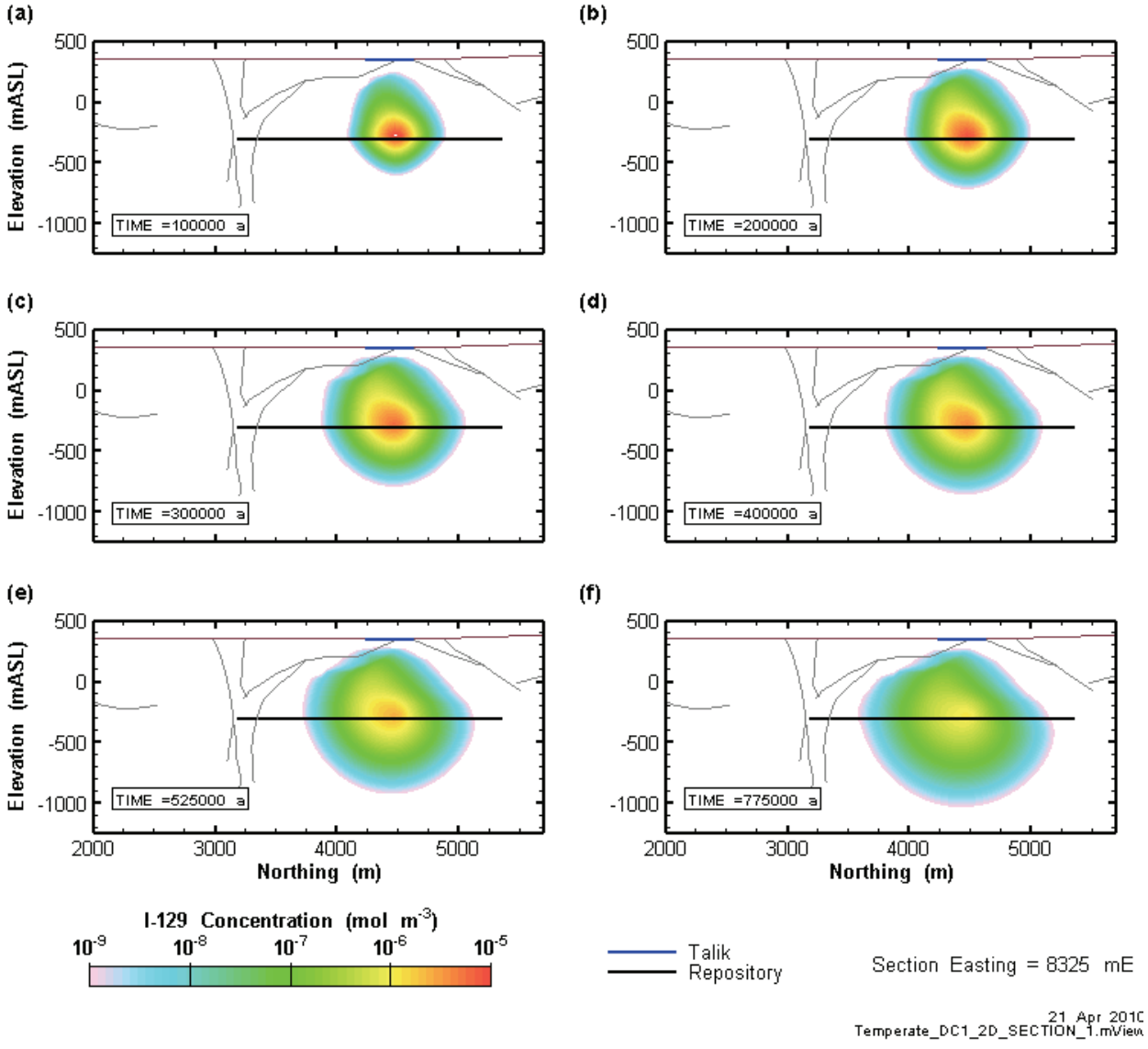

Figure 7.11: GSC-CC (Constant Climate) DC1 Y-Z cross-section of transport model results at 6 times during the simulation period. Section easting of 8325 mE.

Figure 7.12 and Figure 7.13 present snapshots of the transport results for the GSC-HS (High Storage coefficient) case for the DC1 source location. The picture presented in these figures is distinct from the GSC-RC results in Figure 7.8 and Figure 7.9. Although the extent of the plume in the GSC-HS model is similar to that seen for the GSC-RC model, the concentration at the centre of the plume declines much more rapidly in the GSC-HS model. This suggests that, in the GSC-HS case, the radionuclide is being spread further (vertically and horizontally) throughout the model domain due to the increased groundwater flow rates in the model domain (see Section 6.4). Consequently, the plume is more diluted in GSC-HS than in GSC-RC. Furthermore, the plume in Figure 7.13 for the GSC-HS model also appears to have a downward migrating trend, as compared to the GSC-RC plume. This downward movement agrees with the repository velocity analysis from Section 6.4, where it was shown that the average net advective travel direction over the course of a complete glacial cycle was downward within the repository footprint.

Figure 7.14 and Figure 7.15 show the GSC-NF (No-Flow N-S boundaries) case for the DC1 source plume at six times during the simulation period, in plan and cross section respectively, as in previous figures. The GSC-NF plume differs from the GSC-RC plume. The long, low concentration extensions of the radionuclide plume in the upper, more permeable units are significantly stunted in the GSC-NF model. This is a reflection of the generally much lower velocities in the GSC-NF model during glaciation events (compare for example Figure 6.10 and Figure 6.19). The lower velocities are caused by having no-flow North and South boundaries, rather than specified head boundaries. In the GSC-RC model, the difference between the northern and southern specified heads leads to a sizable hydraulic gradient during glaciated periods. This gradient is absent in the GSC-NF model.

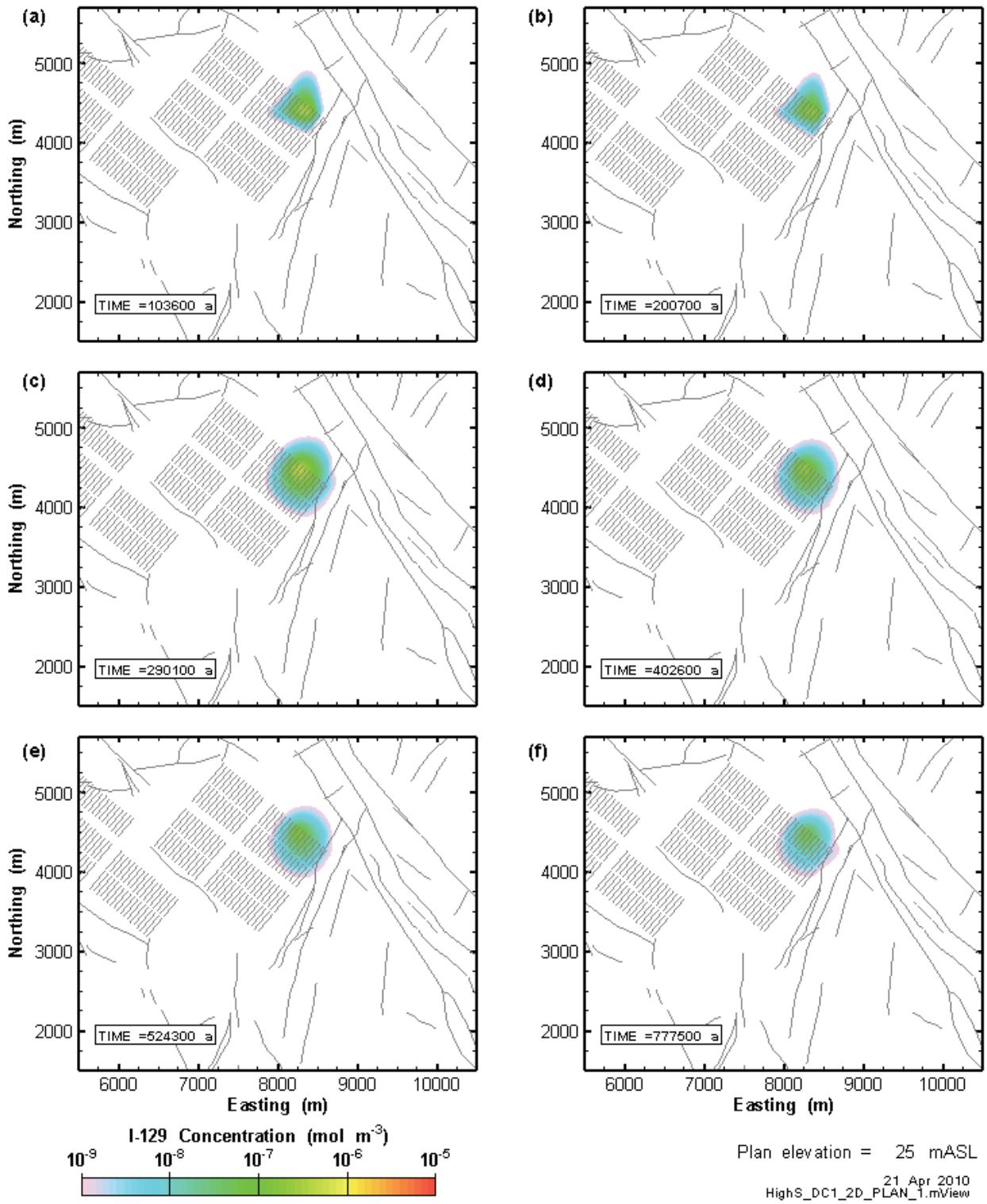

Figure 7.12: GSC-HS (High Storage coefficient) DC1 X-Y planar section of transport model results at 6 times during the simulation period. Section elevation of 0.0 mASL (approximately 370 mBGS).

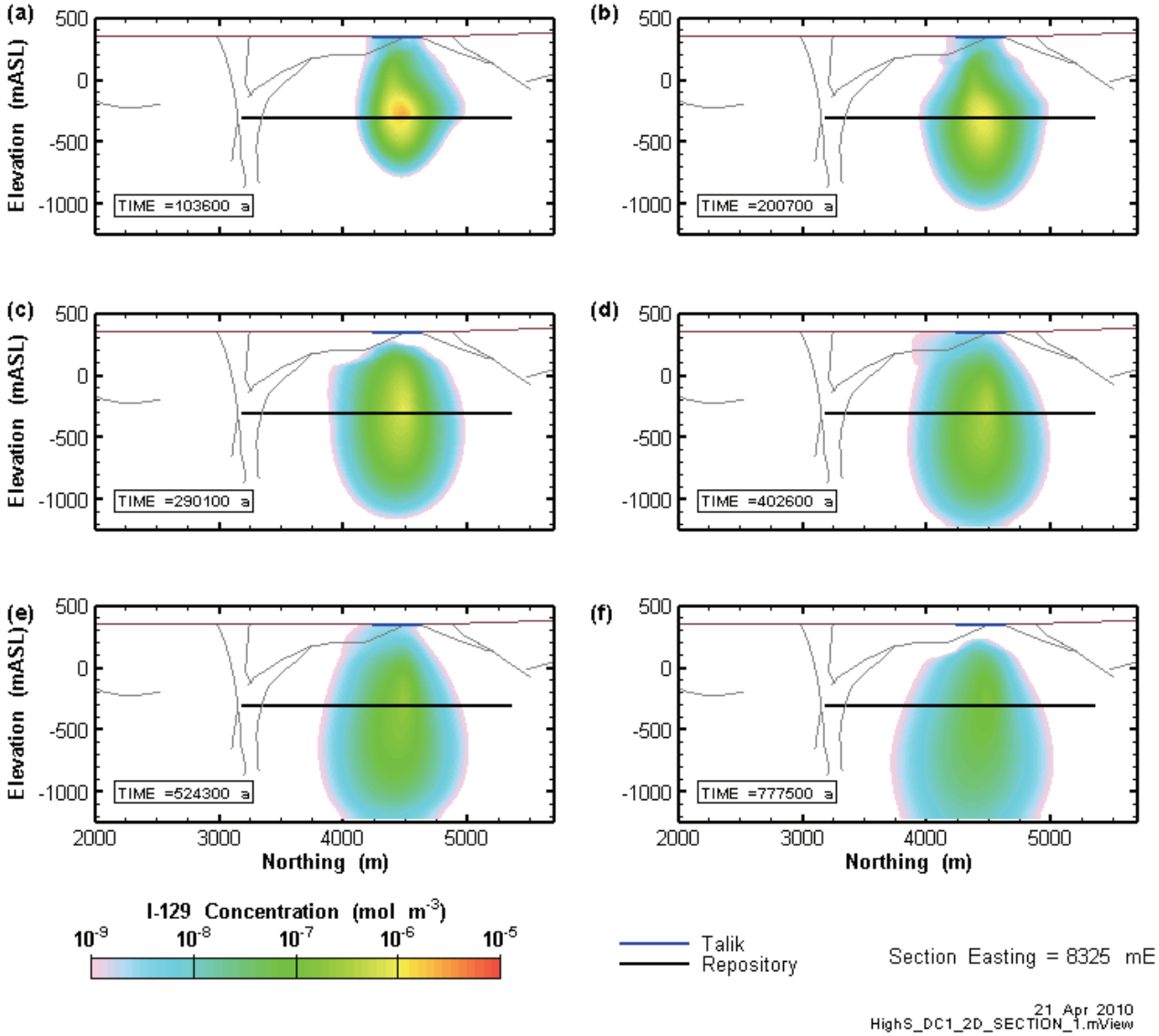

Figure 7.13: GSC-HS (High Storage coefficient) DC1 X Y-Z cross-section of transport model results at 6 times during the simulation period. Section easting of 8325 mE

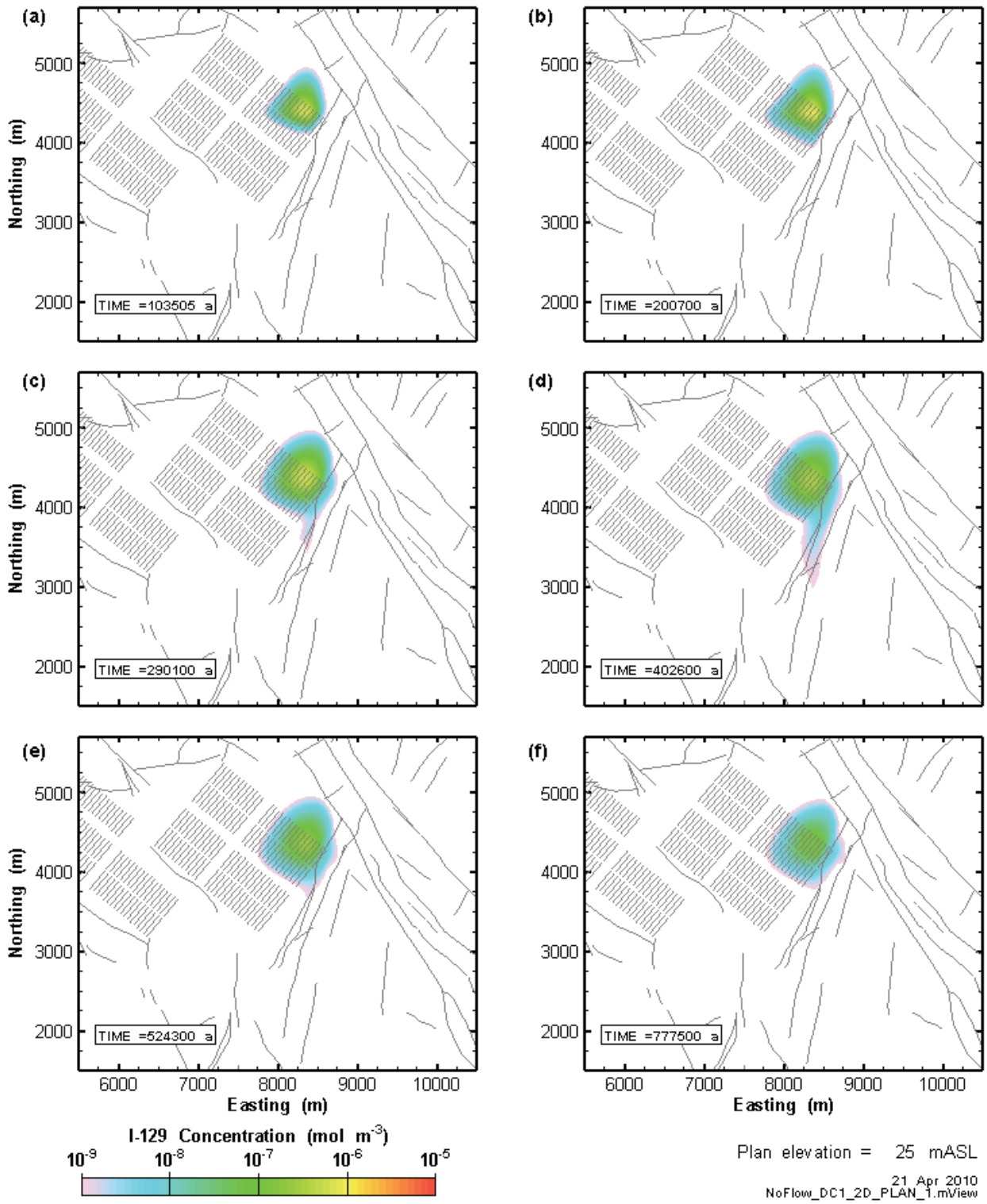

Figure 7.14: GSC-NF (No-Flow North-South boundaries) DC1 X-Y planar section of transport model results at 6 times during simulation period. Section elevation of 0.0 mASL (approximately 370 mBGS).

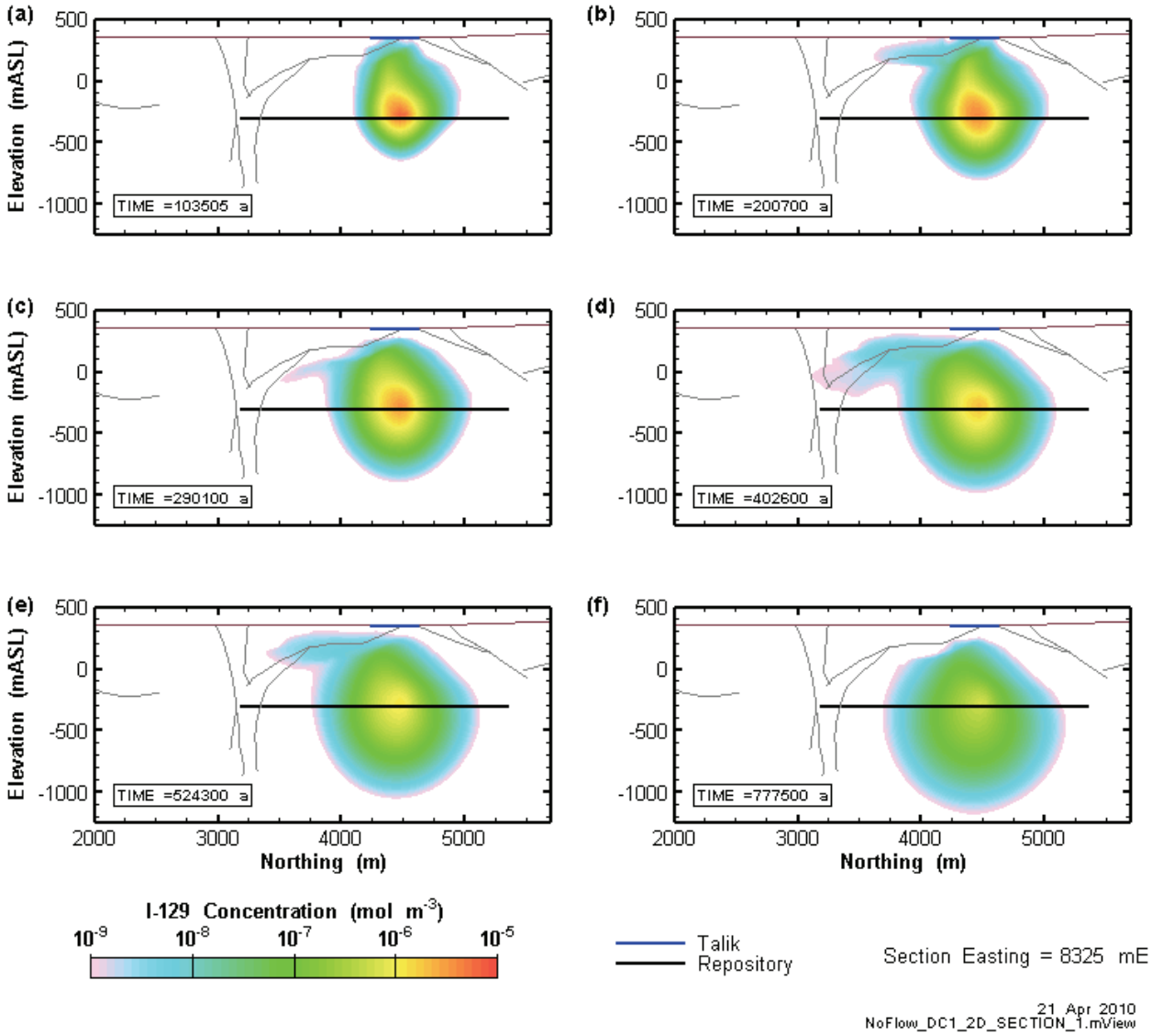

Figure 7.15: GSC-NF (No-Flow North-South boundaries) DC1 Y-Z cross-section of transport model results at 6 times during simulation period. Section easting of 8325 mE.

The effect of having areas of unfrozen ground in the sub-glacial permafrost is shown very clearly in Figure 7.16 and Figure 7.17. These figures show transport results for the model GSC-TK (Talik under glacier), which differs from the reference case only in that the two taliks remain open during cold-based glacial advances. As one would expect, during ice sheet advance, the very high specified heads at the surface of the open taliks lead to water flowing downward through the taliks. This relatively high flow spreads and disperses the upper part of the radionuclide plume to the East, West, and North, leading to a larger but more dilute plume than for case GCS-RC. Nevertheless, the more concentrated core of the plume remains relatively unchanged. This is particularly evident in Figure 7.17.

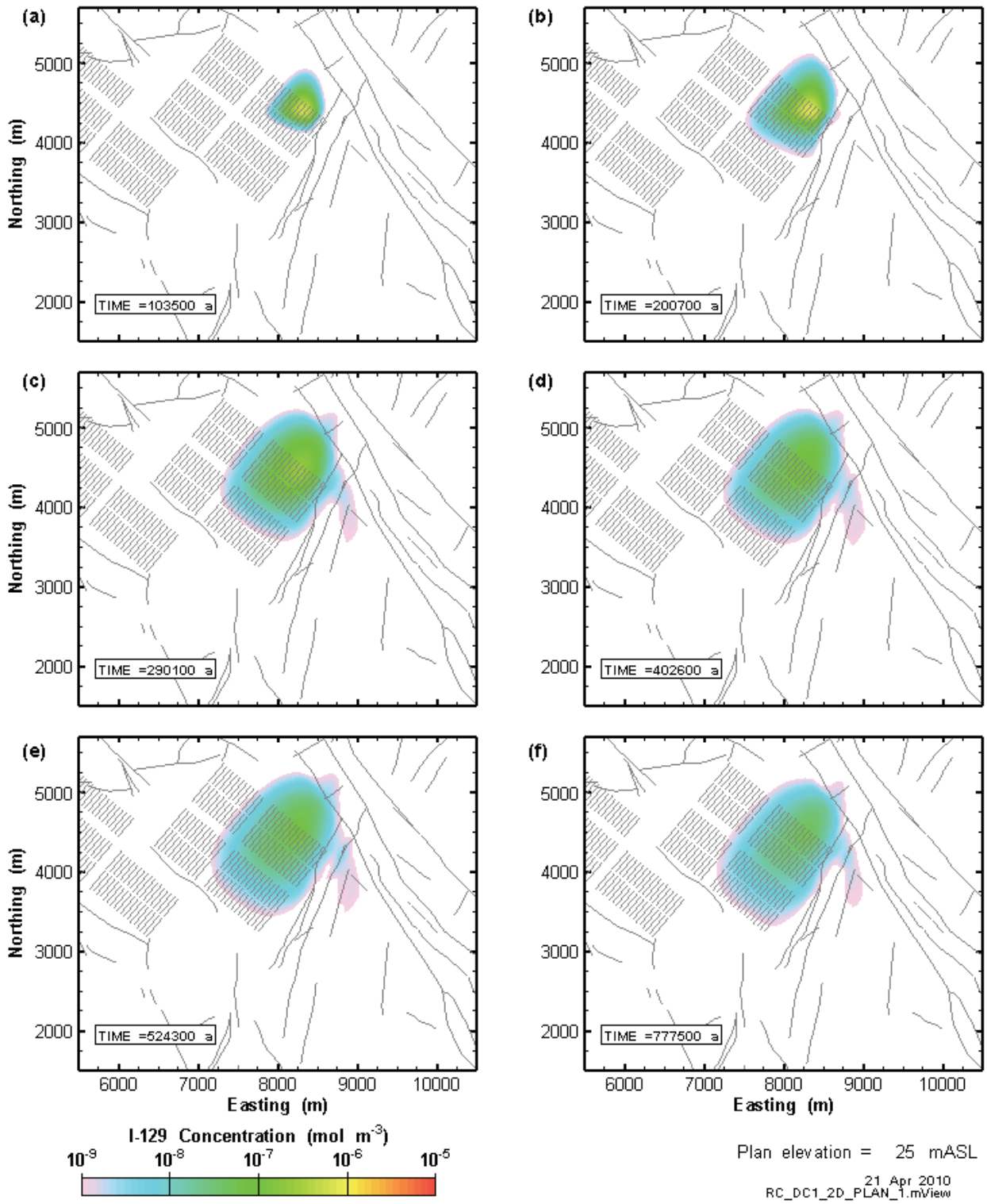

Figure 7.16: GSC-TK DC1 (Talik under glacier) X-Y planar section of transport model results at 6 times during the simulation period. Section elevation of 0.0 mASL (approximately 370 mBGS).

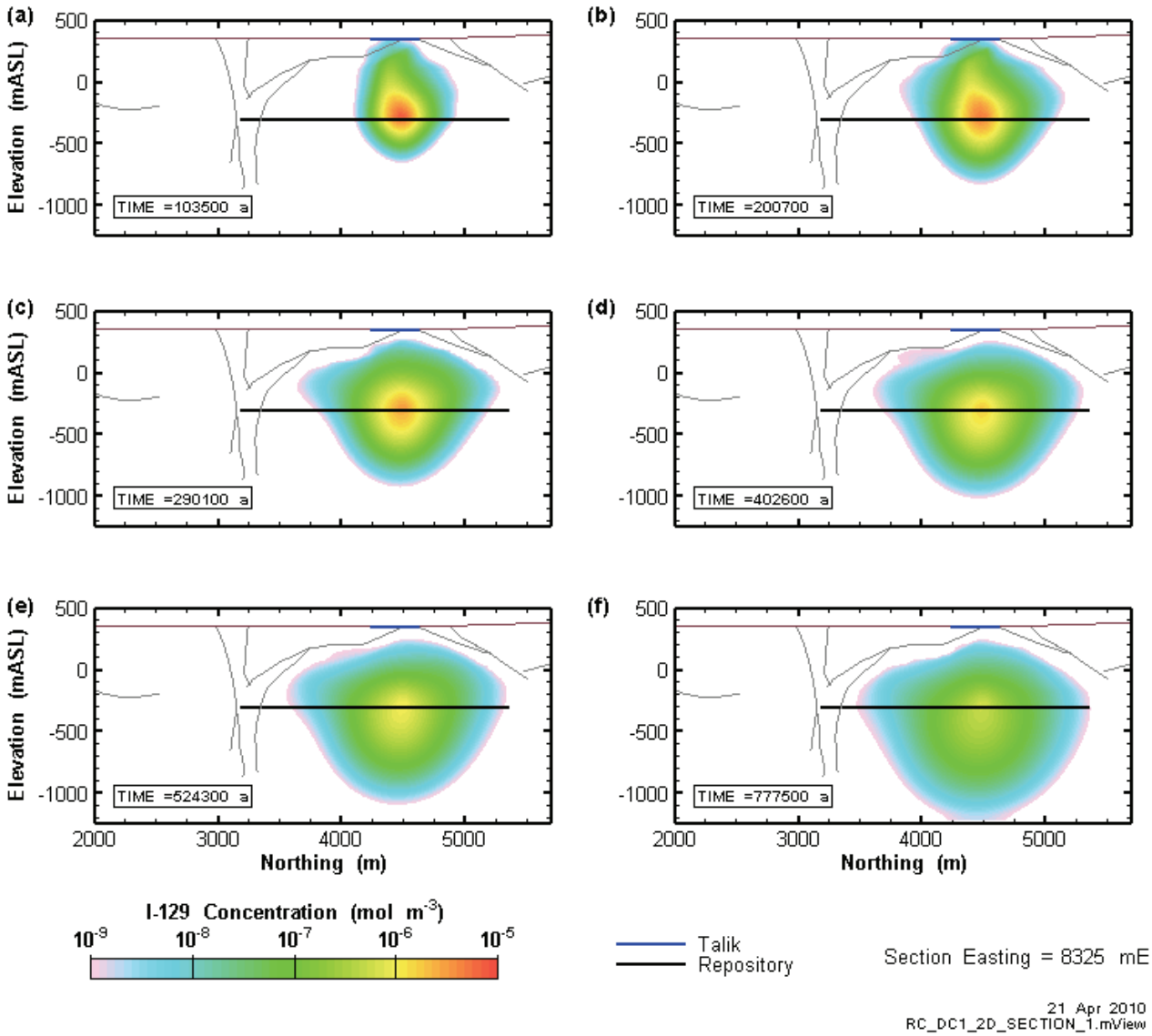

Figure 7.17: GSC-TK (Talik under glacier) DC1 Y-Z cross-section of transport model results at 6 times during the simulation period. Section easting of 8325 mE.

In summary, although the glacial cycles do modify the flow field extensively, the cumulative impact of repeated cycles of advance and retreat tend to effectively “cancel out", leading to a general plume structure that is not substantially different from the steady-state flow transport model. However, at shallower depths, there are significant differences between the various models, as the glacier advance and retreat and flow at the talik disperses I-129 in the upper zones below the permafrost. The higher permeability fracture system is the primary conduit for plume dispersal.

7.6 MASS FLOW PLOTS

Radionuclide mass flow to the biosphere was calculated over the duration of the simulation period. Previous studies had calculated I-129 mass flows to the North Lake and to the major river south of the repository (River). Results from the GSC simulations also showed I-129 mass flow exiting the geosphere in the area several kilometres to the west, due primarily to the dispersal of radionuclides underneath the permafrost during glacial advances. Accordingly, an additional mass flow zone (denoted "Western") was incorporated in the GSC modelling as shown in Figure 7.18. The southern lake, included as a second open talik in the current study, was also included as a mass flow zone (South Lake). All mass flow zones are located at a depth of 30 m below ground surface, and it is assumed that all the I-129 mass crossing this depth will reach the surface biosphere.

Mass flows of I-129 across these zones are presented in the figures on the following pages. Some post-processing of the results has been performed to remove periods of negative (downward) mass flow. These negative flow periods are caused when I-129 transported above the mass flow zones during discharge periods is re-injected into the formation when the flow direction reversed. In reality, radionuclides entering a talik, lake, or catchment zone would likely be diluted and swept downstream in a relatively short time, and not be available for reinjection. Thus, removal of the negative mass flow periods is a conservative approach to addressing possible model errors due to this process.

The mass flow figures below present both I-129 mass flow rates (in moles per year) and cumulative I-129 mass flows (in moles). To maintain legibility of the figures for the transient data, the mass flow rate only for the discharge zone with the highest mass flow is typically presented. Typically the difference between the mass flow across the zone with the highest and second highest mass flows is at least a factor of 10.

The results shown are limited by the minimum value on the Y-axis, which is 10^{-8} mol/a for the mass flow rate and 10^{-4} mol for the cumulative mass. Consequently, not all zones may be displayed in the figures. Thus, for example, if the cumulative mass curve is not shown, this indicates that the cumulative mass never exceeds the minimum value on the Y-axis. In all figures, transient GSC simulation results are compared to corresponding results for the constant (temperate) climate model (GSC-CC) without a well, providing a baseline for comparison between figures. The steady state results without a well are used for comparison because there is no well during most of the transient simulations.

Only the I-129 mass flows to the biosphere for the DC1 source location are presented here, since I-129 releases from this location lead to the highest critical group dose rates. The results for the DC3 source location can be found in Walsh and Avis (2010).

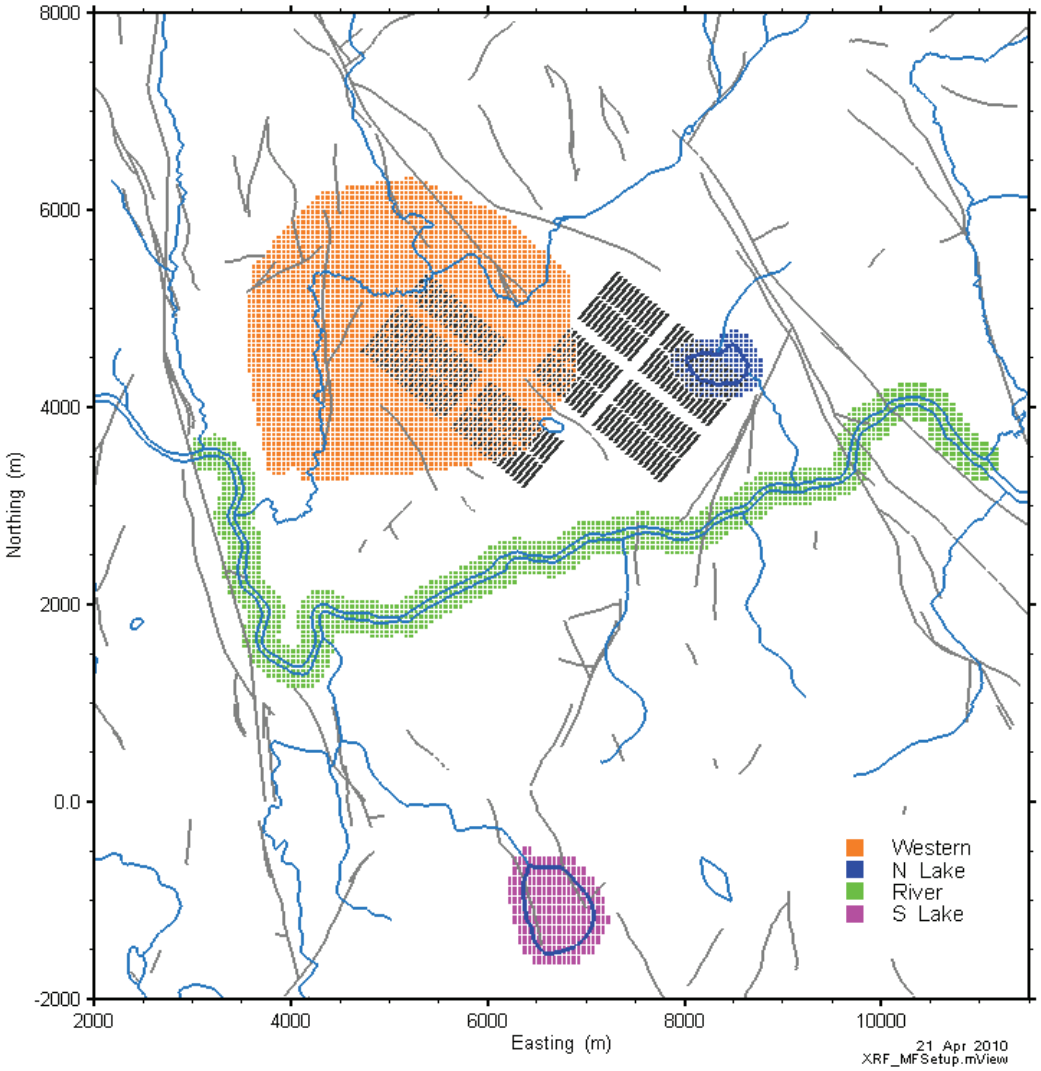

Figure 7.18: GSC transport mass flow calculation zones.

7.6.1 Constant Temperate Climate Model

Figure 7.19 shows the I-129 mass flow rates and cumulative mass flows for case GSC-CC (Constant Climate) for the DC1 source location (see Figure 7.3). The DC1 location lies directly below the North Lake zone, so it is unsurprising that the I-129 mass flows are highest for the North Lake discharge zone for this source location. A small proportion of the contaminant from DC1 also reaches the River zone. No significant amounts of I-129 reach the Western and South Lake zones from the DC1 source location.

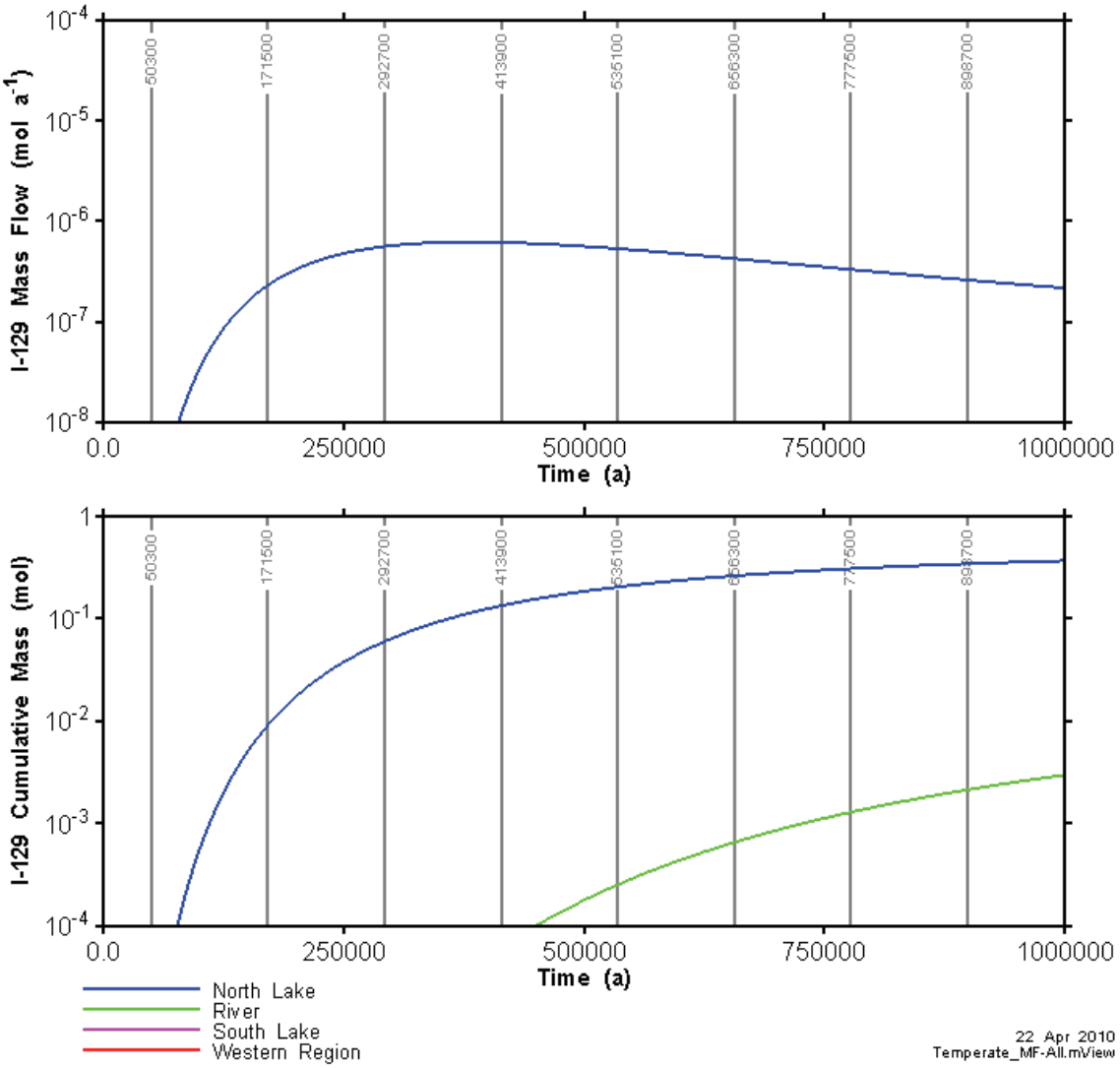

Figure 7.19: GSC-CC (Constant Climate) I-129 mass flow rates and cumulative mass flows for the DC1 source location. Lines in the legend that do not appear on the plot are below the minimum value on the Y-axis. The vertical lines indicate the start of a glacial cycle.

7.6.2 Transient Modelling Cases

Figure 7.20 compares the mass flow results for the Reference Case (GSC-RC) model with the DC1 source with the corresponding GSC-CC results. The mass flow rate curve is clearly quite different for the transient model, with a great variation in the I-129 mass flow rate. However, the overall trend is similar and, by the end of the simulation period, the transient model predicts roughly similar cumulative mass flows into the North Lake zone. The GSC-RC model clearly causes I-129 to be transported over a larger region, as evinced by higher flow at the River region as compared to the GSC-CC model.

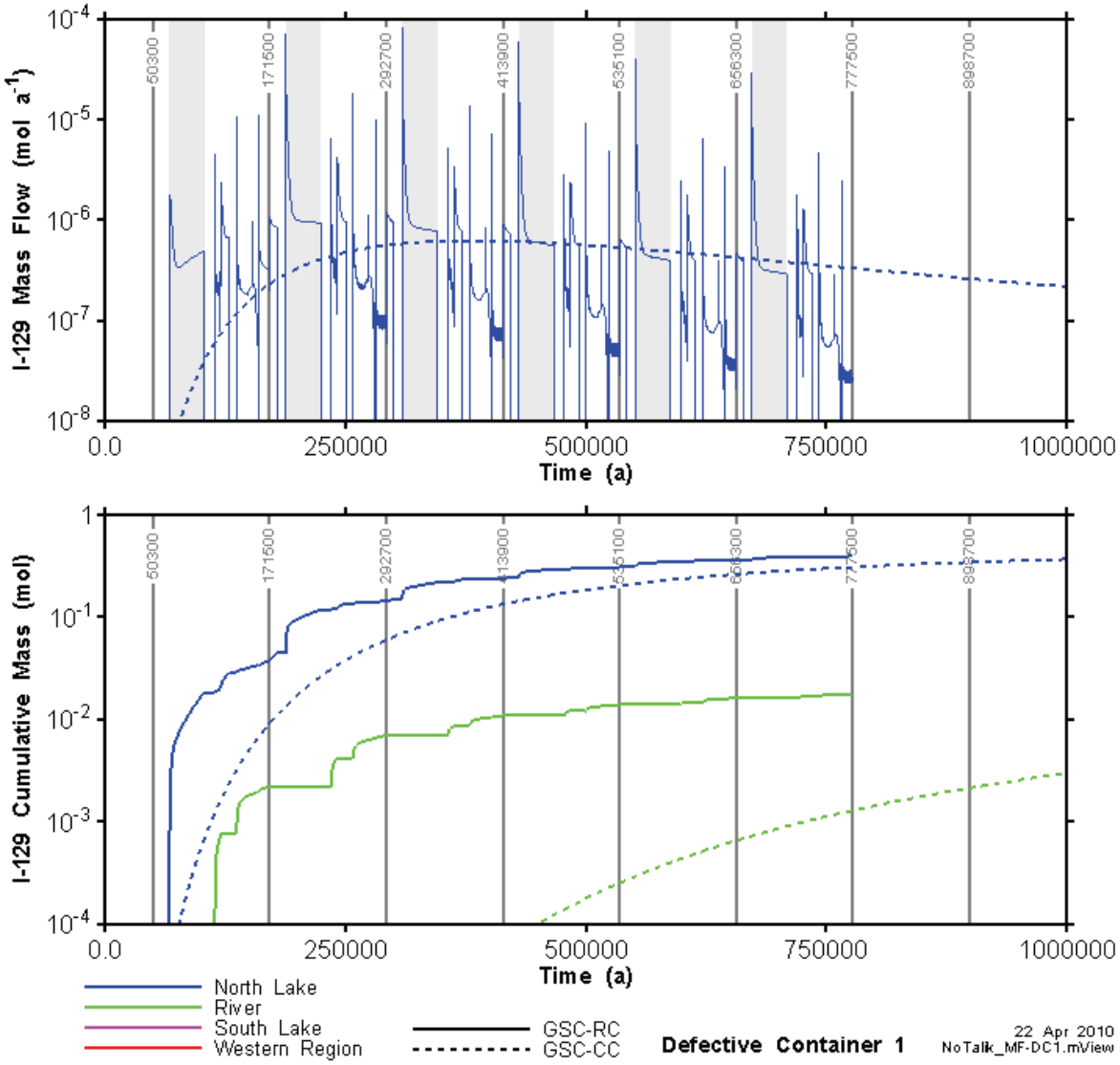

Figure 7.20: GSC-RC I-129 mass flow rate and cumulative mass flow for DC1 source, compared to GCS-CC (without a well). Mass flow only plotted for North Lake to improve legibility of plot. The vertical lines indicate the start of a glacial cycle. Shaded regions show the second Permafrost State in each glacial cycle.

Note that Figure 7.20 shows I-129 mass flows and not concentrations. The variability of the concentration is more muted because the larger I-129 mass flows are associated with higher water discharge rates. Figure 7.21 shows the average concentration of I-129 in water entering the North Lake. The variation in the I-129 concentrations is about one order of magnitude smaller than the variation in the I-129 mass flow rates. Although concentration alone does not explain the variation in mass flow rate, increased mass flow and concentration are correlated, as the more concentrated water flows up from greater depths.

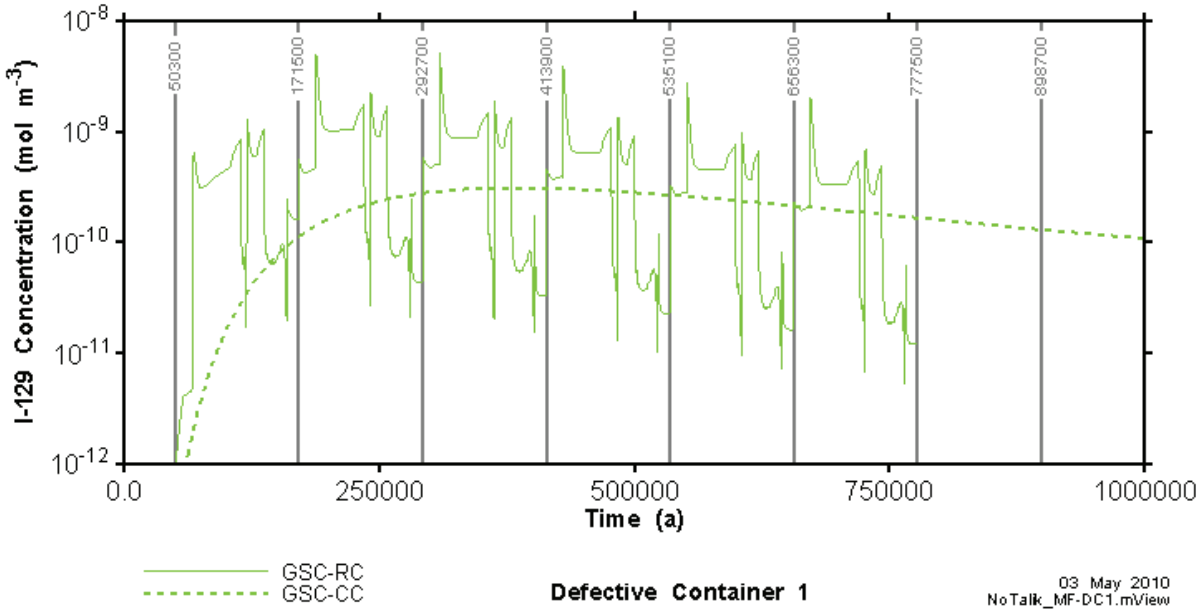

Figure 7.21: I-129 concentration in water entering the North Lake zone, for the GSC-RC and GCS-CC (no well) modelling cases. The vertical lines indicate the start of a glacial cycle.

Some of the mass flow results for this transient model are rather counterintuitive. Figure 7.22 is a close-up of the second glacial cycle. It is evident that the highest mass flows occur at the beginning of Permafrost States, particularly the second permafrost stage (stage 5, Table 3.3). High mass flow rates at the start of this stage are due to the high pressures stored in the subsurface from the preceding glaciation. With the surface largely covered by an impermeable permafrost layer, the North talik, located directly above DC1, is one of the few hydraulic outlets for the system. Thus flow is focussed in the vicinity of this talik, causing high velocities and promoting transport of I-129 from the repository to the surface across this North Lake mass zone (see Figure 6.12).

However, it is clear from Figure 6.15, Figure 6.16 and Figure 6.25 that the glacial retreat (stage 11) and proglacial lake (stage 12) also have relatively high upward advective flows in the vicinity of the repository. The high vertical advective velocity is not reflected in the observed I-129 mass flow. During the glacial retreat, the predominant flow direction shifts from vertically upward to horizontally southward above roughly 200 mASL, due to the variable specified head at the surface that represents the slope of the ice surface. This horizontal flow sweeps the I-129 plume towards the south, away from the area directly below the North talik. Although upward

flow is re-established in the Proglacial Lake State, the I-129 concentration directly below the North Lake zone is now rather low, and the duration of this state is not long enough to bring significant amounts of I-129 from greater depths to the surface. So, although the overall vertical upward gradient is high during both the glacial retreat and the proglacial lake stages, the mass flux across the defined surfaces is low.

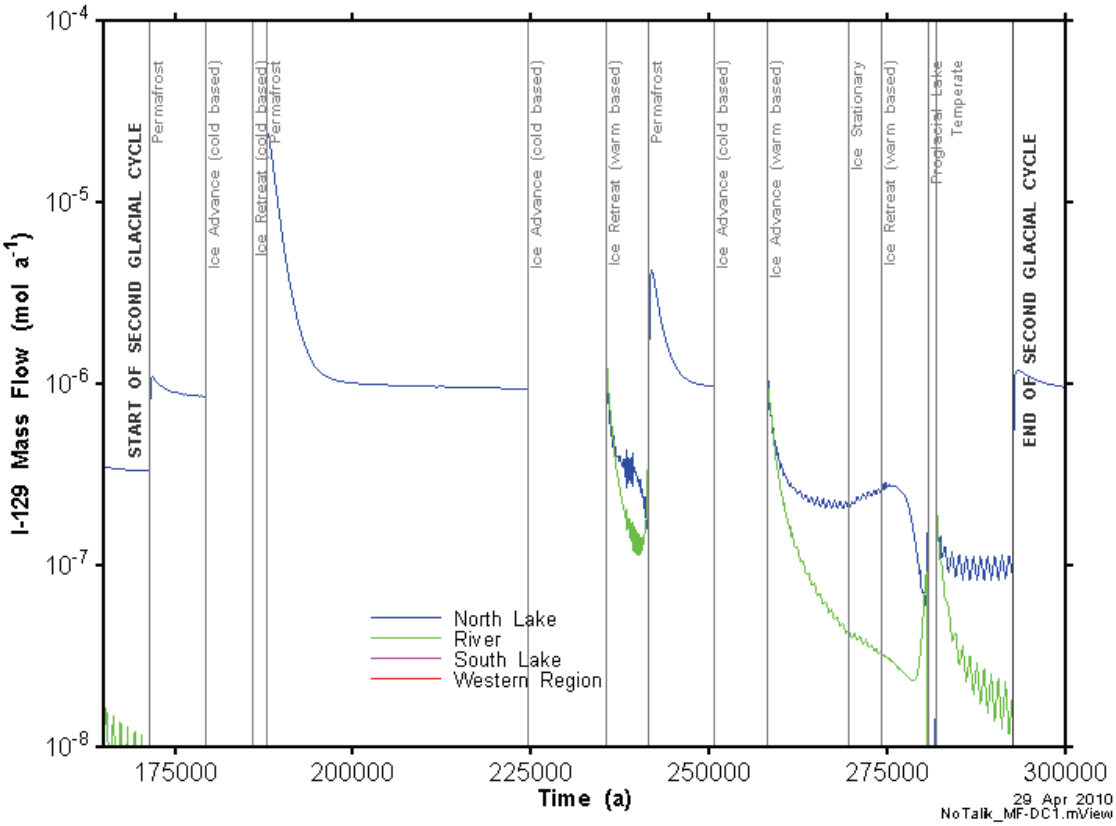

Figure 7.22: GSC-RC I-129 mass flow rates for second glacial cycle and DC1 source location.

Figure 7.22 also shows some evidence of numerical instability in the flow solution, particularly during the second (warm-based) ice retreat between 235,500 and 241,500 years. The oscillations are a direct consequence of the small oscillation in the flow solution (see Figure 6.25). This numerical instability reduces the accuracy of the model to a limited degree during these stages of the glacial cycle. However, the fluctuations remain relatively small and tend to oscillate around a mean correct value so the results are still sufficiently accurate for the purposes of this report.

Figure 7.23 shows the I-129 mass flows for the high storage coefficient (GSC-HS) case. As described earlier, in Section 6.4, the average advective velocity is much higher in the GSC-HS model as compared to the Reference Case. High heads stored in deeper units during glacial advance persist for much longer after the ice has retreated. The difference between the two cases is especially clear in the mass flow curves during the second permafrost period in each glacial cycle (shaded regions in plot). In Figure 7.20, the peak mass flow occur at the beginning

of the second permafrost period, but decays to a steady state flow rate in less than 10,000 years, as the stored pressures in the deep units dissipate. In contrast, in Figure 7.23, the mass flow rate also peaks at the beginning of the second permafrost period, but it never reaches a steady state during this period, meaning that at the beginning of the next ice advance, after 36,800 years of permafrost cover, stored heads from the preceding glaciation are still present in the deeper parts of the geosphere. Naturally, the presence of high vertical gradients for a much longer time promotes increased vertical transport. The cumulative I-129 mass flow across the North Lake mass flow boundary is 26% higher than in the GSC-RC case.

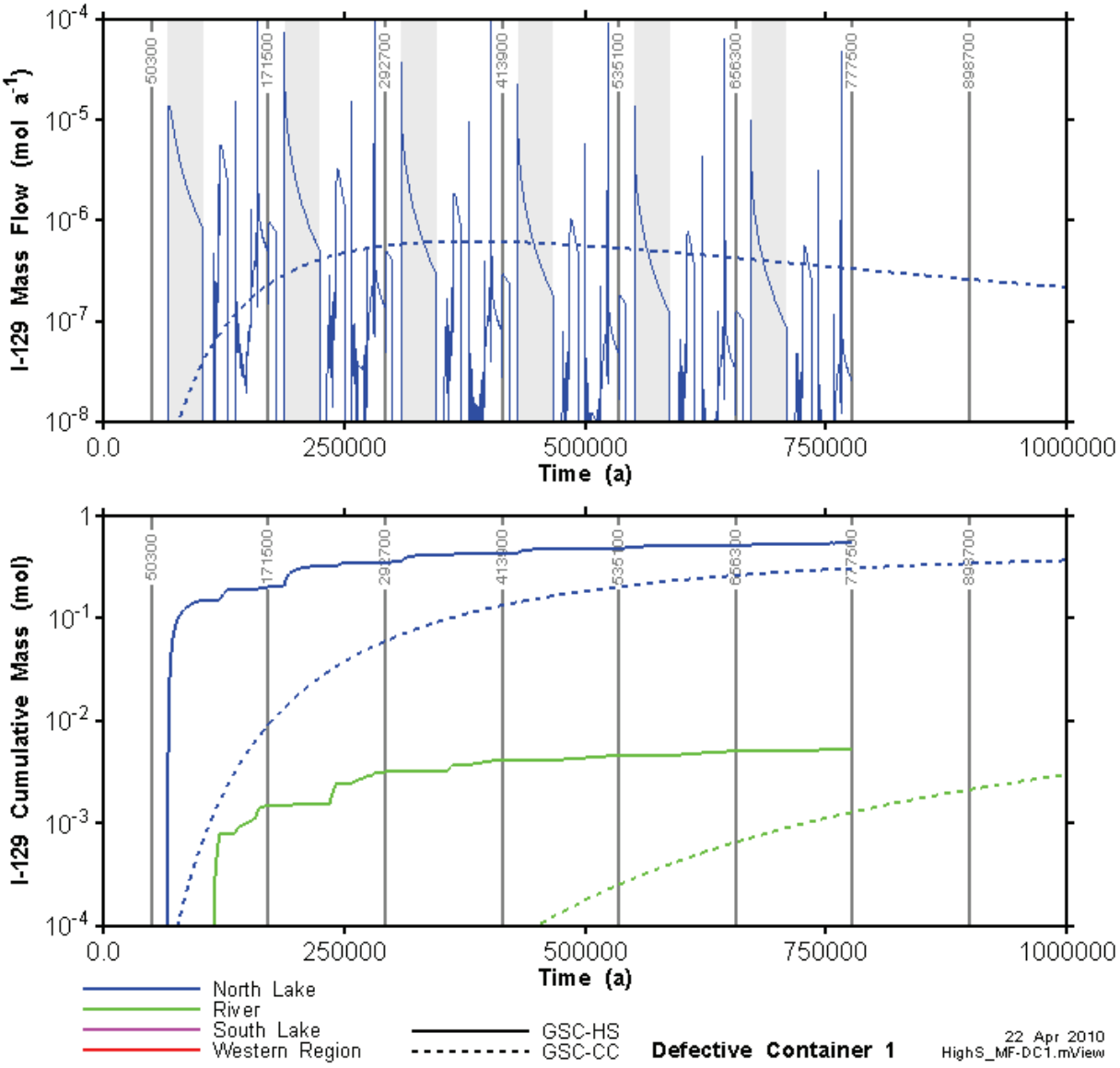

Figure 7.23: GSC-HS I-129 mass flow rate and cumulative mass flow from DC1, compared to GCS-CC (without a well). Mass flow only plotted for North Lake to improve legibility of plot. The vertical lines indicate the start of a glacial cycle. Shaded regions show the second permafrost state in each glacial cycle.

In some ways, the GSC-NF case (No Flow North and South boundaries), mirrors the GSC-HS case, although the mechanism is different (Figure 7.24). The peak mass flow in any given glacial cycle occurs at the beginning of the second permafrost period (shaded regions in plot), when significant heads from the preceding glaciation are stored in the hydrogeological system. Because the no-flow North and South boundaries in the GSC-NF case do not provide hydraulic outlets for the stored pressure, the only route for water to escape is through the two taliks. This forces flow from the entire model domain through these two relatively small areas, and causes the system to require a much longer time to reach steady state (roughly 25,000 years). So, despite the fact that heads in the subsurface do not reach the same level during the preceding cold-based advance and retreat, the GSC-NF model still ultimately has higher cumulative mass flows across the North Lake zone, i.e., 12% higher than in the Reference Case.

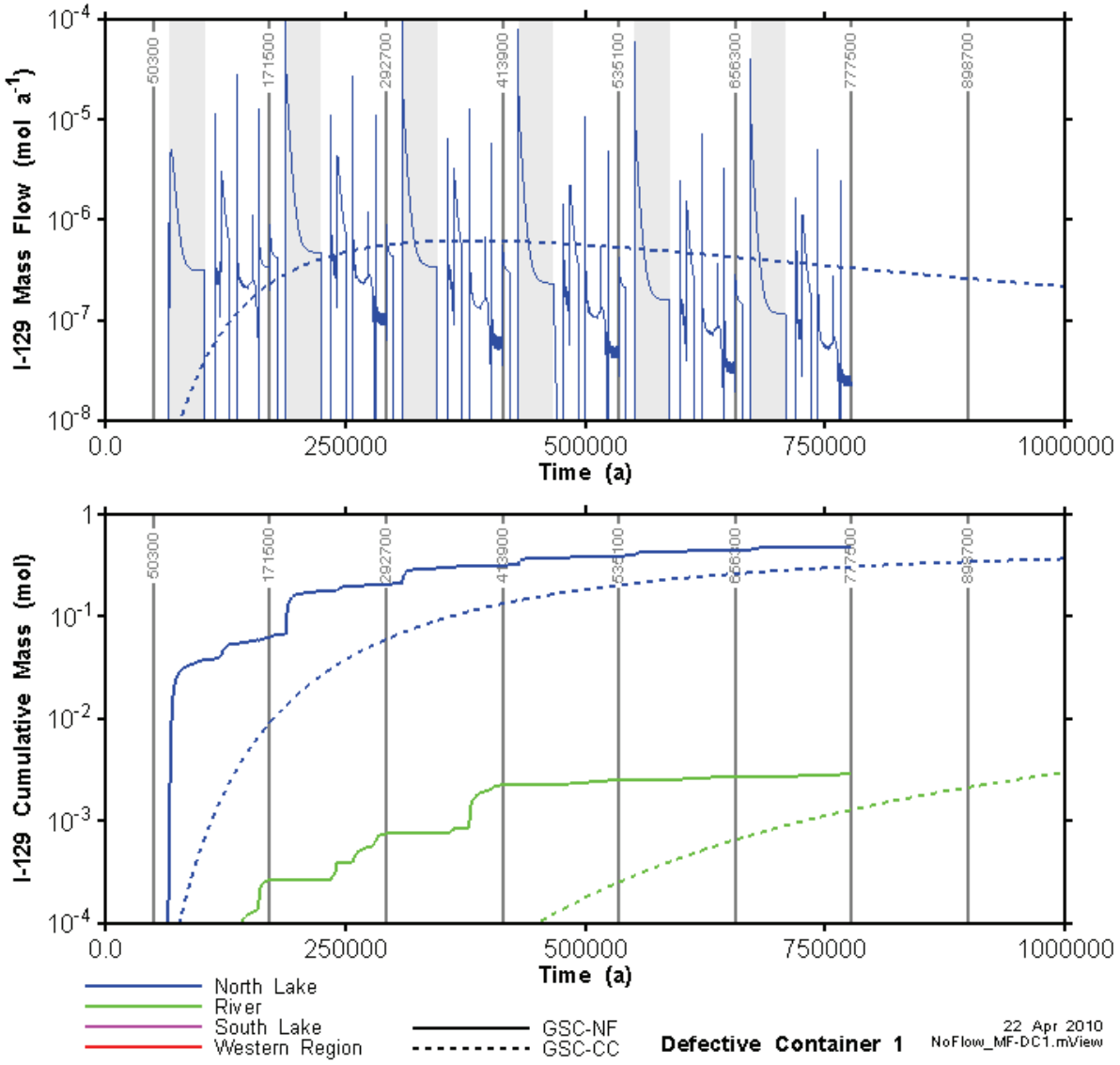

Figure 7.24: GSC-NF I-129 mass flow rate and cumulative mass flow from DC1, compared to GCS-CC (without well). Mass flow only plotted for North Lake to improve legibility of plot. The vertical lines indicate the start of a glacial cycle. Shaded regions show the second permafrost state in each glacial cycle.

The GSC-TK case is similar to the Reference Case, except that the two taliks existing during the Permafrost States remain open under cold-based glacial advances and retreats. During glacial advances and retreats, when the taliks are open, there is a greater spreading and dilution of the upper part of the plume caused by the water inflow across the North talik. However, this has a relatively small effect on the I-129 mass flow rate and the cumulative I-129 mass flow into the North Lake is only 8% less than for the GSC-RC case (Walsh and Avis 2010).

7.6.3 Well Concentrations

Concentrations of I-129 in well water for source location DC1 are presented in Figure 7.25. (Recall that the well is located so as to maximize impacts for this source location.) Peak well water concentrations are highest for the GSC-HS model, the case with the highest groundwater velocities. For all glaciation cases, the I-129 well water concentration peaks at 160,700 years, i.e., at the start of the Temperate State in the first glacial cycle. This is much earlier than for the Constant Climate case (GSC-CC), for which the well concentration peaks at about 400,000 years. This earlier peak is consistent with what was observed for the I-129 mass flow curves in Section 7.6.2 and is due to the impact of ice sheet advance and retreat on the groundwater flow system.

The sharp peaks in the I-129 well water concentrations at the beginning of Temperate States are likely caused by rapid drainage of the proglacial lake. The peak is particularly pronounced for the GSC-HS case. For this case, the peak does not persist for long and within 200 years the concentration drops by about one order of magnitude. For the other glaciation cases, the I-129 well water concentration decreases more slowly. Consequently, if the Farmer critical group arrives at the repository site several thousand years after the end of the Proglacial Lake State, it would not be exposed to the highest well water concentrations and, therefore, the calculated dose rates for this critical group would be marginally lower.

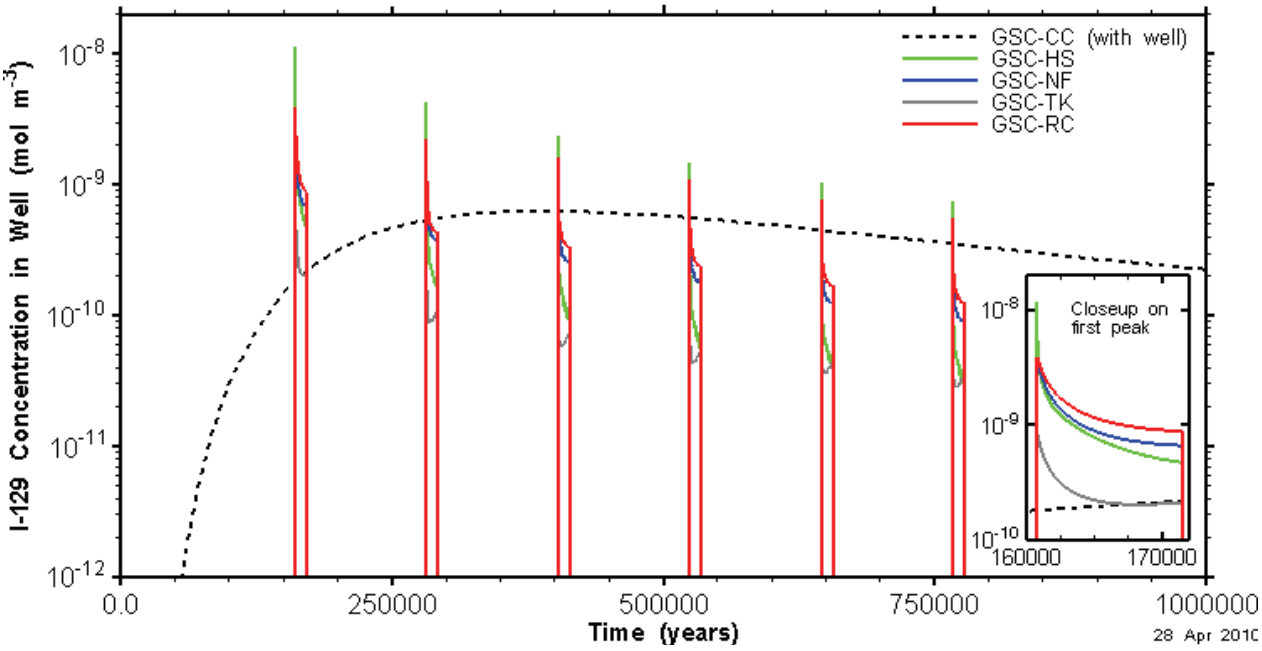

Figure 7.25: I-129 concentrations in well water for all DC1 calculation cases. (Well is located to maximize nuclide concentrations in well water.)

7.7 RAPID DRAINAGE OF PROGLACIAL LAKE

The rapid drainage of a proglacial lake may occur, for instance, due to the failure of an ice dam. In preliminary modelling work, the rapid drainage of the proglacial lake caused a large spike in I-129 mass flows to the surface, due to the sudden change in the hydraulic head at the surface. To examine this possibility in more detail, two additional models were run for the Proglacial Lake State which occurs between 280,700 and 281,900 years, i.e., during the second glacial cycle. This state was chosen because, for the Reference Case, the peak I-129 mass flow rate into the North Lake during a Proglacial Lake State occurs during the second glacial cycle.

In the Reference Case, and all other calculation cases, the surface hydraulic head was held constant for the first 800 years of the Proglacial Lake State, and then reduced slowly over the next 400 years until it reached the surface elevation. In Rapid Drainage Case 1, the surface head was once again left constant for the first 800 years. At this point the head was rapidly reduced (with a drainage time of one year), resulting in a head drop of roughly 165 m in one year. This did lead to a short lived spike in the I-129 mass flow rates as the hydraulic system moved toward a new equilibrium. However, the maximum I-129 mass flow rate of 3.6×10^{-7} mol per year was much lower than that observed during other stages of the glacial cycle (see Figure 7.20). Another simulation (Rapid Drainage Case 2) was performed in which the lake was rapidly drained after only 100 years. The maximum I-129 mass flow rate was comparable to that for Rapid Drainage Case 1.

The results of this modelling are presented in Figure 7.26. Results for the DC3 source location can be found in Walsh and Avis (2010). The simulations indicate that spikes in I-129 mass flow into the North Lake may occur due to rapid drainage of the proglacial lake. However, as the peak I-129 mass flow rates, for both sources DC1 and DC3, are considerably lower for the Rapid Drainage Cases than during other stages of the glacial cycle (see Figure 7.20), they are not further considered in the current safety assessment.

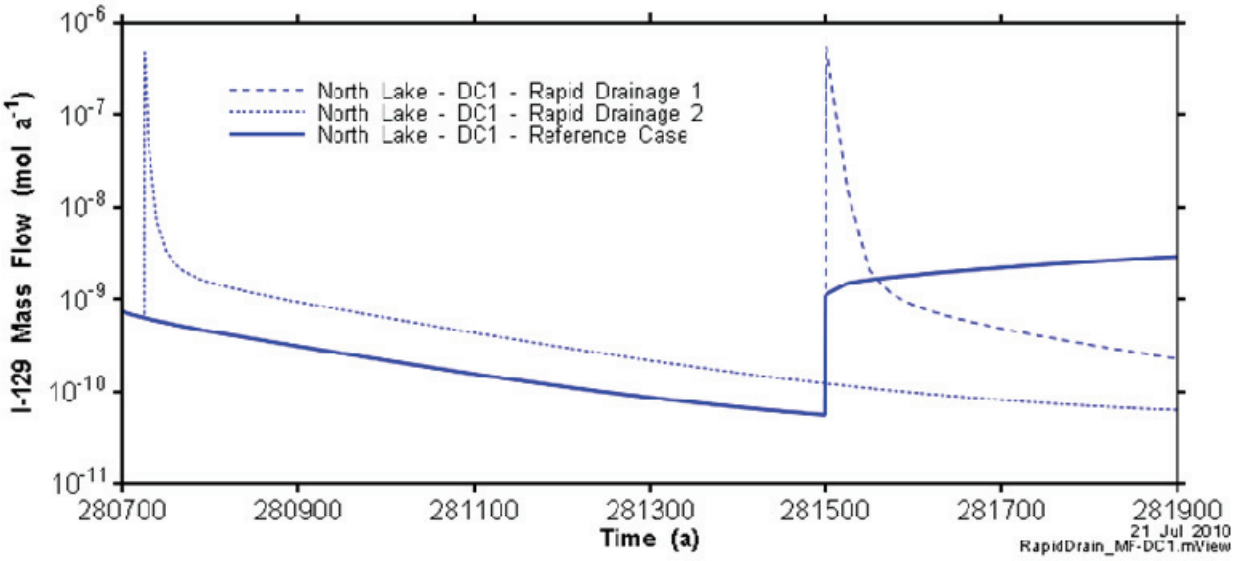

Figure 7.26: I-129 mass flow rate across North Lake control surface for the Rapid Drainage DC1 cases, compared to GCS-RC DC1 result.

8. SYSTEM MODELLING

In this section, safety assessment calculations are carried out with the integrated system model SYVAC3-CC4 (Garisto et al. 2004b, Gierszewski et al. 2004d). SYVAC3-CC4 has an idealized geometric description of the vault, a simple geosphere transport model, and a detailed representation of processes such as radionuclide releases from used fuel and radionuclide transport in the biosphere. Since SYVAC3-CC4 executes much faster than FRAC3DVS, it can be used to assess more quickly a range of cases, e.g., simulation of actinide decay chains, cases with longer simulation times, and simulations studying the effects of variations in system parameters. Finally, SYVAC3-CC4 can also be used to carry out a probabilistic safely assessment for the repository system.

SYVAC3-CC4 consists of two packages. SYVAC3 is the executive shell package, which provides input and output processing, random sampling, and various time series utilities. CC4 is the integrated system model that represents the repository features and processes. The conceptual models for the Defective Container Glaciation Scenario are described in Section 5. Detailed information about the CC4 models can be found in Gierszewski et al. (2004d).

CC4 does not determine the groundwater flow field itself. Rather, this calculation must be done by an external groundwater flow modelling code and the resulting flow field used to determine the geosphere transport network. In this study, FRAC3DVS was used to determine the groundwater flow field, as described in Section 6, and the particle track information from FRAC3DVS was used to develop the networks of one-dimensional flow tubes used by CC4 to approximate radionuclide transport in the geosphere (see Appendix B). The transport network covers only the portion of the geosphere in which the contaminant plume migrates, leading from contaminant sources at the repository/geosphere interface to the discharge locations in the surface biosphere.

All radionuclides identified as of potential importance in the screening calculations for the HBC study were included in the SYVAC3-CC4 deterministic and probabilistic simulations. These radionuclides are listed in Table 8.1.

8.1 CLIMATIC STATES

The climatic states used in the safety assessment of the Glaciation Scenario are based on the information in Section 3. A summary of this information is provided in Table 8.2, for one complete glacial cycle. The current-day glacial cycle is assumed to end following a long (Interglacial) Temperate State (i.e., today's climate) and then a new glacial cycle begins. The new cycle begins at a Permafrost State and proceeds through a sequence of climatic states finishing with a temperate climatic state. The glacial cycle is 121,200 years long. After the first glacial cycle is complete, the climate will cycle over the same sequence of climatic states, starting at the Permafrost 1 state, until the end of the approximately one million year simulation period. Eight complete glacial cycles occur during this simulation period.

Table 8.1: Radionuclides identified as of potential concern by the screening calculations (Garisto et al. 2005a)[1]

Fission products I-129 Cl-36 C-14 Ca-41 Cs-135 Se-79 Tc-99 Bi-208
Nuclides in the "Np-237" actinide decay series Pu-241 Am-241 Np-237 Pa-233 U-233 Th-229 Ra-225 Ac-225
Nuclides in the "U-238" actinide decay series Pu-242 U-238 Th-234 U-234 Th-230 Ra-226 Rn-222 Pb-210 Bi-210 Po-210
Nuclides in the "Pu-239" actinide decay series Pu-239 U-235 Th-231 Pa-231 Ac-227 Th-227 Ra-223
Nuclides in the "Pu-240" actinide decay series Pu-240 U-236 Th-232 Ra-228 Th-228 Ra-224

[1]All radionuclides originate in the UO_2 fuel. Zircaloy nuclides are insignificant contributors to the total dose rate.

Table 8.2: Climatic State Durations

Geosphere State	Permafrost Depth (m)	Start Time (a)	End Time (a)	Duration (a)	Well
(Interglacial) Temperate	0	0	50,300	50,300	Yes
Permafrost 1	100	50,300	5,8100	7,800	No
Ice Sheet 1 Advancing - Cold Based	100	58,100	64,800	6700	No
Ice Sheet 1 Retreating - Cold Based	100	64,800	66,700	1,900	No
Permafrost 2	250	66,700	103,500	36,800	No
Ice Sheet 2 Advancing - Cold based	150	103,500	114,300	10,800	No
Ice Sheet 2 Retreating - Warm Based	0	114,300	120,300	6,000	No
Permafrost 3	250	120,300	129,500	9,200	No
Ice Sheet 3 Advancing - Cold based	200	129,500	136,900	7,400	No
Ice Sheet 3 Advancing - Warm Based	0	136,900	153,000	16,100	No
Ice Sheet 3 Retreating - Warm Based	0	153,000	159,500	6,500	No
Proglacial Lake	0	159,500	160,700	1,200	No
Temperate	0	160,700	171,500	10,800	Yes

Based on the characteristics of the states in Table 8.2, it was possible to define a set of unique geosphere and biosphere states for use in CC4, as shown in Table 8.3. Simplifications were made where possible. For Ice Sheet 1, the two cold based states in Table 8.2 were combined into one cold based Ice Sheet state (ISCB1) because the period of ice sheet retreat is relatively short. Since the Permafrost 2 and Permafrost 3 states are similar, except for their durations, they are described by the same Permafrost State (PERM2). Finally, the retreating warm based phases of Ice Sheet 2 and Ice Sheet 3 are represented by the same Ice Sheet state (ISWB1).

Each unique geosphere state and biosphere state has different properties. For example, the groundwater flow field is different for each geosphere state. These properties remain constant for the duration of the state. All Permafrost States have two open taliks (see Figure 6.2). These are referred to as the North and South talik or, during Temperate States, the North and South Lake. A different critical group is present during the Temperate, Permafrost and Proglacial Lake States, as discussed in Section 5. No people reside near the repository site during Ice Sheet States.

Table 8.3: Unique State Names, Durations, and Cross Reference Indexes

Geosphere State Name	Geosphere Index	Biosphere State Name	Biosphere Index	Time Duration (a)
TEMPR	1	TEMPR	1	50,300
PERM1	2	PERMA	2	7,800
ISCB1	3	ICESH	3	8,600
PERM2	4	PERMA	2	36,800
ISCB2	5	ICESH	3	10,800
ISWB1	6		3	6,000
PERM2	4	PERMA	2	9,200
ISCB3	7	ICESH	3	7,400
ISWB2	8		3	16,100
ISWB1	6		3	6,500
PROLA	9	PROLA	4	1,200
TEMPR	1	TEMPR	1	10,800

Table 8.3 contains the unique state names (mnemonic) for the geosphere and biosphere states and their durations. Also found in this table are the geosphere and biosphere cross-reference indexes, which identify the unique states in CC4. The state names and indexes will be seen on some of the figures in this section. Table 8.4 contains the unique state names and brief descriptions for these states.

Table 8.4: Geosphere and Biosphere State Descriptions

State name	Brief Description
Geosphere	
TEMPR	Temperate (boreal) climate and well (738 m^3/a)
PERM1	Permafrost layer down to 100 m, talik beneath the lake
PERM2	Permafrost layer down to 250 m, talik beneath the lake
ISCB1	Ice sheet - cold based, 100 m permafrost depth, no talik
ISCB2	Ice sheet - cold based, 150 m permafrost depth, no talik
ISCB3	Ice sheet - cold based, 200 m permafrost depth, no talik
ISWB1	Ice sheet - warm based, retreating, no permafrost layer
ISWB2	Ice sheet - warm based, no permafrost layer
PROLA	Proglacial Lake
Biosphere	
TEMPR	Temperate (boreal) climate – Climate conditions like today, self-sufficient farmer household uses water from a well (738 m^3/a)
PERMA	Permafrost – Periglacial climate, inland tundra biosphere, self-sufficient hunter household (caribou main food source) uses water from North talik
ICESH	Ice sheet – no inhabitants due to full glacial coverage
PROLA	Proglacial Lake – Resembles Permafrost State biosphere, self-sufficient hunter-fisher household (similar to hunter but more fish in diet and less caribou) uses water from proglacial lake

Figure 8.1 shows the colour scheme used in many of the figures in this section. The green sections are Temperate States, the tan sections are Permafrost States, the blue sections are Ice Sheet States and the grey section is the Proglacial Lake State. The colour bars show the relative duration of the states, e.g. the first Temperate State lasts 50,300 years compared to the other Temperate States which last 10,800 years.

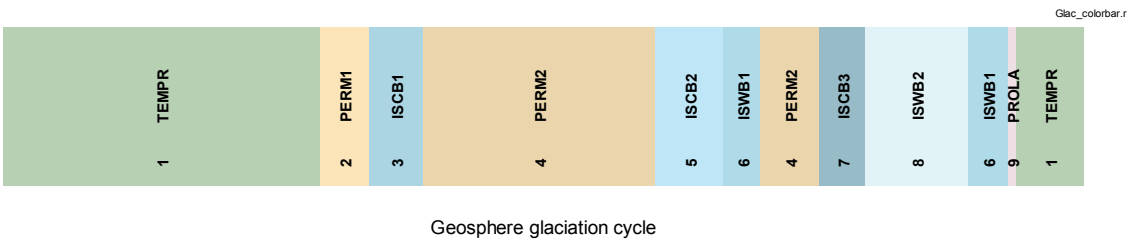

Figure 8.1: Colour scheme for geosphere glaciation states. Both the geosphere state name and geosphere state index are shown (see Table 8.3).

8.2 DETERMINISTIC SAFETY ASSESSMENT: REFERENCE CASE

In this section, the results of the SYVAC3-CC4 deterministic safety assessment calculations for the Reference Case of the Glaciation Scenario are presented. The Reference Case is defined as follows:

- A parameter whose value is described by a probability density function is set equal to its best-estimate value, i.e., the most probable value (or mode) of the probability density function. In cases where there is no unique mode, the median value of the probability density function is used.
- Two container failures occur in Sector 1 of the vault. This corresponds to the best-estimate for the total number of containers with defects in the whole vault, but conservatively assumes they both occur in the vault sector having the shortest groundwater travel time to the surface, as defined by the steady state groundwater flow field for the Temperate State. The DC1 defective container source (see Figure 7.3) used in the FRAC3DVS transport calculations is located in vault Sector 1.
- The climate is described by the reference glacial cycle (see Section 3).
- The groundwater flow field is based on the results of the GSC-RC model described in Section 6.
- The critical group characteristics change as the climate changes, as outlined in Section 5 and detailed in Appendix A.
- Groundwater contacts the fuel in the defective containers at 100 years after start of disposal.

The calculated total dose rates for the Reference Case are shown in Figure 8.2. The peak total dose rate is 3.7×10^{-7} Sv/a and occurs at about 5.2×10^{5} years. This peak dose is well below the dose rate constraint of 3×10^{-4} Sv/a recommended by ICRP 81 (ICRP 2000) for disposal of long-lived solid radioactive waste and the average Canadian natural background dose rate of 1.8×10^{-3} Sv/a (Grasty and LaMarre 2004). The dose rate curve shows many peaks and gaps that correspond to changes in the climatic state with time, in a repeating 11 state cycle. The gaps occur during Ice Sheet States when we assume no humans live near the site and the peaks occur during Permafrost, Temperate and Proglacial Lake States when we assume different critical groups live at the site.

Figure 8.3 shows an expanded view of the total dose rate curve for the 5^{th} glacial cycle. The trends in each state are now more apparent. Humans are not present during Ice Sheet States (blue) and therefore dose rates are zero during these times. Dose rates are very low during the Proglacial Lake State (PROLA, Table 8.4) because the proglacial lake is very large (see Appendix A) and, therefore, radionuclide discharges to the lake are diluted significantly, leading to lower radionuclide concentrations in the water used by the critical group and, hence, lower dose rates.

The dose rate is significantly higher during Temperate States (green) because a well is used by the critical group as the source of domestic water during Temperate States, while a lake is used during the other states. Typically, radionuclide concentrations are several orders of higher in well water than lake water (see Figure 9.3 and Figure 9.4), due to the much greater dilution of radionuclides in the lake than the well, leading to the higher exposure doses for the critical group using water from a well rather than a lake.

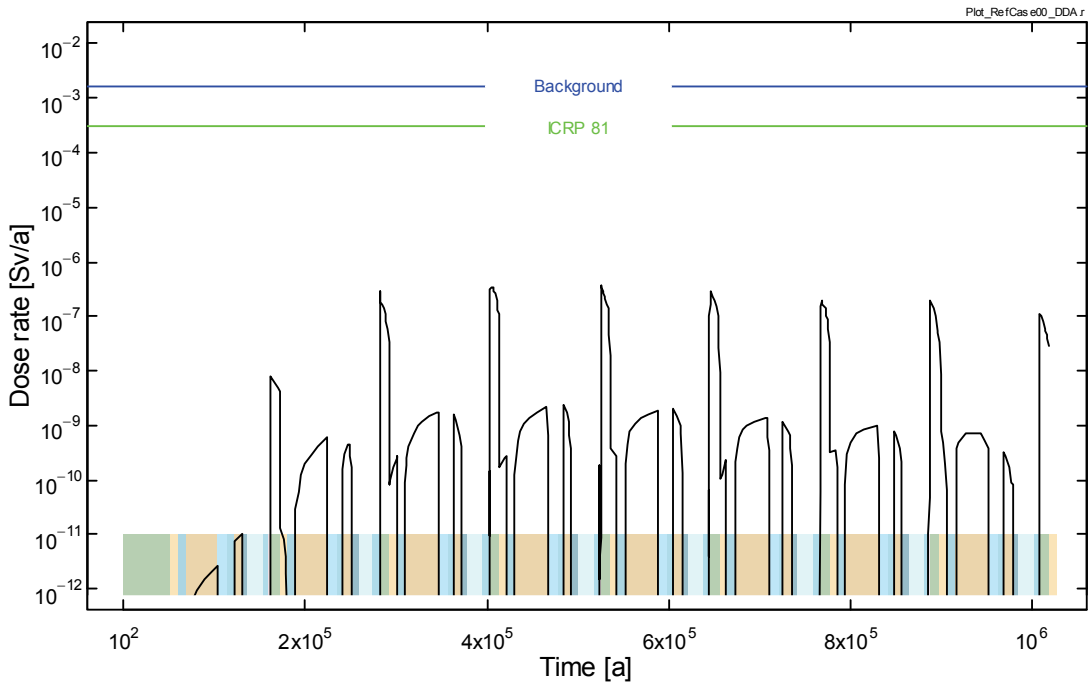

Figure 8.2: Calculated total dose rates for the best-estimate Reference Case.

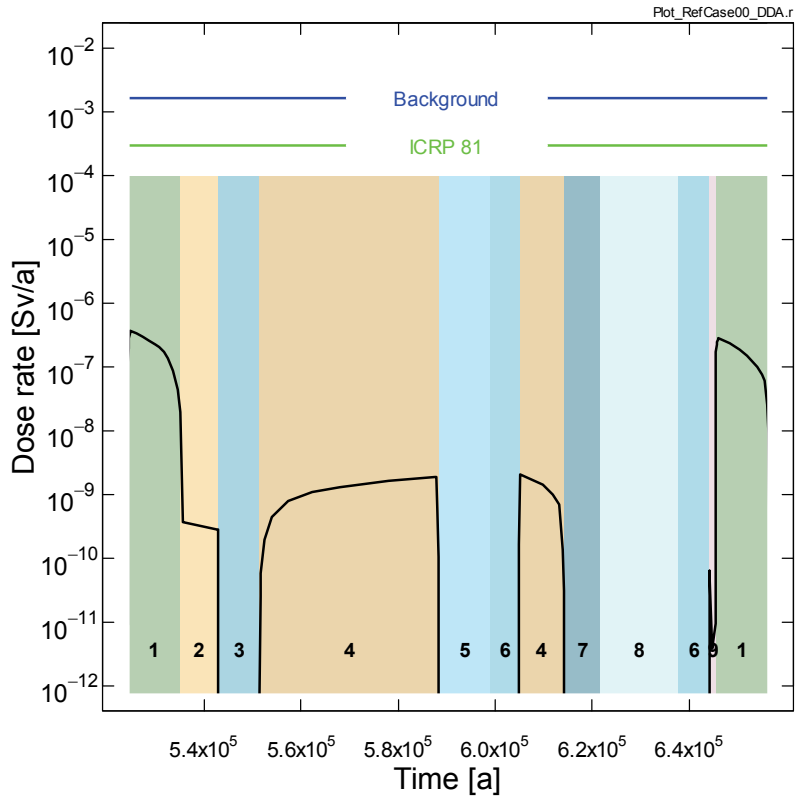

Figure 8.3: Total dose rate for the Reference Case for the 5th glacial cycle.

It is unlikely that a well would be used during Permafrost States because permafrost extends to depths of more than 100 m for these states (see Table 8.4). However, at repository sites where the permafrost extends to a depth of 60 m or less, the permafrost would likely not be continuous and wells might be used by the critical group even living during permafrost periods. In this case, dose rates during Permafrost States could be higher than calculated here, but the large expected differences in the subsurface water flows would also need to be considered.

In Figure 8.4, the dose rate curve is plotted on an overlapping single cycle. The dose rate rises during the first (black line) and second (red line) glacial cycles and then remains relatively invariant for cycles 3 to 8, although a downward trend in the dose rate curve is apparent at longer times. The behaviour of the dose rate curve coincides with the I-129 mass flows to the biosphere (see Figure 9.1). There are no doses during Ice Sheet States (blue sections) since people do not live near the repository during this time. Dose rates increase during the long Permafrost State as radionuclides are slowly transported to the North talik from the repository. Dose rates rise sharply at the start of each Temperate State because the critical group living during Temperate States uses well water rather than lake water, as previously explained. These later dose rates decrease with time as the radionuclides brought towards the surface during the Proglacial Lake State (see Figure 6.34) are slowly depleted.

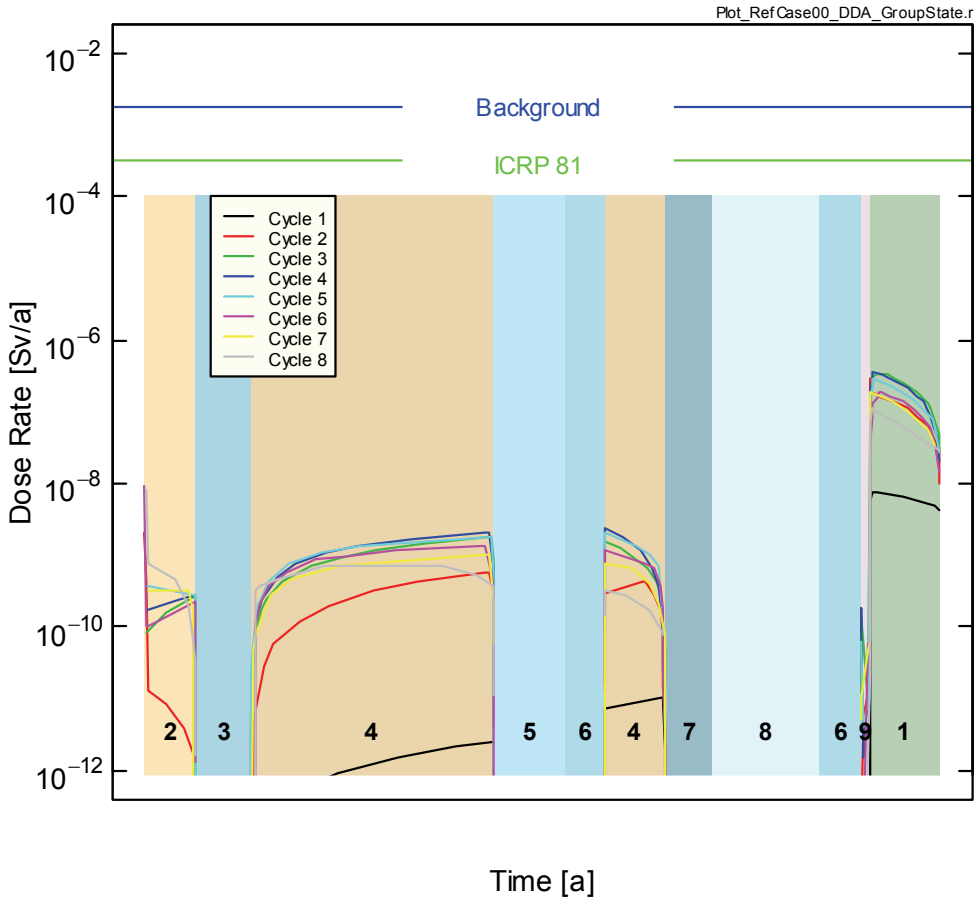

Figure 8.4: Dose rates for the Reference Case shown on an overlapping single cycle.

Figure 8.5 shows the individual nuclide contributions to the total dose rate for the Reference Case for the highest contributors to total dose. The calculated peak dose rates for individual nuclides are given in Table 8.5. Several observations can be made:

- Calculated dose rates are highest for I-129, a long-lived nuclide that has a large instant release fraction and is not sorbed in the vault or geosphere. As indicated in Table 8.7, for I-129, the water ingestion pathway is the most important exposure pathway during Temperate States whereas the meat ingestion pathway it the most important during Permafrost StatesTable 8.7: Peak I-129 Dose Rates for Several Exposure Pathways for Two Scenarios.
- Calculated actinide dose rates are well below 10^{-16} Sv/a during the one million year simulation period. However, actinide dose rates are still slowly increasing at the end of the simulation. The peak dose rates of the actinides occur at late times because the long-lived parents, e.g. U-238 and Np-237, are strongly sorbed in the geosphere and so their transport through the geosphere is appreciably retarded.

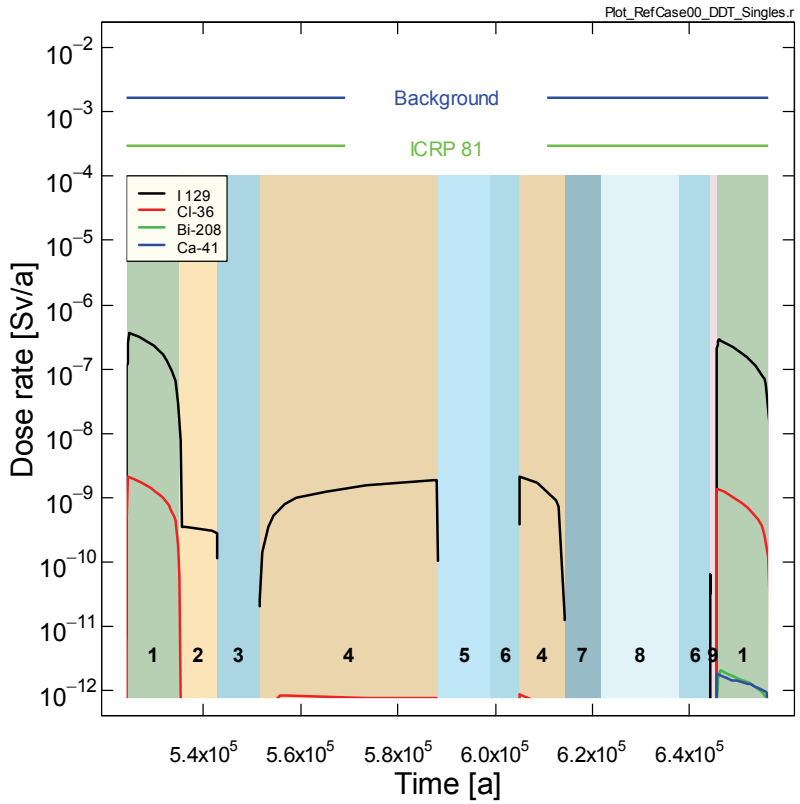

Figure 8.5: Reference Case dose rates for the most important nuclides during the 5th glacial cycle.

Table 8.5: Nuclide Peak Dose Rate and Time of Peak Dose Rate[#]

Nuclide	Peak Dose Rate [Sv/a]	Time of Peak Dose Rate [a]
I-129	3.67×10^{-7}	5.25×10^{5}
Cl-36	3.03×10^{-9}	4.03×10^{5}
Bi-208	8.33×10^{-12}	8.99×10^{5}
Ca-41	2.45×10^{-12}	7.67×10^{5}
Np-237	2.55×10^{-17}	1.01×10^{6}

[#]Calculated peak dose rates are less than 10^{-17} Sv/a for all other radionuclides.

8.3 DETERMINISTIC SAFETY ASSESSMENT: NON-GEOSPHERE SENSITIVITY CASES

A series of sensitivity cases were studied to investigate the effects of

1. No well;
2. The location of the defective containers in the repository;
3. A variation in the glacial cycle in which only Permafrost and Temperate States occur (i.e., there are no Ice Sheet or Proglacial Lake States); and
4. All containers fail simultaneously.

These cases are intended to study particular aspects of the Reference Case for the Glaciation Scenario. Some cases are highly unlikely to occur (e.g., all containers fail simultaneously).

8.3.1 No Well Case

In the Reference Case, the farmer critical group that lives during the Temperate States uses a well as the source of domestic water. In the No Well case, the North Lake is used as the source of domestic water by the farmer critical group. All other parameter values are the same as in the Reference Case. This case is of interest because it illustrates the impact of a well on calculated dose rates.

The calculated total dose rates for the No Well case are shown in Figure 8.6. I-129 is the largest contributor to the total dose rate. The peak total dose rate is 2.2×10^{-9} Sv/a and occurs at about 4.7×10^{5} years, during a Permafrost State. This peak dose is about 2 orders of magnitude lower than the peak total dose rate of 3.7×10^{-7} Sv/a for the Reference Case and well below the ICRP 81 (ICRP 2000) dose rate constraint of 3×10^{-4} Sv/a and the average Canadian natural background dose rate of 1.8×10^{-3} Sv/a.

The most important exposure pathway during Permafrost States is the air-lichen-caribou-man pathway. This pathway is important because the hunter's caribou meat ingestion rate is large, caribou eat mainly lichen, and lichens, which are contaminated via air deposition, retain deposited radionuclides for a long time, resulting in relatively high radionuclide concentrations in lichens.

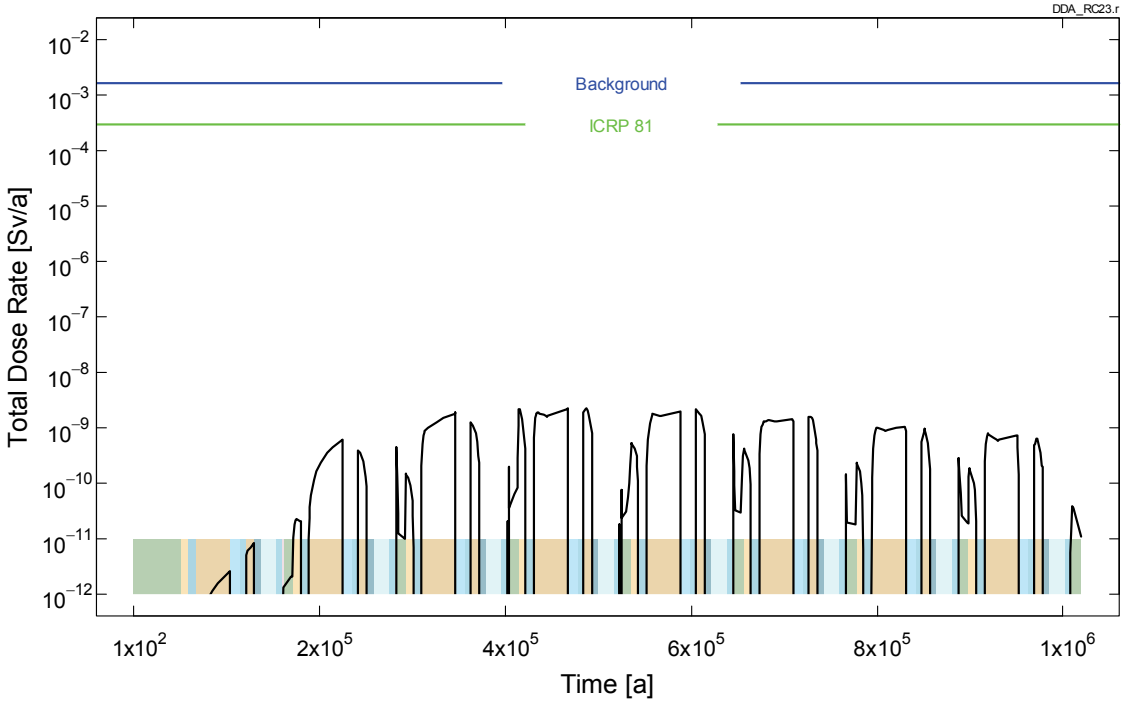

Figure 8.6: Calculated total dose rates for the No Well case.

8.3.2 Container Failure Location Case

In the Reference Case, the failed (i.e., defective) containers are located in Vault sector 1. In the Container Failure Location sensitivity cases, the two defective containers are located in either Vault sector 2, 3, 4, 5 or 6. Thus, there are 5 different Container Failure Location sensitivity cases. All other parameters are the same as for the Reference Case. Only the top five fission products contributing to the total dose rate in the Reference Case were simulated: I-129, Cl-36, Ca-41, C-14 and Bi-208. It is expected that container failures in vault sectors with groundwater flow pathways leading to the well or North Lake, i.e., Vault Sectors 1 and 2 (see Figure B.3), lead to the highest calculated dose rates.

Figure 8.7 and Figure 8.8 compare the total dose rates for the cases where two containers fail in each of the vault sectors. The main contributor to the total dose rate is I-129, followed by Cl-36.

Figure 8.7 shows that, at early times, container failures in Vault Sector 1 lead to the highest dose rates followed by container failures in Sector 2 and then Sector 3. At later times, the calculated dose rates arising from container failures in Sector 1 and Sector 2 are fairly similar. These results are as expected because the groundwater travel time from the repository to the surface is longer for Vault Sector 3 than for the Sectors 1 and 2 (see Appendix B).

Figure 8.8 shows that container failures in Sector 1 lead to much higher calculated dose rates than for container failures in Sectors 4 to 6. Calculated dose rates are lowest for container

failures in Vault Sector 6 because groundwater travel times from the repository to the North Lake or well are longest for this sector (see Appendix B).

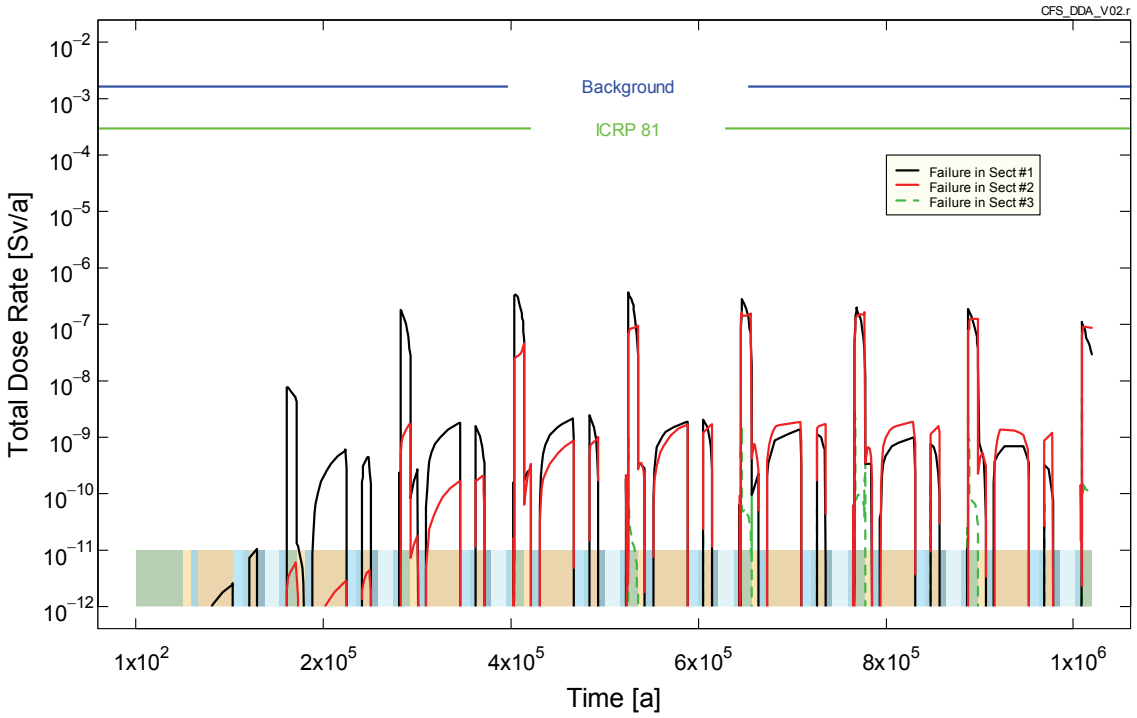

Figure 8.7: Comparison of total dose rates for cases where container failures occur in Vault Sectors 1, 2, and 3. In Reference Case, container failures occur in Vault Sector 1.

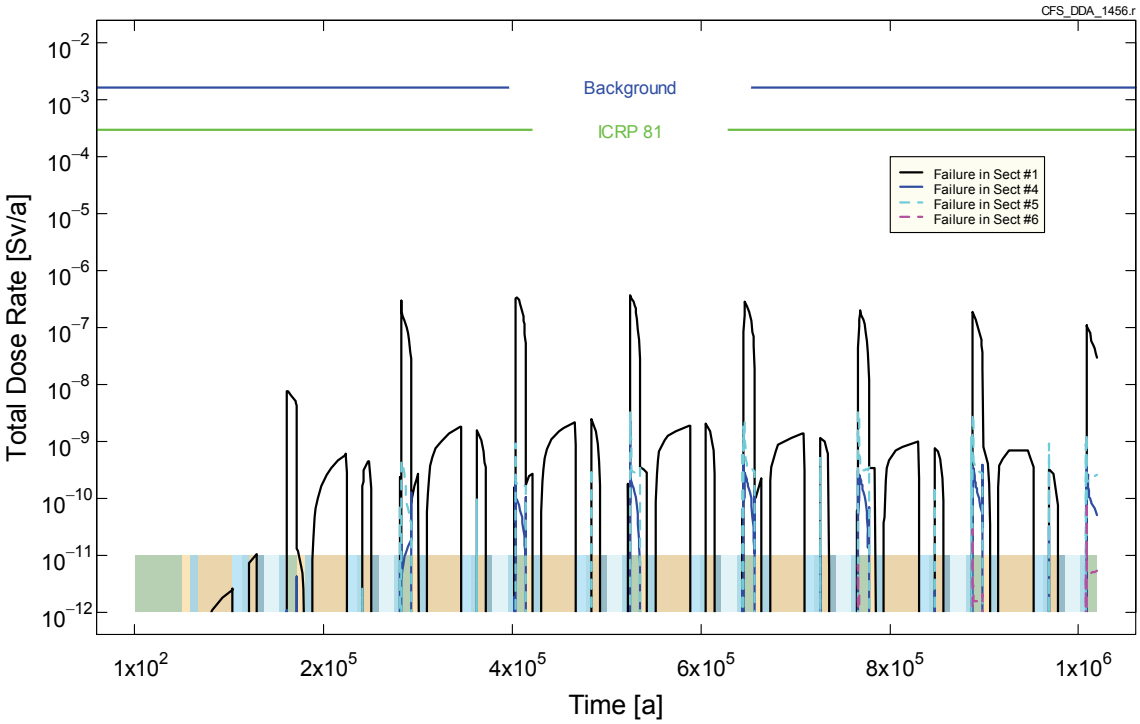

Figure 8.8: Comparison of total dose rates for cases where container failures occur in Vault Sectors 1, 4, 5 and 6. In Reference Case, container failures occur in Vault Sector 1.

Figure 8.9 compares the calculated total dose rates for container failures in each of the six vault sectors for the 5th glacial cycle. As discussed, container failures in Sectors 1 and 2 lead to higher dose rates than container failures in Sectors 3, 4, 5, or 6. Peak dose rates are lowest and occur much later when container failures occur in Sector 6. There are generally no dose rates from container failures in Vault sectors 3 to 6 during Permafrost States because groundwaters from these sectors discharge to the river or the western wetland (see Figure 7.18), which are frozen in by permafrost during Permafrost States. Only groundwaters from Vault sectors 1 and 2 discharge to the North talik. As expected, radionuclide releases from vault sectors with the shortest groundwater travel times to the surface (Sectors 1 and 2) produce the highest calculated dose rates.

As previously noted, the location of the well in the Reference Case was conservatively selected to maximize calculated dose rates for the self-sufficient farmer critical group for cases in which container failures occur in Vault Sector 1. (That is, during the Temperate State, groundwater travel times from the repository to the surface are shortest for Vault Sector 1, as shown in Appendix B.) Thus, for container failures in a different vault sector, the current well location may not maximize calculated dose rates.

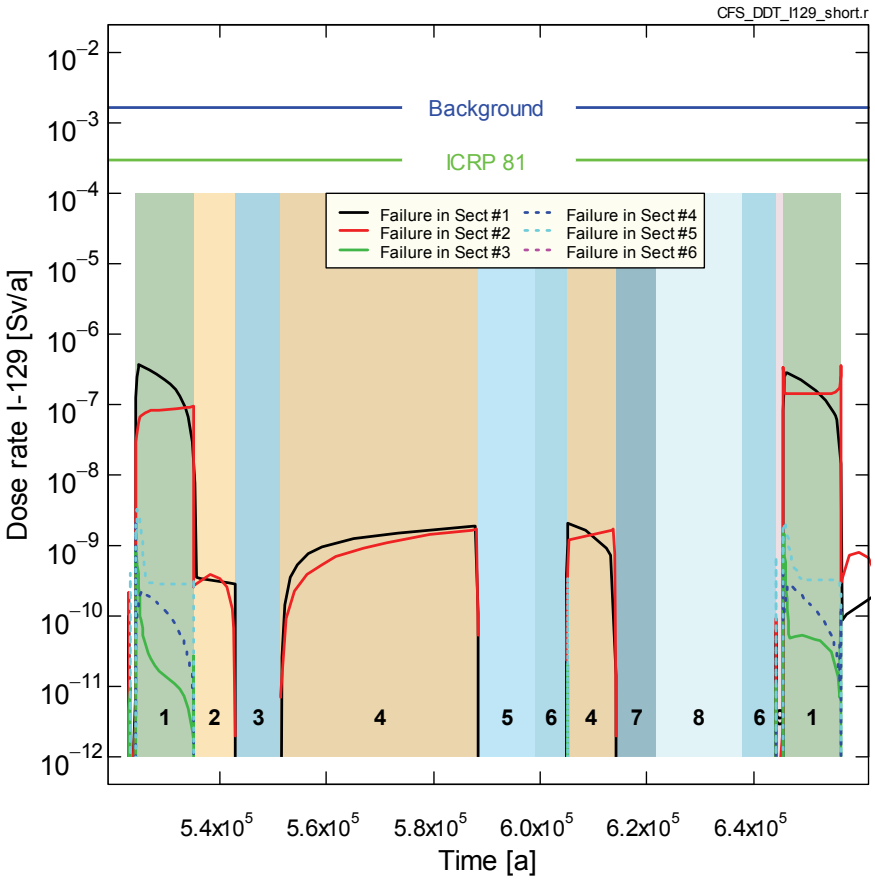

Figure 8.9: Comparison of I-129 dose rates for two container failures in each vault sector for glacial cycle 5.

8.3.3 No Ice Sheet Case

In the No Ice Sheet sensitivity case, the glacial cycle is varied. Specifically, each glacial cycle consists of two alternating states - a standard (10,800 year) Temperate State and a long (110,400 years) Permafrost State (PERM2). There are no Ice Sheet or Proglacial Lake States.

To investigate the effects of a talik, two sub-cases were simulated:

a. Permafrost depth is 250 m (PERM2 – see Tables 8.3 and 8.4) and an open talik exists under the lake, and

b. Permafrost depth is 250 m (PERM2), and no talik exists under the lake.

All parameters remained the same as in the Reference Case except for the time durations of the climatic states and the absence of the talik in one of the sub-cases.

Figure B.5 shows the geosphere schematic diagram with the identification of nodes and the location of the shallow and deep permafrost. The geosphere nodes in the permafrost zones are frozen in, i.e., there is no transport via these nodes, during the PERM2 Permafrost State, except for the nodes leading to the lake. In variant b of the No Ice Sheet State, all geosphere nodes in the permafrost zone are frozen in, i.e., there is no open talik under the lake.

Figure 8.10, the total dose rates calculated for the No Ice Sheet case with and without a talik are compared. The highest dose rates occur during the Temperate State, as in the Reference Case. As expected, calculated dose rates are much lower for the case without a talik. For this later case, radionuclides cannot reach the surface biosphere during the long Permafrost States because permafrost, which acts as a transport barrier, covers the entire model domain.

During the one million year simulation time, calculated dose rates remain lower for the case without a talik even during the Temperate States (see Figure 8.10) because radionuclide migration from the repository to the well is severely limited by the presence of the continuous 250 m thick permafrost layer during periods of permafrost. However, examination of Figure 8.10 indicates that calculated Temperate State dose rates for the No Ice Sheet case without a talik are still increasing at the end of the simulation. Therefore, the simulation for this case was extended to five million years. The calculated peak dose rate for the No Ice Sheet Case without a talik is found to be 3.7×10^{-7} Sv/a and the peak occurs at about 4.5×10^{6} years. This peak dose rate is similar to the peak dose rate for the No Ice Sheet case with a talik. This indicates that the presence of open taliks in permafrost regions greatly facilitates transport of radionuclides to the surface biosphere.

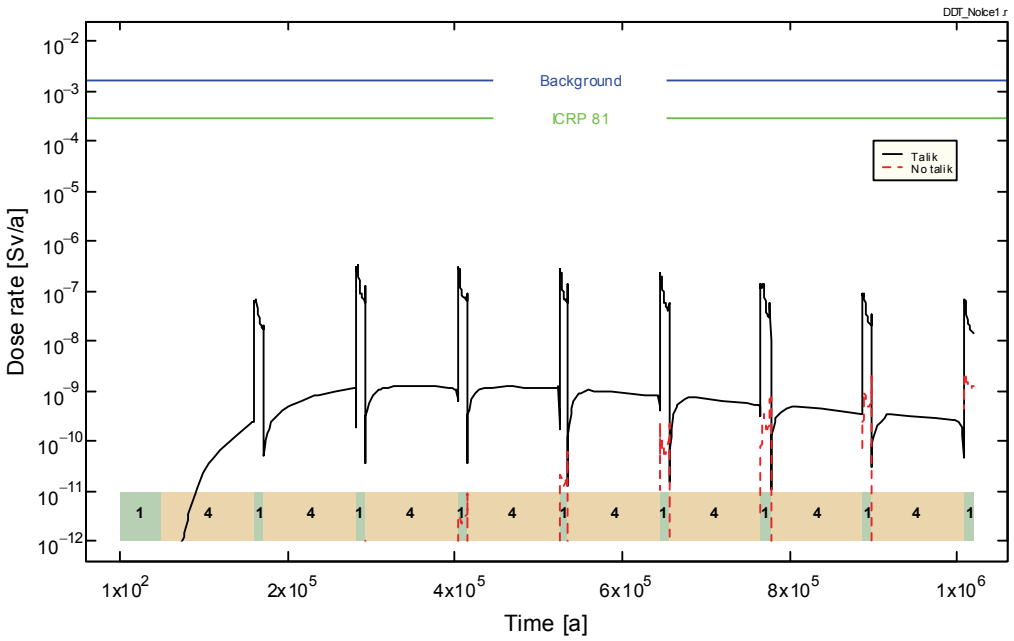

Figure 8.10: Comparison of radionuclide total dose rates for the No Ice Sheet cases with and without a talik. The numbers identify the geosphere state.

8.3.4 All Containers Fail Simultaneously

In the All Containers Fail case, all 11,232 containers are assumed to fail simultaneously at 100,000 years. All other parameter values are the same as those used in the Reference Case (which had two container failures, corresponding to our current knowledge of the number of statistically expected failures). It should be emphasized that it is unlikely that all containers would fail simultaneously. Rather the containers would likely fail over some extended period of time, which depends on the container failure mechanism.

Figure 8.11 shows the calculated total dose rates for the All Containers Fail sensitivity case with a constant temperate climate. For comparison, the results are also shown for the constant temperate climate case in which 2 containers fail (100 years after emplacement) in Vault sector 1. At very early times, dose rates are lower for the All Containers Fail sensitivity case because the containers are assumed to fail at 100,000 years.

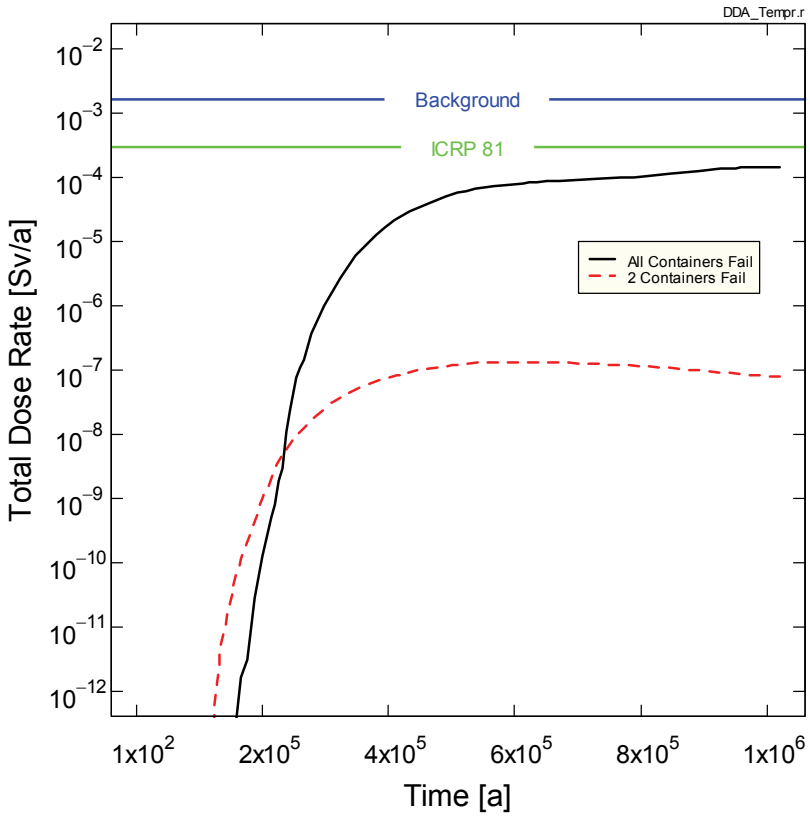

Figure 8.11: Comparison of calculated total dose rates for the All Containers Fail case with a constant climate (all failures occur at 100,000 years) and the corresponding case in which 2 containers fail in Vault Sector 1 (failures occur at 100 years).

The calculated peak total dose rate for the All Containers Fail sensitivity case with a constant climate is 1.5×10^{-4} Sv/a and occurs at 1.0×10^{6} years. These peak dose rates are below the ICRP 81 recommended dose rate constraint of 3×10^{-4} Sv/a and well below the average Canadian background dose rate of 1.8×10^{-3} Sv/a..

The calculated total peak dose rate for the All Containers Fail case is about 1000 times higher than for the case in which only 2 containers fail in Vault Sector 1, even though the number of failed containers is about 5000 times larger. This difference occurs because not all groundwater passing through the repository is captured by the well, which is the dominant exposure pathway for the self-sufficient farmer critical group living during the Temperate State. For example, although groundwater from Vault Sector 1 is mainly captured by the well, groundwater passing through or near the NW corner of the repository discharges mainly to the stream and western wetland areas (see Appendix B).

Figure 8.12 compares the calculated total dose rates for the All Containers Fail case for the Glaciation Scenario with the Reference (Glaciation) Case (in which two containers fail in Vault Sector 1). The calculated peak dose rate for the All Containers Fail case is 4.1×10^{-4} Sv/a and occurs at 7.79×10^{5} years. This peak total dose rate is about 3 orders of magnitude higher than for the Reference Case and exceeds the ICRP 81 recommended dose rate constraint of 3×10^{-4}

Sv/a for brief periods of time during several Temperate State, but remains well below the average Canadian background dose rate of 1.8 x10^{-3} Sv/a.

As previously noted, the All Containers Fail case is not realistic because the containers are not all expected to fail simultaneously. It has been included as a "what if" case to test the robustness of the repository system.

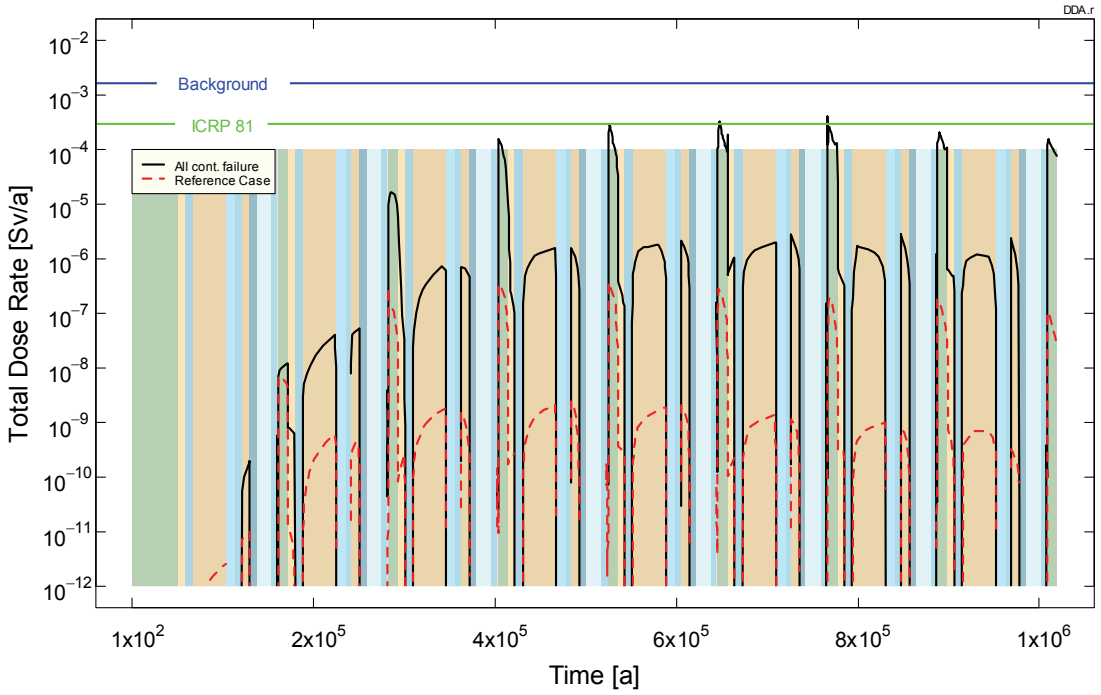

Figure 8.12: Calculated total dose rates for the All Containers Fail case for the Glaciation Scenario. The Reference (Glaciation) Case is shown for comparison.

8.3.5 Summary of Non-Geosphere Sensitivity Cases

The calculated peak dose rates for the non-geosphere sensitivity cases are compared in Table 8.6. As expected, the All Containers Fail case leads to the highest peak dose rate. For this case, the peak total dose rate exceeds the ICRP 81 recommended dose rate constraint of 3x10^{-4} Sv/a for brief periods of time but is well below still below the average Canadian background dose rate of 1.8 x10^{-3} Sv/a.

Examination of Table 8.6 also indicates that dose rates would be significantly lower than in the Reference Case if the self-sufficient farmer critical group, living during Temperate States, does not use a well; or if the failed containers are located in Vault Sectors 3, 4, 5 or 6.

Table 8.6: Calculated Peak Total Dose Rates and Time of the Peak from CC4 for the Non-Geosphere Deterministic Sensitivity Cases

Sensitivity Case	Differences Relative to Reference Case	Peak dose rate (Sv/a)	Time of peak (a)
Reference Case	------	*$3.7x10^{-7}$*	*$5.2x10^{5}$*
Constant Climate Scenario	Climate is temperate throughout the simulation time	$1.3x10^{-7}$	$6.1x10^{5}$
No Well Case	Farmer critical group uses North Lake as water source rather than a well	$2.2x10^{-9}$	$4.7x10^{5}$
Container Failure Location Case	Failed containers located in Vault Sector 2	$1.7x10^{-7}$	$7.8x10^{5}$
	Failed containers located in Vault Sector 3	$3.2x10^{-9}$	$7.7x10^{5}$
	Failed containers located in Vault Sector 4	$2.3x10^{-9}$	$5.2x10^{5}$
	Failed containers located in Vault Sector 5	$3.3x10^{-9}$	$7.7x10^{5}$
	Failed containers located in Vault Sector 6	$2.8x10^{-11}$	$8.9x10^{5}$
No Ice Sheet Case	Glacial cycle includes a long Permafrost State (with permafrost thickness of 250 m) and a 10,800 year long Temperate State.		
	Open talik exists under North Lake	$3.2x10^{-7}$	$2.8x10^{5}$
	No talik under North Lake	$3.7x10^{-7}$	$4.5x10^{6}$
All Containers Fail Case	All containers fail at 100,000 years	$4.1x10^{-4}$	$7.8x10^{5}$

8.4 DETERMINISTIC SAFETY ASSESSMENT: GEOSPHERE SENSISTIVITY CASES

In Section 8.3, we examined the sensitivity of the calculated dose rates for the Reference Case to changes in, for example, the location of the defective containers and the number of defective containers. In all cases, the geosphere properties were the same as those derived from the Reference Case geosphere and, therefore, the GEONET transport network for the Reference Case could be used for these sensitivity cases.

In this section, the effects of changes to the geosphere properties or geosphere boundary conditions on the calculated dose rates are examined. This is carried out using the results of the FRAC3DVS-OPG I-129 transport calculations presented in Section 7. Specifically, the I-129 dose rates to the critical groups are calculated (as described below) for the geosphere sensitivity cases examined in Sections 6 and 7. Since I-129 is, by far, the largest dose rate contributor during the one million year simulation time (see Section 8.1), the total radionuclide dose rate should not differ much from the calculated I-129 dose rate.

The FRAC3DVS-OPG transport calculations provide the I-129 mass flows to the surface biosphere (see Section 7). The dose consequences of these I-129 discharges are calculated with a biosphere model that is basically equivalent to the CC4 biosphere model but implemented using the AMBER V.5.2 modelling environment (Enviros and Quintessa 2008) as was done in preliminary work (Lum and Garisto 2008). This latter model, which will be referred to as the AMBER biosphere model, uses the same parameter data and same major exposure

pathways as used in the CC4 biosphere model (see Appendix A). Thus, for the same I-129 mass flows to the surface biosphere, the CC4 and AMBER biosphere models should provide similar results.

The AMBER biosphere model uses the I-129 mass flows to the North Lake and Well discharge locations to calculate dose rates to the critical groups, as these generally lead to the highest exposures. The critical groups are not exposed to radionuclides discharging to other locations. The critical groups are the same as those described in Section 5 and used in the CC4 simulations: self-sufficient farmer, tundra hunter, and tundra hunter-fisher. The critical group characteristics are provided in Appendix A. Only the self-sufficient farmer critical group, who resides near the repository site during the Temperate States, uses well water for its domestic needs (drinking, irrigation water, bathing, etc.).

8.4.1 Reference Case Dose Rates

The I-129 dose rates calculated by the AMBER biosphere model for the Reference (Glaciation) Case (i.e., for DC1 source location) are shown in Figure 8.13. These dose rates are compared to those calculated with the CC4 biosphere model but using the I-129 discharges to the biosphere from FRAC3DVS. The two biosphere models produce similar results, as expected, lending confidence that the two models are equivalent.

The peak I-129 dose rate calculated using the FRAC3DVS I-129 discharges to the biosphere, 2.5×10^{-7} Sv/a, is somewhat lower than that calculated with the CC4 I-129 discharges to the biosphere, 3.7×10^{-7} Sv/a. However, this agreement is quite good considering the large differences between the two models (see also Appendix C).

Table 8.7 shows the peak I-129 dose rates for several exposure pathways for the Reference (Glaciation) Case and the corresponding Constant Climate Scenario case. The well water-man exposure pathway is the most important for the Temperate State of the Reference Case and corresponding constant climate case. In contrast, the lichen-caribou-man exposure pathway is the most important during the Permafrost States of the Reference Case. This is mainly due to the fact that lichens, which accumulate I-129 via atmospheric deposition, have a very long life and the biological half-life of I-129 in the lichen is very long (5 years, see Table A.4), i.e., the I-129 concentration in lichens becomes relatively high.

Table 8.7: Peak I-129 Dose Rates for Several Exposure Pathways for Two Scenarios

Glaciation Scenario Reference Case (GSC-RC)			**Constant Climate Scenario (GSC-CC with well)**	
Exposure Pathway	Glacial State	Peak Dose (Sv/y)	Exposure Pathway	Peak Dose (Sv/y)
Water Ingestion	Temperate	1.8×10^{-7}	Water Ingestion	4.5×10^{-8}
Meat Ingestion	Permafrost	7.9×10^{-8}	Plant Ingestion	1.9×10^{-8}
Plant Ingestion	Temperate	7.2×10^{-8}	Bird Ingestion	6.6×10^{-9}
Fish Ingestion	Permafrost	6.6×10^{-10}	Milk Ingestion	5.3×10^{-9}
Bird Ingestion	Permafrost	3.4×10^{-11}	Meat Ingestion	2.1×10^{-9}
Milk Ingestion	Temperate	1.1×10^{-12}	Air Inhalation	1.2×10^{-13}

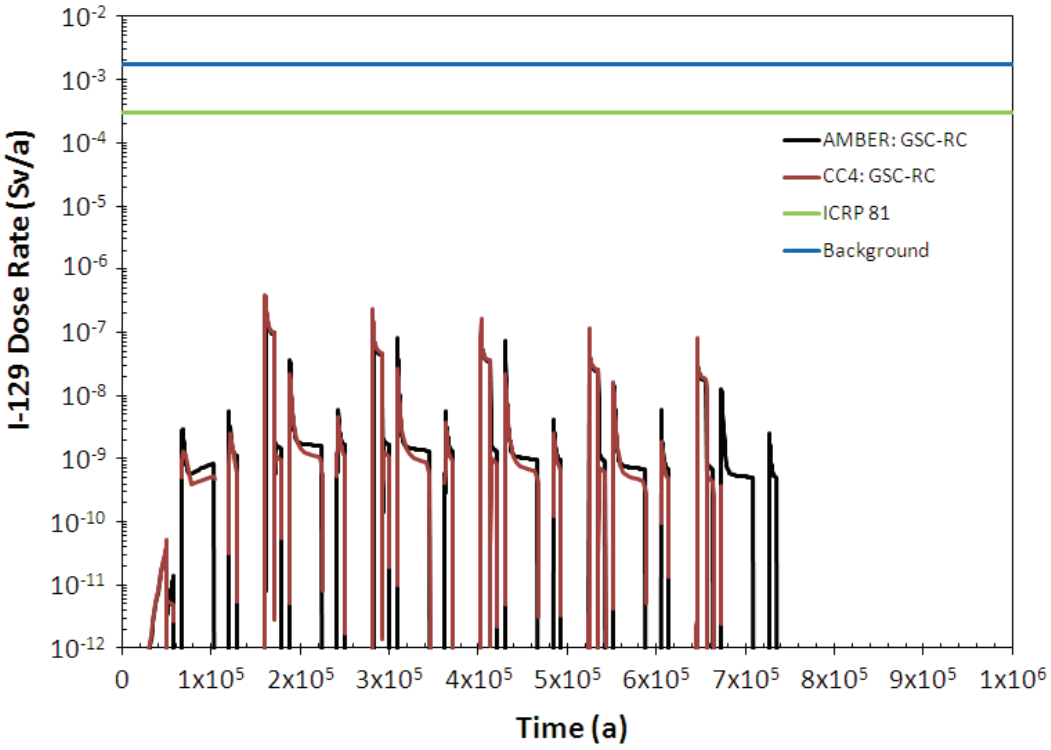

Figure 8.13: Reference Case I-129 dose rates calculated using the FRAC3DVS I-129 discharges (DC1 source) into the biosphere and the AMBER and CC4 biosphere models.

8.4.2 Geosphere Sensitivity Cases

Several geosphere sensitivity cases were run in order to study the effects of various geosphere conditions on the calculated I-129 discharges to the biosphere and, hence, the calculated dose rates (see Table 6.2).

Figure 8.14 compares the calculated I-129 dose rates for geosphere sensitivity case GSC-NF and the Reference Case (GSC-RC). For case GSC-NF, boundary conditions at the north and south boundaries of the model domain were set to no-flow boundaries. The calculated dose rates are similar for the two cases. While no flow boundary conditions may have a considerable effect on the groundwater flows, they have only a minor effect on the calculated peak I-129 dose rates (see Table 8.8).

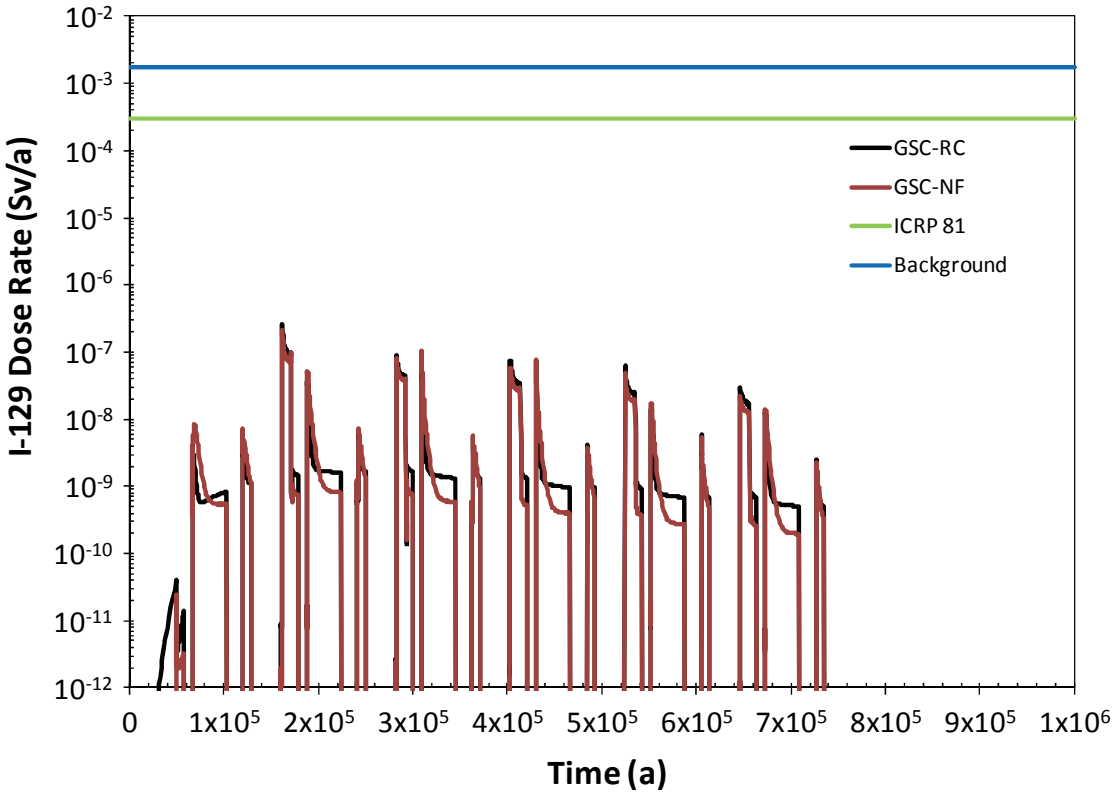

Figure 8.14: Calculated I-129 dose rates for the geosphere sensitivity case GSC-NF compared to those for the Reference Case (GSC-RC) for DC1 source location

Figure 8.15 compares the calculated I-129 dose rates for geosphere sensitivity case GSC-HS and the Reference Case (GSC-RC). For case GSC-HS, the geosphere storage coefficients were increased 10-fold relative to those in the Reference Case. The higher storage coefficients causes the groundwater flow field to respond more slowly to changes in, for example, head boundary conditions. Again, the calculated dose rates are fairly similar for the two cases, although the calculated I-129 dose rates are notably higher at earlier times for case GSC-HS, indicating higher groundwater flow rates at early times for the GSC-HS case (see Section 6).

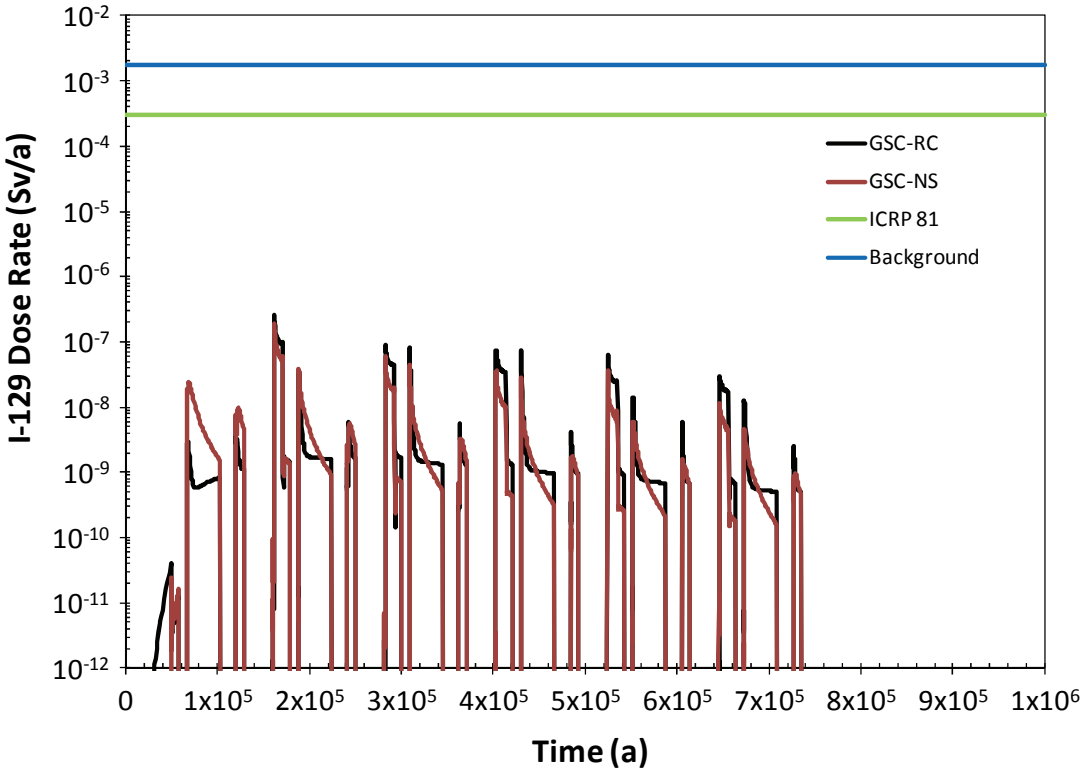

Figure 8.15: Calculated I-129 dose rates for the geosphere sensitivity case GSC-HS compared to those for the Reference Case (GSC-RC) for DC1 source location

Finally, Figure 8.16 compares the calculated I-129 dose rates for geosphere sensitivity case GSC-TK and the Reference Case (GSC-RC). For case GSC-TK, the open taliks that exist during Permfrost States below the North and South Lakes are assumed to remain open when a (cold-based) ice sheet advances over the permafrost. The presence of these unfrozen areas in the sub-glacial permafrost increases the groundwater discharges to the surface at the lake locations during cold-based Ice Sheet States. However, because of the ice cover, there are no inhabitants at the site during this time. Hence, calculated dose rates are similar for case GSC-TK and the Reference Case. Interestingly, the calculated peak dose rates during Temperate States are lower for case GSC-TK than for the Reference Case, suggesting I-129 mass flows to the well are lower for case GSC-TK, as is shown to be the case in Figure 7.25.

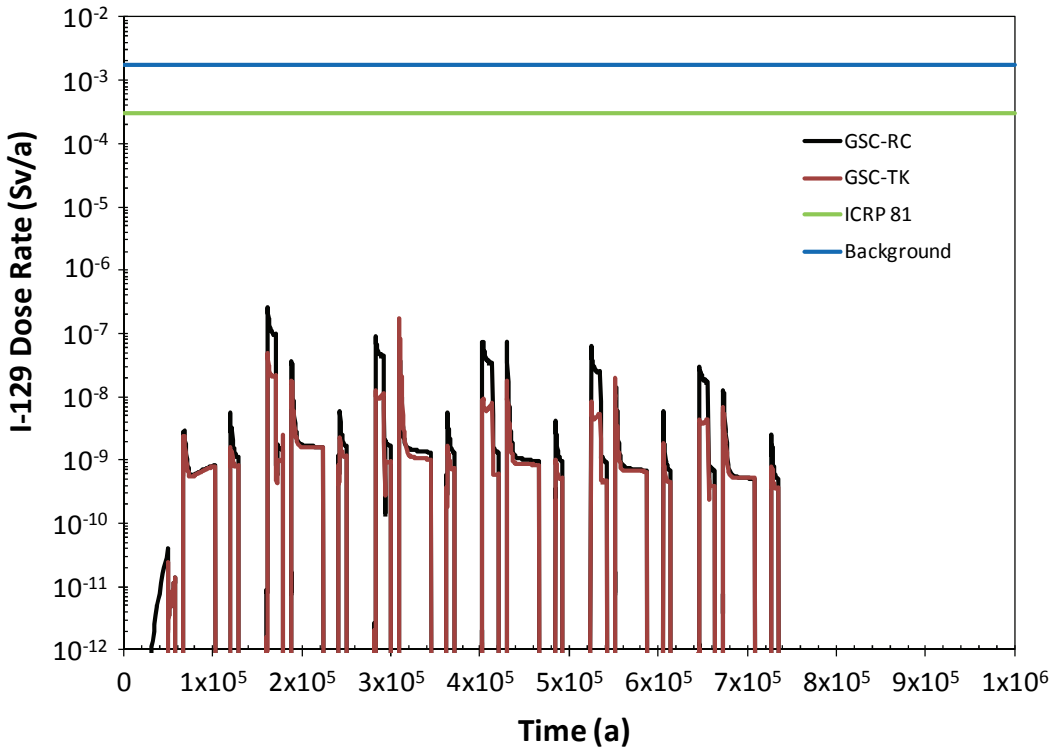

Figure 8.16: Calculated I-129 dose rates for the geosphere sensitivity case GSC-TK compared to those for the Reference Case (GSC-RC) for DC1 source location.

8.4.3 Summary of Geosphere Sensitivity Cases

In this section, the sensitivity of the calculated I-129 dose rates to changes in the geosphere was examined for the (geosphere) sensitivity cases described in Section 6 and 7. The dose rates were calculated using the AMBER biosphere model, which yields results that are essentially identical to results from the CC4 biosphere model.

The calculated peak dose rates for the geosphere sensitivity cases are compared in Table 8.8. For all geosphere sensitivity cases, the calculated peak dose rates are well below the ICRP dose constraint of 3×10^{-4} Sv/a and the average Canadian background dose rate of 1.8×10^{-3} Sv/a.

Although the various geosphere sensitivity cases were found to have a significant impact on the transient groundwater flows during the glacial cycle, there is little impact on the calculated I-129 dose rates. This may be due to the fact that the DC1 source location was conservatively selected, i.e., the groundwater travel time from the repository to the surface (i.e., North Lake) is a minimum for the DC1 repository location during the Temperate State.

Table 8.8: Calculated Peak I-129 Dose Rates and Time of the Peak for the Geosphere Sensitivity Cases and the DC1 Source Location

Geosphere Case	Difference Relative to Reference (Glaciation) Case	Peak dose rate (Sv/a)	Time of peak (a)
GSC-RC	*Reference Case*	2.5×10^{-7}	1.6×10^{5}
GSC-NF	No-flow boundary conditions at North and South vertical boundaries of model	2.2×10^{-7}	1.6×10^{5}
GSC-HS	Geosphere storage coefficients increased 10-fold	1.9×10^{-7}	1.6×10^{5}
GSC-TK	Taliks remain open under cold-based ice sheets	1.7×10^{-7}	3.1×10^{5}

8.5 PROBABILISTIC SAFETY ANALYSES

In previous sections, the dose impacts of a geological repository for used fuel have been assessed using variations on the (best-estimate) Reference Case in which model parameters are assigned specific values. However, many of these model parameters are uncertain (experimental or model uncertainties) or have an inherent degree of variability (in space or time). Consequently, these parameters are more generally characterized by a range or distribution of feasible values. This uncertainty or natural variability in the input parameter values results in uncertainty in the calculated dose consequences. One particular concern is that there could be cases with higher consequences that occur under some combination of parameter values. Thus it is important to investigate the effects of parameter uncertainty on the calculated impacts (Garisto et al 2004a, 2005a,: Goodwin et al. 1994, 1996).

To systematically account for uncertainty, the SYVAC3-CC4 system model was used in probabilistic mode. This approach uses results from hundreds of simulations, based on a sampling strategy that considers the full range of possible values. Each of these simulations produces an estimate of impact. In this way the uncertainty in parameter values is used to generate an empirical distribution of impacts that reflects the underlying uncertainty in the impact of the repository. These SYVAC3-CC4 studies use a simple random sampling strategy, also known as Monte Carlo sampling.

Two probabilistic cases were run. In these cases, one or more sampled parameters are varied randomly as described below while the other parameters were set equal to their values in the Reference (Glaciation) Case:

1. Climate State Duration – In this case the durations of the climate states (see Table 8.3) were varied in 1200 simulations while all other parameters remained at their Reference Case values, including the groundwater flow fields for each unique geosphere state. The duration of a climate state was assumed to be uniformly distributed between 0 and twice the duration of the state in the Reference Case.

2. Container Failure – In this case, the time at which containers fail in a vault sector (i.e., the time when groundwater enters the containers) was varied in 1200 simulations, while the other parameters remained at their Reference Case values. For each sector, there

was a 10% chance that container failure would occur during the one million year simulation time. The failure times were constrained to occur at the beginning of the Ice Sheet States ISCB2 or ISCB3 (see Table 8.3) in one of the eight glacial cycles. Moreover, when container failure occurred in a sector, 10% of the containers in the sector failed. Thus, for each simulation, the time and location (sector number) of container failure can vary. Since each sector contains a different number of containers, there is also a variable number of failed containers in a simulation.

The probabilistic simulations were carried out to 1.02×10^6 years after emplacement. Eight complete glacial cycles occur in this time frame. As in the deterministic simulations, the source of water for the critical group is the well during the Temperate States and the lake during other glacial states. In the following, the average peak total dose rate and the 90th percentile total dose rate (90% of the probabilistic simulations have peak total dose rates that fall below this value) for the probabilistic cases are compared to the Reference Case peak total dose rate.

8.5.1 Variation of Climate State Duration

Figure 8.17 shows the peak total dose rates resulting from the random variation of the duration of each climate state. The plot displays a narrow band of points (approximately 1 order of magnitude in height). A detailed analysis revealed that, for all simulations, the peak total dose rate occurred during a Temperate State (although at different times within the simulation). The two nuclides contributing the most to the peak total dose rate are I-129 and Cl-36.

The average peak total dose rate for the Climate State Duration probabilistic case is 7.4×10^{-7} Sv/a. The maximum peak total dose rate is 6.5×10^{-6} Sv/a and occurs at 6.0×10^5 years during the Temperate State at the end of the 5th glacial cycle. The minimum peak total dose rate is 3.3×10^{-7} Sv/a and it occurs at 5.1×10^5 years during the Temperate State at the end of the 4th glacial cycle. In comparison, for the Reference Case, the peak total dose rate is 3.7×10^{-7} Sv/a and the peak occurs at 5.2×10^5 years during the Temperate State at the end of the 4th glacial cycle. Finally, the 90th percentile calculated dose rate for the Climate State Duration probabilistic case is about 3-fold higher than the peak dose rate in the Reference Case.

Figure 8.18 shows a visual comparison of the maximum, minimum, and Reference Case peak total dose rates. In this figure, the length of the (random) state durations can be compared to those of the Reference case.

Most of the peak total dose rates for the Climate State Duration probabilistic case are higher than in the Reference Case. Detailed examination or the results indicated that this is caused by having one long cold based Ice Sheet State during the simulations. During this long period of "frozen in" conditions, there can be a build up of radionuclides under the permafrost layer beneath the ice sheet (because there are no groundwater discharges to the surface). During a subsequent state, when the permafrost layer is not continuous (e.g., during a Permafrost State with an open talik) or is absent, a slug of radionuclides would begin moving upwards and would eventually reach the biosphere, leading to dose rates higher than in the Reference Case. Since the time duration of each state varies around its Reference Case time duration, there is a high probability that there would be at least one longer period of frozen in conditions (compared to the Reference Case) in a simulation with multiple glacial cycles.

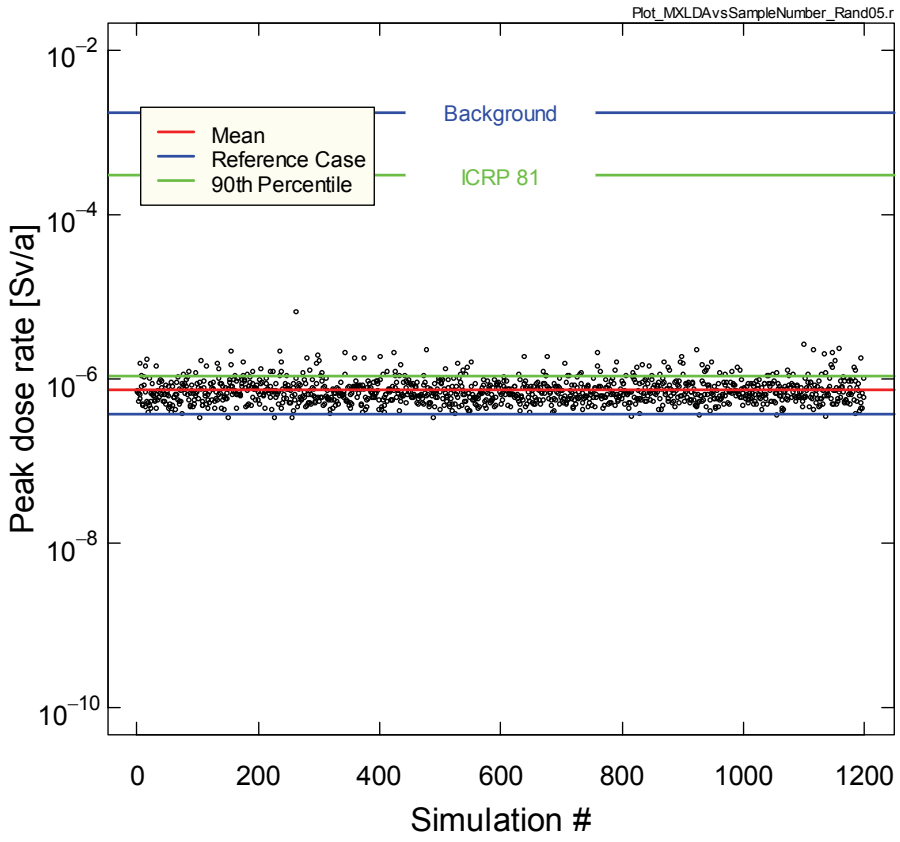

Figure 8.17: Calculated peak dose rates for the Climate State Duration probabilistic case.

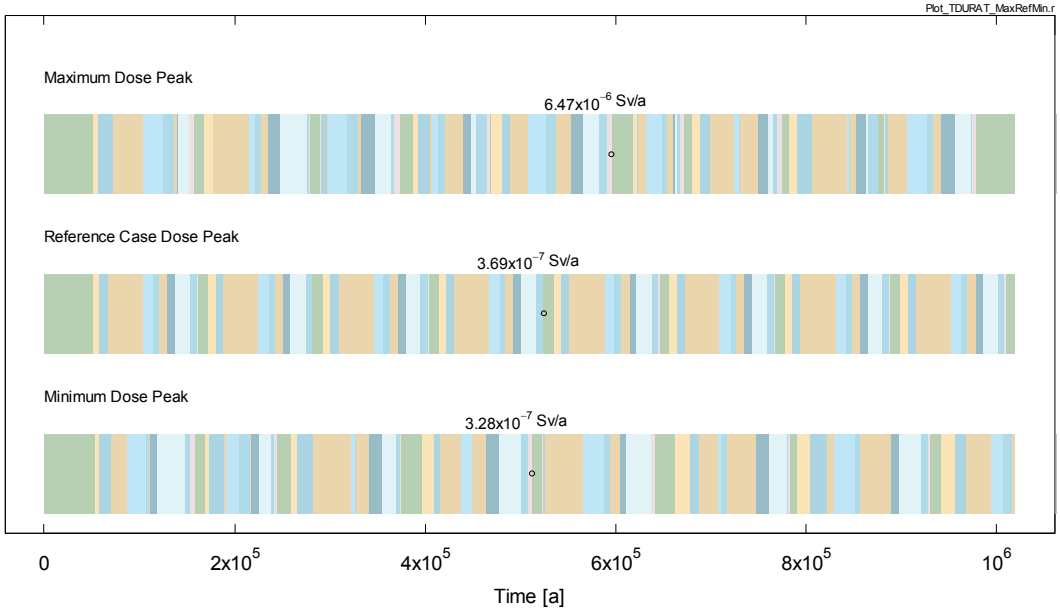

Figure 8.18: Glacial cycles and time of peak dose rates shown visually for three Climate State Duration probabilistic cases.

In carrying out the Climate State Duration probabilistic simulations, it is implicitly assumed that the groundwater flow fields for the unique geosphere states (Table 8.4), derived from the Reference Case (GSC-RC) transient groundwater flow results, can be used without change for the corresponding unique geosphere states in the probabilistic simulations. This assumption has not been tested.

8.5.2 Variation of Container Failure

Figure 8.19 shows the peak total dose rates for the Container Failure probabilistic case. In this set of simulations, the time at which containers fail in each vault sector was varied. These simulations were set up so that, for each vault sector, there was a 10% chance of container failure during the one million year simulation period. If failures occurred then 10% of the containers in the sector failed. Furthermore, the failures, if any, were constrained to occur at the beginning of the Ice Sheet States ISCB2 or ISCB3 (see Table 8.3). On average, about 1100 containers failed in each simulation, i.e., much more than the 2 failed containers in the Reference Case.

For about half of the simulations (626 out of 1200), the calculated total dose rate was zero (not shown in Figure 8.19). Either there were no container failures during the simulation, or the containers failed in vault sectors of the repository for which the groundwater travel time to the well (or lake) was sufficiently long that radionuclides did not reach the well (or lake), or the failures occurred too late during the simulation period for radionuclides to reach the well (or lake).

The calculated total dose rates in Figure 8.19 are spread over 6 orders of magnitude with an average peak total dose rate of 3.6×10^{-6} Sv/a. (I-129 and Cl-36 are the dominant contributors to the total dose rate.) The maximum peak total dose rate of 7.0×10^{-5}, which occurs at 8.9×10^{5} years, is well below the ICRP 81 dose constraint of 3×10^{-4} Sv/a (see Table 8.9). This maximum peak dose rate is about a factor of 10 lower than the total dose rate for the All Containers Fail case (see Section 8.2.3), as would be expected from the relative number of failed containers in the two cases.

The cluster of points around the 90th percentile line in Figure 8.19 represent the total dose rates for simulations in which there are container failures in Vault Sector 1 and/or Sector 2 of the repository. These two sectors have groundwater flow pathways that lead to the well and lake discharges, the well being the most important exposure pathway for the critical group in the Temperate State. Generally the points below the 90th percentile line are for simulations in which either no containers fail in Sectors 1 and 2, or containers fail in Sectors 1 and 2 but near the end of the simulation time.

Table 8.9: Minimum, Average and Maximum Peak Dose Rates for the Probabilistic Cases

Probabilistic Case	Number of Failed Containers	Minimum Peak Dose Rate (Sv/a)	Average Peak Dose Rate* (Sv/a)	Maximum Peak Dose Rate (Sv/a)
Reference Case	2	------	3.7×10^{-7}	------
Climate State Duration	2	3.3×10^{-7}	7.4×10^{-7}	6.5×10^{-6}
Container Failure	1100 (avg.)	0	3.6×10^{-6}	7.0×10^{-5}

*For comparison, the peak total dose rate for the Reference Case is also shown.

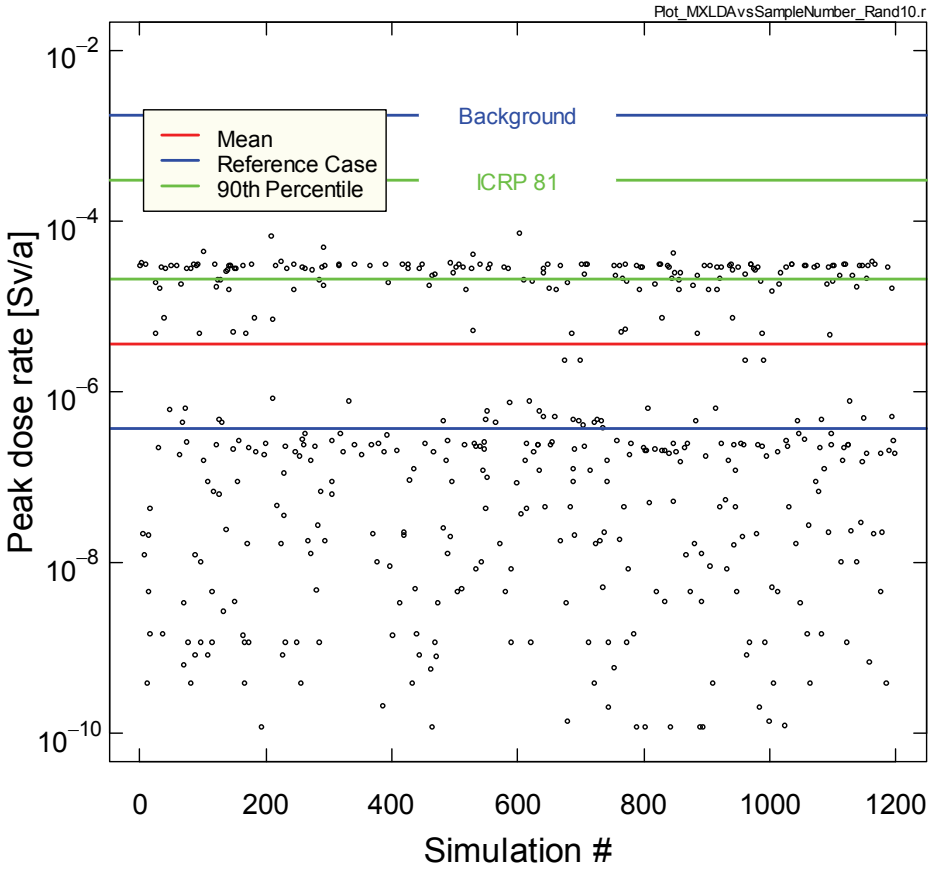

Figure 8.19: Calculated peak total dose rates for the Container Failure probabilistic case. There are on average 1100 failed containers in each simulation, compared to 2 failed containers in the Reference Case.

8.5.3 Summary of Probabilistic Sensitivity Cases

The calculated dose rates for the two probabilistic sensitivity cases are summarized in Table 8.9. The results of the Climate State Duration probabilistic case indicate that the calculated dose rates for the Glaciation Scenario are dependent on the selected glacial cycle. The importance of the number, location and time of container failures on the calculated dose rate is illustrated by the Container Failure probabilistic case. Although the average number of failed containers is 500-fold larger in the Container Failure probabilistic case than in the Reference Case, the average calculated dose rate is only 10-fold higher.

9. COMPARISON OF RESULTS FOR THE GLACIATION AND CONSTANT CLIMATE SCENARIOS

In this report, a safety assessment was carried out for a deep geological repository for used fuel for an illustrative (Defective Container) Glaciation Scenario. In this scenario, some containers are assumed to fail and the potential dose impacts were quantified. In previous sections, the details of the model and results have been presented. This was a very numerically intensive exercise. In this section, the results for the Glaciation Scenario are compared to those for the Constant Climate Scenario, in which the climate is assumed to be constant throughout the simulation period. Of particular importance is the comparison of the calculated peak dose rates for the Glaciation Scenario and the Constant Climate Scenario.

9.1 GROUNDWATER FLOW FIELDS

The groundwater flow field for the Reference (Glaciation) Case is described in Section 6. The groundwater flow field varies extensively with time during the simulation since the boundary conditions vary through the glacial cycle. In particular, the hydraulic heads at the surface of the model change as an ice sheet moves over the model domain. In contrast, for the Constant Climate Scenario (e.g., Garisto et al. 2004a, 2005a), the groundwater flow field is constant.

A key feature during glacial cycles is the generation of high hydraulic heads at depth due to the ice sheet. There are two key mechanisms which control hydraulic heads in the rocks beneath the ice sheet:

1. High fluid pressures at the base of the glacier. In low-permeability rocks, this basal water pressure takes time to penetrate into the rock as the ice sheet advances, and to be released from the rock when the ice sheet retreats. Basal hydraulic head is often very close to the total ice thickness.
2. Mechanically induced pressures in the underlying rock, caused by ice loading compressing the pore space and the pore fluids in the rock. This causes an increase in hydraulic pressure which propagates virtually instantaneously to all depths because it is a function of total stress. This hydromechanically induced pressure is usually a fraction of the total glacial load, and depends on the loading efficiency (see Section 6.2.4), which is a function of pore compressibility.

Both mechanisms are functions of the thickness of the ice sheet, and both change the groundwater flow field.

High basal heads cause large vertical gradients under an advancing glacier because the head in deeper formations is much lower than at the surface. Eventually, however, the hydraulic head in deeper formations will move towards equilibrium with the high basal heads. When the ice subsequently retreats, the hydraulic head near the ground surface will drop relatively rapidly, leaving more pressurised water trapped in deeper formations, and once again inducing higher vertical gradients, but in the opposite direction. The slope of the glacial surface also induces horizontal gradients as regions with different ice thickness have different basal hydraulic head.

If hydromechanical pressurisation is superimposed on the aforementioned hydraulic process it has two effects: (1) vertical hydraulic gradients are reduced, as the difference between the

hydraulic head at the base of the glacier and within the low permeability rock at greater depth is reduced; and (2) horizontal gradients in deeper, low permeability formations are increased in the earlier stages of the glacial advance, before hydraulic heads from the surface would have had a chance to propagate to these depths in the absence of hydromechanical coupling. This increase in horizontal gradients at depth is particularly evident at the ice margins, where the differences between heads beneath and beyond the glacier are very high.

Also, during Permafrost States, open taliks were found to be a dominant factor in controlling groundwater flows, focusing system stresses at a discrete location. These isolated gaps in the permafrost act as pathways for the dissipation of hydraulic pressures from preceding glacial events, i.e., groundwaters from below the permafrost discharge into the taliks.

9.2 NUCLIDE RELEASES FROM THE GEOSPHERE

The large changes in the groundwater flows, caused by the advance/retreat of the ice sheet over the model domain, make the radionuclide transport to the surface highly irregular (see Sections 7 and 8). In particular, a large pulse of nuclide mass is often discharged to the surface following the end of Ice Sheet States; because, at this juncture, groundwater flows are directed upwards due to the high head gradients left in the subsurface by the retreating ice sheet.

In this section, the nuclide mass flow rates from the geosphere to the well and lake discharge locations, the two most important discharges in terms of calculated dose rates, are compared for the Reference (Glaciation) Case and the corresponding Constant Climate case. The comparison is done for I-129 and Ca-41, two radionuclides with very different properties, i.e., I-129 is a non-sorbing radionuclide with a long 15.7 Ma half life and a large instant release fraction, whereas Ca-41 is sorbed in the buffer and geosphere, has a 0.10 Ma half-life, and its instant release fraction is zero. Also, I-129 is the dominant contributor to the total dose rate whereas the Ca-41 dose rate contribution is small (see Figure 8.5).

In Figure 9.1, the I-129 mass flows to the biosphere, as calculated by CC4, are compared for the Reference (Glaciation) Case and the corresponding Constant Climate case with a well. (In CC4, radionuclides discharge only to the well in this Constant Climate case; see Appendix B). The mass flow rates to the biosphere are generally higher in the Reference Case than in the corresponding Constant Climate case, except during cold-based Ice Sheet States, particularly at earlier times. These differences are due to the groundwater flow perturbations caused by the advancing and retreating ice sheet, as discussed in Sections 6 and 7.

During cold-based Ice Sheet States, there is no I-129 mass flow to the land surface (i.e., to the bottom of the ice sheet) since the permafrost layer beneath the ice prevents I-129 from reaching the surface. However, there is some mass flow to the biosphere during warm based Ice Sheet states (blue), i.e., when there is no permafrost under the ice sheet.

Figure 9.2 compares the Ca-41 releases to the biosphere, as calculated by CC4, for the Reference Case and the corresponding Constant Climate case. (Note the difference in the y-axis scale for this figure and Figure 9.1.) For Ca-41, the releases to the biosphere are about 2 orders of magnitude higher in the Reference Case than in the corresponding Constant Climate case.

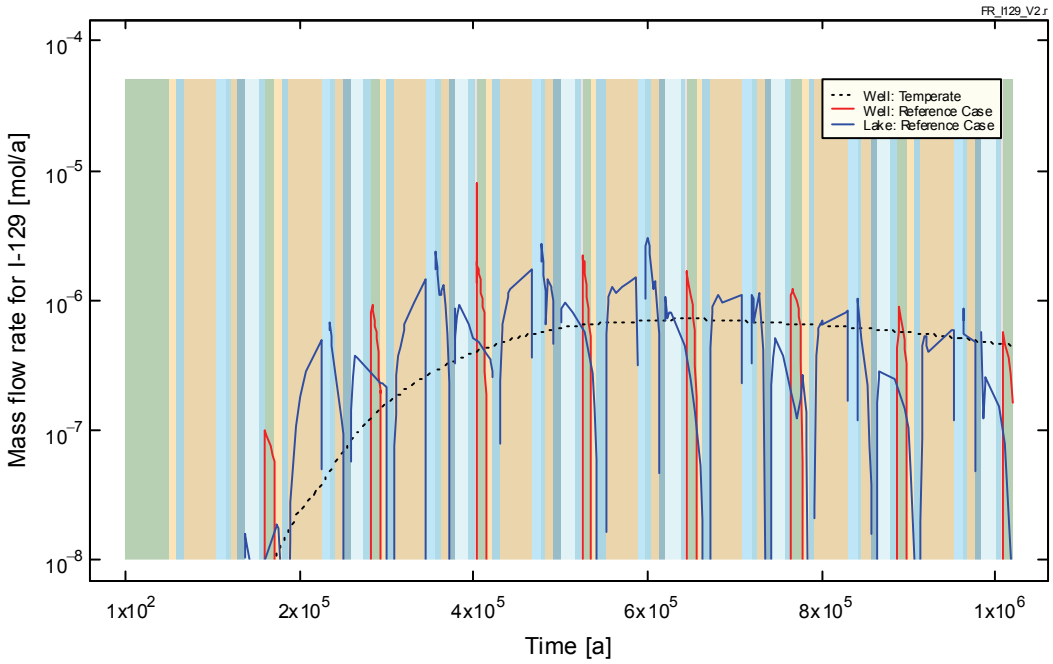

Figure 9.1: Comparison of I-129 mass flow rates to the well and North Lake, as calculated by CC4 for the Reference Case and corresponding Constant (Temperate) Climate case.

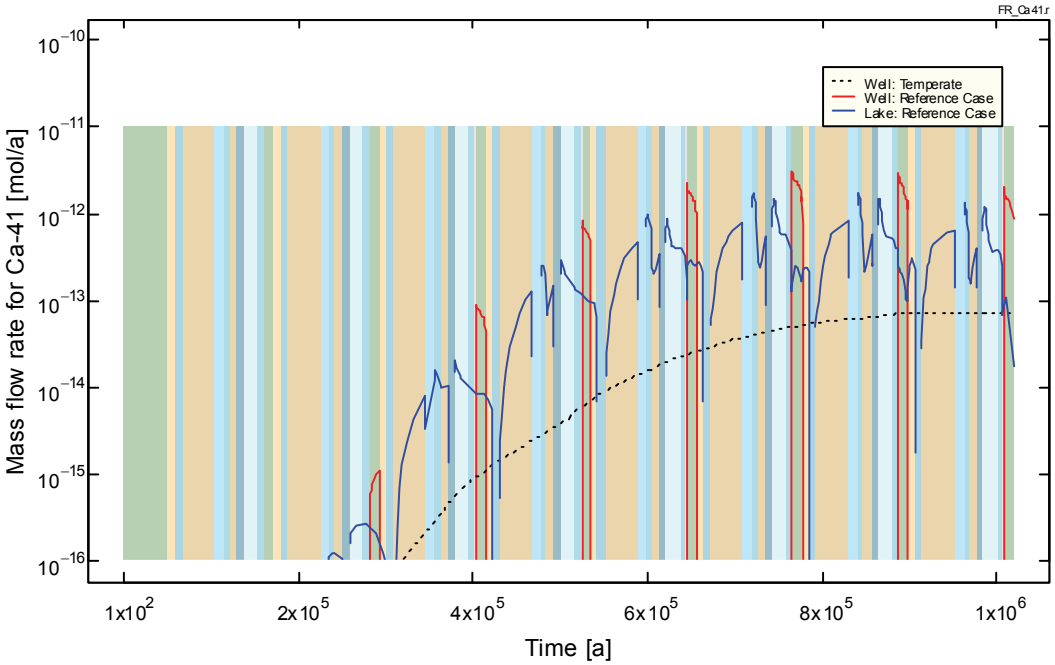

Figure 9.2: Comparison of Ca-41 mass flow rates to the well and North Lake, as calculated by CC4, for the Reference Case and the corresponding Constant Climate case.

The larger differences in Figure 9.2, compared to the differences observed in Figure 9.1 for I-129, can be attributed to the fact that Ca-41 is sorbed in the geosphere. That is, during periods of permafrost, when some of the groundwater pathways to the surface are blocked by permafrost, Ca-41 can accumulate in the groundwater pathways below the permafrost. Relative to I-129, which is not sorbed in the geosphere, much more Ca-41 can accumulate in the groundwater pathways below the permafrost (e.g., in the groundwater pathways leading to the well). This Ca-41 is slowly released into the biosphere after the permafrost melts.

9.3 NUCLIDE CONCENTRATIONS IN THE BIOSPHERE

In this section, nuclide well and lake water concentrations calculated for the Reference Case are compared to those calculated for the corresponding Constant Climate case. As before, the comparison is made for I-129 and Ca-41.

Figure 9.3 compares the I-129 concentrations in the well and North Lake, as calculated by CC4, for the Reference Case and the corresponding Constant (Temperate) Climate case. Since the well is only active during Temperate States, the well concentration peaks during these times. The I-129 concentrations in the well and North Lake are generally higher in the Reference Case than in the corresponding Constant Climate case, reflecting the differences in I-129 mass flow rates to the well and North Lake for these two cases (see Figure 9.1).

Nuclide concentrations in lake water are zero during cold based Ice Sheet States (dark blue) since the ground beneath the ice sheet is frozen during these states. In contrast, nuclide concentrations in the “lake” are non-zero during warm based Ice Sheet States (lighter blues) when the ground is not frozen and, hence, groundwater and radionuclides can discharge to the lake location. A lake would not actually be present during this time; this concentration reflects instead a representation of the radionuclide amount in the surface water under the ice at the lake location. It is conservatively assumed that the radionuclides discharged to the surface, at the lake location, remain in the area and are available when the lake reforms.

Figure 9.4 compares the Ca-41 concentrations in well water and lake water, as calculated by CC4, for the Reference Case and the corresponding Constant Climate case. The differences reflect the differences observed in the Ca-41 mass flows to the biosphere (see Figure 9.2).

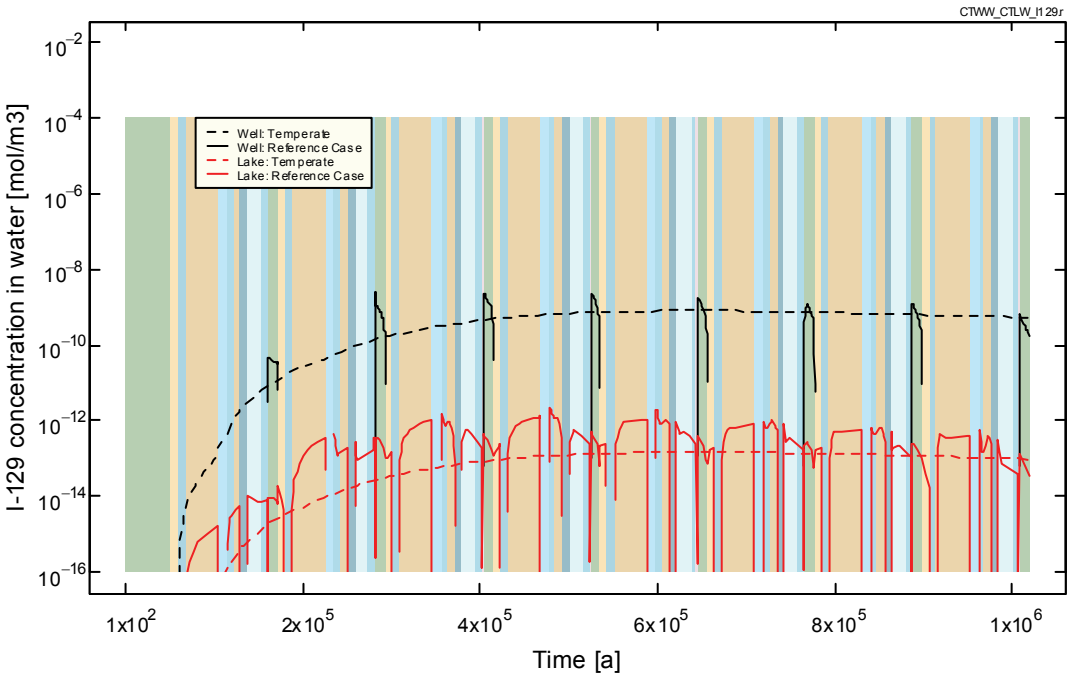

Figure 9.3: Comparison of I-129 concentrations in the well and North Lake, as calculated by CC4, for the Reference Case and the corresponding Constant Climate case.

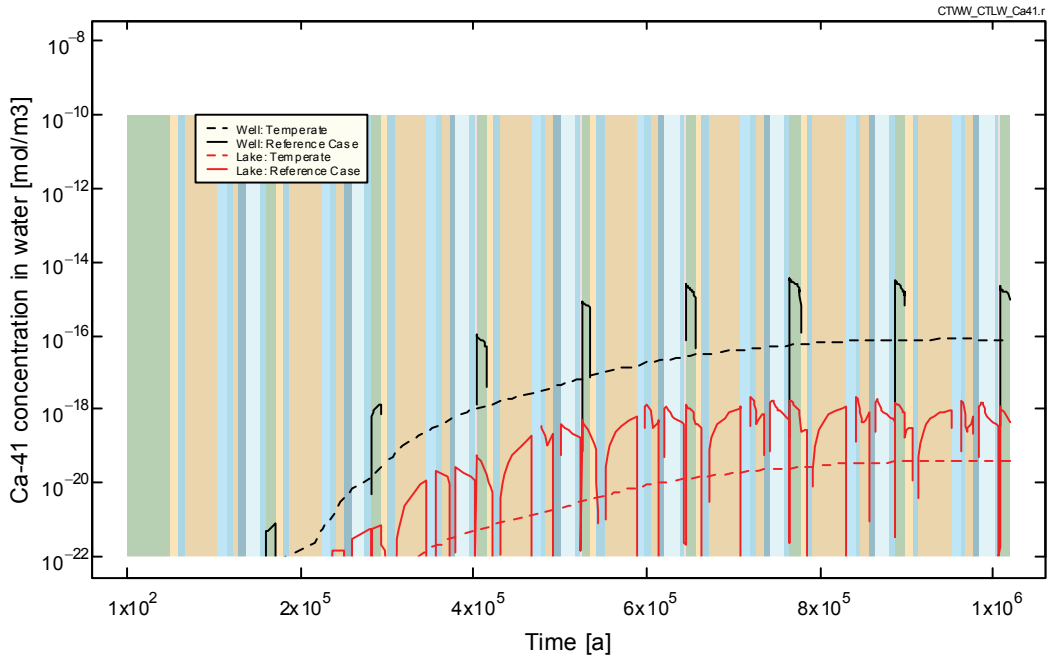

Figure 9.4: Ca-41 concentrations in the well and North Lake for the Reference Case compared to those for the corresponding Constant (Temperate) Climate case.

9.4 CALCULATED DOSE RATES TO THE CRITICAL GROUP

In this section we compare the calculated dose rates to the critical groups for the Reference Case of the (Defective Container) Glaciation Scenario and the corresponding Constant Climate case. In both cases, two of the used fuel containers in the repository are assumed to fail early, leading to early releases of radionuclides from the container and, thereafter, transport of radionuclides through the geosphere and to the surface biosphere.

Because the climate varies markedly during the Reference (Glaciation) Case, three critical groups were defined (see Section 5): a self-sufficient farmer during Temperate States, a tundra hunter during Permafrost States and a tundra hunter-fisher during Proglacial Lake States. In contrast, there is only one critical group during the corresponding Constant (Temperate) Climate case – a self-sufficient farmer, with the same characteristics as the self-sufficient farmer during the Temperate State of the Glaciation Scenario. The critical group characteristics are described in Appendix A.

Figure 9.5 compares the total critical group dose rates, as calculated by CC4, for the Reference (Glaciation) Case and the corresponding Constant Climate case. The calculated dose rates for the Reference (Glaciation) Case are much lower during Permafrost and Proglacial Lake States than during the Temperate State mainly because the critical group uses well water for its domestic needs (drinking, irrigation, bathing, etc.) during the Temperate State, whereas lake water is used for domestic purposes during all other states. As previously observed, nuclide concentrations are much higher in well water than in lake water.

Dose rates are zero during Ice Sheet States because it is assumed that no people reside near the site when it is ice covered.

Figure 9.5 shows that the calculated dose rates for the Constant (Temperate) Climate case are generally higher than for the Reference (Glaciation) Case except during the Temperate States of the glacial cycle. During Temperate States, calculated peak dose rates are somewhat higher for the Reference (Glaciation) Case than for the corresponding Constant Climate case because I-129 well water concentrations are higher for the Reference Case (see Figure 9.3).

Figure 9.6 compares the calculated I-129 dose rates for the Reference (Glaciation) Case with the corresponding Constant Climate case, as calculated using the FRAC3DVS I-129 mass flows to the biosphere and the AMBER biosphere model. The differences are similar to those observed for the CC4 calculated dose rates in Figure 9.5, except for the sharp peaks in the FRAC3DVS dose rates for the Reference Case that occur at the beginning of the second and third Permafrost States of the glacial cycle. These sharp peaks reflect the spikes in the I-129 mass flows to the North talik observed in the FRAC3DVS transport results (see Section 7.6).

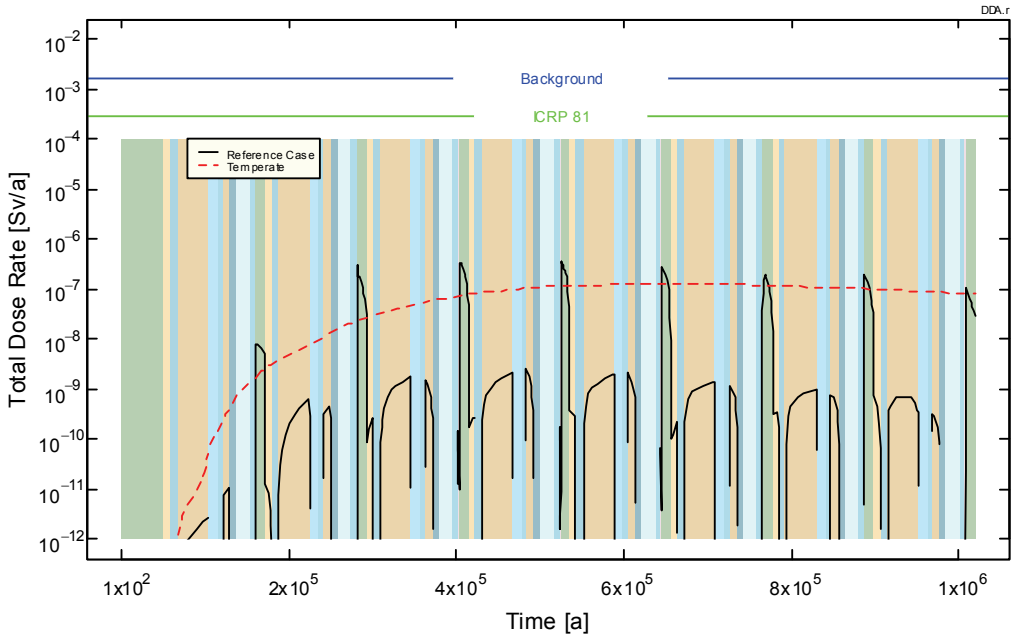

Figure 9.5: Comparison of total dose rates, as calculated by CC4, for Reference Case of the Glaciation Scenario, and the corresponding Constant (Temperate) Climate case.

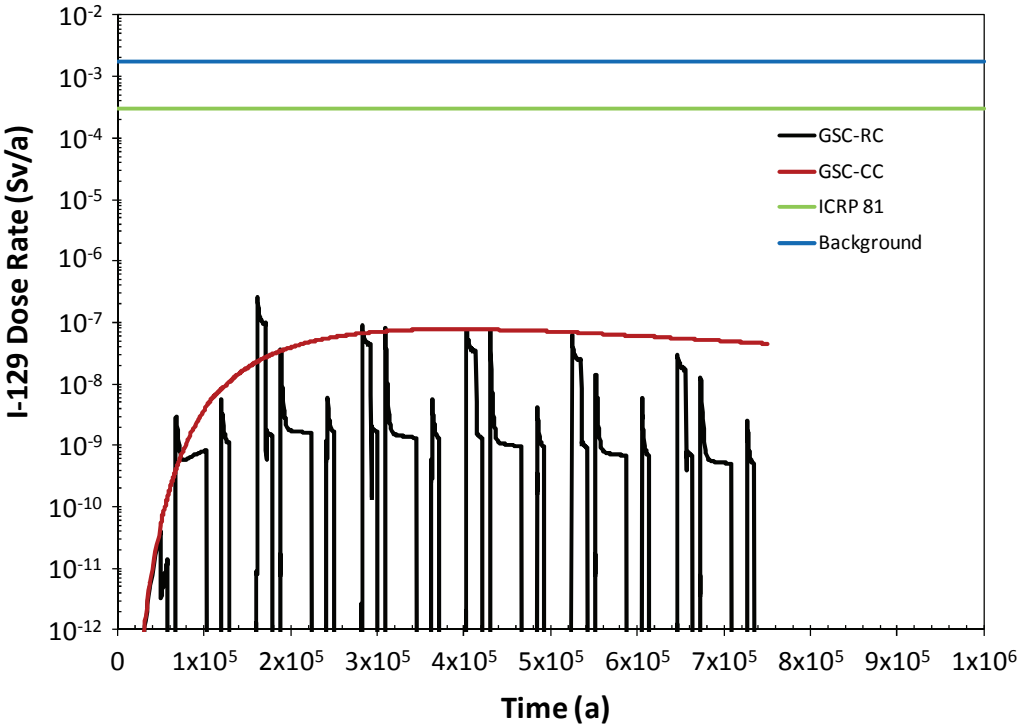

Figure 9.6: Comparison of I-129 dose rates, calculated using FRAC3DVS (DC1 source) and AMBER biosphere model, for Reference (Glaciation) Case (GSC-RC) and the corresponding Constant (Temperate) Climate case (GSC-CC).

The comparisons shown above indicate that calculated peak dose rates are somewhat higher for the Reference (Glaciation) Case than for the corresponding Constant (Temperate) Climate case. The question then arises is how sensitive are the calculated Reference Case dose rates to the selected reference glacial cycle (see Section 3).

To partially address this issue, the Climate State Duration probabilistic safety assessment case was run (see Section 8.5). In this case, the durations of the climate states (see Table 8.3) were varied in 1200 simulations while all other parameters remained at their Reference Case values, including the groundwater flow fields for each unique geosphere state. The results for this case, which are shown in Figure 8.17, indicate that varying the glacial cycle could lead to higher calculated dose rates compared to the Reference Case. Although the 90th percentile calculated dose rate in this probabilistic simulation was 3-fold higher than in the Reference Case, it remained well below the dose rate constraint of 3×10^{-4} Sv/recommended by the ICRP and the average natural Canadian background dose rate of about 1.8×10^{-3} Sv/a.

These results need to be balanced with the reminder that they are particularly sensitive to the conservative assumption that a well is used by the farmer critical group (living during Temperate States) immediately after drainage of the Proglacial Lake, and to the placement of both the well and failed containers in the most conservative locations.

In addition to the glacial cycle, the properties of the geosphere and the geosphere boundary conditions, which affect the transient groundwater flow field, can also affect calculated dose rates. The sensitivity of calculated dose rates to changes in the geosphere properties or geosphere boundary conditions were examined in Section 8.4. Specifically, the I-129 dose rates received by the critical groups were calculated for the geosphere sensitivity cases examined in Section 6. Since I-129 is, by far, the largest dose contributor during the one million year simulation time (see Section 8.1), the total radionuclide dose rate should not differ much from the calculated I-129 dose rate.

The calculated peak dose rates for the geosphere sensitivity cases are summarized in Table 8.8 for defective containers at the DC1 source location (see Figure 7.3). For the geosphere sensitivity cases studied here, the calculated peak I-129 dose rates are similar to those for the Reference Case. This is likely due to the fact that the peak dose rate occurs during the Temperate State, when a well is used as the source of domestic water, and the geosphere changes for these sensitivity cases do not greatly impact I-129 mass flows to the well, as shown in Figure 7.25.

10. SUMMARY AND CONCLUSIONS

In this report, we have carried out a safety assessment of a deep geological repository for used fuel for the so-called Glaciation Scenario. For this assessment, the repository was assumed to be located at the hypothetical Third Case Study site on the Canadian Shield (Gierszewski et al. 2004a).

In the Glaciation Scenario, in contrast to previous Canadian safety assessments (Goodwin et al. 1884, Goodwin et al. 1996, Gierszewski et al. 2004a, Garisto et al. 2005a), the climate is not constant but varies according to a defined reference glacial cycle. The reference glacial cycle used in this study was based on a reconstruction of the last glaciation that occurred over the last 120,000 years (Peltier 2006, see Section 3). The glacial cycle was divided in four distinct states: the Temperate, Permafrost, Ice Sheet and Proglacial Lake States, as described in Sections 3 and 4.

The impact of glacial cycles on the groundwater flow system at the site was investigated using a quasi-transient 3-D model with equivalent porous medium representation of fractures, depth dependent permeabilities and no salinity. The results indicated that the glaciation related changes to surface boundary conditions have an extensive effect on the groundwater flow system, affecting velocity direction, and magnitude. As expected, the effects were greatest near the surface but extended to the repository level. The open taliks during Permafrost States, in particular, are a dominant factor, focusing system stresses at a discrete location.

Sensitivity studies examined the effects of some geosphere assumptions on the groundwater flow. Changes to the geosphere storage coefficient (GSC-HS), and to the southern and northern boundaries (GSC-NF), had a significant effect on the groundwater flow system particularly near the surface. However, these changes had a much more muted impact on the contaminant mass flows to the biosphere. The analyses (Section 6) suggest that this is partially due to the low groundwater flow around the repository itself, as well as the cancellation of the effects arising from glacial advance and retreat, i.e., the periods of positive and negative vertical velocity tend to cancel one another. The largest effects of glaciation occur on groundwater flow closer to the surface, and therefore the edges of any contaminant plume are affected more than the central portion of the plume around the repository.

The groundwater modelling results presented in this report represent a small set of parameter choices and conceptual models, many of which are uncertain, e.g., glacier profile, geosphere storativity, fracture permeability, salinity, loading efficiency, permafrost properties and site features (talik locations). The instantaneous changes in permeability in the upper layers, used to simulate the application of permafrost, also have an uncertain impact and may potentially magnify spikes in I-129 mass flows to the surface (see Section 7). However, although the groundwater flow details will clearly change if other parameter values or conceptual models are used, the parameters considered here are plausible and in some cases bounding, e.g., the presence of open taliks during Permafrost States. Therefore, the main impacts of glaciation are likely captured by the models used here. Of course, analysis of more cases would improve our confidence in the conclusions.

The safety assessment calculations for the Glaciation Scenario were carried out using the system model SYVAC3-CC4. In this system model, the time-dependent geosphere and biosphere are described by a series of defined geosphere and biosphere states with constant

(i.e., time independent) properties (Section 8). To confirm the validity of this approximation to the transient groundwater flow, the CC4 model results for I-129 were compared to those calculated using the detailed FRAC3DVS results. The comparisons, described in Appendix C, indicate that the CC4 system model could adequately reproduce the major features of the FRAC3DVS-CC4 results, and was appropriate to use for the purposes of this report.

Due to the very different climates that occur during the glacial cycle, several different critical groups were defined: the self-sufficient farmer for Temperate States, the tundra hunter for Permafrost States and the tundra hunter-fisher for Proglacial Lake States.

The calculated total dose rates for the Reference Case of the Glaciation Scenario are shown in Figure 10.1. The calculated dose rates are highest during the Temperate State. This occurs because only the critical group during the Temperate State uses a well, rather than a lake, as its domestic water source and nuclide concentrations in well water are typically a few orders of magnitude higher than in lake water (see Section 9). The nuclides contributing the most to the total dose rate are I-129 and Cl-36, followed by Ca-41, Bi-208 and C-14, in that order.

In the Reference Case, the peak total dose rate is about 3.7×10^{-7} Sv/a and occurs at about 520,000 years. This peak dose is similar to the peak dose rate of 1.3×10^{-7} Sv/a for the corresponding Constant (Temperate) Climate case and well below the dose rate constraint of 3×10^{-4} Sv/a recommended by ICRP 81 (ICRP 2000) for disposal of long-lived solid radioactive waste and the average Canadian natural background dose rate of 1.8×10^{-3} Sv/a (Grasty and LaMarre 2004).

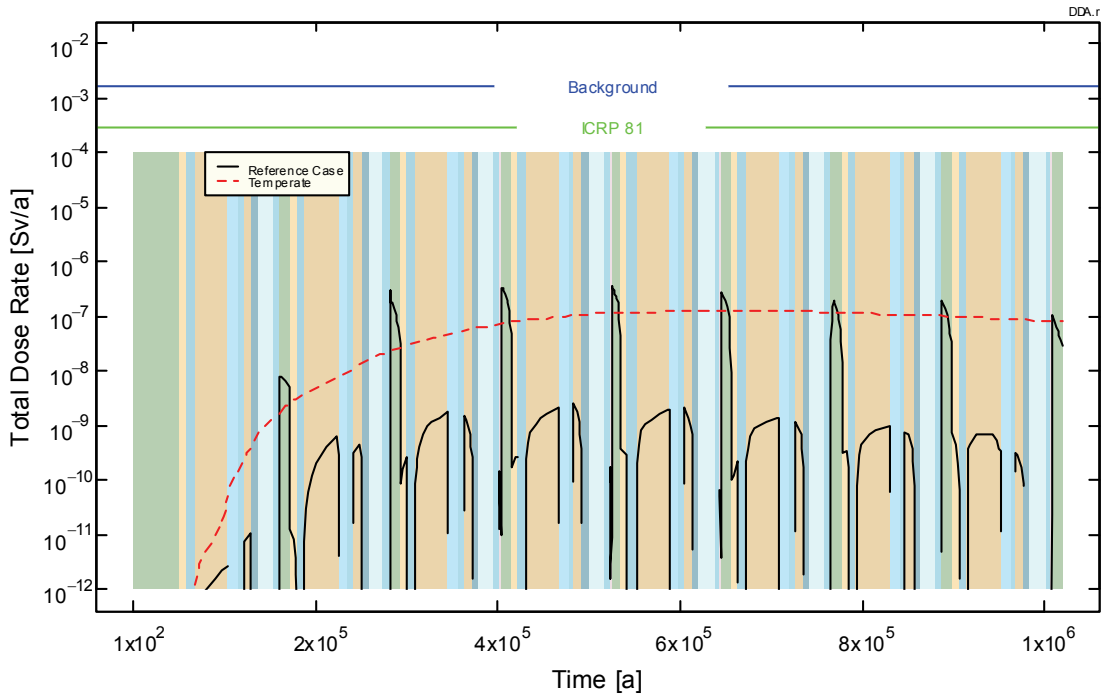

Figure 10.1: Comparison of calculated total dose rates, as calculated by CC4, for the Reference Case of the Glaciation Scenario, and the corresponding Constant (Temperate) Climate case. For the Reference (Glaciation) Case, dose rates are highest during the Temperate State and zero during Ice Sheet States when no humans live near the site.

A series of sensitivity cases studied the effects, on calculated dose rates, of: (1) container failures in different vault sectors, (2) a glacial cycle with no Ice Sheet States and (3) a "what if" scenario in which all containers fail simultaneously. For the first two sensitivity cases, the calculated dose rates were similar or lower than in the Reference (Glaciation) Scenario. However, calculated doses were, as expected, significantly higher for the All Containers Fail case. For this case, the peak calculated dose rate of $4x10^{-4}$ Sv/a, which occurs during a Temperate State, exceeds the ICRP 81 dose rate constraint of $3x10^{-4}$ Sv/a but is well below the average Canadian background dose rate of $1.8x10^{-3}$ Sv/a. However, the calculated dose rate exceeds the ICRP 81 dose constraint for only brief periods of time, as shown in Figure 8.12.

The sensitivity of the calculated I-129 dose rates to changes in the geosphere assumptions was investigated in Section 8.4 using the AMBER biosphere model and the I-129 releases to the biosphere calculated by FRAC3DVS. Although the various geosphere sensitivity cases were found to have a significant impact on the transient groundwater flows during the glacial cycle, there was little impact on the calculated dose rates. This may be partially due to the conservatively selected locations of the defective containers and well in the Reference Case, i.e., the groundwater travel time from the repository to the surface is shortest for the sector of the repository containing the defective containers and the well is placed so as to intercept the radionuclide plume from the repository. In addition, as previously noted, there is a cancellation of effects arising from glacial advance and retreat, i.e., the periods of positive and negative vertical velocity tend to cancel one another making the net effect of glacial advances and retreats small. This would also tend to mute the impact of glaciation on calculated dose rates.

Two probabilistic analyses were carried out using SYVAC3-CC4 to study the consequences of randomly varying the time durations of the glaciation states, and of the number, time and location of container failures. In the Reference Case, the glaciation states have fixed durations (see Table 8.3) and two containers fail in Vault Sector 1. For each probabilistic analysis, the calculated average peak total dose rates were higher than the peak total dose rate for the Reference Case. However, in both cases the 90^{th} percentile total dose rate was well below the ICRP 81 dose rate constraint, as shown in Table 8.9, as were the maximum total dose rates.

Finally, the calculated dose rates to the critical groups for the Reference Case of the Glaciation Scenario were compared to those calculated for the corresponding Constant Climate case (Section 9). The calculated peak dose rate in the Reference Case was found to be about 3-fold higher that in the corresponding Constant Climate case. However, the impacts of glaciation could be greater, depending on the glacial cycle. For example, in the Climate State Duration probabilistic case, the 90^{th} percentile peak dose rate was 3-fold higher than for the Reference Case. Nevertheless, the peak dose rates remained well below the ICRP 81 dose constraint of $3x10^{-4}$ Sv/a.

In conclusion, for the Third Case Study hypothetical site and repository, calculated peak dose rates for the Glaciation Scenario were found to be approximately of the same order of magnitude as for the corresponding constant (temperate) climate case. The calculated peak dose rates for the Reference (Glaciation) Case were well below the ICRP 81 dose constraint of $3x10^{-4}$ Sv/a and the average natural Canadian background dose rate of about $1.8x10^{-3}$ Sv/a. Thus, it can be concluded that for the hypothetical Third Case Study site and repository, the impacts of a deep geological repository would be well below regulatory limits when the effects of glaciation are considered.

ACKNOWLEDGEMENTS

The authors would like to thank Bruce Goodwin for his review and comments on the report. His comments have improved the report.

REFERENCES

Adams, J. 1989. Postglacial faulting in eastern Canada: Nature, origin and seismic hazard implications. Tectonophysics 163, 323-331.

AECL (Atomic Energy of Canada Limited). 1994. Environmental impact statement on the concept for disposal of Canada's nuclear fuel waste. Atomic Energy of Canada Limited Report, AECL-10711, COG-93-1. Chalk River, Canada.

Ahlbom, K., T. Aikas and L. Ericsson. 1991. SKB/TVO ice age scenario. SKB Technical Record TR 91-32. Stockholm, Sweden.

Archer, D. and Ganopolski, A. 2005. A movable trigger: Fossil fuel CO_2 and the onset of the next glaciation. Geochemistry Geophysics Geosystems 6 (5).

Arcos, D., J. Bruno, S. Benbow and H. Takase. 2000. Behaviour of bentonite accessory minerals during the thermal stage. Swedish Nuclear Fuel and Waste Management Company SKB Technical Report TR-00-06. Stockholm, Sweden.

Berger, A. and M.F. Loutre. 2002. An exceptionally long interglacial ahead? Science 297, 1287-1288.

Blyth, A., S. Frape, R. Blomqvist and P. Nissinen. 2000. Assessing the past thermal and chemical history of fluids in crystalline rock by combining fluid inclusion and isotope investigations of fracture calcite. Applied Geochemistry 13, 1417-1437.

Brown, R.J.E. 1974. Distribution and environmental relationships of permafrost. In Permafrost Hydrology, Proceedings of Workshop Seminar, 1974, pp. 1- 5. Canadian National Committee, International Hydrological Decade, Environment Canada. Ottawa, Canada.

Cedercreutz, J. 2004. Future climate scenarios for Olkiluoto with emphasis on permafrost. Posiva Oy Report POSIVA 2004-06. Olkiluoto, Finland

Chan, T., R. Christiansson, G.S. Boulton, L.O. Eriksson, J. Hartikainen, M.R. Jensen, D. Mas Ivars, F. W. Stanchell, P.Vistrand, and T. Wallroth. 2005. DECOVALEX III/BENCHPAR PROJECTS. The thermal-hydro-mechanical responses to a glacial cycle and their potential implications for deep geological disposal of nuclear fuel waste in a fractured crystalline rock mass. Report of BMT3/WP4. SKI Report 2005:28. Stockholm, Sweden.

Chan, T. and F.W. Stanchell. 2008. DECOVALEX THMC TASK E – Implications of glaciation and coupled thermohydromechanical processes on shield flow system evolution and performance assessment. Nuclear Waste Management Organization Technical Report NWMO TR-2008-03. Toronto, Canada

Chan, T. and F.W. Stanchell. 2004. DECOVALEX III BMT3 (The Glaciation Bench Mark Test) Final Research Team Report. Ontario Power Generation, Nuclear Waste Management Division Report 06819-REP-01300-10091-R00. Toronto, Canada.

Chan, T., F.W. Stanchell, T. Wallroth, J. Hernelind and G. Boulton. 2003. A finite-element study of potential coupled hydromechanical effects of glaciation on a crystalline rock mass. Proceedings of the International Conference on Coupled T-H-M-C Processes in Geo-systems: Fundamentals, Modelling, Experiments and Applications (GEOPROC, 2003), Stockholm, Sweden. (Editors, O. Stephansson, J. A. Hudson and L. Jing), 277-282.

CNSC (Canadian Nuclear Safety Commission). 2004. Managing Radioactive Waste. CNSC Regulatory Policy P-290. Ottawa, Canada.

CNSC (Canadian Nuclear Safety Commission). 2006. Assessing the long term safety of radioactive waste management. CNSC Regulatory Guide G-320. Ottawa, Canada.

CSA (Canadian Standards Association). 2008. Guidelines for calculating derived release limits for radioactive material in airborne and liquid effluents for normal operation of nuclear facilities. CSA Guideline Report N288.1-08. Toronto, Canada.

Davis, P.A., R. Zach, M.E. Stephens, B.D. Amiro, G.A. Bird, J.A.K. Reid, M.I. Sheppard and M. Stephenson. 1993. The disposal of Canada's nuclear fuel waste: The biosphere model, BIOTRAC, for postclosure assessment. Atomic Energy of Canada Limited Report AECL-10720. Pinawa, Canada.

Davison, C.C., T. Chan, A. Brown, M. Gascoyne, D.C. Kamineni, G.S. Lodha, T.W. Melnyk, B.W. Nakka, P.A. O'Connor, D.U. Ophori, N.W. Scheier, N.M.Soonawala, F.W. Stanchell, D.R. Stevenson, G.A. Thorne, S.H. Whitaker, T.T. Vandergraaf and P. Vilks. 1994. The disposal of Canada's nuclear fuel waste: The geosphere model for postclosure assessment. Atomic Energy of Canada Limited Report, AECL-10719, COG-93-9. Chalk River, Canada.

Environment Canada. 2009. See Environment Canada website: http://www.ec.gc.ca/soer-ree/English/Framework/Nardesc/canada_e.cfm

Enviros and Quintessa. 2008. AMBER 5.2 Reference guide. Enviros Consulting Limited. Abingdon, UK.

Frind, E. 1988. Solution of the advection-dispersion equation with free exit boundary. Numerical Methods for Partial Differential Equations 4, 301-313.

Garamszeghy, M. 2008. Nuclear fuel waste projections in Canada – 2008 update. Nuclear Waste Management Organization Technical Report NWMO TR-2008-18. Toronto, Ontario.

Garisto, F., J. Avis, N. Calder, P. Gierszewski, C. Kitson, T. Melnyk, K. Wei and L. Wojciechowski. 2005a. Horizontal borehole concept case study. Ontario Power Generation, Nuclear Waste Management Division Report 06819-REP-01200-10139-R00. Toronto, Canada.

Garisto, F., T. Kempe, P. Gierszewski, K. Wei, C. Kitson, T. Melnyk, L. Wojciechowski, J. Avis and N. Calder. 2005b. Horizontal borehole concept case study: Chemical toxicity risk. Ontario Power Generation Report, Nuclear Waste Management Division Report 06819-REP-01200-10149-R00. Toronto, Canada.

Garisto, F., J. Avis, N. Calder, A. D'Andrea, P. Gierszewski, C. Kitson, T. Melnyk, K. Wei and L. Wojciechowski. 2004a. Third case study - Defective container scenario. Ontario Power Generation, Nuclear Waste Management Division Report 06819-REP-01200-10126-R00. Toronto, Canada.

Garisto, F., A. D'Andrea, P. Gierszewski and T. Melnyk. 2004b. Third Case Study - Reference Data and Codes. Ontario Power Generation, Nuclear Waste Management Division Report 06819-REP-01200-10107-R00. Toronto, Canada.

Gascoyne, M. 2004. Hydrogeochemistry, groundwater ages and sources of salts in a granitic batholith on the Canadian Shield, southeastern Manitoba. Appl. Geochem. 19, 519-560.

Gascoyne, M. 2000. Hydrogeochemistry of the Whiteshell Research Area. Ontario Power Generation Report, Nuclear Waste Management Division Report 06819-REP-01200-10033-R00, Toronto, Canada.

Gascoyne, M. 1999. Long-term maintenance of reducing conditions in a spent nuclear fuel repository. A re-examination of critical factors. SKB Research Report R-99-41. Stockholm, Sweden.

Gascoyne, M., J. McMurry and R. Ejeckam. 2004. Paleohydrogeological case study of the Whiteshell Research Area. Ontario Power Generation, Nuclear Waste Management Division Report 06819-REP-01200-10121-R00. Toronto, Ontario.

Gierszewski, P., J. Avis, N. Calder, A. D'Andrea, F. Garisto, C. Kitson, T. Melnyk, K. Wei and L. Wojciechowski. 2004a. Third case study - Postclosure safety assessment. Ontario Power Generation, Nuclear Waste Management Division Report 06819-REP-01200-10109-R00. Toronto, Canada.

Gierszewski, P., M. Jensen and P. Maak. 2004b. Third case study - Site and design description. Ontario Power Generation, Nuclear Waste Management Division Report 06819-REP-01200-10124-R00. Toronto, Canada.

Gierszewski, P., F. Garisto and K. Wei. 2004c. Third case study - Features, events and processes. Ontario Power Generation, Nuclear Waste Management Division Report 06819-REP-01200-10125-R00. Toronto, Canada.

Gierszewski, P., T.W. Melnyk, S.C. Sheppard and J. Tait. 2004d. SYVAC3-CC4 theory. Ontario Power Generation, Nuclear Waste Management Division Report 06819-REP-01300-10072-R00. Toronto, Canada.

Glynn, P.D., C.I. Voss, and A.M. Provost. 1997. Deep penetration of oxygenated meltwaters from warm based ice sheets into the Fennoscandian Shield. In: Use of hydrogeochemical information in testing groundwater flow models, Workshop Proceedings, pp. 201-241.

Gogineni, D. Tammana, D. Braaten, C. Leuschen, T. Aikins, J. Legarsky, P. Kanagaratnam, J. Stiles, C. Allen and K. Jezek. 2001. Coherent radar ice thickness measurements over the Greenland ice sheet. J. Geophysical Research 106, 33,761-33,772.

Goodwin, B.W., D. McConnell, T. Andres, W. Hajas, D. LeNeveu, T. Melnyk, G. Sherman, M. Stephens, J. Szekely, P. Bera, C. Cosgrove, K. Dougan, S. Keeling, C. Kitson, B. Kummen, S. Oliver, K. Witzke, L. Wojciechowski and A. Wikjord. 1994. The disposal of Canada's nuclear fuel waste: Postclosure assessment of a reference system. Atomic Energy of Canada Limited Report AECL-10717, COG-93-7. Pinawa, Canada.

Goodwin, B.W., T. Andres, W. Hajas, D. LeNeveu, T. Melnyk, J. Szekely, A. Wikjord, D. Donahue, S. Keeling, C. Kitson, S. Oliver, K. Witzke and L. Wojciechowski. 1996. The disposal of Canada's nuclear fuel waste: A study of postclosure safety of in-room emplacement of used CANDU fuel in copper containers in permeable plutonic rock. Volume 5: Radiological Assessment. Atomic Energy of Canada Limited Report AECL-11494-5, COG-95-552-5. Pinawa, Canada.

Goodwin, B.W., P. Gierszewski and F. Garisto. 2001. Radionuclide screening model (RSM) version 1.1 - Theory. Ontario Power Generation, Nuclear Waste Management Division Report 06819-REP-01200-10045-R00. Toronto, Canada.

Government of Canada. 2004. Climate change impacts and adaptation: A Canadian perspective. Government of Canada publication. Ottawa. Canada. Available at: http://adaptation.nrcan.gc.ca/perspective/pdf/report_e.pdf

Grasty R.L., and J. R. LaMarre. 2004. The annual effective dose from natural sources of ionising radiation in Canada. Radiation Protection Dosimetry 108, 215-226.

Hanna, S. And D. Arguner. 2001. Radiation dose rates from used-fuel containers and attenuation characteristics of selected materials. Ontario Power Generation, Nuclear Waste Management Division Report 06819-REP-01300-10020-R00. Toronto, Canada.

Hökmark, H., B. Fälth and T. Wallroth. 2006. T_H_M couplings in rock. Overview of results of importance to the SR-Can safety assessment. SKB Research Report R-06-88. Stockholm, Sweden.

Huybrechts, P. 1986. A three dimensional time-dependent numerical model for polar icesheets:Some basic testing with a stable and efficient finite difference scheme. Report 86-1. Geografisch Instituut, Vrije Universiteit Brussel, Pleinlaan 2, B-1050 Brussels, Belgium.

IAEA (International Atomic Energy Agency). 2004. Safety assessment methodologies for near surface disposal facilities. Results of a co-ordinated research project. Vol. I: Review and enhancement of safety assessment approaches and tools. IAEA. Vienna, Austria.

ICRP (International Commission on Radiological Protection). 2000. Radiation protection recommendations as applied to the disposal of long-lived solid radioactive waste. Annals of the ICRP 28(4). ICRP Publication 81, Pergamon Press, Oxford, UK.

IPCC (Intergovernmental Panel on Climate Change). 2007. Climate change 2007. Synthesis report. Contribution of Working Groups I, II and III to the Fourth Assessment Report of the Intergovernmental Panel on Climate Change. IPCC, Geneva, Switzerland. Available at http://www.ipcc.ch

Jaquet, O. and P Siegel. 2006. Regional groundwater flow model for a glaciation scenario. Simpevarp subarea – version 1.2. SKB Research Report R-06-100. Stockholm, Sweden.

Lemire R.J. and F. Garisto. 1989. The solubility of U, Np, Pu, Th and Tc in a geological disposal vault for used nuclear fuel. Atomic Energy of Canada Limited Report AECL-10009. Pinawa, Canada.

Loutre, M.F. and A. Berger. 2000. Future climate changes: Are we entering an exceptionally long interglacial? Climate Change 46, 61-90.

Lum, P. and F. Garisto. 2008. Glaciation biosphere model for a Canadian used fuel repository. Proceedings of the 2008 International High Level Radioactive Waste Management Conference, Las Vegas, USA. P. 513-520.

Maak, P. and G. Simmons. 2001. Summary report: A screening study of used-fuel container geometric designs and emplacement methods for a deep geologic repository. Ontario Power Generation, Nuclear Waste Management Division Report 06819-REP-01200-10065-R00. Toronto, Canada.

Maak, P., P. Gierszewski and M. Saiedfar. 2001. Early failure probability of used-fuel containers in a deep geologic repository. Ontario Power Generation, Nuclear Waste Management Division Report 06819-REP-01300-10022-R00. Toronto, Canada.

Marsh, G.E. 2008. Climate stability and policy: A synthesis. Available on the web at arXiv:0801.3830v1 [physics.ao-ph].

Marshall, S.J. and G.K.C. Clarke, 1997a. A continuum mixture model of ice stream thermodynamics in the Laurentide Ice Sheet: Theory. J. Geophys. Res. 102, 20599-20614.

Marshall, S.J. and G.K.C. Clarke, 1997b. A continuum mixture model of ice stream thermodynamics in the Laurentide Ice Sheet 2: Application to the Hudson Strait Ice Stream. J. Geophys. Res. 102, 20615-20638.

McMurry, J. 2004. Reference water compositions for a deep geologic repository in the Canadian Shield. Ontario Power Generation, Nuclear Waste Management Division Report 06819-REP-01200-10135-R1. Toronto, Canada.

McMurry, J. 2000. Evaluating effects of deep recharge by a low-salinity, oxidizing groundwater: A geochemical modeling case study. Ontario Power Generation, Nuclear Waste Management Division Report 06819-REP-01300-10007-R0. Toronto, Canada.

McMurry, J. and R.B. Ejeckam. 2002. Paleohydrogeological study of fracture mineralogy in the Whiteshell Research Area. Ontario Power Generation Report, Nuclear Waste Management Division 06819-REP-01200-10082-R00. Toronto, Canada.

McMurry, J., D.A. Dixon, J.D. Garroni, B.M. Ikeda, S. Stroes-Gascoyne, P. Baumgartner and T.W. Melnyk. 2003. Evolution of a Canadian deep geologic repository: Base scenario. Ontario Power Generation, Nuclear Waste Management Division Report 06819-REP-01200-10092-R00. Toronto, Canada.

McMurry, J., B.M. Ikeda, S. Stroes-Gascoyne, D.A. Dixon and J.D. Garroni. 2004. Evolution of a Canadian deep geologic repository: Defective container scenario. Ontario Power Generation, Nuclear Waste Management Division Report 06819-REP-01200-10127-R00. Toronto, Canada.

Neuzil, C. 2003. Hydromechancial coupling in geological processes. Hydrogeology Journal, 11, 41-83.

Normani, S.D. 2009. Paleoevolution of pore fluids in glaciated geologic settings. Ph.D. Thesis, University of Waterloo, Department of Civil Engineering.

Normani, S.D., Y.-J. Park J.F. Sykes and E.A. Sudicky. 2007. Sub-regional case study 2005-2006 status report. Nuclear Waste Management Organization Technical Report NWMO TR-2007-07. Toronto, Canada.

NWMO (Nuclear Waste Management Organization). 2005. Choosing a way forward: The future management of Canada's used nuclear fuel. Final study. Toronto, Canada.

Oerlemans, J. 2005. Analytical ice-sheet models", Karthaus 2005 Lecture Notes. On web at http://igitur-archive.library.uu.nl/phys/2007-0504-200658/oerlemans_05_lecturenotes_analyticalicesheetmodels.pdf

Passe, T. 2004. The amount of glacial erosion of the bedrock. SKB Technical Report TR-04-25. Stockholm, Sweden.

Payne, A.J. and P.W. Dongelmans. 1997. Self-organization in the thermomechanical flow of ice sheets. J. Geophys. Res. 102 (B6), 12219-12234.

Payne, A.J., P. Huybrechts, A. Abe-Ouchi, R. Calov, J.L. Fastook, R. Greve, S.J. Marshall, I. Marsiat, C. Ritz, L. Tarasov, and M.P.A. Thomassen. 2000. Results from the EISMINT model intercomparisons: The effects of thermomechanical coupling. J. Glaciology 46, 227-238.

Peltier, W.R. 2006. Boundary conditions data sets for spent fuel repository performance assessment. Ontario Power Generation, Nuclear Waste Management Division Report 06819-REP-01200-10154-R00. Toronto, Canada.

Peltier, W.R. 2003. Long-term climate change – glaciation. Ontario Power Generation, Nuclear Waste Management Division Report 06819-REP-01200-10113-R00. Toronto, Canada.

Poon, G., M. Saiedfar and P. Maak. 2001. Selection of a primary load-bearing component conceptual design for used-fuel containers. Ontario Power Generation, Nuclear Waste Management Division Report 06819-REP-01200-10051-R00. Toronto, Canada.

Raymo, M.E. and K. Nisancioglu. 2003. The 41 kyr world: Milankovitch's other unsolved mystery. Paleoceanography 18, **11**-1 to **11**-6.

Ritz, C., A. Fabre and A. Letreguilly. 1996. Sensitivity of a Greenland ice sheet model to ice flow and ablation parameters: Consequences for evolution through the last climatic cycle. Clim. Dyn. 11-24.

Seidler, W. and B. Faucher. 2004. EU's Esdred initiative. Nucl. Eng. Internat. 49 (July), 19-21.

Shoesmith, D. 2008. The role of dissolved hydrogen on the corrosion/dissoluton of spent nuclear fuel. Nuclear Waste Management Organization Technical Report NWMO TR-2008-19. Toronto, Canada.

SKB (Svensk Kärnbränslehantering AB). 2006a. Long-term safety for KBS-3 repositories at Forsmark and Laxemar – a first evaluation. Main report of the SR-Can project. SKB Technical Report TR-06-09. Stockholm, Sweden.

SKB (Svensk Kärnbränslehantering AB). 2006b. Climate and climate-related issues for the safety assessment SR-Can. SKB Technical Report TR-06-23. Stockholm, Sweden.

SKB (Svensk Kärnbränslehantering AB). 2006c. Geosphere process report for the safety assessment SR-Can. SKB Technical Report TR-06-19. Stockholm, Sweden.

SKB (Svensk Kärnbränslehantering AB). 1999. Deep repository for spent nuclear fuel. SR-97 – Post-closure safety. SKB Technical Report TR-99-06. Stockholm, Sweden.

Smith, P., L. Johnson, M. Snellman, B. Pastina and P. Gribi. 2007.. Safety assessment for a KBS-3H spent fuel repository at Olkiluoto: Evolution report. Posiva Oy Report POSIVA 2007-08. Olkiluoto, Finland.

Spiessl, S.M., K.U. Mayer and K.T.B. MacQuarrie. 2009. Reactive transport modelling in fractured rock – Redox stability study. Nuclear Waste Management Technical Report NWMO TR-2009-04.

Srivastava, R.M. 2002a. The discrete fracture network model in the local scale flow system for the Third Case Study. Ontario Power Generation, Nuclear Waste Management Division Report 06819-REP-01300-10061-R00. Toronto, Canada.

Srivastava, R.M. 2002b. Probabilistic discrete fracture network models for the Whiteshell Research Area. Ontario Power Generation, Nuclear Waste Management Division Report 06819-REP-01200-10071-R00, Toronto, Canada.

Stewart, I.S., J. Sauber and J. Rose. 2000. Glacio-seismotectonics: Ice sheets, crustal deformation and seismicity. Quaternary Science Reviews 19, 1367-1389.

Sudicky, E. A. 1990. The Laplace transform Galerkin technique for efficient time-continuous solution of solute transport in double-porosity media. Geoderma 46, 209-232.

Sykes, J.F., S.D. Normani and E.A. Sudicky. 2003a. Regional scale groundwater flow in a Canadian Shield setting. Ontario Power Generation, Nuclear Waste Management Division Report 06819-REP-01200-10114-R00. Toronto, Canada.

Sykes, J.F, S.D. Normani and E.A. Sudicky. 2003b. Modelling strategy to assess long-term regional-scale groundwater flow within a Canadian Shield setting, Proceedings 4th Joint IAH/CGS Conference. Winnipeg, Canada.

Sykes, J.F., S.D. Normani, E.A. Sudicky and R.G. McLaren, 2004, Sub-regional scale groundwater flow within an irregular discretely fractured Canadian Shield setting. Ontario

Power Generation Report, Nuclear Waste Management Division 06819-REP-01200-10133-R00. Toronto, Canada.

Therrien, R. and E. Sudicky. 1996. Three-dimensional analysis of variably-saturated flow and solute transport in discretely-fractured porous media. J. of Contaminant Hydrology 23, 1-44.

Therrien, R., R. McLaren, E. Sudicky, S. Sanday, and V. Guvanasen. 2007. FRAC3DVS_OPG: A Three-Dimensional Numerical Model Describing Subsurface Flow and Solute Transport (DRAFT). Groundwater Simulations Group, University of Waterloo.

Vidstrand, P., U. Svensson and S. Follin. 2006. Simulation of hydrodynamic effects of salt rejection due to permafrost. SKB Research Report R-06-101. Stockholm, Sweden.

Walsh, R. And J. Avis. 2010. Glaciation Scenario: Groundwater and radionuclide transport studies. Nuclear Waste Management Organization Technical Report NWMO TR-2010-09. Toronto, Canada.

Wang, H.F. 2000. Theory of linear poroelasticity with application to geomechanics and hydrogeology. Princeton University Press, Princeton, NJ.

Zhang, M., and S.K. Frape. 2002. Permafrost: Evolution of shield groundwater compositions during freezing. Ontario Power Generation, Nuclear Waste Management Division Report 06819-REP-01200-10098-R00. Toronto, Canada.

APPENDIX A: BIOSPHERE INFORMATION AND DATA

CONTENTS

A.1 INTRODUCTION

The reference glacial cycle, which is described in Section 3 of the report, is divided into four distinct states: the Temperate, Permafrost, Ice Sheet and Proglacial Lake States. Some features of these states are described in Section 4. In this Appendix, we provide information and data on the biospheres states used in the calculation of dose rates to the critical groups. Data on ice sheet advance and retreat rates are also summarized here.

It is assumed that people (or non-human biota) do not reside near the repository site during Ice Sheet States so dose rates are zero during these times; therefore, biosphere data are not needed for this state. Therefore, the Ice Sheet State is not discussed further in this appendix.

A.2 GENERAL CRITICAL GROUP CHARACTERISTICS

The critical group is a group of individuals expected to receive the largest annual dose rate from radionuclides released from the repository. Conservative assumptions are made to ensure the dose rates are not underestimated. This group is assumed to spend their entire lives in the vicinity of the site and to obtain all their needs (food, water, shelter, etc.) from this area.

During the Temperate State, a self-sufficient farmer household, as described in the HBC study (Garisto et al. 2005a), is assumed to be the critical group. Animals raised on the farm include cattle, dairy cows and poultry. The farmer grows crops and obtains fish from a nearby lake. Enough food is grown for all humans and animals living on the farm. All water needs are met by a well, which is located so as to intercept any contaminated plume from the repository. Water is used for bathing, irrigation and drinking by humans and animals.

During the Permafrost State, a self-sufficient tundra hunter, characteristic of the inland tundra region, is assumed to be the reference critical group. The hunter diet consists mainly of meat from caribou herds, supplemented with some wild plants, fish and migratory wild birds. Humans and animals consume water taken from a nearby lake. Lake water is also used for bathing. Contaminated groundwater from the repository discharges into the lake even during the Permafrost State since the lake is assumed to support an open talik during this time. The biosphere characteristics of the Permafrost State for the Canadian Shield area are discussed by Sheppard et al. (1995).

As noted, caribou herds are assumed to graze near the repository site for a half a year. While at the site, the caribou eat lichen. Lichen becomes contaminated via deposition from the air of radionuclides released from the nearby lake due to degassing and aerosol suspension, and from the soil due to dust resuspension. Canada geese, the representative wild bird in this model, eat forage plant that grows near the lake. Wild plants, represented by berries, gathered by the hunter contribute a small part of the overall diet.

The surface of the lake is assumed to be frozen for part of the year. This decreases degassing and aerosolization rates for radionuclides in the lake during the Permafrost State compared with those during the Temperate State (Sheppard et al. 1995) since winters are longer during Permafrost States.

As previously mentioned, due to the full glacial coverage, no inhabitants are assumed to live in the vicinity of the repository area during Ice Sheet States. Hence, the value of "Overall Human Occupancy Factor" is set to zero (0) during Ice Sheet States. (Where biosphere data are required for Ice Sheet States in the SYVAC3-CC4 data files, data from the Permafrost State are arbitrarily used.)

The Proglacial Lake climate was assumed to resemble that of the Permafrost State. Thus, the main difference between these two climate states is the presence of a large proglacial lake.

The critical group during the Proglacial Lake State is a self-sufficient tundra hunter-fisher who moves into the area after the last glaciation period. This group resembles the tundra hunter group in that a large fraction of their diet consists of caribou meat; however, due to the availability of fish in the proglacial lake, the hunter-fisher diet contains a much greater proportion of fish than the hunter diet. The proglacial lake is the source of drinking and bathing water for humans and animals, as well as a major food source (fish) for the critical group.

A.3 BIOSPHERE DATA

Due to the large number of data, the parameters have been divided into the following categories for discussion: climate, site and surface water, human physical and lifestyle, plant and animal, volatilization and transfer factors. Temperate State parameters are mainly from the HBC study (Garisto et al. 2005a) unless otherwise specified. Parameters for the Permafrost and Proglacial Lake States are from a variety of sources referenced throughout this appendix.

For the most part, the safety assessment calculations reported here used best-estimate parameter values. The median value of the parameter was used if a best-estimate value was unavailable. However, for conservatism and consistent with the critical group concept, human food consumption and air inhalation parameters were 90^{th} or 95^{th} percentile values.

A.3.1 Climate Parameters

Climate parameters for each state are summarized in Table A.1. Cooler climates during the Permafrost and Proglacial Lake States result in less precipitation and higher wind speeds than for the Temperate State.

Table A.1: Climate Parameters

Parameter	Temperate	Permafrost and Proglacial Lake
Average Precipitation Rate (m/a)	0.78	0.29 (1)
Average Annual Temperature (°C)	1 (2) *	-8 (1)
Average Wind Speed (m/s)	2.36	3.8 (1)

(1) Sheppard et al. 1995.
(2) Environment Canada. 2008a.
* Climate parameters for the temperate state are based on the Environment Canada Boreal Shield Ecozone average summer and winter temperatures.

A.3.2 Site and Surface Water Parameters

Site and surface water parameters are summarized in Table A.2.

The Temperate and Permafrost site and surface water parameters are identical because it is assumed that the same lake is present during both these states. The lower precipitation rate during the Permafrost State compared with the Temperate State is assumed to have a negligible effect on lake properties. Site and surface water parameter data in the Proglacial Lake state are estimated values (see below). Radionuclide loss rates to lake sediments for the Permafrost and Proglacial Lake States are approximately 25% of the Temperate State loss rates (Sheppard et al. 1995).

The parameter values for the Proglacial Lake State were derived as follows:

- Based on data from Chan and Stanchell (2006), Boulton et al. (2001a) and SKB (1999), the ice sheet melt rate can be described by a uniform probability density function with limits 0.05 to 0.15 m/a, giving a median value of 0.1 m/a.
- The watershed area for the proglacial lake was calculated assuming that only one major ice tunnel feeds into the lake. Major ice tunnels are typically 10 to 100 km long and are spaced 5 to 20 km apart (Boulton et al. 2001b). Thus, the watershed area feeding one major ice tunnel is in the range $5x10^8$ to $2x10^{10}$ m^2. A loguniform distribution between these limits gives a median value of about $3x10^9$ m^2.
- The proglacial lake was arbitrarily assumed to have a surface are 100-fold larger than the lake in the Temperate State.
- Finally, the depths of the proglacial lakes in the GST simulations (Peltier 2006) ranged from 25 to 190 m. A nominal median value of 100 m was selected for the calculations.

Table A.2: Site and Surface Water State Parameters

Parameter	Temperate	Permafrost	Proglacial Lake
Watershed Area (m^2)	$6x10^6$	$6x10^6$	$3.2x10^9$
Watershed Runoff Rate (m/a)	0.31	0.12 (1)	0.12 (1)
Meltwater Production Rate (m/a)	0	0	0.1
Lake Surface Area (m^2)	$1.5x10^5$	$1.5x10^5$	$1x10^7$
Lake Depth (m)	4.6	4.6	100

(1) Sheppard et al. 1995.

A.3.3 Human Physical and Lifestyle Parameters

Physical and lifestyle parameters for humans are summarized in Table A.3.

Human physical and lifestyle parameters for the Temperate State are from various sources, including Davis et al. (1993) and CSA (2008). The relative ingestion rates for the different food types are based on CSA (2008, Table 6.9a) rather than Davis et al. (1993). Hence, food ingestion rates for the self-sufficient farmer are different from those used in the HBC study (Garisto et al. 2004, 2005a). For the Permafrost and Proglacial Lake States data are taken from Garisto et al. (2005b), where available, and are largely based on a traditional aboriginal self-

sufficient tundra hunter lifestyle. In cases where a range of values was provided for a parameter, the mean value was selected.

The Southern Arctic Ecozone (Environment Canada 2008a), a model for the Permafrost and Proglacial Lake States, contains an irregular tree line, where clumps of stunted trees grow on warmer, sheltered sites (Environment Canada 2008c). These trees provide firewood for the hunter and hunter-fisher critical groups.

Table A.3: Human Physical and Lifestyle Parameters

Parameter	Temperate	Permafrost [3]	Proglacial Lake [3]
People per Household (-)	3	6 [2]	6 [2]
Overall Human Occupancy Factor	1	1	1
Building Height (m)	2.4	2 [2]	2 [2]
Building Width (m)	9.7	3 [2]	3 [2]
Building Material Hold Up Time (d)	180 wood 30 inorganic	180 wood 30 inorganic	180 wood 30 inorganic
Building Lifetime, i.e., Replacement Time for Building (a)	50	8 [2]	8 [2]
Building Occupancy Factor (-)	0.8	0.5 [2]	0.5 [2]
Outdoor/Ground Exposure Factor (-)	0.2	0.5 [2]	0.5 [2]
Domestic Water Demand per Person (m^3/a)	130	8 [2]	8 [2]
Human Water Ingestion Rate (m^3/a)	0.77	0.77	0.77
Human Water Holdup Time (d)	0	0.25 [2]	0.25 [2]
Air Inhalation Rate (m^3/a)	$8.4x10^3$ [1]	$8.4x10^3$ [1]	$8.4x10^3$ [1]
Cattle Ingestion Rate (kg/a)	73 [1]	-	-
Milk Ingestion Rate (m^3/a)	0.20 [1]	0	0
Poultry Ingestion Rate (kg/a)	38 [1]	-	-
Crop Ingestion Rate (kg/a)	566 [1]	-	-
Fish Ingestion Rate (kg/a)	5.6 [1]	35	321
Fish Hold Up Time (d)*	0.5	30 [2]	30 [2]
Caribou Ingestion Rate (kg/a)	-	495	350
Caribou Hold Up Time (d)*	-	15 [2]	15 [2]
Canada Geese Ingestion Rate (kg/a)	-	10.4	12
Canada Geese Hold Up Time (d)	-	1 [2]	1 [2]
Berry Ingestion Rate (kg/a)	-	6.9	7.9
Soil Ingestion Rate (kg/a)	0.02	0.024[2]	0.024[2]
Irrigation Rate (m/a)	0.1	0	0
Irrigation Period (a)	100	0	0

(1) Air inhalation rate set at 95th percentile value (CSA 2008). Food ingestion rates are scaled values based on the median ingestion rates (CSA 2008, Table G.9a) and the 90th percentile energy intake value of 15060 kJ/d (Beak 2002). The energy content of food is calculated using data in Davis et al. (1993).
(2) Garisto et al. 2005b.
(3) Caribou and fish make up a large fraction of the human diet during Permafrost and Proglacial Lake States. Ingestion rates are scaled so that the human energy intake rate is approximately 15060 kJ/a.
*Longer period for fish and caribou hold up time accounts for outdoor drying of fish and caribou meat.

Total human energy need is assumed to be 15060 kJ/day (Beak 2002) for all the critical groups, similar to the value of 14600 kJ/day used in the HBC study (Garisto et al. 2004, 2005a). Food consumption rates are estimated based on meeting energy demands. Cattle, milk, poultry and crops are ingested during the Temperate State because the self-sufficient farmer raises animals and grows crops. The irrigation rate is only applicable during the Temperate State as the farmer is assumed to irrigate his crops. Only crops grown for human consumption are irrigated. Fish are consumed by all critical groups because a lake is present in all climate states (except the Ice Sheet State); however, much more fish are consumed during the Proglacial Lake State due to the abundance of fish in the large proglacial lake.

Caribou and Canada geese are hunted during the Permafrost and Proglacial Lake states, and some berries are also gathered. Because plant food is scarce during these periods, much more meat is consumed during the Permafrost and Proglacial Lake States than during the Temperate State. Also, fish is a major food source during the Proglacial Lake State.

Human occupancy factors are used to describe the presence of the critical group in the repository area vicinity. Human occupancy factors for the corresponding critical groups are 1 for the Temperate, Permafrost and Proglacial Lake States since they are assumed to spend their entire lives in the vicinity of the repository site, whereas the human occupancy factor is 0 during the Ice Sheet State when no humans reside in the vicinity of the repository.

A.3.4 Plant and Animal Parameters

Plant and animal parameters are summarized in Table A.4. These are primarily from Garisto et al. (2005b) and Garisto et al. (2008).

During the Temperate State, garden and forage plants are used by humans and farm animals, respectively. In the Permafrost and Proglacial Lake States, lichens and forage plants are the two types of plants consumed by caribou and Canada geese, respectively. The forage plant in the Permafrost and Proglacial Lake States is considered to have the same properties as the forage plant in the Temperate State unless otherwise specified, and is the primary food source for Canada geese. Although a study by Garisto et al. (2005b) suggests that wild plants are a negligible part of the inland tundra hunter or tundra hunter-fisher, berries are assumed to comprise a small portion of the their diet to assess its impact on dose rates. The nutrient content of berries is based on raw blueberry data (USDA 2008). The berry yield is based on average US cultivated yields.

The air to lichen to caribou to man exposure pathway is a new pathway modelled in the Permafrost and Proglacial Lake States. While at the site, the caribou eat lichens that grow near the repository site. Lichens become contaminated via deposition of airborne radionuclides, which originate from the lake (due to degassing and aerosol suspension) and soil (due to dust resuspension). Because lichens are contaminated primarily due to air deposition and live for long periods of time, they can integrate contamination over an extended period; hence, radionuclide concentrations in lichens cannot be calculated using a plant/soil concentration ratio as forage plants. Thus, the plant/soil concentration ratio for lichen is assumed to be zero. Also, parameters (such as cropping frequency, cropping period, etc.), which apply to modelling forage plant concentrations, are not applicable to lichen.

Two important lichen parameters are (1) the fraction of air deposition intercepted and retained on lichen surfaces and (2) the environmental (weathering) half-life for radionuclides deposited

and retained on lichens. A deposition fraction of 0.5 and an environmental (weathering) half-life of 5 years (1825 days) have been selected based on a literature survey (Ellis and Smith 1987, Golikov et al. 2004, Beresford et al. 2003; Palsson et al. 2009, IAEA 1996, Paatero et al. 1998, Topcuoglu et al. 1995). The deposition fraction is less than unity because, for example, not all the ground is covered with lichens, and radionuclides deposited on snow covered lichens may be washed away during snow melt. The selected environmental (weathering) half-life is conservative for most radionuclides such as Pb, Pu and Am (Paatero et al. 1998, Ellis and Smith 1987), and perhaps I (Daillant et al. 2009), but is realistic for Cs, for which a wide range of effective environmental half-lives (3 to 12 years) have been measured.

Table A.4: Plant and Animal Parameters

Parameter	Temperate	Permafrost and Proglacial Lake
Cattle Water Ingestion Rate (m^3/a)	14.6	-
Dairy Cow Water Ingestion Rate (m^3/a)	21.9	0
Poultry Water Ingestion Rate (m^3/a)	0.15	-
Fish Occupancy Factor (-)	1	1
Wild Mammal Occupancy Factor (-)[#]	1	0.5 (2)
Wild Bird Occupancy Factor (-)[#]	1	0.5 (2)
Caribou Water Ingestion Rate (m^3/a)	-	3.5 (1)
Caribou Soil Ingestion Rate (kg/a)	-	88 (1)
Caribou Forage Rate (kg/a)	-	2.9×10^3 (1)
Fraction of Caribou Diet that is Lichen (-)	-	0.75 (2)
Fraction of Caribou Diet that is Forage Plant (-)	-	0.25 (2)
Caribou Inhalation Rate (m^3/a)	-	9.9×10^3 (2)
Canada Goose Water Ingestion Rate (m^3/a)	-	5.5×10^{-2} (2)
Canada Goose Forage Rate (kg_{ww}/a)	-	128 [##] (1)
Canada Goose Soil Ingestion Rate (kg/a)	-	2.6 (1)
Canada Goose Inhalation Rate (m^3/a)	-	3.3×10^2 (2)
Blueberry Yield (kg/m^2)	-	0.57 (3)
Blueberry Carbohydrate Content (g/kg)	-	145 (4)
Blueberry Fat Content (g/kg)	-	3.3 (4)
Blueberry Protein Content (g/kg)	-	7.4 (4)
Forest Renewal Time (a)	50	300 (5)
Lichen Yield Density (kg_{ww}/m^2)	-	0.5 (2)
Duration of Lichen Exposure to Atmospheric Deposition (s)	-	1×10^{10} (2)
Lichen environmental (weathering) half-life (d)	-	1825
Fraction of Deposition Intercepted by Lichen (-)	-	0.5
Probability of using Sediments on Fields (-)	0.01	0
Depth of Surface Soil (m)	0.3	0.2
Total Soil Depth (m)	1.5	0.3
Leaching Fraction (-)	0.55	0

(1) Garisto et al. 2005b. (2) Garisto et al. 2008. (3) University of Georgia 2008.
(4) US Department of Agriculture 2008. (5) Laberge et al. 2000.
[#]During Permafrost and Proglacial Lake States, wild mammal refers to caribou and wild bird refers to Canada goose.
[##]In CC4 this is set to zero if the caribou-lichen pathway is modelled simultaneously (see text).

A sandy soil is assumed to exist during all three modelled states. In the Permafrost and Proglacial Lake States, a shallow soil model is used because permafrost is present and only a shallow layer is assumed to melt during the summer.

As noted above, the self-sufficient farmer (during the Temperate State) eats beef, dairy products, chicken, fish and garden produce. In the CC4 database, these food types are assigned generic properties representative of beef, milk, bird, fish and garden plants. The hunter and hunter-fisher, in contrast, eat caribou, geese, fish, and some berries. Thus, for CC4 simulations, the properties of caribou, geese and berry replace those for beef, bird and garden plants during Permafrost and Proglacial Lake States.

Caribou eat lichens. Thus, in CC4 simulations, lichen properties replace those for the forage plant during Permafrost and Proglacial Lake States. Geese are also eaten by the critical groups during the Permafrost and Proglacial Lake States. However, because there is only one forage plant in CC4 (which is used to represent lichen during the Permafrost and Proglacial Lake States) it is assumed in CC4 that geese are only contaminated via water and soil ingestion and air inhalation. This approximation is not expected to greatly affect calculated total dose rates because the geese make up a small fraction of the total diet (see Table A.3). Similarly, although caribou also eat plants other than lichens, it is assumed that lichens make up 100% of the caribou diet.

The duration of exposure of plants to contaminants depends on the plant type. During the Temperate State, exposure values of 50-100 days are used for domestic plants eaten by humans and animals, and up to 50 years for wild plants eaten by wild mammals. The diet of wild birds during the Temperate State is considered to be primarily seasonal growth, conservatively estimated as having 180 day exposure.

During the Permafrost State, since the main human meat source is caribou, the exposure period for the forage plant (which is eaten by caribou) is set to that of lichen, which is the caribou's main food source (Table A.4). Plants eaten by humans during the Permafrost State are based on berries, and the exposure period is set at 180 days. The diet of wild birds is considered to be primarily seasonal growth, conservatively estimated as having 180 day exposure. Wild plants during the Permafrost State are assumed on average to have 50 years exposure, recognizing in part their slow growth in permafrost conditions. Finally, the exposure times of the various plants during the Proglacial Lake State are assumed to be the same as for the corresponding plants in the Permafrost Period.

A.3.5 Volatilization Parameters

Volatilization parameters are summarized in Table A.5.

The air deposition velocity is a parameter used to calculate nuclide concentrations in, for example, lichen due to atmospheric deposition. The majority of the Permafrost and Proglacial Lake atmospheric parameters refer to data from Sheppard et al. (1995). Soil degassing rates decrease due to decreased biological activity in colder climates. Lake evasion rates decrease due to a shorter ice-free season and lower diffusion rates. For all the Permafrost and Proglacial Lake parameters without references, an assumption is made that the lake and soil surface is frozen half the year; thus, there is no degassing or aerosol formation for that portion of the year.

The iodine mass loading parameter (IMLA) describes the ratio of the iodine concentration in air above a lake (or other water body) to the iodine concentration in the lake. It is an equilibrium value, i.e., it applies to a closed system in which there is no mass transport of iodine out of the air mass (or compartment) above the lake. However, in reality, the iodine in the air mass above the lake water body is constantly being swept away by wind action. In this case, the concentration of iodine in the air mass above the lake is controlled by the volatilization rate of iodine from the lake. Because scoping calculations indicated use of the equilibrium value of the IMLA would be overly conservative for calculation of doses from the air-lichen-caribou-man pathway, we have determined steady-state values of IMLA, based on the volatilization rate of iodine from the lake, the properties of the lake and the wind speed.

Table A.5: Volatilization Parameters

Parameter	Temperate [1]	Permafrost, Proglacial Lake
Dry (Air) Deposition Velocity (m/s)	0.006	0.006
Washout Ratio ( )	6.3×10^{5} [6]	6.3×10^{5}
C Water to Air Loss Rate (1/a)	0.92	0.14 [2]
I Aquatic Mass Loading Parameter (m^3_{water}/m^3_{air})	1.8×10^{-8} [3]	7×10^{-9}; 6×10^{-8} [3]
Rn Aquatic Transfer Coefficient (m/s)	6.7×10^{-6}	3.4×10^{-6}
Rn Emission Rate from Soil ((mol/m^2s)/(mol/kg))	2.7×10^{-9}	1.4×10^{-9}
Rn Soil to Indoor Air Transfer Factor ((mol ^{222}Rn m^{-3}_{air})/(mol ^{226}Ra $kg^{-1}_{dry\ soil}$))	1×10^{-5} [5]	5×10^{-6}
C Soil Degassing Rate (1/a)	13.6	4.4 [2]
Cl Soil Degassing Rate (1/a)	9.5×10^{-4}	4.8×10^{-4}
I Soil Degassing Rate (1/a)	0.021	0.016 [2]
Se Soil Degassing Rate (1/a)	0.032	0.016 [2]
Frequency of Agricultural Fires (1/a)	1	0 [4]
Land Clearing Frequency (1/a)	1/50	0
Probability of being located Downwind from Energy Fires (-)	0.25	0.5 [4]
Probability of Burning Peat for Energy Source (-)	0.01	0

(1) Davis et al. (1993) unless otherwise mentioned. (2) Sheppard et al. 1995.
(3) Calculated in this report (see text). Values are different for the Permafrost (7×10^{-9}) and Proglacial Lake (6×10^{-8}) states.
(4) Garisto et al. 2005b. (5) Sheppard et al. 2005.
(6) CSA (2008)

The calculation of the steady-state IMLA value is based on a simple atmospheric box model. The atmospheric box is assumed to be 2 m high and has a width equal to the square root of the lake surface area. The width of the atmospheric box is perpendicular to the wind direction. Using these assumptions the steady-state air concentration of iodine above the lake, C_a, is given by

$$C_a = k_v A_w C_w/(U_w Z_a W_a) \equiv \text{IMLA } C_w \qquad \text{(A.1)}$$

where

k_v = iodine volatilization rate (m/a)

A_w = area of lake (m^2)
C_w = iodine concentration in the lake (mol/m^3)
U_w = wind speed (m/a)
Z_a = thickness of the air layer (= 2 m)
W_a = width of the air compartment (= $(A_w)^{1/2}$ m)

The value of k_v was calculated from the data in Connan et al. (2008) to be $8.8x10^{-3}$ m/a. Values of (k_v/D), where D is the depth of the lake, have been reported by Stephenson and Motycka (1995) and Bird et al. (1995). For a lake with a depth of 4.6 m, the k_v values are found to be $8.7x10^{-3}$ m/a (Stephenson and Motycka 1995) and $5.5x10^{-4}$ m/a (Bird et al. 1995). It should be noted that the reported k_v/D values, which are based on laboratory flask experiments, have been extrapolated to whole-lake ecosystems by applying a correction factor based on the ratio of the measured volatilization rate of C-14 from the experimental flask to the volatilization rate of C-14 from fresh water lakes (Davis et al. 1993).

The three values of k_v are similar and we have selected the value of $8.8x10^{-3}$ m/a, which is based on field measurements (Connan et al. 2008). This value applies to ice free water bodies. To account of the presence of ice during winter months and the lower temperatures, this value was reduced by a factor of 0.8, 0.5 and 0.5 for the Temperate, Permafrost and Proglacial Lake States, respectively. (Note that the C water to air loss rate during the Permafrost State is 15% of the loss rate during the Temperate State, as shown in Table A.5.) Using the data in Tables A.1 and A.2 we find the following values:

IMLA (Temperate) = $1.8x10^{-8}$ m^3 water/m^3 air,
IMLA (Permafrost) = $0.7x10^{-8}$ m^3 water/m^3 air, and
IMLA (Proglacial Lake) = $0.6x10^{-7}$ m^3 water/m^3 air.

A.3.6 Transfer Factor Parameters

The soil to berry transfer factors (TFs) shown in Table A.6 are from recent soil and blueberry sampling results (S.C Sheppard, private communication) or from Garisto et al. (2008). For radionuclides for which data are not available in these two sources, the values for garden plants (Temperate State) were used.

Caribou ingestion TFs were calculated using ingestion TFs for (beef) meat and allometrically scaling them for caribou. An average weight of 525 kg was used for cattle and 135 kg was used for caribou. With these values, the caribou transfer factors are about 2.77 times larger than for cattle. This concept and these values are described in the Garisto et al. (2008).

Caribou ingestion TFs for Pb, Po, Ra and U were calculated based on measurements by Thomas and Gates (1999) using the following equation:

$$F_c = C_c/C_l U_l \qquad (A.2)$$

where:
F_c = caribou ingestion transfer factor (d/kg_{ww}),
C_c = caribou concentration (Bq/kg_{ww}),
U_l = caribou lichen ingestion rate (kg_{ww}/d), and
C_l = radionuclide concentration in lichen (Bq/kg_{ww}).

These calculated ingestion TFs, which agree reasonably well with allometrically scaled ingestion TFs (differences range from 16% to 112% of allometrically scaled values), were used in the database. Ingestion TFs for caribou are summarized in Table A.7.

Table A.6: Soil to Berry Transfer Factors (kg/kg_{ww})#

Element	Permafrost and Proglacial Lake
Bi	$2x10^{-3}$ (1)
C	0.21 (2)
Cl	21 (2)
Co	$7.5x10^{-4}$ (1)
Cs	$5.7x10^{-3}$ (1)
I	$7x10^{-4}$ (1)
Kr	0
Mo	0.021 (1)
Nb	$5.7x10^{-4}$ (1)
Ni	$6.8x10^{-3}$ (1)
Np	0.003 (2)
Pb	$2.1x10^{-4}$ (1)
Po	0.001 (2)
Ra	$4.6x10^{-3}$ (2)
Rn	0
Sb	$3.9x10^{-3}$ (1)
Sn	0.027 (1)
Sr	0.018 (1)
Tc	0.45 (2)
U	$2.3x10^{-4}$ (1)
Y	$1.8x10^{-4}$ (1)
Zr	0.014 (1)

#These are assumed to be geometric mean values. The geometric standard deviations are assumed to be the same as for garden plants in the temperate state.
(1) S.C. Sheppard (private communication). Wet weight to dry weight ratio is 5.6.
(2) Garisto et al. 2008. Wet weight to dry weight ratio is assumed to be 3.3.

There are few data available for estimating caribou air inhalation transfer factors, FI_c. The FI_c values are estimated based on allometrically scaling beef inhalation transfer coefficients as suggested by Zach et al. (1996). FI_c is given by the following equation:

$$FI_c = FI_m F_c / F_m \quad (A.3)$$

where:
FI_m = beef inhalation transfer factor (d/kg),
F_c = caribou ingestion transfer factor (d/kg_{ww}), and
F_m = beef ingestion transfer factor (d/kg).

The caribou air inhalation transfer factors so-calculated are generally 2.77 times larger than the beef inhalation transfer factors. Caribou air inhalation TFs are shown in Table A.7.

The air inhalation transfer factors for wild birds consumed during Permafrost and Proglacial Lake States are assumed to be similar to those for domestic birds during the Temperate State.

Table A.7: Caribou Ingestion Transfer Factors (d/kg $_{ww}$)*

Element	Ingestion Transfer Factors	Inhalation Transfer Factors
Ac	6.92×10^{-5}	0.036
Am	9.69×10^{-6}	2.8×10^{-3}
Bi	1.11×10^{-3}	0.012
C	1.77×10^{-1}	0.18
Cl	5.54×10^{-2}	0.22
Co	2.77×10^{-2}	0.016
Cs	7.20×10^{-2}	0.072
I	3.32×10^{-2}	0.019
Kr	0	0
Mo	1.88×10^{-2}	0.021
Nb	6.92×10^{-1}	10.5
Ni	5.54×10^{-3}	0.061
Np	5.54×10^{-4}	2.3×10^{-3}
Pa	2.77×10^{-5}	4.2×10^{-3}
Pb	9.29×10^{-4} (1)	3.3×10^{-3}
Pd	1.11×10^{-2}	1.11
Po	0.0151 (1)	0.069
Pu	5.54×10^{-6}	8.3×10^{-3}
Ra	5.30×10^{-3} (1)	3.6×10^{-3}
Rn	0	0
Sb	2.77×10^{-3}	0.015
Se	4.15×10^{-2}	0.047
Sn	2.22×10^{-1}	5.8
Sr	2.24×10^{-3}	0.005
Tc	2.35×10^{-2}	0.026
Th	1.66×10^{-5}	0.012
U	1.16×10^{-3} (1)	0.006
Y	8.31×10^{-4}	1.25
Zr	5.54×10^{-2}	13.8

*Only data for potentially important radionuclides are shown in the table.
(1) Thomas and Gates 1999.

A.4 ICE SHEET ADVANCE AND RETREAT RATES

A literature survey was carried out of ice sheet advance and retreat rates during the last continental scale glaciation and deglaciation. Only data from the eastern North American continent were selected. The compiled data are shown in Table A.8. This information was used to constrain the rate of ice sheet travel over the model area, as described in Section 3.4.

Table A.8: Ice Sheet Advance and Retreat Rates During Last Ice Age

Location	Retreat (m/a)	Advance (m/a)	Notes	Reference
Erie lobe (Ohio)	-----	94 - 120	24 - 16 ka BP[#]. After Erie lobe split into two, advance rate decreased to 17 – 33 m/a (4-fold smaller)	Goldthwait (1959)
Appalachians of SE Quebec	200	-----	13 ka – 12 ka BP	Parent and Occhietti (1999)
NW and S margins of Wisconsin Laurentide Ice Sheet	260	-----	10 and 7 ka BP	Andrews (1973)
NE margin of Wisconsin Laurentide Ice Sheet	20			
Rainy Lobe	190*	110*	25- 20 ka BP	Mooers and Lehr (1997)
Superior Lobe	220*	-----	18 - 15 ka BP	
Rainy Lobe	230*		18 - 15 ka BP	
Superior Lobe	200	-----		Johnson et al. (1999)
Lake Michigan and Lake Erie Lobes	85*	35*	Advance 26 - 20 ka BP and retreat 20 - 12 ka BP	Colgan et al. (2003)
Green Bay and L. Superior Lobes	45*	35*		
Ungava Peninsula De Geer Moraine Zone on Hudson Bay coast	120 - 160	-----	10 ka – 5 ka BP	Lauriol and Gray (1987)
Ungava Peninsula Riviere Korik Basin	100 - 140			
Laurentide Ice Sheet (during Wisconsinan)	-----	75*	33 - 27 ka BP, from N. Ontario towards Michigan	Vincent and Prest (1987)
		94*	33 - 27 ka BP, from N. Ontario towards Minnesota	
Green Bay Lobe	50 - 100	-----	26 - 13 ka BP	Colgan (1999)

[#]BP = Before Present

*Values calculated from figures of ice sheet location with time.

REFERENCES

Andrews, J.T. 1973. The Wisconsin Laurentide ice sheet: Dispersal centers, problems of rates of retreat, and climatic implications. Arctic and Alpine Res. 5, 185-199.

Beak International. 2002. Guidance for calculation of derived release limits for radionuclides in airborne and liquid effluents from Ontario Power Generation nuclear facilities. Ontario Power Generation Report N-REP-03482-10000-R00. Toronto, Canada.

Beresford, N.A., S.M. Wright, J.E. Brown and T. Sazykina (Eds). 2003. Review of approaches for the estimation of radionuclide transfer to reference Arctic biota. A deliverable report for Environmental Protection from Ionising Contaminants (EPIC), Project ICA2-CT-2000-10032.

Bird, G.A., W.J. Schwartz and J. Rosentreter. 1995. Evolution of 131I from freshwater and its partitioning in simple aquatic microcosms. Sci. Total Environment 164, 151-159.

Boulton, G.S., U Kautsky, L. Morén, and T. Wallroth. 2001a. Impact of long-term climate change on a deep geological repository for spent nuclear fuel. SKB Technical Report TR-99-05. Stockholm, Sweden.

Boulton, G.S., S. Zatsepin, and B. Maillot. 2001b. Analysis of groundwater flow beneath ice sheets. SKB Technical Report TR-01-06. Stockholm, Sweden

Chan. T. And F. Stanchell. 2006. DECOVALEX THMC TASK E – Implications of glaciation and coupled thermohydromechanical processes on shield flow system evolution and performance assessment. Nuclear Waste Management Organization Technical Report NWMO TR-2008-03. Toronto, Ontario.

Colgan, P.M., D.M. Mickelson and P.M. Cutler. 2003. Ice-marginal terrestrial landsystems: Southern Laurentide ice sheet margin. In Glacial Landsystems, D.A. Evans and B.R. Rea (eds), p. 111–142. Edward Arnold, London.

Colgan, P.M. 1999. A reconstruction of the Green Bay Lobe, Wisconsin, USA, from 26,000 to 13,000 radiocarbon years B.P. In Glacial Processes Past and Present, D.N. Mickelson and J.W. Attig (eds), p. 137-150. Geological Society of America Special Paper 337. Geological Society of America, Boulder, USA.

Connan, O., E. Tessier, D. Maro, D. Amouroux, D. Hebert, M. Rozet, C. Vaiseux and L. Solier. 2008. Water to atmosphere fluxes of ^{131}I in relation with alkyl-iodide compounds from the Sein Estuary (France). J. Environ. Radioactivity 99, 1102-1110.

CSA (Canadian Standards Association). 2008. Guidelines for calculating derived release limits for radioactive material in airborne and liquid effluents for normal operation of nuclear facilities. CSA Guideline N288.1-08. Toronto, Canada.

Daillant, O.R., A. Bernollin, M. Josset and K.I. Fifield. 2009. Potential of lichens for monitoring iodine-129 and chlorine-36. J. Radioanal. Nucl. Chem. DOI 10.1007/s10967-009-0110-y. Published online: 27 June 2009.

Davis, P.A., R. Zach, M.E. Stephens, B.D. Amiro, G.A. Bird, J.A.K. Reid, M.I. Sheppard, S.C. Sheppard and M. Stephenson. 1993. The disposal of Canada's nuclear fuel waste: The biosphere model, BIOTRAC, for postclosure assessment. Atomic Energy of Canada Report AECL-10720. COG-93-10. Pinawa, Canada.

Ellis, K.M. and J.N. Smith. 1987. Dynamic model for radionuclide uptake in lichen. J. Environ. Radioactivity 5, 185-208.

Environment Canada. 2008a. Landforms and Climate of the Boreal Shield Ecozone. (http://www.ec.gc.ca/soer-ree/English/vignettes/Terrestrial/bs/land.cfm, accessed 2008).

Environment Canada. 2008b. Southern Arctic Ecozone. (http://www.ec.gc.ca/soer-ree/English/vignettes/Terrestrial/sa/default.cfm, accessed 2008).

Environment Canada. 2008c. Plants of the Southern Arctic Ecozone. (http://www.ec.gc.ca/soer-ree/English/vignettes/Terrestrial/sa/plants.cfm, accessed 2008).

Garisto, F., J. Avis, N. Calder, P. Gierszewski, C. Kitson, T. Melnyk, K. Wei, and L. Wojciechowski. 2005a. Horizontal borehole concept case study. Ontario Power Generation, Nuclear Waste Management Division Report 06819-REP-01200-10139-R00. Toronto, Canada.

Garisto, F., A. D'Andrea, P. Gierszewski and T. Melnyk. 2004. Third case study - Reference data and codes. Ontario Power Generation, Nuclear Waste Management Division Report 06819-REP-01200-10107-R00. Toronto, Canada.

Garisto, N.C., S.L. Fernandes and I. V. Ham. 2008. No-effect concentrations for screening radiological impacts on non-human biota. Nuclear Waste Management Organization Report NWMO TR-2008-02. Toronto, Canada.

Garisto, N.C., Z. Eslami and F. Bhesania. 2005b. Alternative exposure groups, characteristics and data for the post-closure safety assessment of a deep geological repository. Ontario Power Generation, Nuclear Waste Management Division Report 06819-REP-01200-10150-R00. Toronto, Canada.

Goldthwait, R.P. 1959. Scenes in Ohio during the last ice age. The Ohio J. Science 59, 193-216.

Golikov, V., I. Logacheva, G. Bruk, V. Shutov, M. Balonov, P. Strand, S. Borghuis, B. Howard and S. Wright. 2004. Modelling of long-term behaviour of caesium and strontium radionuclides in the Arctive environment and human exposure. J. Environ. Radioactivity 74, 159-169.

IAEA (International Atomic Energy Agency). 1996. Modelling of radionuclide interception and loss processes in vegetation and of transfer in semi-natural ecosystems. Second report of the VAMP Terrestrial Working Group. IAEA Technical Document IAEA-TECDOC-857. Vienna, Austria.

Johnson, J.D., K.L. Addis, L.R. Ferber, C.B. Hemstad, G.N. Meyer and L.T. Komai. 1999. Glacial lake Lind, Wisconsin and Minnesota. Geol. Soc. America Bulletin 111, 1371-1386.

Laberge, M., S. Payette and J. Bousquet. 2000. Life Span and Biomass Allocation of Stunted Black Spruce Clones in the Subarctic Environment. Journal of Ecology 88, 584-593.

Lauriol, B. And J.T. Gray. 1987. The decay and disappearance of the late Wisconsin Ice Sheet in the Ungava Peninsula, Northern Quebec, Canada. Arctic and Alpine Res. 19, 109-126.

Mooers, N.D. and J.D. Lehr. 1997. Terrestrial record of Laurentide ice sheet reorganization during Heinrich events. Geology 25, 987-990.

Paatero, J., T. Jaakkola and S. Kulmala. 1998. Lichen (sp. *Cladonia*) as a deposition indicator for transuranium elements investigated with the Chernobyl fallout. J. Environ. Radioactivity 38, 223-247.

Palsson, S.E., L. Skuterud, S. Fesenko and V. Golikov. 2009. Radionuclide transfer in arctic ecosystem. In Quantification of radionuclide transfer in terrestrial and freshwater environments for radiological assessments. IAEA Draft Technical Document. Accessed on the web in 2009 at http://www-ns.iaea.org/downloads/rw/projects/emras/draft-final-reports/trs-364-wg-tecdoc.pdf

Parent, M. and S. Occhietti. 1999. Late Wisconsinan deglaciation and glacial lake development in the Appalachians of southeastern Quebec. Géog. physique et Quaternaire 53, 117-135.

Peltier, W.R. 2006. Boundary conditions data sets for spent fuel repository performance assessment. Ontario Power Generation, Nuclear Waste Management Division Report 06819-REP-01200-10154-R00. Toronto, Canada

Sheppard, M.I., J.C. Tait, B.L. Sanipelli, S.C. Sheppard. 2005. Recommended biosphere model values for radium and radon. Ontario Power Generation, Nuclear Waste Management Division Report 06819-REP-01200-10144-R00. Toronto, Canada.

Sheppard, M.I., B.D. Amiro, P.A. Davis and R. Zach. 1995. Continental glaciation and nuclear fuel waste disposal: Canada's approach and assessment of the Impact on nuclide transport through the biosphere. Ecological Modelling 78, 249-265.

SKB (Svensk Kärnbränslehantering AB). 1999. Deep repository for spent nuclear fuel. SR 97 - Post-closure safety. Main Report, Vol. II, Chapter 10. SKB Technical Report TR-99-06. Stockholm, Sweden

Stephenson, N. and M. Motycka. 1995. Volatility of ^{125}I in fresh water. J. Environmental Radioactivity 28, 295-311.

Thomas, P.A. and T.E. Gates. 1999. Radionuclides in the Lichen-Caribou-Human Food Chain Near Uranium Mining Operations in Northern Saskatchewan, Canada. Environmental Health Perspectives 107, 527-537.

Topcuoglu, S., A.M. Van Dawen and N. Gungor. 1995. The natural depuration rate of ^{137}Cs radionuclides in a lichen and moss species. J. Environ. Radioactivity 29, 157-162.

USDA (United States Department of Agriculture). 2008. USDA National Nutrient Database for Standard Reference. Release 20. Individual Food Reports. (http://www.nal.usda.gov/fnic/foodcomp/Data//SR20/reports/sr20fg09.pdf, accessed 2008).

University of Georgia. 2008. (http://www.uga.edu/fruit/bluberi.html, accessed 2008).

Vincent, J.-S., and V.K. Prest. 1987. The early Wisconsinan history of the Laurentide ice sheet. Géog. physique et Quaternaire 41, 199-213.

Zach, R., B.D. Amiro, G.A. Bird, C.R. Macdonald, M.I. Sheppard, S.C. Sheppard and J.G. Szekely. 1996. The disposal of Canada's nuclear fuel waste: A study of postclosure safety of in-room emplacement of used CANDU fuel in copper containers in permeable plutonic rock. Volume 4: Biosphere model. Atomic Energy of Canada Report AECL-11494-4, COG-95-552-4. Pinawa, Canada.

APPENDIX B: DERIVATION OF CC4 GEOSPHERE TRANSPORT NETWORK

CONTENTS

B.1 GENERAL APPROACH

The SYVAC3-CC4 system model represents the geosphere as a network of one-dimensional flow tubes and uses this network to approximate radionuclide transport in the geosphere. This geosphere transport network is referred to as GEONET.

The starting point for the generation of GEONET is a steady-state groundwater flow field for the site. However, for the Glaciation Scenario, a transient groundwater flow field is needed, as discussed in Section 6. Hence, to use SYVAC-CC4 for analysis of the Glaciation Scenario, it was necessary to approximate the transient groundwater flow field using a series of fixed groundwater flow fields. Thus, from the transient groundwater flow fields calculated for the Reference Case (GSC-RCA, see Section 6), a different fixed groundwater flow field was selected for each unique geosphere state (see Section 8). Table B.1 contains the state name identifiers and brief descriptions of the unique geosphere states.

The fixed groundwater flow field selected to represent groundwater flow during a state was either the steady state flow field (e.g., TEMPR and PERM2) or the groundwater flow field at around the mid-point of the state (e.g., PROLA and ISCB1).

Table B.1: Geosphere State Name Descriptions

Geosphere State Name	Brief Description
TEMPR	Temperate (boreal) climate and well (738 m^3/a)
PERM1	Permafrost layer down to 100[m], talik beneath the lake
PERM2	Permafrost layer down to 250[m], talik beneath the lake
ISCB1	Ice sheet - cold based, 100[m] permafrost depth, no talik
ISCB2	Ice sheet - cold based, 150[m] permafrost depth, no talik
ISCB3	Ice sheet - cold based, 200[m] permafrost depth, no talik
ISWB1	Ice sheet - warm based, retreating, no permafrost layer
ISWB2	Ice sheet - warm based, no permafrost layer
PROLA	Proglacial Lake

For each fixed flow field, a set of particle tracks was generated using FRAC3DVS to map how particles released from the repository footprint would move with the groundwater flow field and discharge to the surface. These particle tracks, one set for each unique geosphere state, were then used to generate the GEONET network for use in the system model for the Reference (Glaciation) Case.

In the development of the geosphere network, it was implicitly assumed that the maximum simulation time would be approximately one million years (hence, for example, particle tracks with much longer travel times to the surface could be ignored) and that the network should be able to reflect the important groundwater pathways from the repository to the surface discharges for all geosphere states.

Assembly of the transport network consists of the following sequential steps:

- Sector Selection – The vault is divided into sectors. A sector is typically defined so that its properties are uniform. For instance, a sector would have the same waste form type and room length, and would connect to a portion of the groundwater flow field whose properties (e.g., particle track pathways) are approximately uniform. Different sectors would have different properties, and often the properties of the surrounding geosphere are the delineating factors.

- Selection of Representative Tracks – A representative particle track for each sector is generally chosen that gives the shortest travel time to a surface discharge. Tracks may merge with tracks from other sectors along the flow path and may diverge as the well or terrestrial discharge areas capture portions of the groundwater flow.

- Selection of Nodes along Tracks – Nodes are generally selected at material property boundaries so that the resulting segments of the flow path have constant properties. Additional nodes are selected to approximate curved flow paths.

- Addition of Well and Near-Surface Nodes – Additional nodes are required for the well – for example, upper and lower reference nodes define the range of positions for the well and drawdown nodes, which give a better representation of the drawdown cone in the vicinity of the well. Also, near-surface nodes are added to define an overburden and a sediment segment for each discharge location, and possible terrestrial and wetland discharges associated with the (default) aquatic discharge.

- Effect of Climatic State on Transport Properties and Pathway – The transport properties and pathways of each segment are adjusted to reflect the particle track information for each climatic state. In some cases conservative approximations are made. These include, for example, keeping the flow direction focussed towards the talik discharge regardless of changes in flow direction during some glaciation states and ignoring downward flows during ice sheet advance by simply using a zero groundwater velocity during this time.

- Assembly of Data Files – Data are assembled for use in the SYVAC3-CC4 input file. These include the Cartesian coordinates of the nodes, the hydraulic head and temperature of the nodes, hydraulic and chemical properties of the geosphere zones, and the effect of each unique state on the properties of the geosphere, e.g., radionuclide transport is assumed to be completely inhibited in geosphere zones affected by permafrost.

- Add Well Model – The effects of the well drawdown on adjacent node heads is accounted for via an analytical well model within the aquifer, and by a site-specific well model outside the aquifer.

- Verify – The geosphere network model should be checked against detailed models. For example, contaminant fluxes to the biosphere calculated by the SYVAC3-CC4 system model could be compared to the corresponding results from FRAC3DVS. Appendix C compares results from FRAC3DVS and SYVAC3-CC4.

B.2 SECTOR SELECTION

In the current study, all the containers in the repository contain the same used fuel wasteform, and the emplacement room design is common across the vault. Therefore, the main distinction between the vault sectors is the influence of the surrounding groundwater flow field.

For each unique geosphere state, a set of 1600 particle tracks was obtained from the FRAC3DVS-OPG simulation of the Reference Case (Walsh and Avis 2010). These tracks start at the repository horizon and are uniformly distributed over the entire repository footprint.

Figure B.1 shows a composite of the discharge locations of the particle tracks generated using the steady-state groundwater flow field for the Temperate State. The origins of these tracks at the repository horizon are shown in Figure B.2 using the same colour coding. The legend on Figure B.2 applies for both figures.

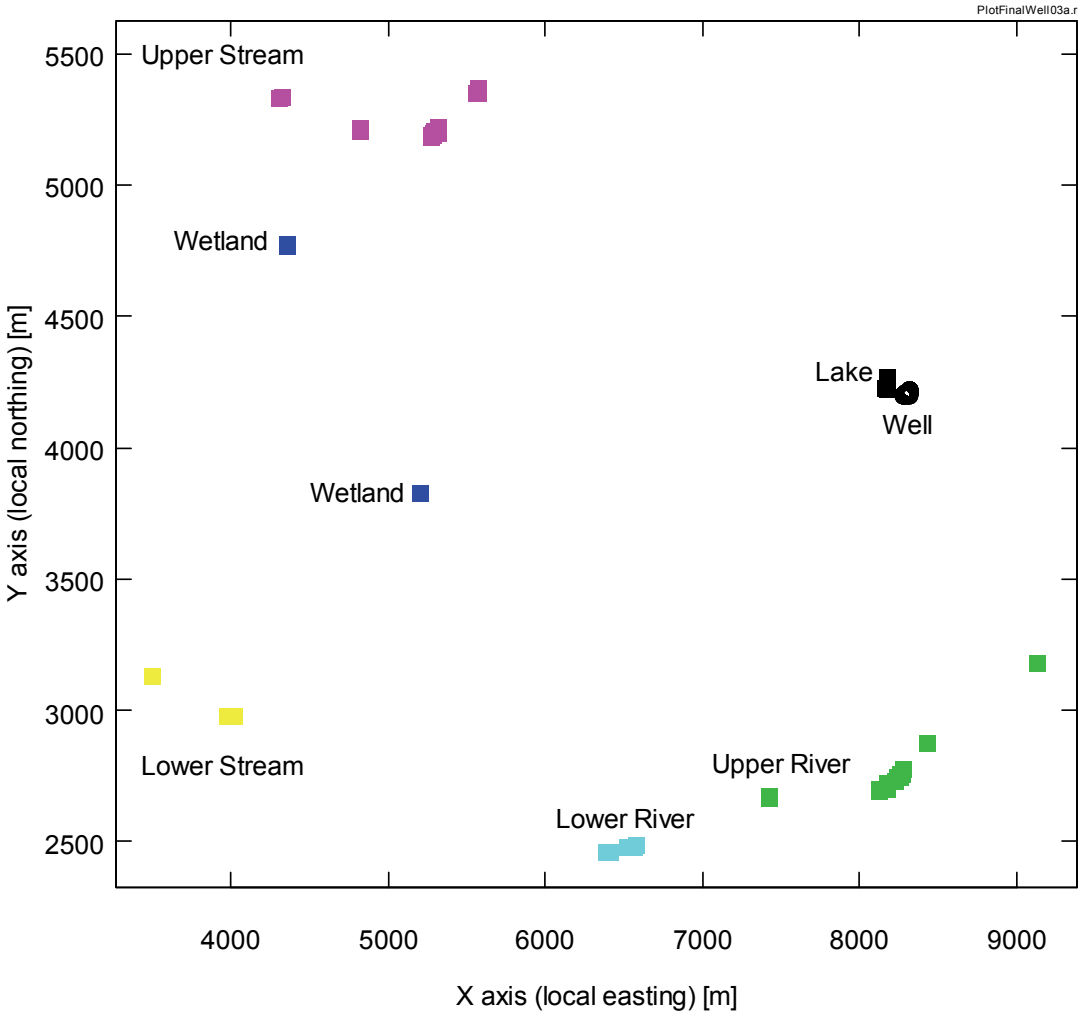

Figure B.1: Discharge locations of the particle tracks for the Temperate State.

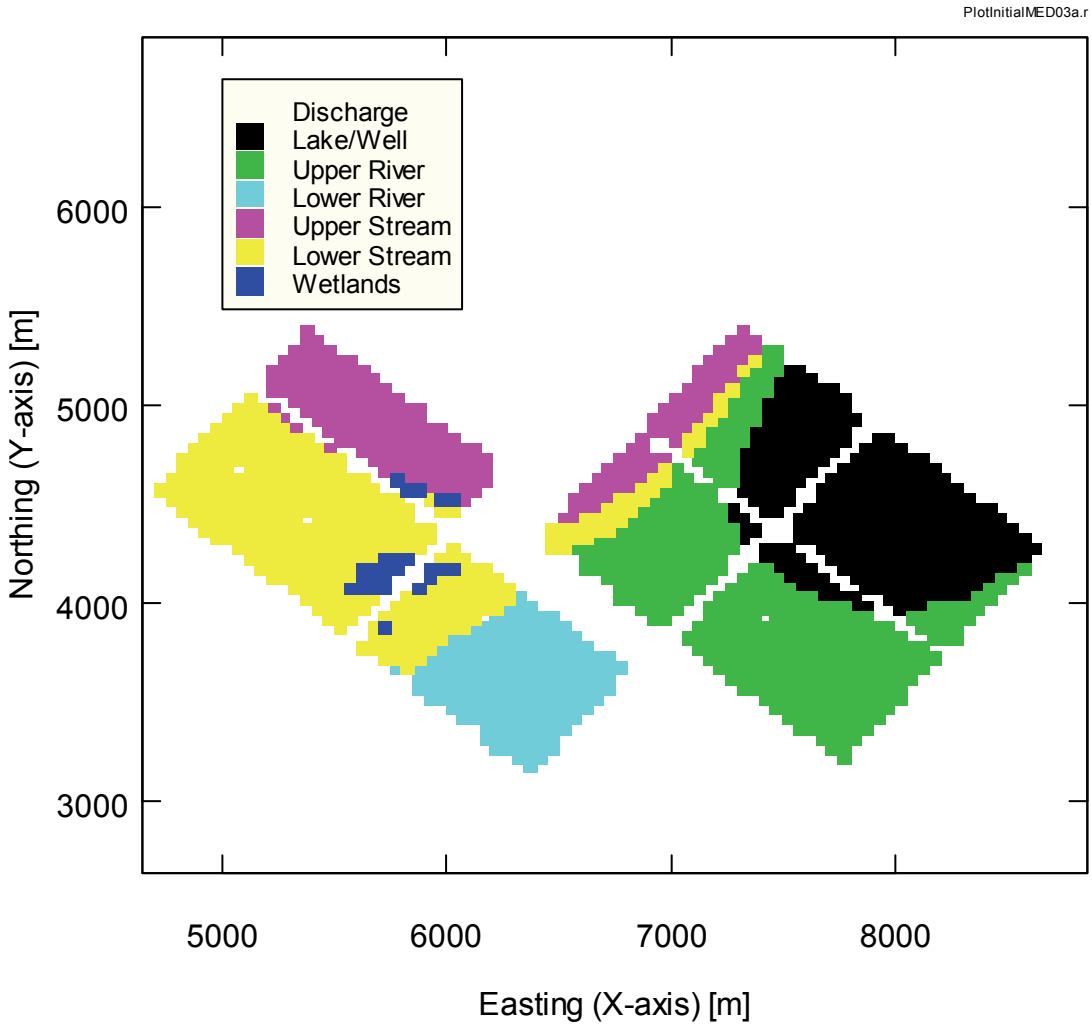

Figure B.2: Origin of particle tracks to discharge locations shown in Figure B.1

This analysis of the discharge patterns of the particle tracks gives a natural initial division of the vault into six (vault) sectors, where the particle tracks from the vault lead to:

1. either the Lake or Well
2. the Upper River
3. the Lower River
4. the Upper Stream
5. the Lower Stream, and
6. the Wetland

The final selection of the vault sectors for the Glaciation Scenario studies was done with the following priorities:

i) The initial vault divisions by discharge location for significant transport pathways should be maintained.
ii) The maximum simulation times would be approximately one million years or eight glacial cycles. Hence, for some geosphere states, the groundwater pathways that had excessively long travel times to the surface (i.e., greater than the maximum simulation time) were not incorporated explicitly in the network and instead shorter "more conservative" transport pathways were used.
iii) The pathways from the repository to the surface discharge should be chosen, where possible, to represent the groundwater pathways for the Temperate, Permafrost and, to a lesser extent, the Proglacial Lake States. For these states, humans are assumed to reside near the repository site and, hence, are exposed to radionuclides discharged from the repository.

The final division of the repository into representative vault sectors is shown in Figure B.3. This layout is not radically different from the initial division shown in Figure B.2, although the division of the Lake/Well discharge into two sectors, based on groundwater transport time to the surface, does give a different visual look to the layout. The modifications made to arrive at the vault sectors shown in Figure B.3 include:

i) Addition of the particle tracks from the Upper River discharge found in the lower right vault panel to the Lake/Well discharge. This is a conservative adjustment since the Lake/Well pathway is the shortest in terms of distance and travel time to the surface.
ii) Division of the Lake/Well discharge region into two sectors because of significant differences in the transport time across this region.
iii) Combining the Wetland and Lower Stream discharge regions into one sector.
iv) The Upper and Lower Stream sectors could not be combined because the groundwater pathways for these two sectors are quite different. In particular, the effect of Permafrost States on the groundwater pathways and travel times is not the same for these two sectors. Similarly, it was not possible to combine the Upper and Lower River vault sectors because the groundwater pathways and travel times behave differently for these two sectors during Permafrost States. These differences are illustrated in Tables B.2 below.

B.3 SELECTION OF REPRESENTATIVE TRACKS

For each of the vault sectors presented in Figure B.3, a representative particle track was selected to approximate the groundwater flowpath from the sector to the discharge point at the surface. These tracks may converge and combine with others on the way to the surface or diverge and lead to different discharge points, depending on conditions such as well demand or geosphere state (e.g., presence of permafrost).

The representative track from each sector was chosen to have the shortest travel time, as a conservative approximation. The minimum travel times from the vault sectors to the different discharge locations are presented in Table B.2 for each unique geosphere state. The representative tracks are shown in Figure B.4.

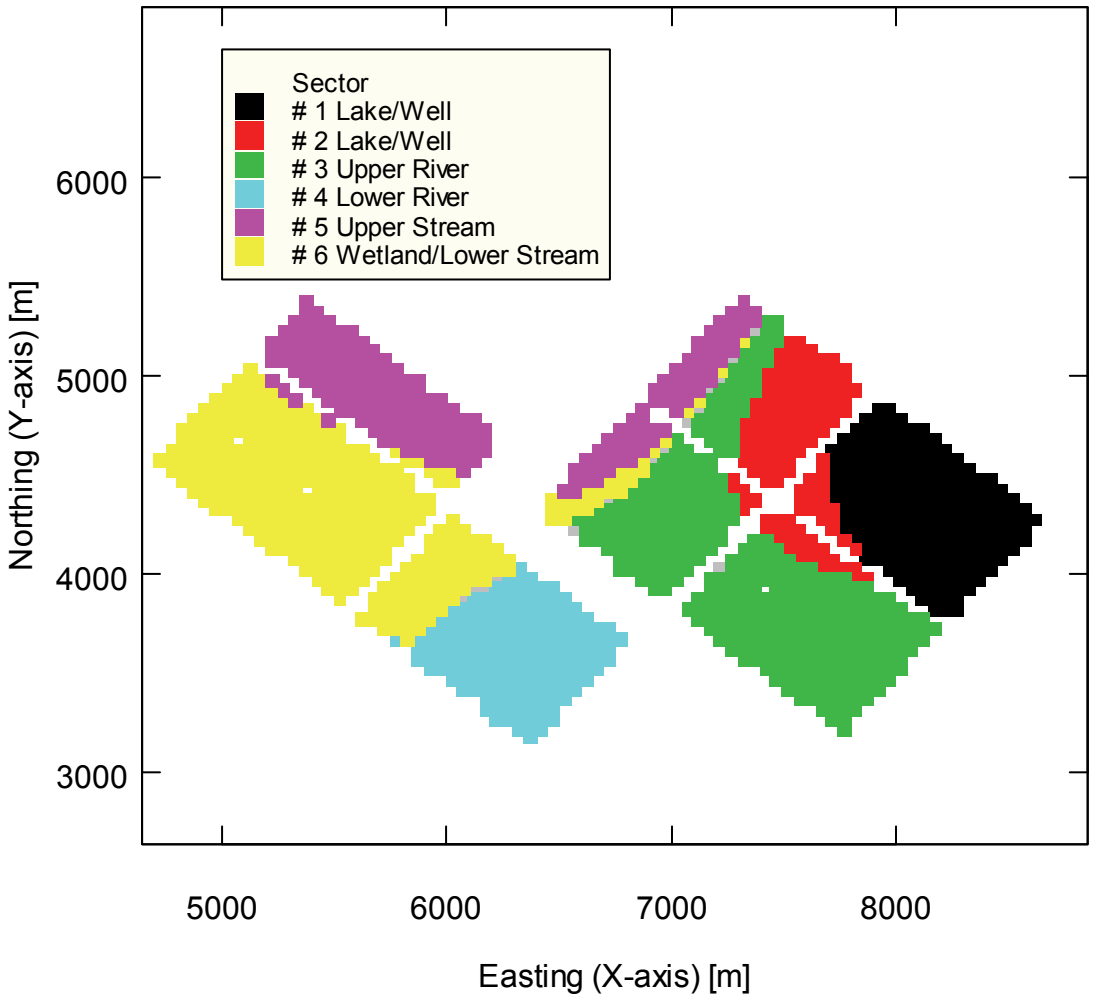

Figure B.3: Six vault sectors defined for the Glaciation Scenario study.

Table B.2: Reference Case particle track travel times to the surface discharge for the representative tracks for each vault sector and unique geosphere state

Vault Sector	Number of Containers	Groundwater Travel Time [Ma]						Discharge Location
		TEMPR	PERM1	PERM2	ISWB1	ISWB2	PROLA	
1	1646	0.61	0.38	0.30	0.21	0.51	2.30	Well/Lake
2	1036	0.83	0.84	0.74	0.21	0.59	1.48	Well/Lake
3	2810	0.93	2.28	2.03	0.31	0.69	1.16	River
4	1298	0.88	13.58	32.0	0.18	0.60	0.65	River
5	1575	1.58	13.84	67.1	0.21	0.95	1.85	Stream
6	2867	2.56	8.12	14.5	0.79	1.17	1.14	Stream

The geosphere states ISCB1, ISCB2 and ISCB3 are not shown in Table B.2. These geosphere states represent times during the reference glacial cycle when a cold based ice sheet is present over the site. During these times, the groundwater flow is predominantly downwards, based on the fixed groundwater flow fields that were selected to be representative of the transient groundwater flow field during these three cold-based Ice Sheet States. Consequently, the particle tracks (derived using the fixed flow fields) never reach the surface.

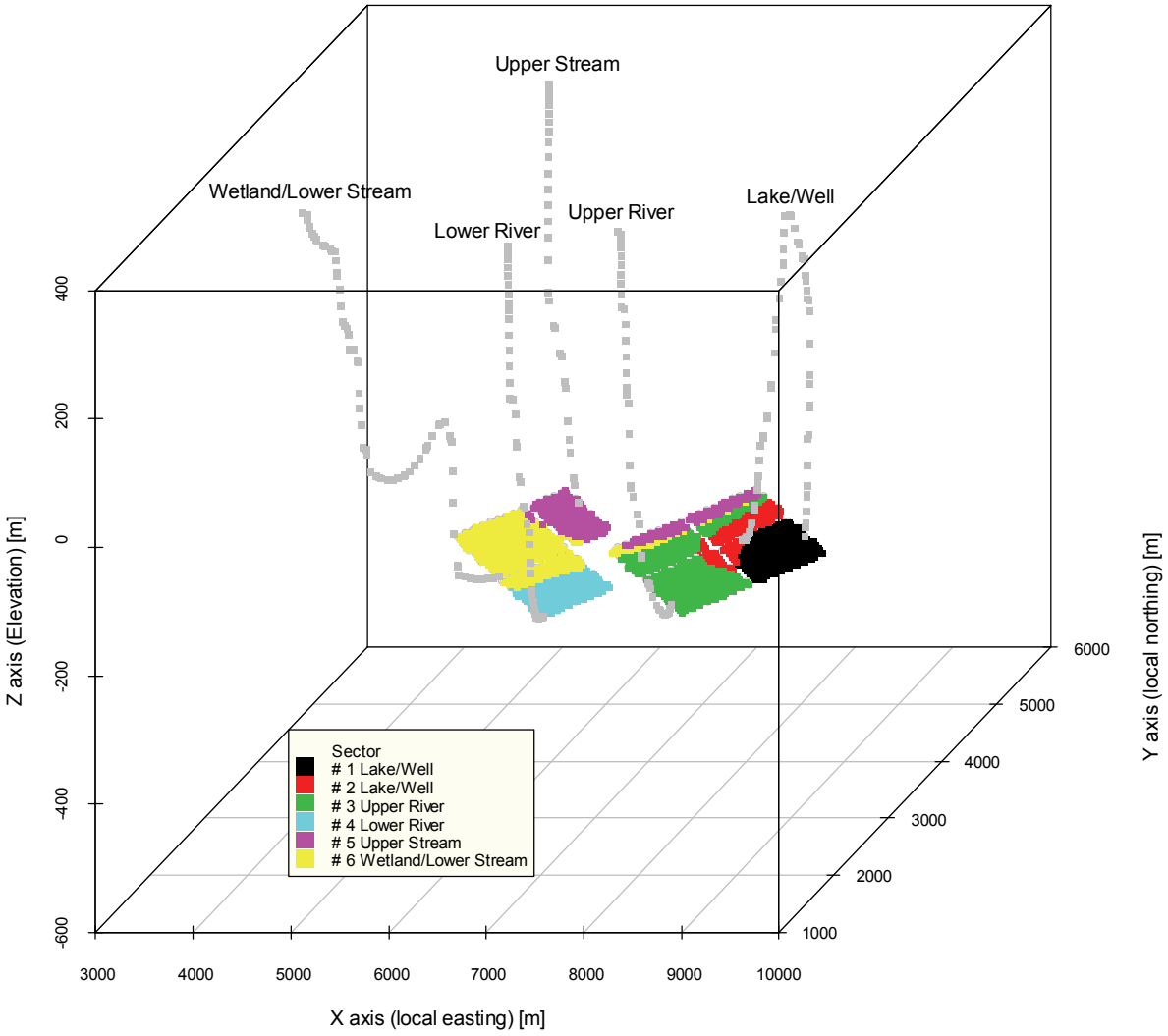

Figure B.3: Vault sectors for the Glaciation Scenario study and the representative particle tracks for the Temperate State

The travel times presented in Table B.2 are the minimum times for the representative particle to travel from the repository horizon to the discharge locations assuming that the groundwater flow field is fixed. Inherently, the GEONET transport model, which is based on these representative tracks, can only capture the principal features of the groundwater flow fields and, thus, can only approximate radionuclide transport from the repository to the surface as compared to the FRAC3DVS model which uses the transient groundwater flow field.

The geosphere transport network (GEONET) used for modelling the Glaciation Scenario is shown in Figure B.5. The locations of the shallow and deep permafrost zones are also shown in the figure.

B.4 ADDITION OF GLACIATION STATE EFFECTS ON THE GEOSPHERE NETWORK

The initial geosphere network, including nodal locations and segment properties, is based on the Temperate State groundwater flow field information. This state was the natural starting point because of its expected importance in the safety assessment calculations. This is particularly true since the critical group is assumed to use a well, which intercepts the contaminant plume from the repository, for its water needs. Dose rates to critical groups using well water have been found to be much higher than for those using lake water (Garisto et al. 2004).

The Temperate State geosphere network is then used as a basis for all other geosphere states with the following changes made, as needed, to correctly represent each unique geosphere state:

i) modification of groundwater velocities,
ii) changes in the partition of the flow, for segments where flow diverges,
iii) the freezing in of segments (with no radionuclide transport allowed for frozen in segments) affected by permafrost, during both Permafrost and cold-based Ice Sheet States, and
iv) the effect of the open talik during Permafrost States.

As an example of the changes made to the Temperate State geosphere network, we will discuss the transport pathway from Vault Sector 1 to the Well/Lake discharge location. This particular Well/Lake pathway has the shortest travel time to the surface during the Temperate State (see Table B.2) and also has the shortest distance to the surface.

The particle track chosen to represent the pathway from Vault Sector 1 to the Well/Lake discharge is shown in Figure B.6 for three unique geosphere states: Temperate (TEMPR), Permafrost 1 (PERM1), and Permafrost 2 (PERM2). There is very little difference in these three pathways even though the particle travel times are quite different for each geosphere state, as shown in Table B.2.

In order to account for the differences in travel times, a scaling factor (GSCALE) was determined for each segment in the pathway from Vault Sector 1 to the Well/Lake discharge and for each of the geosphere states listed in Table B.3. This scaling factor is then used to calculate the groundwater velocity in a segment, for a particular geosphere state, given the groundwater velocity in the segment for the Temperate State. Thus, for example, Table B.4 indicates that groundwater velocity in Segment 1 is 4.2 times larger in geosphere state ISWB1 than in the Temperate State (TEMPR). The scaling factors for all pathways from the vault horizon to the surface shown in Figure B.5 are available in the CC4 database for the Glaciation Scenario.

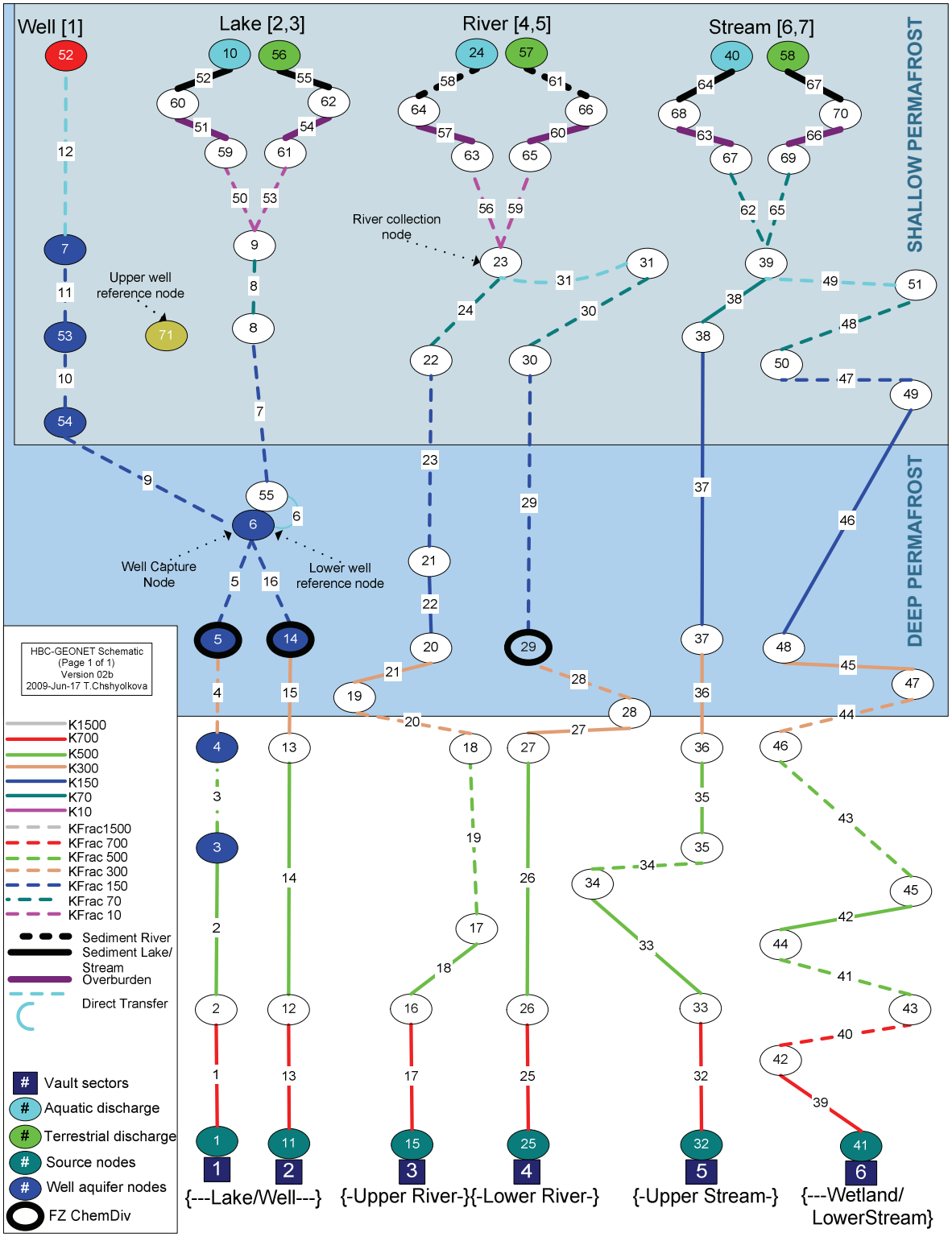

Figure B.5: Schematic showing connectivity of geosphere transport network. Only nodes with a particular function are colour coded. The line segments, representing the 1-dimentional transport pathways, are colour coded to indicate the geosphere zone through which they pass.

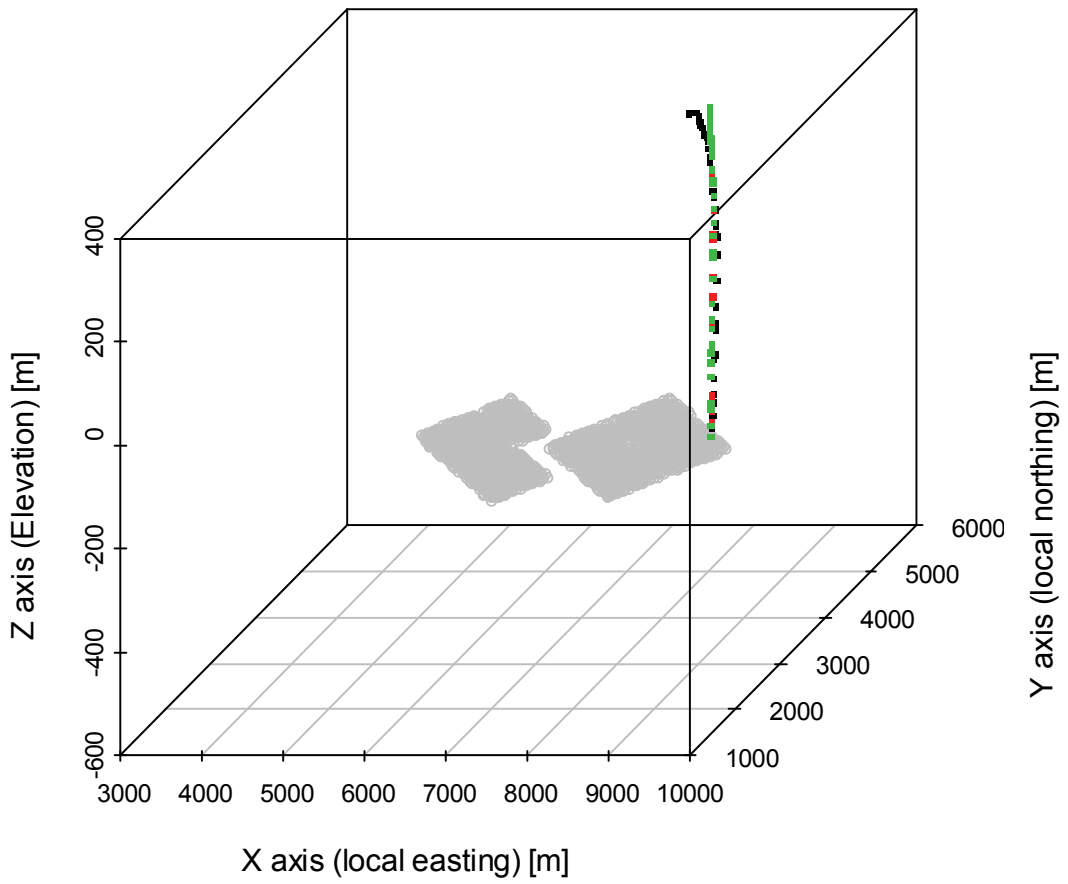

Figure B.6: Particle track selected for Vault Sector 1, Temperate (TEMPR, black), Permafrost 1 (PERM1, red), and Permafrost 2 (PERM2, green) States.

In general, for geosphere states with permafrost, the pathways leading to the Well/Lake discharge tend to have higher velocities than during the Temperate State, although the scaling factor is not the same for each segment. For the geosphere states that arise during cold-based Ice Sheet States (ISCB1, ISCB2 and ISCB3), all groundwater velocities are set to zero because, in this case, the particles travel vertically downwards. Consequently, during these states, radionuclide transport along the pathways can occur only by diffusion. However, if a segment is in the permafrost zone, then it is considered “frozen in” and there is no radionuclide transport along the segment until after the permafrost melts in a subsequent glaciation state.

Finally, particle tracks move vertically upwards during warm-based Ice Sheet and Proglacial Lake States.

Table B.3: Reference Case scaling factor (GSCALE) values for the different geosphere states, for the pathway leading from Vault Sector 1 to the Well/Lake discharge

Segment	Geosphere State						
	TEMPR	PERM1	ISCB1 ISCB2 ISCB3	PERM2	ISWB1	ISWB2	PROLA
1	1	1.6	0	2.0	4.2	1.3	1.0
2	1	2.4	0	3.1	1.8	1.0	0.3
3	1	0.4	0	0.4	0.2	0.6	0
4	1	0.5	0	1.6	0.3	0.7	0
5	1	5.5	0	2.3	0.4	0.8	0
7	1	4.8	0	1.4	0.6	0.6	0
8	1	1.3	0	0.4	1.3	1.3	0
50 & 53	1	1.3	0	0.4	1.3	1.3	0
51 & 54	1	1.3	0	0.4	1.3	1.3	0
52 & 55	1	1.3	0	0.4	1.3	1.3	0

During Permafrost States (PERM1 and PERM2), particle track travel times are significantly longer for pathways that do not lead to the Well/Lake discharge, as shown in Table B.2. The increase in travel time is caused by two factors. First, the groundwater velocities in the immediate rock zone around the vault are reduced, adding significantly to the travel time. Second, the pathway to the surface, that initially follows the same path as in the Temperate State, is diverted as it approaches the permafrost layer. However, since the maximum simulation time for this study is approximately one million years, these diverted pathways (for Vault Sectors 3, 4, 5 and 6) leading to the river or stream discharges were not included in the GEONET network for the Permafrost States and, therefore, the representative tracks remain the same as for the Temperate State. This is expected to be a conservative assumption since radionuclides are not diverted towards long pathways to the surface but are retained within the shorter pathways, from where they can more quickly reach the surface during subsequent Temperate States. The scaling factor (GSCALE) values for the pathway leading from Vault Sector 5 to the stream discharge are shown in Table B.4.

B.5 ADDITION OF THE OPEN TALIK TO THE GEOSPHERE NETWORK

During Permafrost States PERM1 and PERM2, an open talik exists under the Lake, i.e., there is no permafrost under the lake. Thus, all groundwater pathways that flow from the repository to the Well/Lake discharge are assumed to be within the talik region during Permafrost States. (Only groundwater pathways from Vault Sectors 1 and 2 discharge to the Well/Lake). Thus, during these states, radionuclide transport (diffusive and advective) continues to occur along the pathways from Vault Sectors 1 and 2 to the Well/Lake discharge. In contrast, all other transport segments above the permafrost depth (see Figure B.4), that are not identified as being within the talik, are “frozen in”, i.e., radionuclide transport does not occur in these segments. During cold based Ice Sheet States, the talik does not exist and therefore all transport segments above the permafrost depth are frozen in.

B.6 ADDITIONAL GEOSPHERE NETWORK REQUIREMENTS

For finalization of the geosphere transport network there are a number of additional steps required, including addition of extra nodes and segments for the well, and for the overburden, and sediment layers. These steps are identical to those described in detail in Garisto et al. (2005, Appendix B).

Table B.4: Reference Case scaling factor (GSCALE) values for the different geosphere states, for the pathway leading from Vault Sector 5 to the Stream discharge

Segment	TEMPR	PERM1	ISCB1 ISCB2 ISCB3	PERM2	ISWB1	ISWB2	PROLA
River 2							
25	1	0.1	0	0	7.3	1.6	2.8
26	1	0.8	0	2	2.1	0.8	0.3
27	1	5.8	0	0.2	0.2	0.5	0.1
28	1	1.1	0	0.8	0	0.7	0
29	1	0.5	0	0.1	0	0.7	0
30	1	0.1	0	0.1	0.3	0.9	0
56 & 59	1	0.1	0	0	0.4	0.9	0
57 & 60	1	0.1	0	0	0.4	0.9	0
58 & 61	1	0.1	0	0	0.4	0.9	0

REFERENCES

Garisto, F., J. Avis, N. Calder, P. Gierszewski, C. Kitson, T. Melnyk, K. Wei, and L. Wojciechowski. 2005. Horizontal borehole concept case study. Ontario Power Generation Report, Nuclear Waste Management Division 06819-REP-01200-10139-R00. Toronto, Canada.

Garisto, F., J. Avis, N. Calder, A. D'Andrea, P. Gierszewski, C. Kitson, T.W. Melnyk, K. Wei and L. Wojciechowski. 2004. Third case study – Defective container scenario. Ontario Power Generation, Nuclear Waste Management Division Report 06819-REP-01200-10126-R00. Toronto, Canada.

Walsh, R. And J. Avis. 2010. Glaciation Scenario: Groundwater and radionuclide transport studies. Nuclear Waste Management Organization Technical Report NWMO TR-2010-09. Toronto, Canada.

APPENDIX C: COMPARISON OF FRAC3DVS AND CC4 RESULTS

CONTENTS

C.1 INTRODUCTION

In the current study, the CC4 geosphere model has a simplified description of the repository site geometry, relative to the FRAC3DVS model. The geosphere in CC4 is represented by a network of 1-dimensional transport segments (see Appendix B), whereas FRAC3DVS uses a three dimensional numerical model to represent the geosphere (see Section 6 and Walsh and Avis (2010)). Furthermore, CC4 uses a series of (fixed) groundwater flow fields to represent the transient groundwater flow field during a glacial cycle.

The FRAC3DVS model does not include a representation of the repository in the geosphere model; rather the nuclide mass flows out of the repository previously developed for the HBC study (Garisto et al. 2005a) were used as source terms for the current FRAC3DVS transport modelling, as described in Section 6. In contrast, the CC4 model includes a representation (albeit appropriately simplified) of the repository (Garisto et al. 2005a). In addition, a large dispersivity value was used in the FRAC3DCS transport calculations to maintain numerical stability.

In this appendix, the SYVAC-CC4 and FRAC3DVS model results for I-129 are compared as a consistency check between these two numeric models. (FRAC3DVS transport results are only available for I-129.) In particular, we compare the I-129 release rates from the geosphere (to the biosphere) and the calculated I-129 dose rates to the critical groups. The I-129 release rates from the repository are not compared, as was done in previous studies (Garisto et al. 2005, 2004), because the repository is not explicitly represented in the current FRAC3DVS transport model and, hence, I-129 release rates out of the repository are not calculated by FRAC3DVS (see Section 7).

The comparisons between the SYVAC-CC4 and FRAC3DVS model results are first done for several cases of (Defective Container) Constant Climate Scenario and then for the Reference Case of the (Defective Container) Glaciation Scenario.

C.2 COMPARISON OF FRAC3DVS AND CC4 FOR CONSTANT CLIMATE CASES

In this section, we compare the CC4 and FRAC3DVS results for various cases of the Constant Climate Scenario. We consider the following Constant Climate cases:

1. The DC1 Temperate case, in which the defective containers are in the Defective Container 1 source location (see Figure 7.3). Except for the constant climate, this calculation case is identical to the Reference Case of the Glaciation Scenario.
2. The DC3 Temperate case, in which the defective containers are in the Defective Container 3 source location (see Figure 7.3). Except for the constant climate and source location, this calculation case is identical to the Reference Case of the Glaciation Scenario.
3. Temperate All Containers Fail case, in which all containers fail at 100,000 years. Except for the constant climate, this calculation case is identical to the All Containers Fail case of the Glaciation Scenario.

C.2.1 Comparison of Geosphere Releases

The source locations DC1 and DC3 are associated with Vault Sector 1 and 5, respectively (cf. Figures 7.3 and B.3). Groundwater from Sector 1 discharges to the Well or North Lake, whereas groundwater from Sector 5 discharges to the Stream (see Appendix B). The Stream discharge in CC4, which represents the sum of the discharges to the Upper Stream and Wetland/Lower Stream, as shown in Figure B.5, corresponds with the Western Region discharge in FRAC3DVS (see Figure 7.18).

The approximate groundwater travel times (from particle tracking) from the repository to the surface for the different vault sectors are shown in Table B.2. Groundwater travel times to the surface are shorter for the DC1 location than the DC3 location. For the DC3 location (Vault Sector 5), the groundwater travel time to the Well or Lake is so long (i.e., much longer than the simulation time) that this groundwater pathway was not modelled in CC4 (see Appendix B).

The total I-129 mass flow rates to the biosphere are presented in Figure C.1 for the DC1 and DC3 Temperate cases. Overall the agreement between the two models is fairly good for these cases; although, in FRAC3DVS, the peak I-129 mass flows occur earlier because the FRAC3DVS model uses a larger longitudinal dispersivity value (80 m in FRAC3DVS versus 50 m in CC4).

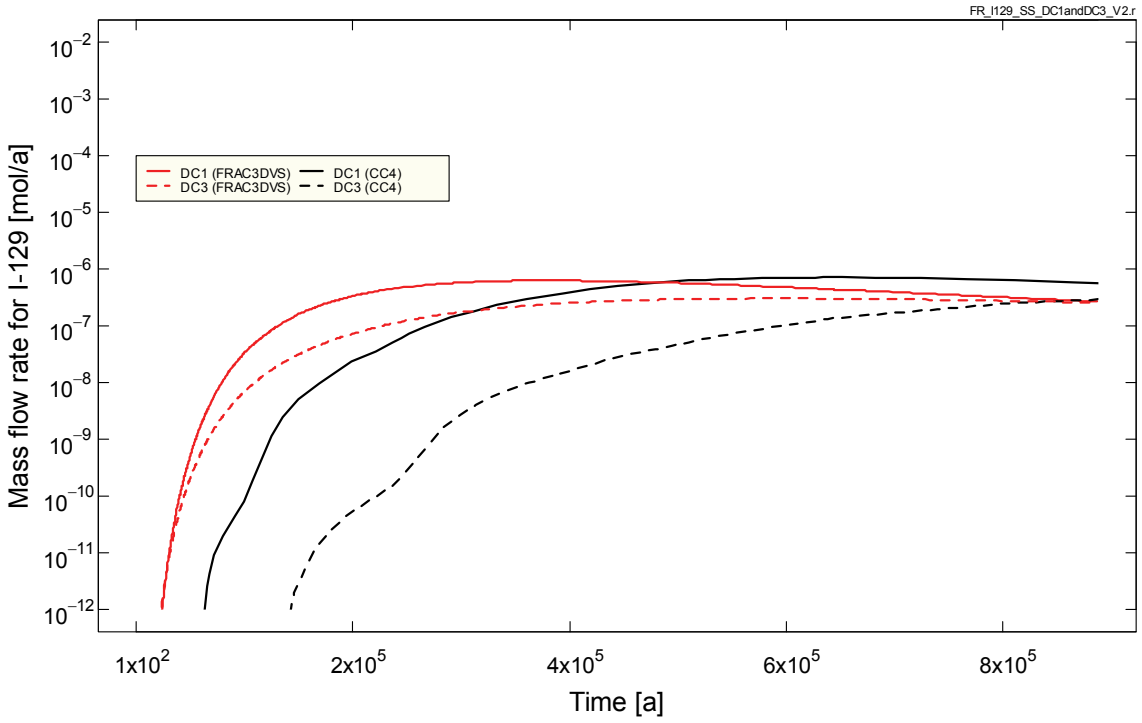

Figure C.1: Comparison of I-129 geosphere releases to the biosphere for CC4 and FRAC3DVS for the DC1 Temperate and DC3 Temperate cases of the Constant Climate Scenario.

For the DC1 Temperate case, all I-129 is discharged to the biosphere via the well in CC4; whereas, in FRAC3DVS, only a portion of the I-129 plume is captured by the well and some I-129 is also discharged to the (North) Lake. This difference arises because the CC4 geosphere transport network was conservatively constrained, by the choice of data values for well capture, so that the well captures the entire contaminant plume from Vault Sector 1. Thus, for this case, CC4 overestimates the contaminant mass flows to the well relative to FRAC3DVS. For the DC3 Temperate case, the FRAC3DVS releases are to the Western Region and the CC4 releases are to the Stream, which, as noted, corresponds to the Western Region discharge in FRAC3DVS.

Table C.1 summarizes the calculated peak I-129 mass flows for the DC1 and DC3 Temperate cases. The peak mass flow rates to the well and stream are similar in CC4 and FRAC3DVS, although the peak mass flow rates occur earlier in FRAC3DVS. These differences are similar to those observed in Section 7.4 in the comparison of the current FRAC3DVS model with that used in the HBC study (Garisto et al. 2005). The earlier arrival time in FRAC3DVS is mainly due to the higher dispersivity value used in the FRAC3DVS transport model.

Table C.1: Comparison of CC4 and FRAC3DVS I-129 releases to the biosphere for the DC1 Temperate and DC3 Temperate cases

Nuclide	Peak mass flow rate [mol/a]			Time of Peak [a]		
	CC4	FRAC3DVS	Ratio[1]	CC4	FRAC3DVS	Ratio[1]
DC1 Source						
Well	7.4×10^{-7}	4.7×10^{-7}	1.2[#]	6.2×10^{5}	4.0×10^{5}	1.5
Lake	0.0	1.7×10^{-7}		NA	3.5×10^{5}	NA
DC3 Source						
Stream	2.8×10^{-7}	3.1×10^{-7}	0.9	8.9×10^{5}	6.0×10^{5}	1.5
Lake.	0.0	8.4×10^{-17}	NA	NA	1.0×10^{6}	NA

[1]Ratio is the CC4 result divided by the FRA3DVS result.
[#]This is the ratio of the peak total mass flow to well and lake.

C.2.2 Comparison of Dose Consequences

In this section, the dose rates calculated with the SYVAC3-CC4 system model are compared with the dose rates calculated using SYVAC3-CC4 biosphere model and the I-129 release rates into the biosphere from FRAC3DVS. The latter dose rates will simply be referred to as the FRAC3DVS dose rates. In effect, this provides a direct comparison of the dose impacts of the CC4 and FRAC3DVS mass flows shown in the previous section.

The calculated dose rate curves for the two models are compared in Figure C.4 for the DC1 Temperate and DC3 Temperate cases. The calculated dose rates are much higher for the DC1 source location than the DC3 source location. The agreement is fairly good for the DC1 source location but the dose rate peaks much earlier in FRAC3DVS for the DC3 source location. The differences in these dose rate curves mirror the differences observed in the I-129 releases to the biosphere in Section C.2.1.

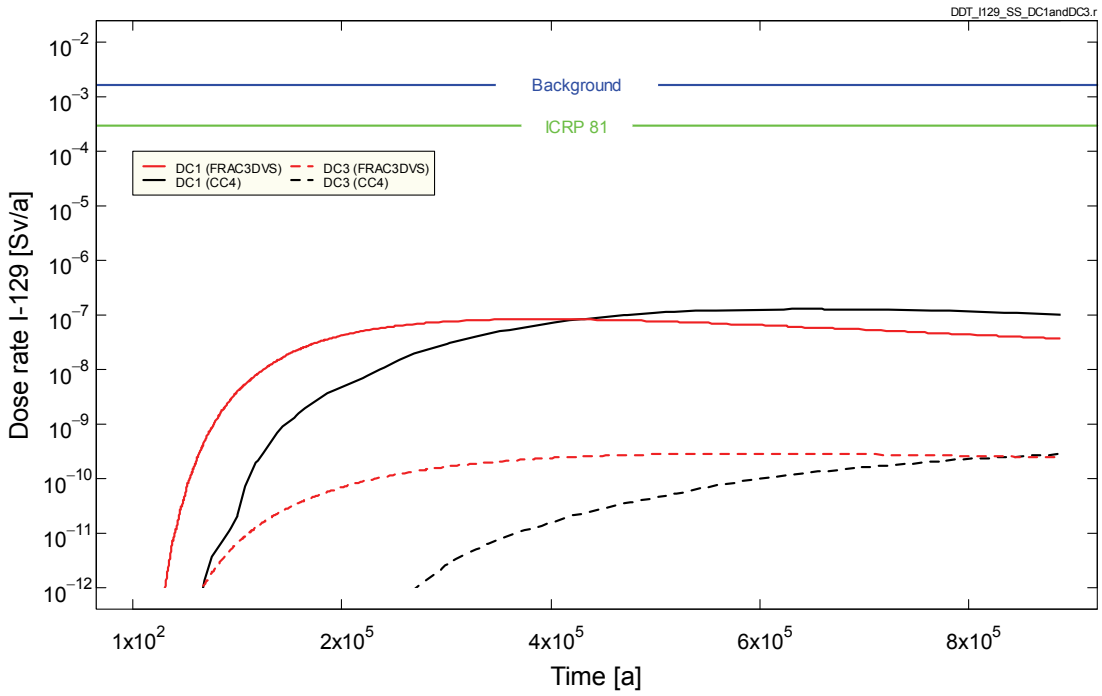

Figure C.2: Comparison of calculated I-129 dose rates from CC4 and FRAC3DVS for the DC1 Temperate and DC3 Temperate cases.

Table C.2 summarizes the calculated peak I-129 dose rates for the DC1 and DC3 Temperate cases. The calculated peak I-129 dose rates from CC4 are somewhat higher than the FRAC3DVS dose rates. However, the peak dose rate occurs earlier in FRAC3DVS because a higher dispersivity value is used in the FRAC3DVS transport calculations than in the CC4 calculations.

Table C.2: Comparison of the calculated I-129 dose rates from CC4 and FRAC3DVS for the DC1 Temperate and DC3 Temperate cases

Source Location	Peak dose rate [Sv/a]			Time of Peak [a]		
	CC4	FRAC3DVS	Ratio[1]	CC4	FRAC3DVS	Ratio[1]
DC1	1.3×10^{-7}	8.4×10^{-8}	1.6	6.1×10^{5}	4.0×10^{5}	1.5
DC3	3.3×10^{-10}	2.9×10^{-10}	1.2	1.0×10^{6}	6.0×10^{5}	1.7

[1]Ratio is the CC4 result divided by the FRA3DVS result

C.2.3 Comparison of Analytical and Multi-compartment Transport Solutions

The CC4 model was modified significantly for this study. Of particular note, were the changes needed to handle a time-varying geosphere. The analytical solutions to the geosphere transport equations used in CC4 cannot be used for a time-varying geosphere (Gierszewski et al. 2004). Therefore, a multi-compartment approach was developed for solving the geosphere transport equations for the Glaciation Scenario calculations. The multi-compartment approach was found to work well and improves as the number of compartments increases.

A comparison of CC4 results obtained with the analytical and mutli-compartment solutions is shown in Figure C.3. A comparison is possible only for constant climate cases, since the analytical solution is only valid for these cases.

The multii-compartment solution (GRF=5) agrees well with the analytical solution (GRF=1) at long times but gives higher dose rates at earlier times, which is conservative. The higher dose rates at the earlier times arise because the contaminant plume from the repository reaches the well earlier due to numerical dispersion. The agreement could be improved by increasing the number of compartments.

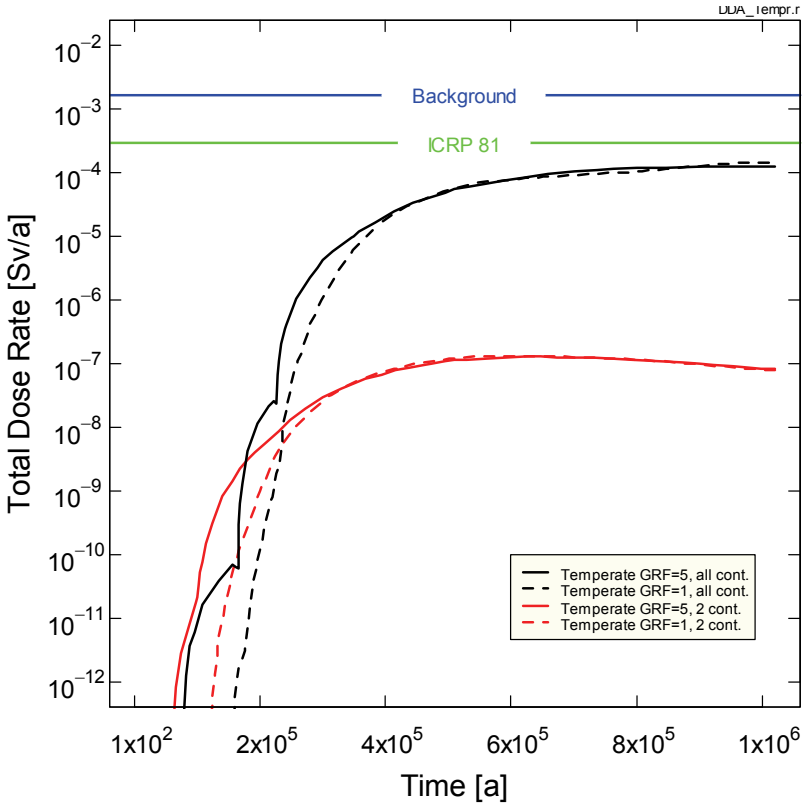

Figure C.3: Comparison of CC4 dose rates calculated using analytical solutions (GRF=1) and multi-compartment solutions (GRF=5) to the geosphere transport equations. Two cases are shown: the Temperate All Containers Fail sensitivity case and the DC1 Temperate case with 2 container failures in Vault Sector 1.

In Figure C.3, the wiggles in the curves for the multi-compartment solutions are artefacts of the time series calculations in CC4 and would disappear if more time series points are used in the calculations.

C.3 COMPARISON OF FRAC3DVS AND CC4 FOR GLACIATION CASES

In this section, we compare the CC4 and FRAC3DVS results for various Glaciation Scenario cases. We consider the following two Glaciation Scenario cases:

1. The Reference Case, in which the defective containers are in the Defective Container 1 source location (see Figure 7.3).
2. The DC3 Glaciation case, in which the defective containers are in the Defective Container 3 source location (see Figure 7.3). Except for the source location, this calculation case is identical to the Reference Case.

C.3.1 Comparison of Geosphere Releases

In Figure C.4, the I-129 mass flows from the geosphere to the biosphere from CC4 and FRAC3DVS are compared for the Reference (Glaciation) Case. (The colour scheme used for the geosphere glaciation states is shown in Figure 8.1.)

Initially, the FRAC3DVS mass flow rates to the biosphere are larger than those from CC4, because the contaminant plume reaches the surface faster in FRAC3DVS, as was the case in the constant climate cases. However, the agreement becomes better after about 3×10^5 years and, at longer times, the CC4 I-129 geosphere releases generally exceed the FRAC3DVS releases except at particular times during each glacial cycle (such as at the beginning of the long Permafrost State).

A prominent difference between the two models occurs at the beginning of the second and longest Permafrost State (PERM2 or geosphere state 4, see Figure 8.1) in the glacial cycle. In FRAC3DVS, a pulse of I-129 mass is released into the biosphere at the start this Permafrost State because groundwater flow velocities are generally higher (and upwards) at the beginning of the second Permafrost State (see Section 6) due to pressurization of the groundwater flow system during the Ice Sheet State preceding this Permafrost State. This I-129 pulse is not present in the CC4 results. Rather, in CC4, the I-129 release rate increases rapidly at the start of this Permafrost State and reaches a fairly constant value after several thousand years.

This difference is likely due to the fact that the two codes use different approaches to handle the time-dependent groundwater flow field. In FRAC3DVS, the groundwater flow field is transient. In contrast, in CC4, a (fixed) snapshot of the groundwater flow field is selected for use during each unique geosphere state. (For PERM2, the snapshot is taken near the end of the state.) Thus, the CC4 model does not include a complete representation of the transient groundwater flow field. In particular, the higher groundwater flows into the North talik, which occur at the beginning of the second Permafrost State, are absent in the CC4 model (see Section 6). In FRAC3DVS, these high flows carry a pulse of I-129 mass into the North talik at the start of the second Permafrost State. Similar, but more muted, differences are also noticeable during the start of the other Permafrost States.

Another apparent difference between the two models occurs during cold-based ice sheet states (geosphere states 3, 5 and 7). In FRAC3DVS, the I-129 mass flow rate into the biosphere is lower during these stated (compared to preceding or subsequent states); but, in CC4, it is zero. This difference arises because the properties of the permafrost zone are different in the two models. In CC4, the permafrost is considered impermeable and so there is no mass transport through the permafrost. In contrast, in FRAC3DVS, permafrost has an unrealistically high water filled porosity (similar to granite), allowing radionuclides to be transported (both by advection and diffusion) through the permafrost.

In summary, although there are some differences, the comparisons indicate that, even though the peak I-129 mass flows occur earlier in FRAC3DVS, these two significantly different models predict similar trends for the I-129 mass flow rates into the biosphere.

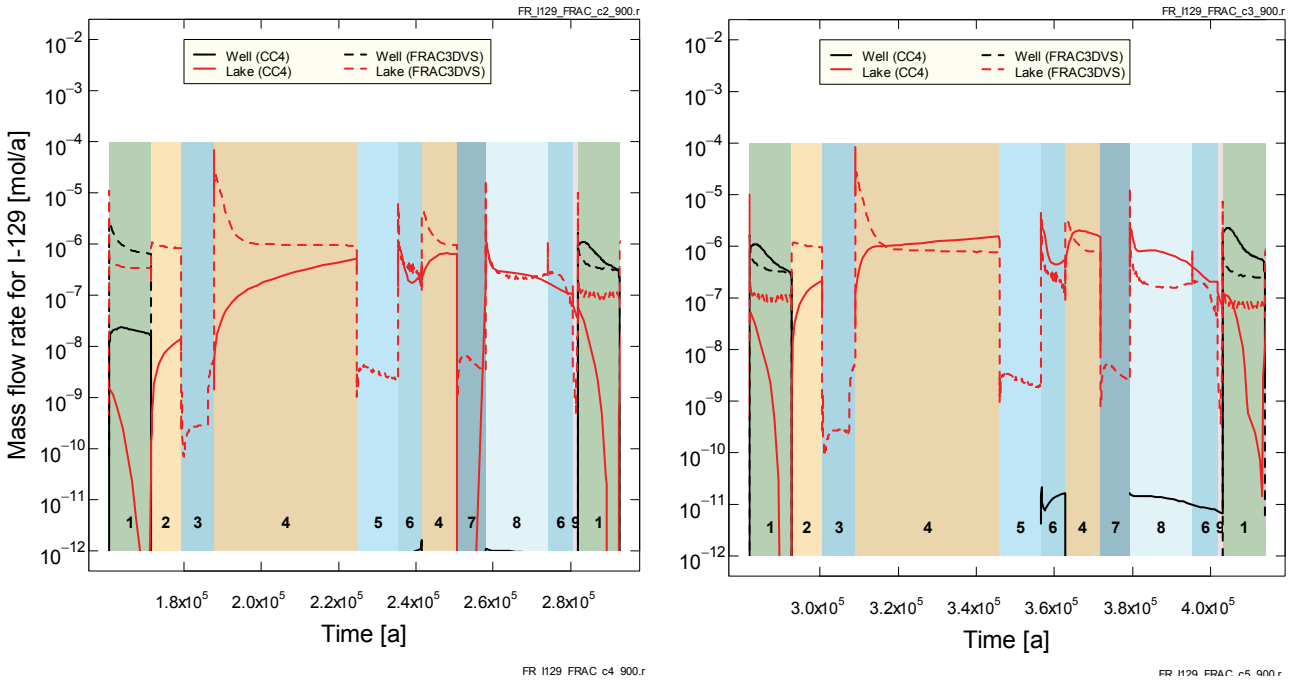

Figure C.4: Comparison of the I-129 geosphere releases to the biosphere for CC4 and FRAC3DVS for the Reference Case and glacial cycles 2 and 3. For the other glacial cycles, the I-129 releases to the biosphere are similar to those for cycle 3. .

The I-129 mass flow rates to the biosphere from FRAC3DVS and CC4 are compared in Figure C.5 for the DC3 Glaciation case. For the DC3 source location, the I-129 discharges to the biosphere are mainly to the Stream in CC4 or equivalently the Western Region in FRAC3DVS. The results in Figure C.5 indicate that the I-129 plume reaches the biosphere much earlier in FRAC3DVS than in CC4 for the DC3 source location. This difference is likely due to the larger dispersivity values used in the FRAC3DVS model.

The major difference between the FRAC3DVS and CC4 models for the DC3 Glaciation case occurs during Permafrost and cold-based Ice Sheet States. During these periods, permafrost exists below the Stream or Western discharge location. Therefore, the differences in the two models during these periods arise because the permafrost (transport) properties are different in the two models. In CC4, the permafrost is impermeable and so there is no mass transport through the permafrost. Therefore, in CC4, I-129 discharges to the Stream are zero during Permafrost and cold-based Ice Sheet States. In FRAC3DVS, the permafrost is conservatively assigned the same transport properties as granite, so although I-129 mass flows to the Western discharge are much reduced during these periods they are not zero.

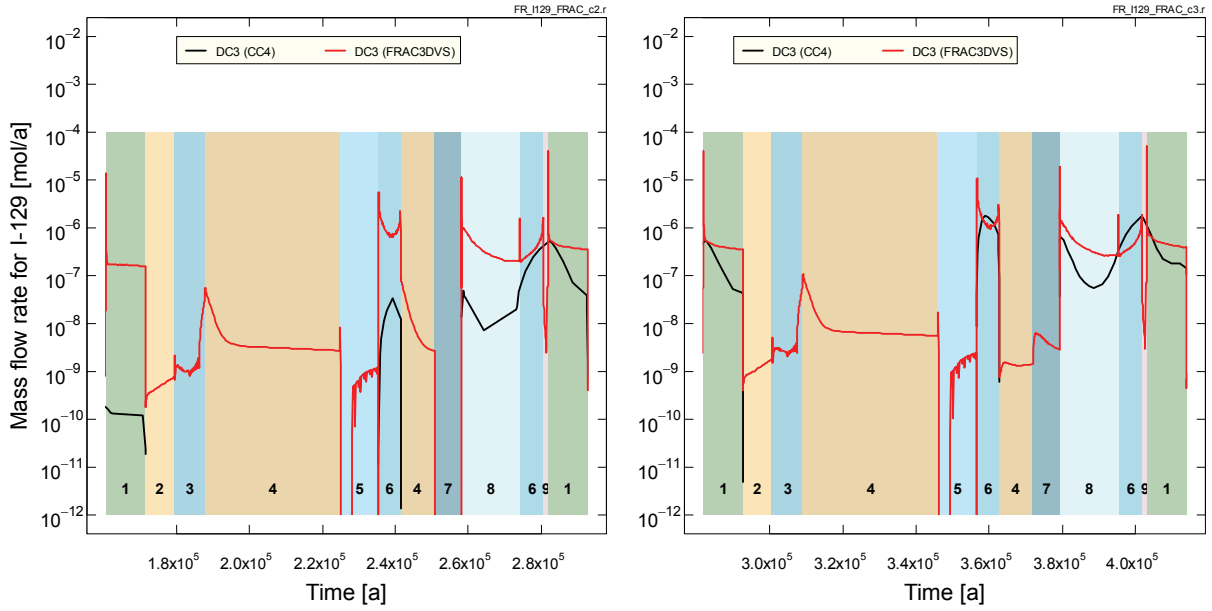

Figure C.5: Comparison of the I-129 geosphere releases to the stream discharge for CC4 and FRAC3DVS for the DC3 Glaciation case for glacial cycles 2 and 3. For the other glacial cycles, the I-129 releases to the biosphere are similar to those for cycle 3.

C.3.2 Comparison of Dose Consequences

In this section, the dose rates calculated by the SYVAC3-CC4 system model, using the CC4 geosphere release rates into the biosphere, are compared with the dose rates calculated with by SYVAC3-CC4 model but using the I-129 release rates into the biosphere calculated by FRAC3DVS. In effect, this provides a direct comparison of the dose impacts of the CC4 and FRAC3DVS mass fluxes shown in the previous section.

The dose rates calculated by CC4 and FRAC3DVS are compared in Figure C.6 for the Reference (Glaciation) Case. The calculated dose rates are in fairly good agreement except at earlier times. At early times the larger differences arise because the I-129 plume reaches the biosphere earlier in FRAC3DVS as discussed in Section C.3.1. At intermediate times (between 300,000 and 500,000 years) the agreement is quite good and at longer times the CC4 calculated doses rates are generally slightly higher.

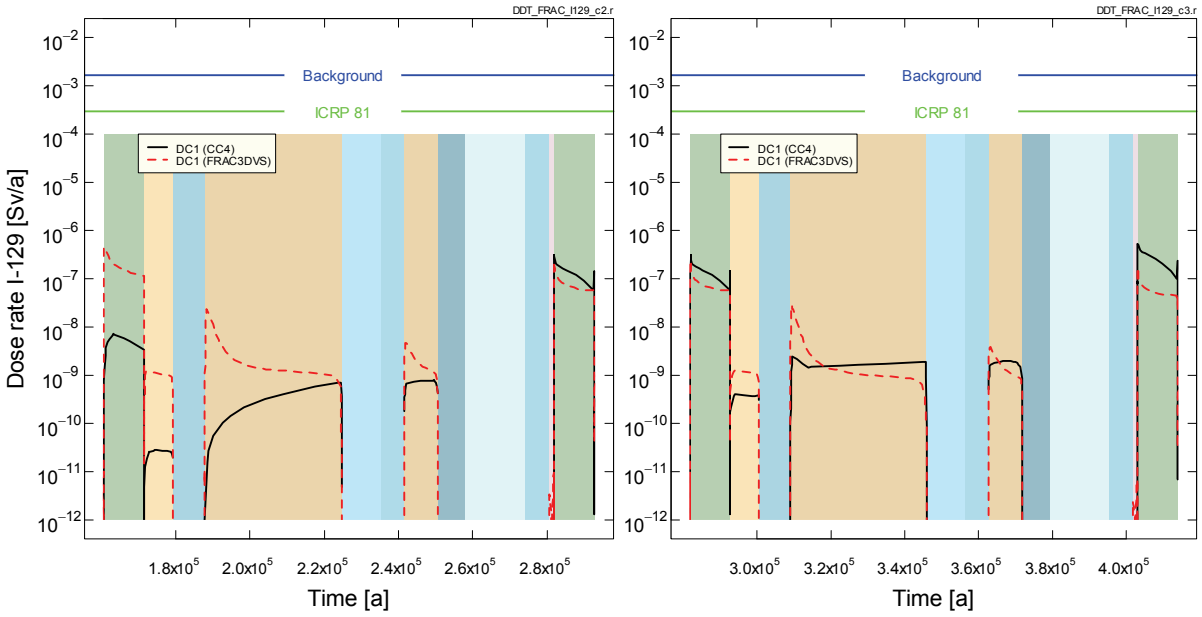

Figure C.6: Comparison of calculated I-129 dose rates from CC4 and FRAC3DVS for the Reference Case for glacial cycles 2 and 3. For the other glacial cycles, the I-129 dose rates are similar to those for cycle 3.

At intermediate times when agreement is good, there are two main differences. First, during Temperate States, the calculated I-129 dose rates from CC4 are larger than those from FRAC3DVS. This occurs because in CC4 the well, by conservative assumption, captures essentially all the I-129 plume from the repository whereas in FRAC3DVS only a portion of the plume is captured by the well. Consequently, I-129 concentrations in well water are higher in CC4. Since the well is the most important exposure pathway for the farmer critical group living during Temperate States, the calculated CC4 dose rates are larger that the FRAC3DVS dose rates during these periods.

Second, the calculated FRAC3DVS dose rates are generally higher than the CC4 dose rates at the beginning of Permafrost States. This follows the pattern observed in the I-129 mass flow rates to the biosphere in Section C.3.1 and, as explained there, arises mainly due to the different methods used to model groundwater flow in the two models.

The I-129 dose rates calculated by CC4 and FRAC3DVS for the DC3 Glaciation Case are compared in Figure C.7. The calculated dose rates, which are much lower than for the Reference Case, are higher for FRAC3DVS at early times because the I-129 reaches the surface earlier in FRAC3DVS than in CC4. The FRAC3DVS dose rates are also, in general, higher than the corresponding CC4 values during Temperate States; but the differences decrease with time.

Another difference between the calculated dose rates occurs during Permafrost States. During these periods the critical group is exposed to radionuclides discharged to the North Lake or North talik. Calculated dose rates are zero in CC4 because there are no I-129 releases to the North Lake during these times for the DC3 source location. In contrast, FRAC3DVS dose rates are non-zero because there are I-129 releases, albeit low, to the North Lake during these periods even for the DC3 source location.

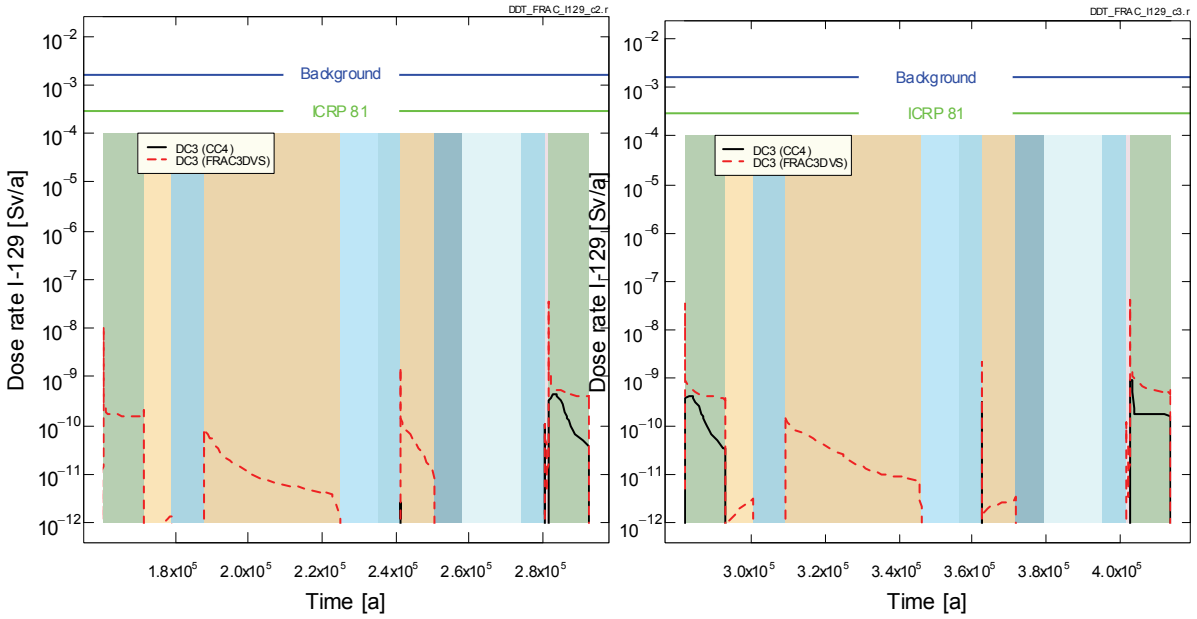

Figure C.7: Comparison of calculated I-129 dose rates from CC4 and FRAC3DVS for the DC3 Glaciation case for glacial cycles 2 and 3. For the other glacial cycles, the I-129 dose rates are similar to those for cycle 3.

C.4 CONCLUSIONS

The purpose of the CC4 and FRAC3DVS comparisons presented in this appendix is two-fold: (1) to increase confidence in the numerical transport models by providing independent confirmation and review of their respective results, and (2) to check if the geosphere model used in the system model SYVAC3-CC4 provides an acceptable representation of the more detailed FRAC3DVS geosphere model. As previously noted, a series of “snapshots” of the transient groundwater flow field (that exists during the glacial cycle) is used to represent the groundwater flow in the CC4 simulations for the Glaciation Scenario.

The results of the comparisons made in this appendix indicate that the SYVAC3-CC4 system model generally reproduces the key results from FRAC3DVS. This suggests that the approach taken to represent the transient groundwater flow field (generated by FRAC3DVS) in CC4 is acceptable. Since CC4 executes much faster (hours versus months) than FRAC3DVS, it can be used to more quickly assess a range of cases, e.g., simulation with other nuclides (particularly long chains) and long-time simulations, and it can be used for probabilistic safety analyses (see Section 8).

REFERENCES

Garisto, F., J. Avis, N. Calder, P. Gierszewski, C. Kitson, T. Melnyk, K. Wei and L. Wojciechowski. 2005. Horizontal borehole concept case study. Ontario Power Generation, Nuclear Waste Management Division Report 06819-REP-01200-10139-R00. Toronto, Canada.

Garisto, F., J. Avis, N. Calder, A. D'Andrea, P. Gierszewski, C. Kitson, T. Melnyk, K. Wei and L. Wojciechowski. 2004. Third case study - Defective container scenario. Ontario Power Generation, Nuclear Waste Management Division Report 06819-REP-01200-10126-R00. Toronto, Canada.

Gierszewski, P., T.W. Melnyk, S.C. Sheppard and J. Tait. 2004. SYVAC3-CC4 theory. Ontario Power Generation, Nuclear Waste Management Division Report 06819-REP-01300-10072-R00. Toronto, Canada.

Walsh, R. And J. Avis. 2010. Glaciation Scenario: Groundwater and radionuclide transport studies. Nuclear Waste Management Organization Technical Report NWMO TR-2010-09. Toronto, Canada.